

**Development of Small Molecules Towards Novel Protein Targets:
From Selective Androgen Receptor Modulators to Affinity Probes for a Novel
Immunological Target**

by

Chih-Hsuan Lin

A thesis submitted in partial fulfillment of the requirements for the degree of

Doctor of Philosophy

Department of Chemistry
University of Alberta

© Chih-Hsuan Lin, 2023

Abstract

Cancer is a group of diseases that result from the uncontrollable growth of cells, which eventually can metastasize to other parts of the body, resulting in spread of the cancer. Chemotherapy, radiotherapy, surgery, and immunotherapy are the main pillars of cancer therapeutics. In recent years, immunotherapy achieved a revolutionary breakthrough with the identification of immune checkpoint proteins and their inhibitors, which has led to the development of several antibody treatments.

Target deconvolution remains an important task in studying pathologically and clinically significant processes, which pave the way to the development of a drug candidate. Protein identification requires the involvement of medicinal, biological, and organic chemistry. Synthesis of novel small molecules plays an essential role in the process. Small molecules with diverse structures and functionalities are used to probe an active site, such as a ligand binding pocket or protein–protein interaction. Over the years, scientists have developed various techniques and cutting-edge chemistry towards protein identification.

Barakat and coworkers discovered a novel hit compound with promising immunological activities by being able to promote the production of T cells and cytokine interleukin 2 (IL-2). The target deconvolution revealed that the mechanism of the compound triggering the downstream immune response involves neither of the two common pathways, the programmed cell death protein 1 (PD-1/PD-L1) or cytotoxic T-lymphocyte-associated protein 4 (CTLA-4/B7-1). Instead, the compound binds to an unknown protein and triggers the downstream immune response. In this project, we executed the structural modifications of the lead compound with different

functionalities, which were applied in different strategies in order to identify the unknown protein and probe its mode of action (MOA).

Chapter 2 outlines the molecular design and preparation of the first- and second- generation probe molecules. The first-generation probe molecule was synthesized with a biotin functionality, which was used towards the streptavidin–biotin affinity purification. The second-generation probe molecules were proposed and synthesized for a proof-of-concept photoaffinity labelling experiment. Benzophenone was incorporated as the photo-crosslinker; the synthesized probe molecules were treated to bovine serum albumin (BSA) for photoaffinity labelling.

Chapter 3 addresses the utilization of third-generation trifunctional probe molecules and a fourth-generation fluorescent probe molecule. Two distinct trifunctional molecules were prepared by incorporating a photo-crosslinker and a bio-orthogonal handle, affording the benzophenone (BP) and the trifluoromethyl phenyl diazirine (TPD) probe. Later, the TPD probe found applications in a successful BSA photoaffinity labelling experiment by increasing the molecular weight of the protein under UV irradiation. Also, it was used in the synthesis of the fifth-generation probe molecule, in which a biotin handle was installed prior to the cell-based assay. On the other hand, a fluorescent molecule containing a BODIPY fluorophore was prepared and used in multiple microscopic experiments, including real-time high content imaging and confocal microscopy.

In Chapter 4, a different project aiming at the preparation of a selective androgen receptor modulator (SARMs)-based compounds will be addressed. The compound library consists of SARMs with distinct chemical structures, including aryl

propionamide, quinolinone, *N*-substituted tropine/tropinone, and hydantoin. These compound classes have previously shown to possess performance-enhancing properties, such as increasing body mass and muscle strength; consequently, they have been reported to be abused in the athlete community. These properties also give them the potential to treat muscle wasting conditions. The synthesized analogs were proposed to be analyzed by two-dimensional gas chromatography (GC × GC) by studying their physicochemical properties and retention behaviour, which would be used toward the development of a machine-learning algorithm in order to flag suspicious performance-enhancing drugs (PEDs) in clinical samples. The compounds await for the opportunity to be tested in a cachexia model when an appropriate collaborator is secured.

Chapter 5 provides a set of general conclusions for the projects that were mentioned in this thesis. Also, it illustrates possible future directions for the immunological chemistry project and reiterates objectives for the SARMs project.

Preface

Chapter 2 will be published at a future date upon completion of key additional experiments as Lin, C.-H; Tabana, Y.; Yu, S.; Ponich, A.; Zhang, S.; Babu, D.; Moon, T.-C.; Siraki, A.; Fahlman, R.; Barakat, K.; West, F. G. “Synthesis and Evaluation of 1-Methyl-3-nitro-4-(piperazin-1-yl)quinolin-2(1*H*)-one-based Immunostimulators Towards the Development of Immunotherapy”. The project was conceived by Barakat, K. and West, F. G. who supervised me; Barakat, K., Moon, T.-C., and Babu, D. supervised Tabana, Y. I was responsible for the design, synthesis, and characterization of all compounds. Yu, S. contributed equally to the synthesis and data collection of compounds **9** and **10**. Yu, S. contributed equally to the photoaffinity labelling experiments of bovine serum albumin (BSA). Tabana, Y. was responsible for all the cell-based assay and immunological evaluations of the synthesized compounds **1**, **9**, and **10**.

Chapter 3 will be published at a future date upon completion of key additional experiments as Lin, C.-H; Tabana, Y.; Yu, S.; Ponich, A.; Zhang, S.; Babu, D.; Moon, T.-C.; Siraki, A.; Fahlman, R.; Barakat, K.; West, F. G. “Synthesis and Evaluation of 1-Methyl-3-nitro-4-(piperazin-1-yl)quinolin-2(1*H*)-one-based Immunostimulators Towards the Development of Immunotherapy”. I was responsible for the design, synthesis, and characterization of all compounds. Ponich, A., an NSERC USRA summer undergraduate researcher, contributed to significant portions of the synthesis of compound **3** and was responsible for the characterization of compound **3**. I performed the photoaffinity labelling experiment of BSA with compound **3** and the fluorescent analysis of compound **29**. Tabana, Y. was responsible for all the affinity pull-down purification and immunological assays of compound **1**, **3**, **29**, and **30**. Zhang, S. and Tabana, Y. were responsible for the design and performance of real-time high content microscopy and confocal microscopy.

In Chapter 4, I was responsible for the synthesis and characterization of compound **1a-1g** and **2aa-2gb**. Dr. Thomas Scully was responsible for the synthesis and characterization of all the other compounds mentioned in the compiled library.

Dedication

This thesis is dedicated to my beloved parents, my brother, and all my friends who have supported me relentlessly throughout the journey.

Acknowledgement

First and foremost, I would like to express my deepest gratitude to my supervisor, Dr. Frederick G. West, for his continuous support and guidance as well as all the caring words and encouragement. Thank you for welcoming me to the group, giving me the opportunity to learn, and the best environment to express myself. I have learned so much from you in terms of knowledge in organic chemistry, communication skills, and useful laboratory skills. I am also extremely grateful for the mentorship and support you have offered to help me overcome the challenges on the research projects. Thank you for being such an amazing mentor throughout the journey.

I also would like to express my gratefulness to my supervisory committee members, Dr. John C. Vederas and Dr. Matthew Macauley, for the knowledgeable opinions and suggestions I received. I want to thank all the senior collaborators, Dr. Khaled Barakat, Dr. Tae-Chul Moon, Dr. Arno Siraki, and Dr. Richard Fahlman for all the guidance on the research projects. My appreciation goes to Yasser Tabana, who has been a hard-working researcher, for all the input you made for the project.

Words cannot express how grateful I am to be able to work with all the talented West group members. I want to thank former group members, Dr. Thomas Sully, Dr. Claudia Weilbeer, Dr. Yury Karpov, Dr. Marius Constantin, Dr. Ahmed Elemenoufy, Dr. Natasha Rana, Dr. Luna Ismat, and Dr. Ahmed Oraby, for the assistance you provided to help me adapt to the lab. I also want to thank James Donnelly, Maxwell Boateng, Christian Jankovic, Richard Yuen, Seif Khalifa, Andrew Daszczyński, Karim Elbaz, Israel Najar, Erin Fitch, Emily Schmidt, and Shivesh Baburam for your presence in the lab. Thanks to all of you for embracing me with the warmest and friendly atmosphere. I would like to especially express my gratitude to Ashley Ponich, who has been an extremely talented friend and co-worker; it has been a pleasure working with you. I would also like to thank Dr. Yen-Ku Wu for embarking me to this wonderful experience. Words cannot express how grateful I am to Dr. Shaohui Yu who I have learned so much from, not only in the lab but also in life. Thanks to all of you for broadening my knowledge; it is you that makes this journey so amazing.

I would like to take this chance again to thank all the supporting staff of NMR, analytical lab, mass spectroscopy facility, and biological lab in the Department of Chemistry. They work diligently and do their best to offer professional suggestions and resolutions to any technical problems I have encountered. I also want to express my appreciation to Dr. Anna Jordan for annotating my thesis with valuable feedbacks. I feel extremely proud of the result; this would not be possible without your help.

Finally, words cannot express how grateful and thankful I am to my family for the endless love and encouragement over the years. My deepest gratitude goes to my dad Jung-Mao Lin, my mom Yen-Chen Yang, and my beloved brother Ting-Yu Lin. I want to thank my friends Serena Chang, Riley Hsiao, Hansol Park, and many many others for making this an unforgettable journey. I am so lucky to have you all by my side through all the tough and stressful moments. Your love makes me who I am today. Love you all immensely.

Table of Content

Chapter 1. Introduction: Synthesis and Evaluation of Probe Molecules as Immunostimulators Toward Immunotherapy	1
1.1 Cancer.....	1
1.2 Immune System and Immunoediting	2
1.2.1 Immune System.....	2
1.2.2 Immunoediting.....	3
1.2.3 Immune Checkpoints.....	4
1.3 Immunotherapy.....	5
1.3.1 History of Immunotherapy.....	5
1.3.2 Immune Checkpoint Inhibitors	6
1.3.2.1 Anti-CTLA-4 Antibodies.....	7
1.3.2.2 Anti-PD-1/Anti-PD-L1 Antibodies	9
1.4 Development of Small-molecule Immune Checkpoint Inhibitors.....	11
1.4.1 Recent Development of Small Molecule Inhibitors.....	11
1.4.2 Previous Work.....	14
1.5 Protein Identification.....	17
1.5.1 Biotin-tagged Approach	20
1.5.2 Trifunctional Approach	22
1.5.2.1 Photoaffinity Labelling.....	23
1.5.2.2 Bio-orthogonal Reactions	28
1.6 Conclusion and Statement of Problem.....	31
1.7 References.....	33
Chapter 2. Design and Synthesis of Small-molecule Probes Based on The Biotin-tagged Approach and The Photoaffinity Labelling Technique.....	48
2.1 Introduction	48
2.1.1 Biotinylation of Small Molecules	48
2.1.2 Synthetic Strategies of Benzophenones.....	50
2.1.3 Synthetic Strategies of Trifluoromethyl Phenyl Diazirines.....	54
2.1.4 Project Objectives	57
2.2 Result and Discussion	59
2.2.1 Synthesis of The First-Generation Biotinylated Probe Molecules.....	59

2.2.2 Immunological Evaluation of Biotinylated Probe 1	63
2.2.3. Design and Synthesis of Two Second Generation Photoaffinity Labelling Probe Molecules.....	65
2.2.4 Immunological Results of Photoaffinity Labelling Probe 9 and 10	68
2.2.5 Photoaffinity Labelling Experiment Using Bovine Serum Albumin (BSA)	69
2.3 Conclusion.....	71
2.4 Experimental.....	73
2.4.1 Synthesis of 1-Methyl-3-nitro-4-(piperazin-1-yl)quinolin-2(1 <i>H</i>)-one 5	73
2.4.2 Reduction of 4-Nitrobenzaldehyde to 4-Aminobenzaldehyde	75
2.4.3 Synthesis of Biotinylated Probe 1	75
2.4.4 Synthesis of Photoaffinity Probe 9	77
2.4.5 Synthesis of Photoaffinity Probe 10	78
2.4.6 Photoaffinity Labelling Experiment With BSA.....	80
2.5 References	81

**Chapter 3. Design, Synthesis, and Applications of the Trifunctional Probe
Molecules and the Fluorescent Probe Molecules..... 85**

3.1 Introduction	85
3.1.1 The Trifunctional Probe Molecules.....	86
3.1.2 The Fluorescent Small-molecule Probe.....	87
3.1.2.1. The Selection of Fluorophores	88
3.2 Results and Discussion.....	89
3.2.1 The Trifunctional Probe Molecules.....	89
3.2.1.1 Synthesis of BP Probe Molecules 1 and 2	90
3.2.1.2 Synthesis of TPD Probe Molecule 3	91
3.2.1.3 The Immunological Result of the Synthesized Probes 1 and 3	94
3.2.2 Optimization of the Click Reaction and Photoaffinity Labelling	95
3.2.2.1 Stability Test of Diazirine in Click Reaction Conditions	95
3.2.2.2 Comparison of Two Reducing Agents	96
3.2.2.3 Photoaffinity Labeling Experiment With Probe 3 in Methanol	97
3.2.3 Proof-of-concept BSA Labelling Experiment Using the Probe 3	98
3.2.4 The Biological Workflow Using Probe 3	101

3.2.4.1 The Result of Immunoblotting	102
3.2.5 The Fluorescent Probe Molecules	102
3.2.5.1 Synthesis of the Fluorescent Molecules.....	103
3.2.5.2 The Immunological Result of the Fluorescent Probe Molecules ..	104
3.2.5.3 Fluorescent Analysis.....	104
3.2.5.4 Confocal Microscopy and High-content Live Cell Imaging.....	106
3.2.6 The Biotin–TPD Probe Molecule.....	108
3.2.6.1 Synthesis of the Biotin–TPD Probe Molecule 30	108
3.2.6.2 The Immunological Result of the Biotin–TPD Probe Molecule...	109
3.2.6.3 The Pull-down Purification Using the Biotin–TPD probe 30	110
3.2.6.4 Preliminary LC-MS Result	113
3.3 Conclusion	113
3.4 Experimental.....	114
3.4.1 Synthesis of the Trifunctional Probe Molecule 1	115
3.4.2 Synthesis of the Trifunctional Probe Molecule 2	117
3.4.3 Synthesis of the Trifunctional Probe Molecule 3	119
3.4.4 Synthesis of the Fluorescent Probe Molecule 29	121
3.4.5 Synthesis of the Biotin–TPD Probe Molecule 30	124
3.4.6 The Stability Test of The TPD Trifunctional Probe 3	127
3.3.7. The Selection of Reducing Agent for the Click Reaction Condition ..	127
3.3.8. The Optimization of Photoaffinity Labelling Reaction.....	128
3.3.9. The BSA Labelling Experiment.....	128
3.5 References	129

Chapter 4. Synthesis and Characterization of Aryl Propionamide Derivatives as Potential Selective Androgen Receptor Modulators 132

4.1 Introduction	132
4.1.1 Androgen and Androgen Receptor (AR).....	132
4.1.1.1 The Structure of AR	133
4.1.1.2 Mechanism of Action of Androgens	134
4.1.1.3 Clinical Applications of Androgen.....	135
4.1.2 Selective Androgen Receptor Modulators (SARMs).....	136

4.1.2.1 Tissue Selectivity of SARMs	137
4.1.2.2 Potential Abuse of SARMs	138
4.1.3 Different Categories of SARMs.....	138
4.1.3.1 Aryl Propionamides	139
4.1.3.2 Hydantoins	140
4.1.3.3 Quinolinones	141
4.1.3.4 <i>N</i> -Aryl Tropine	142
4.1.3 Project Objectives	144
4.2 Result and Discussion	144
4.2.1 Synthesis of Aryl Propionamide Analogues.....	145
4.2.1. Compound Library	147
4.3 Conclusion.....	149
4.4 Experimental.....	150
4.5 References	168
Chapter 5. General Conclusions and Future Directions	173
5.1 The Identification of Immunostimulator Compound A	173
5.2 Synthesis of the Biotinylated Probe Molecule for Affinity Purification and the Photoaffinity Labelling Probe Molecules for a Protein Labelling Experiment	174
5.3 Synthesis of the Trifunctional Probe Molecules and the Fluorescent Probe Molecule, and Their Applications	175
5.4 Development of Selective Androgen Receptor Modulators (SARMs).....	176
5.5 Future Directions	177
5.6 Conclusion.....	178
5.7 References	179
Compiled References	180
Appendix: NMR Spectra	207

List of Tables

Chapter 2

Table 2.1. Reduction of 4-Nitrobenzaldehyde with Various Reductive Agents 62

Table 2.2. The Amide Coupling to the Corresponding Aldehyde **11** 66

Chapter 4

Table 4.1. Synthesis of the Anilide Intermediate **1a-g** and Aryl Propionamide

Derivatives **2** 145

List of Figures

Chapter 1

Figure 1.1. Signaling pathway of PD-1.	4
Figure 1.2. Immune checkpoint inhibitors (ICI): anti-PD-1 antibodies, anti-PD-L1 antibodies, and anti-CTLA-4 antibodies.	7
Figure 1.3. Stimulatory and inhibitory pathway by CD28/CTLA-4 and B7.	8
Figure 1.4. Anti-CTLA-4 antibodies.	9
Figure 1.5. Interaction of PD-1/PD-L1 leads to reduced immune response.	10
Figure 1.6. Anti-PD-1 and anti-PD-L1 antibodies.	10
Figure 1.7. BMS-57 and BMS-71.	12
Figure 1.8. 1,2,4-oxadiazole or 1,3,4-oxadiazole containing peptidomimetic compounds by Aurigene.	13
Figure 1.9. Small molecule inhibitors by the BMS containing phoxymethyl biphenyl scaffold.	14
Figure 1.10. Selected small molecule inhibitors for comprehensive in vitro assays. .	15
Figure 1.11. a) Chemical structure of Compound A . b) IL-2 ELISA assay in peripheral blood mono lear cells stimulated by staphylococcal enterotoxin B (SEB). c) CD8+ proliferation assay in response to anti-CD3, anti-PD-1 antibody (Pembrolizumab) and Compound A using PBMCs labelled with 1.25µM of carboxyfluorescein succinimidyl ester (CFSC) from ThermoFisher Scientific. d) CellTiter-Glo® Luminescent Cell Viability Assay with HepG2 cells in various concentrations of Compound A using CCK-8 assay. (Copied and modified with permission from Barakat et al. ¹¹⁵)	16
Figure 1.12. The biotin-tagged approach and the trifunctional approach.	19
Figure 1.13. Structure of biotin.	20
Figure 1.14. Biotin-tagged approach workflow.	21
Figure 1.15. Molecular design of biotinylated stauprimide.	21
Figure 1.16. Trifunctional approach.	23

Chapter 2

Figure 2.1. The biotin and activated biotin esters for amide bond formation.....	49
Figure 2.2. a) Naturally occurring compounds containing benzophenone. b) Commercial drugs with benzophenone scaffold.	50
Figure 2.3. The chemical structure of the lead compound, Compound A	57
Figure 2.4. Overview and design of different generations of molecules.	58
Figure 2.5. The first and the second generation probe molecules.	59
Figure 2.6. Proposed biotinylated molecules with an amide or an ester linker.....	60
Figure 2.7. The proposed retrosynthetic strategies of biotinylated probes 1 and 2	60
Figure 2.8. The immunological result of the biotinylated probe 1	64
Figure 2.9. Proposed photoaffinity probe molecules 8 , 9 , and 10	65
Figure 2.10. The immunological result of the photoaffinity labelling probe 9 and 10	69
Figure 2.11. MALDI results of the photoaffinity labelling model experiments. a) Only BSA in water. b) BSA incubated with probe 9 and irradiate with UV light for 2 h. c) BSA incubated with probe 10 and irradiate with UV light for 2 h.....	70
Figure 2.12. Molecular design of the first and the second generation probe molecules.	71
Figure 2.13. The schematic representation depicting the design of the trifunctional probe molecules.....	72

Chapter 3

Figure 3.1. The molecular design of the trifunctional, fluorescent, and biotin-TPD probe molecules.....	86
Figure 3.2. The molecular design of DA-1 and DA-2 based on the trifunctional approach.....	87
Figure 3.3. Fluorophores that have been used commonly in bioimaging.....	88
Figure 3.4. The proposed trifunctional probe molecules.	89
Figure 3.5. The immunological result of trifunctional probes 1 (panel a) and probe 3 (panel b).	95

Figure 3.6. The workflow of the proof-of-concept BSA labelling experiment.	98
Figure 3.7. The MALDI result of the first photoaffinity labelling experiment.....	99
Figure 3.8. The revised workflow of the proof-of-concept BSA labelling experiment.	100
Figure 3.9. The MALDI result of the labelling experiment utilizing the TPD- containing probe 3	101
Figure 3.10. The biological workflow utilizing probe 3 in attempts to isolate the protein of interest.....	102
Figure 3.11. The immunological result of the fluorescent probe 29	104
Figure 3.12. a) The fluorescence analysis of probe 29 and the concentration- dependent fluorescent analyses when b) 490 nm or c) 400 nm excitation was applied.	105
Figure 3.13. The real-time high content imaging of probe 29 with PBMCs.	106
Figure 3.14. Confocal microscopy using the probe 29	107
Figure 3.15. The proposed biotin–TPD probe 30	108
Figure 3.16. The comparison between the biological activity of probe 30 and other probe molecules.....	109
Figure 3.17. The control experiment with or without UV irradiation.	110
Figure 3.18. The result of the UV irradiation control experiment.....	111
Figure 3.19. Pull-down assay with probe 30	112
Figure 3.20. One of the Western blot results from utilizing probe 30 and the PBMCs.	113
Figure 3.21. Overview of the synthesized probe molecules.	114
 Chapter 4	
Figure 4.1. Chemical structure of testosterone and dihydrotestosterone.	133
Figure 4.2. The schematic representation of AR structure.	134
Figure 4.3. The schematic representation of AR mechanism.	134
Figure 4.4. SARMs with different chemical structures.	137
Figure 4.5. LGD2226 and LGD2941 by Ligand Pharmaceuticals.	141

Figure 4.6. The chemical structures of AC262536 and ACP-105.....	143
Figure 4.7. Library of the synthesized SARMs.....	148
Figure 4.7. Library of the synthesized SARMs (cont.).....	149

Chapter 5

Figure 5.1. Project overview.	174
Figure 5.2. The overview of the molecular design in Chapter 2.	175
Figure 5.3. The overview of the molecular design in Chapter 3.	176
Figure 5.4. Feasible future directions of the project.	178

List of Schemes

Chapter 1

Scheme 1.1. Benzophenone (BP), trifluoromethyl phenyl diazirine (TPD), and the corresponding reactive intermediates.	24
Scheme 1.2. Excitation pathways of BP.....	25
Scheme 1.3. Photoactivation mechanism of BP.	26
Scheme 1.4. Structural design of PIK-BP ₂ yne.....	26
Scheme 1.5. a) Photolysis of TPD and possible reactive intermediates. b) Bond insertion by a singlet carbene. c) Formation of alkene from aliphatic diazirine 1,2-hydride shift.	27
Scheme 1.6. The Staudinger reaction and the Staudinger ligation.	29
Scheme 1.7. Mechanism of Copper-catalyzed azide–alkyne cycloaddition (CuAAC).	30
Scheme 1.8. Strain-promoted [3+2] cycloaddition.	31

Chapter 2

Scheme 2.1. Synthesis of norbiotinamine from naturally occurring biotin.....	49
Scheme 2.2. a) The Friedel–Crafts acylation to benzophenones catalyzed by a Lewis acid. b) the variation of Friedel–Crafts proposed by Hwang et al. in the presence of TfOH. c) The Weinreb–Nahm ketone synthesis to benzophenone.	51
Scheme 2.3. The palladium-catalyzed carbonylative coupling to benzophenone.	52
Scheme 2.4. Carbon monoxide-free syntheses to benzophenone.	53
Scheme 2.5. Metal-catalyzed C–H activation of aryl aldehyde to diaryl ketone.	54
Scheme 2.6. Synthetic routes utilizing liquid ammonia. a) Zeifmann and co-workers established the key transformation from trifluoroacetophenone <i>O</i> -tosyl oxime to trifluoromethyl phenyl diaziridine. b) Brunner et al. later proposed the first synthesis of TPD with this transformation.....	55
Scheme 2.7. Ammonia-free synthesis to the TPD.	55
Scheme 2.8. The synthesis of building block 5	61
Scheme 2.9. The amide coupling of compound 6	61

Scheme 2.10. The synthesis to the final biotinylated probe 1 .	63
Scheme 2.11. The synthesis of photoaffinity probe 9 .	67
Scheme 2.12. The synthesis of photoaffinity probe 10 .	68

Chapter 3

Scheme 3.1. The synthetic strategy of the BP-bearing trifunctional probe 1 .	90
Scheme 3.2. The proposed synthetic strategy for a BP-bearing trifunctional probe.	90
Scheme 3.3. The synthetic strategy of the BP-bearing trifunctional probe 2 .	91
Scheme 3.4. TPD synthesis utilizing liquid ammonia or the nitrogen surrogate, MSH.	92
Scheme 3.5. The synthesis of the imine 11 , MSH 13 , and the attempted synthesis of diaziridine 14 .	93
Scheme 3.6. The synthesis of the trifunctional probe 3 using liquid ammonia.	94
Scheme 3.7. The stability test of TPD under the selected reaction conditions.	96
Scheme 3.8. The comparison between sodium ascorbate and TCEP as the reducing agent.	97
Scheme 3.9. Photoaffinity labelling using methanol as the substrate.	98
Scheme 3.10. The synthesis of the BODIPY-containing fluorescent probe 25 .	103
Scheme 3.11. The synthesis of the fluorescent probe molecule 29 .	104
Scheme 3.12. The synthesis of the biotin-TPD probe 30 .	109

Chapter 4

Scheme 4.1. General synthetic procedure of aryl propionamide derivatives.	139
Scheme 4.2. Enantioselective route to aryl propionamides.	140
Scheme 4.3. Synthesis of BMS-564929 reported by Bristol-Myers Squibb.	140
Scheme 4.4. Synthesis of quinolinone-containing SARMS.	142
Scheme 4.5. Synthesis of N-aryl tropine SARMS.	143

Abbreviation

Ac	acetyl
app.	apparent (spectral)
APCs	antigen-presenting cells
aq	aqueous solution
Ar	aryl
AR	androgen receptors
Bn	benzyl
BP	benzophenone
br	broad (spectral)
Bu	butyl
BSA	bovine serum albumin
Calcd	calculated
cat.	indicates that the reagent was used in a catalytic amount
cDCs	conventional dendritic cells
cm ⁻¹	wavenumber
CO	carbon monoxide
conc.	concentrated
CTLA-4	cytotoxic T-lymphocyte-associated protein 4
CTL	cytotoxic T lymphocytes
CuAAC	copper(I)-catalyzed azide-alkyne cycloaddition
d	day(s); doublet (spectral)
DBU	1,8-Diazabicyclo[5.4.0]undec-7-ene
DBD	DNA binding domain
DCC	<i>N,N'</i> -Dicyclohexylcarbodiimide
DCE	1,2-dichloroethane
DCM	dichloromethane
DCs	dendritic cells
DHT	5 α -dihydrotestosterone
DMF	dimethylformamide

DMSO	dimethyl sulfoxide
DMAP	4-(dimethylamino)pyridine
dd	doublet of doublets (spectral)
ddd	doublet of doublets of doublets (spectral)
DIBAL-H	diisobutylaluminum hydride
dt	doublet of triplets (spectral)
EC ₅₀	half maximal effective concentration
EDC/EDCI	1-ethyl-3-(3-dimethylaminopropyl)carbodiimide
EDG	electron-donating group
EI	electron impact (mass spectrometry)
ELISA	enzyme-linked immunosorbent assay
equiv.	equivalent(s)
ESI	electrospray ionization (mass spectrometry)
Et	ethyl
EtOAc	ethyl acetate
EWG	electron-withdrawing group
ex/em	excitation/emission
FT-IR	Fourier-transform infrared spectroscopy
FDA	Food and Drug Administration
GC-MS	gas chromatography–mass spectrometry
HATU	hexafluorophosphate azabenzotriazole tetramethyl uronium
HBTU	hexafluorophosphate benzotriazole tetramethyluronium
HSQC	heteronuclear single quantum coherence (spectral)
HRMS	high resolution mass spectrometry
HRT	hormone replacement therapy
HTS	high throughput screening
hν	light
IC	inhibitory concentration
ICI	immune checkpoint inhibitor
IL	interleukin

irAEs	immune-related adverse effects
ISC	intersystem crossing
<i>J</i>	coupling constant
<i>K_d</i>	dissociation constant
kDa	kilodaltons
L	liter(s); unspecified ligand
LBD	ligand binding domain
LC-MS	liquid chromatography–mass spectrometry
LDA	lithium diisopropylamide
LD	lethal dose
m	multiplet (spectral)
mABs	monoclonal antibodies
MALDI	matrix-assisted laser desorption/ionization
mCPBA	meta-chloroperoxybenzoic acid
Me	methyl
MeCN	acetonitrile
mg	milligram(s)
MHC	major histocompatibility complex
MOA	mode of action
mp	melting point
MSH	<i>O</i> -mesitylenesulfonyl hydroxylamine
<i>m/z</i>	mass to charge ratio
<i>n</i> -BuLi	<i>n</i> -butyllithium
NHS	<i>N</i> -hydroxysuccinimide ester
NIR	near infrared
NK	nature killer
NMR	nuclear magnetic resonance
NTD	N-terminal domain
O/N	overnight
PAL	photoaffinity labelling

PBMC	peripheral blood mononuclear cells
PEDs	performance enhancing drugs
PEG	polyethylene glycol
PD-1	programmed cell death protein 1
PD-L1	Programmed death-ligand 1
Ph	phenyl
q	quartet (spectral)
quint	quintet
R	generalized alkyl group of substituents
R_f	retention factor (in chromatography)
rt	room temperature
s	singlet (spectral)
SARMs	selective androgen receptor modulators
SDS-PAGE	sodium dodecyl sulfate–polyacrylamide gel electrophoresis
sept	septet (spectral)
SEB	Staphylococcal Enterotoxin B
SERMs	selective estrogen receptor modulators
SET	single electron transfer
S_NAr	nucleophilic aromatic substitution
SPAAC	strain-promoted azide–alkyne cycloaddition
t	triplet (spectral)
T	temperature, testosterone
TBTA	tris((1-benzyl-4-triazolyl)methyl)amine
<i>t</i> -Bu	<i>tert</i> -butyl
TCR	T cell receptor
TCEP	tris(2-carboxyethyl)phosphine
TCGF	T-cell growth factor
TEA	triethylamine
Tf	trifluoromethanesulfonyl
TfOH	trifluoromethanesulfonic acid

TFA	trifluoroacetic acid
TFAA	trifluoroacetic anhydride
THF	tetrahydrofuran
TLC	thin layer chromatography
T_m	melting temperature
TMS	trimethylsilyl
TPD	trifluoromethyl phenyl diazine
Ts	<i>p</i> -toluenesulfonyl
<i>p</i> -TsOH	<i>p</i> -toluenesulfonic acid
δ	chemical shift
λ	wavelength
ϵ_{\max}	absorptivity coefficient

CHAPTER 1

Introduction: Synthesis and Evaluation of Probe Molecules as Immunostimulators Toward Immunotherapy

1.1 Cancer

Cancer is one of the leading causes of death in the world. According to the World Health Organization (WHO), over 19.3 million people were diagnosed with cancer in 2020, and cancer accounts for the death of nearly 10 million cases in the same year.^{1,2} Cancer is a group of diseases that causes the systematic breakdown of the host's immunity. Cancer is able to bypass the immune surveillance through immunoediting.^{3,4} Immunoediting is the interaction between the immune system and tumor cells, it includes elimination, equilibrium, and escape phase. Elimination phase represents the main stage where anticancer activity is provoked by the host's immunity. However, cancer cells can develop further, thus enabling the masking of cancer cells, which eventually prevents the detection by the immune cells.^{3,5} It works by manipulating the recognition of immune cells and the environment of the cancerous site. This leads to the exponential and uncontrolled growth of tumor cells.⁶ Once the host immunity has been compromised, cancers now has entered the "equilibrium" and "escape" phases and possess the ability to metastasize to different parts and organs of the body, causing the detrimental collapse of the immune system.

So far, surgery, radiotherapy, chemotherapy, and immunotherapy remain the four most used ways for treating cancer.⁷ Although surgical operation offers a good chance of cure during the early stage of cancer, and around 80% of the cancer patients receive surgery, it is still an invasive treatment that might be accompanied various postoperative complexities. Radiotherapy is used to treat cancer by applying a high energy ionizing radiation, such as X-rays, gamma rays, or proton beams, at the cancerous site. The high energy radiation will damage the DNA of the cancerous tissue to initiate cancer cell death. It often is used to treat a solid tumor that is localized in one part of the body but has to be targeted with a precise angle and

exposure dose in order to reach the cancerous tissue.⁸ Chemotherapy uses one or a combination of cytotoxic drugs to systematically eliminate cancer cells through different mechanisms.⁹⁻¹¹ For example, cisplatin is used to treat many advanced stage cancers by causing the cross linking of nucleic acids of cancer cells to inhibit their DNA replication and cell division.¹²

Immunotherapy, on the other hand, emerged as a new generation of cancer treatment by modulating patients' immune system, particularly with the use of immune checkpoint inhibitors (ICIs). The consensus is that ICIs are able to increase immunity toward cancer by inhibiting a negative immune response.¹³⁻¹⁵ Among them, inhibitors of cytotoxic T-lymphocyte antigen-4 (CTLA-4) and programmed death protein (PD-1) or its ligand (PD-L1) have been studied extensively.^{16,17} Ipilimumab, an anti-CTLA-4 antibody, was brought first to the market in 2011 to treat malignant melanoma.^{18,19} Pembrolizumab, an anti-PD-1 antibody and one of the first therapeutics that target PD-1, was approved for melanoma by the Food and Drug Administration (FDA) in 2014.^{17,20} Although immunotherapy proved to be effective for some cancers in clinical trials, other cancer patients still suffer from low response rate and side effects, such as autoimmune responses.²¹ To reach an elevated immune activity, a more extensive understanding of the relationship between the immune system, cancer, and potential immunological targets are required.

These cancer treatments can be used as a monotherapy but more often are used in synergy with another treatment to reach best anticancer activity. Despite many treatments being available for cancers, problems like drug resistance, low survival rate, low response rate, and severe side effects, still remain big challenges to be overcome.²²⁻²⁵ In sum, a new therapy to reach best anticancer activity with less side effects and cost is still in urgent need.

1.2 Immune System and Immunoediting

1.2.1 Immune System

Innate and adaptive immune systems are the two main lines of defense against foreign pathogens, including cancers. The innate immune system offers a rapid first line of defense as well as initiating the adaptive immune system to provide a more specific

and long-term immune response. The adaptive immune system is composed mainly of T cells and B cells; it contributes to most of the anticancer activity in the process of eliminating cancer cells.²⁶⁻²⁸

1.2.2 Immunoediting

During the early stage of cancer development, the genetic mutation of cancer cells will cause the production of neo-antigens, modified proteins that can be recognized by antigen-presenting cells (APCs), such as dendritic cells (DCs). DCs are myeloid cells that engulf tumor cells and present antigens on their surfaces through class II major histocompatibility complex (MHC). The binding of antigen–MHC II complex to T cell receptor (TCR) initiates the stimulatory signal to activate T cells. A secondary co-stimulatory signal is necessary to achieve full activation of T cells and their proliferation. This secondary pathway is provided by the recognition of co-receptor CD28 to B7 on the surface of APCs.²⁹ On the other hand, the presentation of processed antigen by MHC I to cytotoxic T cells will promote immune response against foreign substances. These events trigger the activation and proliferation of T cells, and cancer cells are eliminated when encountered by the activated CD8⁺ T cells,^{30,31} while CD4⁺ T cells can differentiate into different subtypes in response to various cytokines.^{32,33} This stage is referred to as the “elimination” phase and is critical for killing cancer cells. However, cancer cells also possess the ability to bypass immune surveillance by immunoediting.

Cancer variants that develop according to Darwinian selection can escape the immune system through different mechanisms.^{3,6,27,31,34} One of the most common pathways is by causing the dysfunction of conventional dendritic cells (cDCs) or the disruption of priming. Primary tumors can affect hematopoiesis and the formation of DCs; this leads to immature and dysfunctional DCs. The ability of DCs to present antigens is, therefore, influenced and subsequently causes the diminishing of T cell activity. Also, tumor cells can alter their resistance toward apoptosis by secreting immunosuppressive cytokines, such as vascular endothelial growth factor (VEGF), transforming growth factor- β (TGF- β), IL-4, and IL-10, to create an

immunosuppressive state in the tumor microenvironment, making them less prone to cytotoxicity by the cytotoxic T cells.

1.2.3 Immune Checkpoints

Another mechanism of immunoeediting targets the immune checkpoint receptor PD-1. PD-1 controls negative immune regulation to promote self-tolerance and prevent autoimmunity when it binds to its ligand PD-L1. PD-1 is expressed on the surface of activated T cells and interacts with PD-L1 once a series of cytokines are produced to initiate an inflammatory process. Binding of PD-1 to PD-L1 down-regulates immune responses through different mechanisms, for example, activation of the STAT3 pathway, leading to T cell deactivation and declined level of cytokine production.^{35–38} This mechanism is also utilized by tumor cells, where various cancer cell lines can overexpress PD-L1 on their surfaces to suppress immune response by activated T cells (Figure 1.1). It has been found that PD-L1 is upregulated constantly in different tumors³⁹ and mouse models expressing PD-L1 showed reduced T cell mediated anticancer activity.⁴⁰

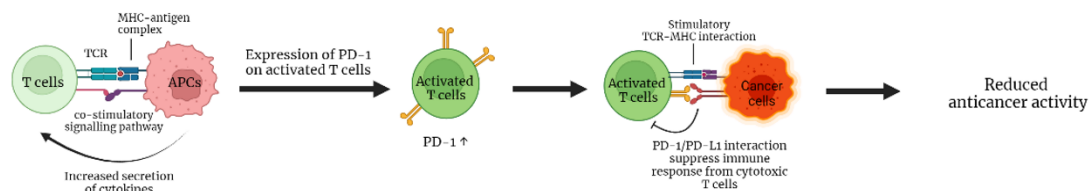


Figure 1.1. Signaling pathway of PD-1.

This finding has led to the development of a new generation of immunotherapy, immune checkpoint inhibitors (ICIs), based upon the rationale that interaction between PD-1 of activated T cells and PD-L1 on tumor cells leads to dampened antitumor activity. ICIs were antibodies proposed to block the interaction between PD-1/PD-L1 to enhance immune response, either by the blockage of PD-1 or PD-L1.^{13,15,37} Other ICIs include anti-CTLA-4, which targets inhibitory immune receptors cytotoxic T-lymphocyte antigen-4 (CTLA-4).⁴¹

1.3 Immunotherapy

1.3.1 History of Immunotherapy

The research studies in immunotherapy led to breakthroughs in the recent decade and has started to establish promising results in clinical trials.⁴²⁻⁴⁴ The high-impact journal *Science* selected it as the topic of the year in 2013.⁴⁵ The history of immunoncology can be dated back to more than a century ago. In 1891, William Coley, who is now recognized as the “Father of Immunotherapy”, injected cancer patients with a mixture of live and inactivated *Streptococcus pyogenes* and *Serratia marcescens*. The cocktail of bacteria also is known as Coley’s toxin and is the first documented immunotherapy used in clinical applications to achieve remission in a patient with various melanomas.^{28,43,46,47} However, the lack of the understanding in its mechanism raised the concern of infecting patients with pathogenic bacteria, causing it to be replaced by other treatments, like surgery and chemotherapy, until decades later.

In 1967, Miller and co-workers published a study in *Nature* on the discovery of T cells and their vital role in immunity⁴⁸ followed by the discovery of dendritic cells⁴⁹ and a deeper understanding about the function of nature killer (NK) cells.^{50,51} Around the same time, Stutman further elaborated the concept of immune surveillance with mouse models. In these studies, the mice model with a deficient immune system were more prone to develop cancer than the wild-type mice models.^{52,53} Others also found that T lymphocytes are related closely to antigen recognition and anticancer activity.⁵⁴ These findings in immunology and oncology established the conditions necessary for the field of immunotherapy to flourish.⁴³

Immunotherapy has started a major therapeutic improvement era later in 1976. In 1976, IL-2 was discovered as a “T-cell growth factor” (TCGF) that sustains the growth of T lymphocytes. It was approved later by the FDA for treating metastatic renal cell carcinoma and metastatic melanoma.⁵⁵ IL-2 immunotherapy can be used in a monotherapy but is more often used in combination with other therapies for metastatic melanoma.^{56,57}

In 1987, Brunet and colleagues reported the first immune checkpoint, CTLA-4.⁵⁸ However, it was not until 1995 that James Allison and his team elucidated the inhibitory and competitive mechanism in opposition to CD28. This also linked the

critical relationship between blockage of CTLA-4 and increased antitumor activity.^{59,60} Almost around the same time, programmed death-1 (PD-1) was discovered in 1991 by the Honjo group at the University of Tokyo when in search of a gene related to self–nonself recognition of the immune system.⁶¹ After several years of studying, the same research group revealed that PD-1 is not directly related to apoptosis/programmed death of immature T cells but an inhibitory modulator of T cell associated immune responses.^{62–64} Together, researchers from the Allison group and the Honjo group had demonstrated that the blocking of these immune checkpoints can lead to an elevated antitumor activity that possesses a therapeutic potential.^{60,65}

These results have paved the way for the development of ICIs such as ipilimumab (anti-CTLA-4 antibody) and pembrolizumab (anti-PD-1 antibody) in clinical trials. Ipilimumab was the first ICI that was brought to the market by Bristol-Myers Squibb (BMS) in 2011. It was approved for the treatment of metastatic melanoma.^{65,66} During the next several years, several ICIs targeting the interaction between PD-1 and PD-L1 such as pembrolizumab, atezolizumab, durvalumab, and avelumab were approved for various cancers.⁴³ The ICIs are undoubtedly the most promising antibody therapies that are currently in use. In fact, the 2018 Nobel Prize in Physiology or Medicine was awarded jointly to James Allison and Tasuku Honjo for their significant contribution on discovering immune checkpoints, which forged the path to cancer immunotherapy.^{67,68}

1.3.2 Immune Checkpoint Inhibitors

Immunotherapy has emerged as the fourth most used methods to treat cancers in recent years. Unlike other conventional therapies that aim to kill cancer cells directly, immunotherapy focuses on modulating patients' immune response to suppress cancer survival. Among immunotherapies, ICIs have been a revolutionary breakthrough in the recent decade and have shown clinical success against various cancers. ICIs fall under three different categories, anti-CTLA-4 antibodies, anti-PD-1 antibodies, and anti-PD-L1 antibodies (Figure 1.2).^{13,15,37} They are antibodies that block the protein-protein interaction between receptor and ligand, and thus interfere with the inhibitory

immune signalling pathway. As a result, there is a boost to immune responses against cancerous cells.

Although this type of therapy can be highly effective, unintended immune activation gives rise to the undesirable side effects that are termed immune-related adverse effects (irAEs).^{69–73} Immune-related adverse effects (irAEs) describe the treatment-specific adverse events that originated following the administration of the ICI therapies. These irAEs can happen in any organ system; the most common adverse events observed in ICI therapies include diarrhea, colitis, and skin disorders. According to statistics, irAEs caused by anti-PD-1/anti-PD-L1 antibodies are less severe than those of anti-CTLA-4 antibodies.^{73–75} In order to tackle the toxicities and complexities associated with ICI-mediated immunotherapies, guidelines have been published to provide better care.^{75–77}

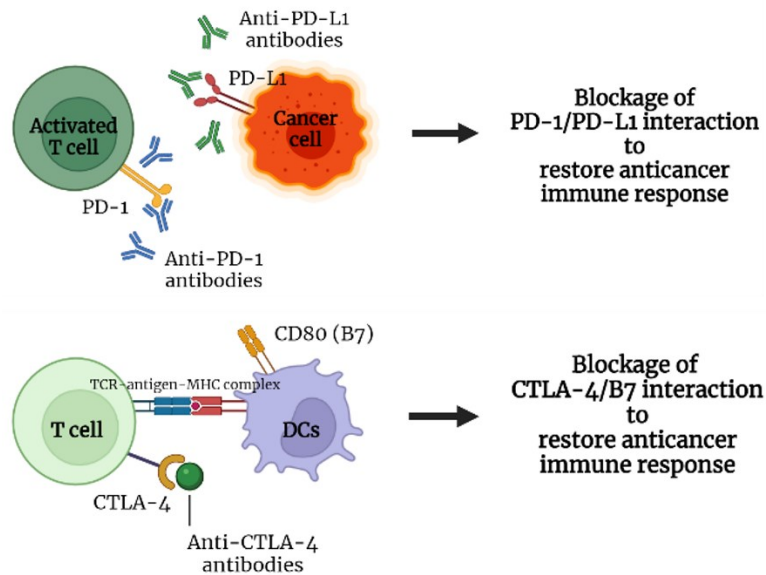


Figure 1.2. Immune checkpoint inhibitors (ICI): anti-PD-1 antibodies, anti-PD-L1 antibodies, and anti-CTLA-4 antibodies.

1.3.2.1 Anti-CTLA-4 Antibodies

CTLA-4 is a homolog of CD28, which presents on the surface of activated T cells and binds to B7-1/B7-2 in competition to CD28. When CD28 binds to B7, a stimulatory response is initiated and upregulates the activity of T cells. On the other hand, when

CTLA-4 competes with CD28 and binds to B7, a decreased T cell response will be observed (Figure 1.3).^{16,29,41}

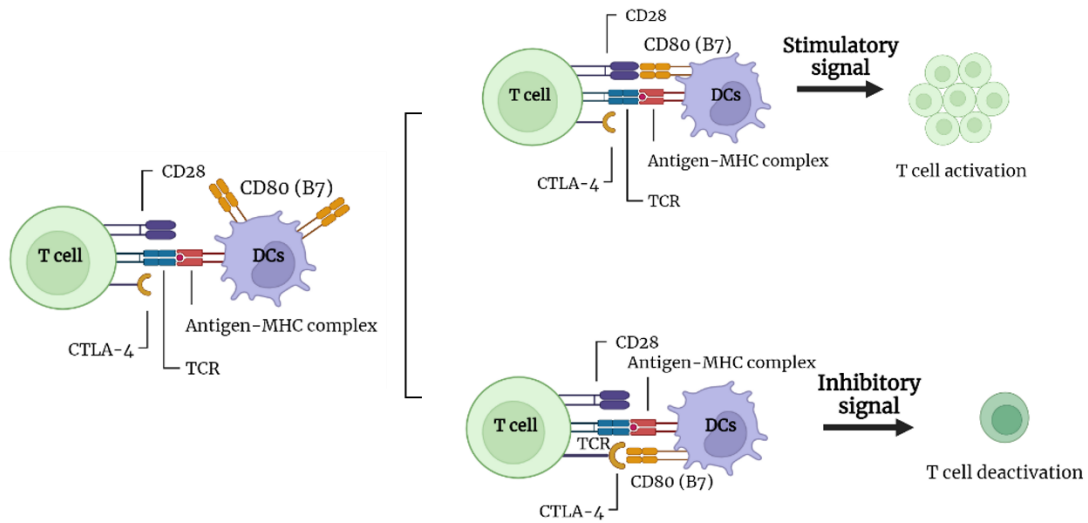


Figure 1.3. Stimulatory and inhibitory pathway by CD28/CTLA-4 and B7.

Anti-CTLA-4 antibodies are able to block the interaction between CTLA-4 and B7 by binding to CTLA-4 (Figure 1.4). It has been shown in clinical trials that blockage of CTLA-4 with anti-CTLA-4 antibodies is the predominant mechanism for T cell activation against cancer.⁷⁸ Ipilimumab is an anti-CTLA-4 antibody that was approved in 2011 by the FDA for late-stage melanoma.^{66,79} It is sold under the trade name Yervoy and should be administered to patients intravenously. It has been evaluated extensively for the response rate and survival rate as both a monotherapy and a combined therapy.

Maker and co-workers performed a study by administering a combination of ipilimumab (0.1, 0.3, 1.0, 2.0, or 3.0 mg/kg every three weeks) and IL-2 to a group of patients hoping to see a synergistic effect from the combined therapies. However, the authors concluded that the 22% response rate was the sum of individual treatments.⁸⁰ According to other case analyses, patients that received ipilimumab combined with dacarbazine showed a significantly higher response rate and overall survival.^{81,82} Other trials using anti-CTLA-4 antibodies as a monotherapy in patients with renal carcinoma or metastatic melanoma demonstrated a response rate of 12–19%.^{29,83,84} Although the response rates vary with the types of cancer and patients' conditions,

statistics still showed that ipilimumab provides an alternative with improved overall survival rate and more lasting response compared to conventional therapies.⁷⁹

However, putting a break on inhibitory immune response often comes with immune-related toxicity and autoimmunity. These immune related adverse events are the results of the provoked immunity. Skin lesions, colitis, hepatitis, and sarcoidosis are all irAEs that have been documented in patients that received treatment with ipilimumab or tremelimumab.^{29,79,85}

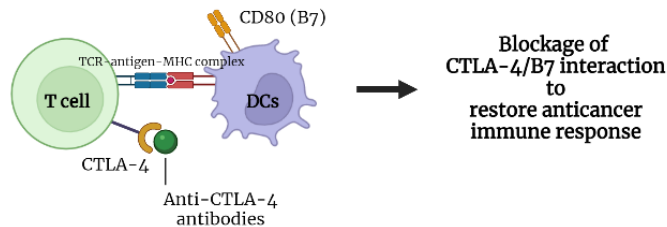


Figure 1.4. Anti-CTLA-4 antibodies.

1.3.2.2 Anti-PD-1/Anti-PD-L1 Antibodies

PD-1 is a transmembrane glycoprotein of 50–55 kDa mass; its ligands, PD-L1 and PD-L2, are glycoproteins of the B7 family. The difference between PD-L1 and PD-L2 is that PD-L1 expressed ubiquitously on all inflamed tissues while PD-L2 only expressed on APCs like DCs and macrophages. When PD-1 interacts with PD-L1, it initiates the phosphorylation of a tyrosine residue on the cytoplasmic domain of PD-1. The phosphorylation recruits Src homology-2 domain-containing the protein tyrosine phosphatase-2 (SHP-2), which causes the phosphorylation of the downstream spleen tyrosine kinase (Syk) and phospholipid inositol-3-kinase (PI3K). This series of signaling pathways results in the exhaustion of T cell-related function, including cytokine production and the proliferation of cytotoxic T lymphocytes (CTLs), which enables the evasion of cancer cells (Figure 1.5).^{35,86,87}

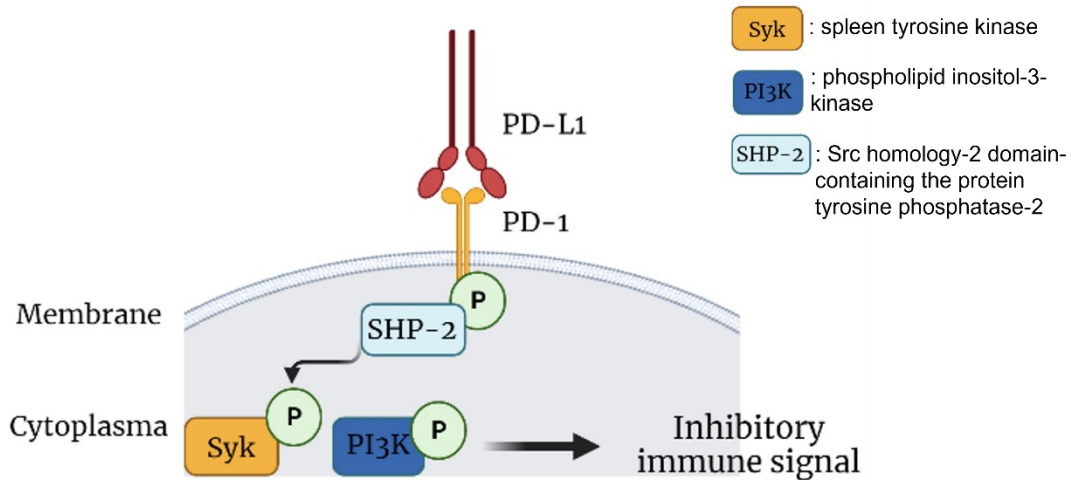


Figure 1.5. Interaction of PD-1/PD-L1 leads to reduced immune response.

Anti-PD-1 and anti-PD-L1 antibodies can cause a blockade of this interaction (Figure 1.6). Pembrolizumab is the first anti-PD-1 antibody approved by the FDA in 2014. It is sold under the name Keytruda and is currently on the World Health Organization's List of Essential Medicines.⁸⁸ Results from a phase I clinical trial showed that pembrolizumab was effective against advanced melanoma.⁸⁹ Similar results were seen in another phase I clinical trial, where a 33% overall objective response rate and a 35% progression-free survival rate were reported among advanced melanoma treated with pembrolizumab.⁸⁶ Another result from a phase II clinical trial demonstrated that pembrolizumab provided prolonged survival without showing progression and showed less severe toxicity compared to patients treated with ipilimumab.^{86,87,90}

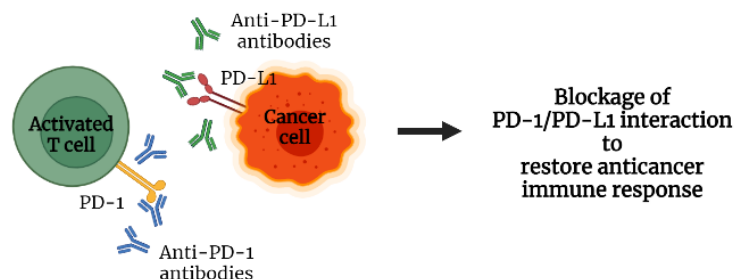


Figure 1.6. Anti-PD-1 and anti-PD-L1 antibodies. When the anti-PD-1 antibodies bind to PD-1 or anti-PD-L1 antibodies bind to PD-L1, the suppressive immune response is blocked, leading to increase anticancer activity.

Like anti-CTLA-4 antibodies, the occurrence of irAEs is not uncommon in anti-PD-1/anti-PD-L1 therapy. Some frequent adverse events include fatigue, rash, skin disorders, gastrointestinal events, diarrhea, and endocrinopathies.³⁵

1.4 Development of Small-molecule Immune Checkpoint Inhibitors

1.4.1 Recent Development of Small Molecule Inhibitors

There has been significant progress on the development of antibodies as ICIs over the last decade. But disadvantages still are present in therapies with these biomacromolecules. One obvious drawback is the occurrence of the previously mentioned irAEs. The circulation time of these monoclonal antibodies (mABs) varies from several days to weeks; therefore, patients can only be given with palliative care to manage these serious symptoms before the drug is cleared. Other downsides include a complex production process, high cost, low stability, immunogenicity, and low tissue permeability.^{91,92} In order to overcome these problems, the study and development of small molecules as an alternative for the blockade of immune checkpoint pathways has started to gain more attention over the years, particularly targeting the PD-1/PD-L1 immune checkpoint.⁹³⁻⁹⁹ Small molecules, in comparison to antibodies, are able to achieve better bioavailability as well as lower production cost and increased stability. Although the clinical progress of small molecule inhibitors remains inferior to antibody therapies, it is certain that these incentives have fueled the development of small molecules toward immunotherapy.

There have been many studies on the small molecule inhibitors since the X-ray structure of the PD-1/PD-L1 complex was published.¹⁰⁰ The human PD-1 (hPD-1) protein belongs to the immunoglobulin (Ig) superfamily and is made up of 288 amino acids. hPD-1 is composed structurally of three parts: a cytoplasmic domain, a transmembrane domain, and an extracellular domain. PD-1 binds to PD-L1 in a 1:1 ratio, and when they bind, this signal promotes tolerance to self-antigens to protect normal tissues. Tumor cells can take advantages of the PD-1/PD-L1 immune checkpoint signalling pathway by overexpressing PD-L1 on their surface to suppress antitumor activity by the T lymphocytes.

The development of small molecule inhibitors targeting this pathway can be categorized based on different mode of actions: (1) direct blockade of PD-1 or PD-L1; (2) interfering with the expression of PD-L1, and (3) promoting the degradation of PD-L1.^{93,99} These include peptides, macrocyclic peptides, peptidomimetics, and low-molecular weight compounds.⁹³

AUNP-12 is a peptide designed to block this interaction by binding to PD-1. After the analyses of several related patents, the structure of AUNP-12 was proposed to be a branched 29 amino acid peptide.^{101,102} It was shown to interfere with the binding of PD-L2 to PD-1 with a EC_{50} of 0.72 nM. This result also was in agreement with another rat peripheral blood mononuclear cell (PBMC) proliferation assay, where AUNP-12 showed an EC_{50} of 0.41 nM in rat cells expressing PD-L1.¹⁰¹

Macrocyclic peptides also were used to substitute antibodies to block the PD-1/PD-L1 signalling pathway. BMS-57 and BMS-71 were developed by the BMS company under the research of PD-1/PD-L1 antagonists (Figure 1.7).^{103,104} Soon after, Magiera-Mularz and co-workers provided more details on the binding of two macrocyclic peptides to PD-1/PD-L1. They suggested that the macrocyclics bind to PD-L1 directly and are able to restore the function of T lymphocytes by antagonizing the immune checkpoint pathway.¹⁰⁵

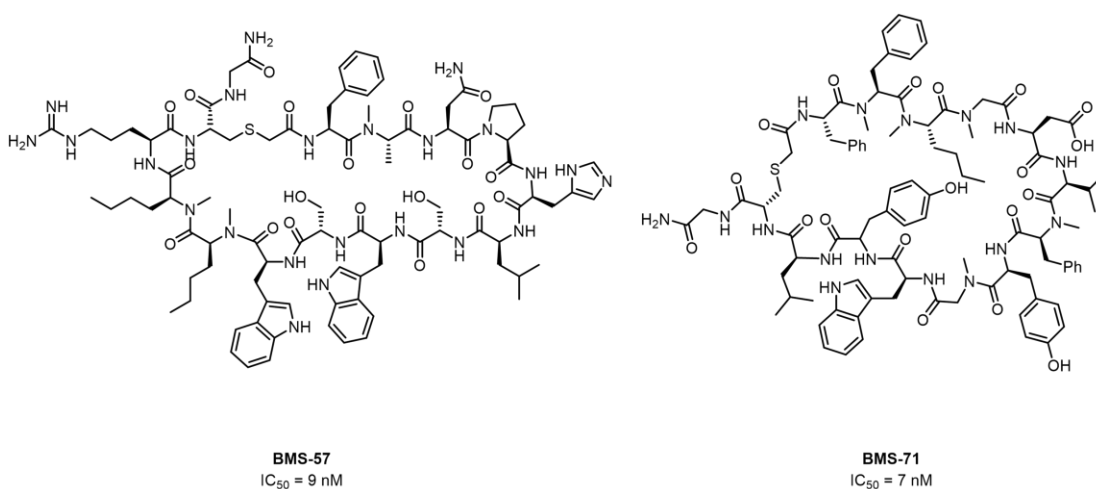


Figure 1.7. BMS-57 and BMS-71.

Aurigene Discovery Technologies and Curis Pharmaceuticals jointly came up with an oral inhibitor, CA-170, that targets not only the PD-1/PD-L1 pathway but also the V-domain immunoglobulin suppressor of T cell activation (VISTA) pathway.¹⁰⁶ Preclinical data showed that the compound is able to promote the proliferation of T cells and the secretion of IFN- γ by blocking PD-L1. Also, CA-170 showed low toxicity and no obvious irAEs at the maximum dose of 1200 mg/d.^{99,107,108} CA-170 was the first small molecule that entered clinical study and is currently under a phase II clinical trial. The structure of CA-170 contains a 1,2,4-oxadiazole scaffold, according to their recently published patent.¹⁰⁷ Aside from CA-170 (**1**), Aurigene also patented a series of compounds containing similar scaffolds (**2,3**) that were reported to be able to disrupt the PD-1/PD-L1 pathway (Figure 1.8).^{94,109,110} These compounds have demonstrated the advantageous characteristics of small molecule inhibitors, for example, better bioavailability and easier production processes, which populate the development of small molecule inhibitors.

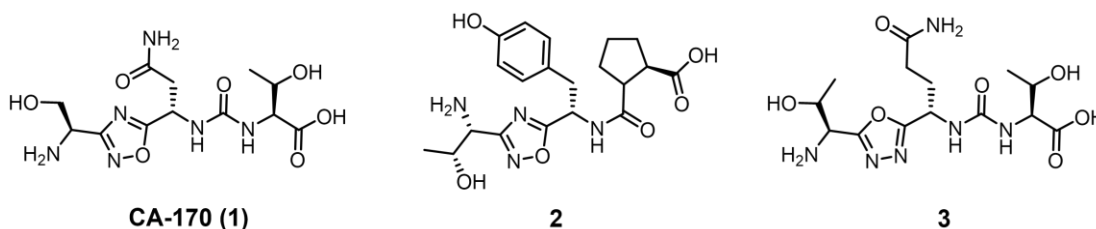


Figure 1.8. 1,2,4-oxadiazole or 1,3,4-oxadiazole containing peptidomimetic compounds by Aurigene.

BMS has also led the development of non-peptide small molecule inhibitors targeting the PD-1/PD-L1 pathway.^{94,111} The core structure of the proposed small molecule inhibitors is centered around a phoxymethyl biphenyl scaffold (Figure 1.9). The IC₅₀ values of BMS-200 and BMS-202 were determined to be 80 nM and 18 nM, respectively, by homogeneous time-resolved fluorescence (HTRF)-binding assays.^{112,113} The mechanism of BMS-202 was later described by Zak et al. They found that BMS-202 and BMS-8 bind to the hydrophobic pocket between the interface of PD-L1 homodimers. This inhibitor-PD-L1 interaction can lock PD-L1 molecules into a tetramer, which prevents the binding of PD-1, resulting in the

suppression of the PD-1/PD-L1 pathway that eventually leads to the restoration of T cell activity.^{99,100,114}

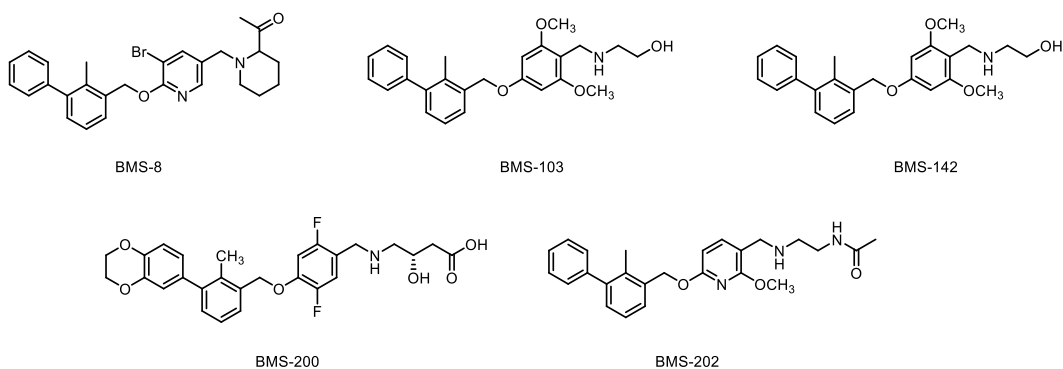


Figure 1.9. Small molecule inhibitors by the BMS containing phoxymethyl biphenyl scaffold.

1.4.2 Previous Work

The above-mentioned compounds have represented the significant improvement of small molecules against the PD-1/PD-L1 pathway. These compounds typically work by occupying the shallow hydrophobic cavity on the protein surface or between the interface of proteins. In order to have a thorough understanding of the structural activity relationship and toxicity of these compound, Barakat and co-workers proceeded with a systematic in vitro analysis of several small molecule inhibitors (Figure 1.10).¹¹⁵ In this study BMS-57, BMS-103, BMS-142 and Aurigene-1(2) were selected, and their ability to interfere with PD-1/PD-L1 interaction was validated through competitive ELISA assays. Also, their affinity for PD-L1 was tested using differential scanning fluorimetry (DSF) assays, microscale thermophoresis (MST), surface plasmon resonance (SPR), and NMR. Results from these experiments unanimously showed that BMS small molecule inhibitors bind to PD-L1 and are able to disrupt PD-1/PD-L1 interaction. However, results from multiple assays suggested that Aurigene-1 (2) does not bind to PD-L1 in these assays nor block PD-1/PD-L1 interaction in an ELISA assay. They also proposed that there is no suitable hydrophobic pocket between the PD-L1 dimer interface through computational studies. Thereby, they concluded that Aurigene-1 (2) does not act directly at the

PD-1/PD-L1 axis, and more studies are required to identify the mode of action (MOA) of Aurigene-1.

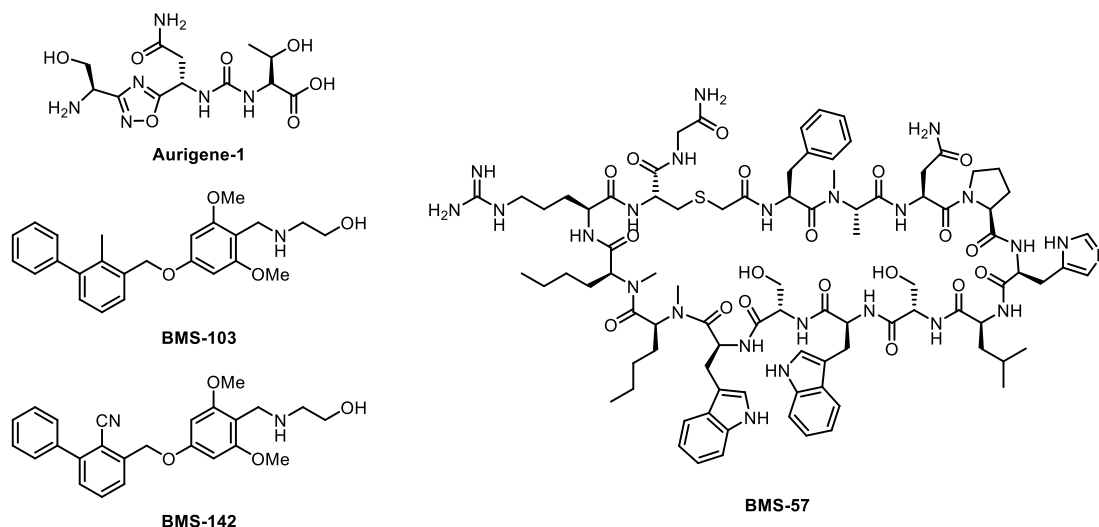


Figure 1.10. Selected small molecule inhibitors for comprehensive in vitro assays.

During these analyses and as part of their continuing research on novel immunomodulators, they identified a series of compounds exhibiting promising immunological results in the cell-based assay. Among all derivatives, **Compound A** shows potent immunological activity in the biological assays (Figure 1.11a). **Compound A** induces production of the cytokine IL-2 and promotes the proliferation of T cells in PBMC stimulated with Staphylococcal Enterotoxin B (SEB) (Figure 1.11b-c).^{116–118} SEB was used as a super-antigen to activated T-cell related immune responses in the absence of foreign antigen. Low toxicity was observed with **Compound A** in HepG2 cells with concentrations starting from 45 μ M (Figure 1.11d).

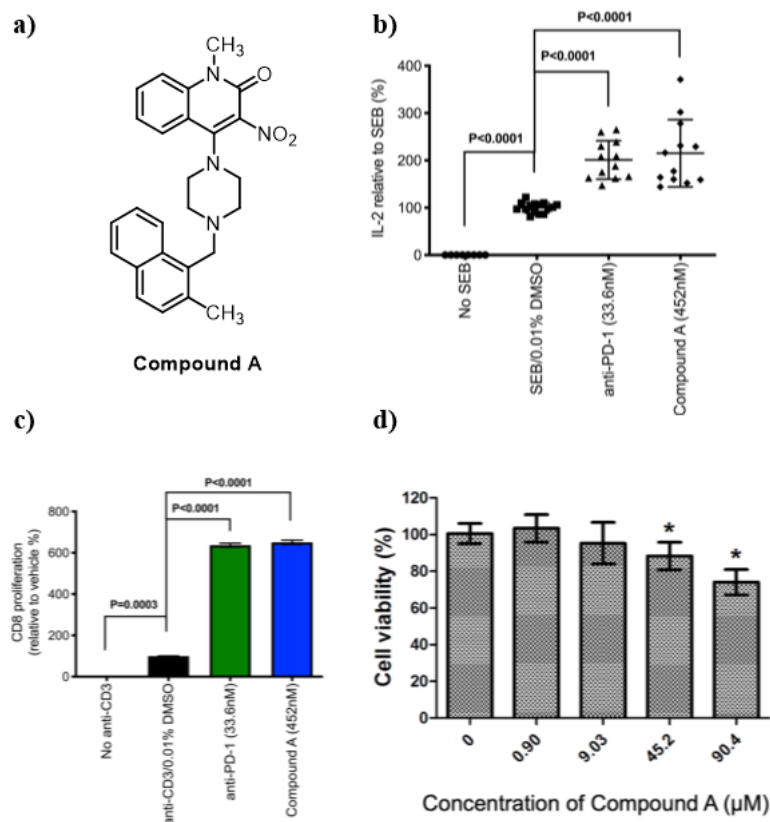


Figure 1.11. a) Chemical structure of **Compound A**. b) IL-2 ELISA assay in peripheral blood mononuclear cells stimulated by Staphylococcal Enterotoxin (SEB). c) CD8⁺ proliferation assay in response to anti-CD3, anti-PD-1 antibody (Pembrolizumab) and **Compound A**. T cell proliferation assay was conducted using PBMCs labelled by 1.25 μM of carboxyfluorescein succinimidyl ester (CFSE) from ThermoFisher Scientific d) CellTiter-Glo® Luminescent Cell Viability Assay with HepG2 cells in various concentrations of **Compound A** using CCK-8 assay. (Copied and modified with permission from Barakat et al.¹¹⁵)

When they attempted to verify the MOA of **Compound A**, they found that **Compound A** did not act as an inhibitor through blocking to the PD-1/PD-L1 interface. They hypothesized that **Compound A** triggers the immune response through an unidentified protein target that is yet to be discovered. This may lead to the discovery of a potential new protein target and a previously unidentified immune activation pathway.

Therefore, the important objective of this project is to identify and isolate the unknown protein target of interest that **Compound A** acts on and study the MOA of **Compound A**. In order to do that, we synthesized a series of molecules that maintain structural similarity with the lead **Compound A** to serve as probe molecules that can help identify the unknown protein target. These probe molecules were designed based

on well-developed methods in the field of protein identification, including the biotin-tagged approach, the photoaffinity labelling, and the trifunctional approach.

1.5 Protein Identification

Protein identification remains an important area of research.^{119–126} The discovery of clinically significant targets helps understand the etiology of diseases and assists the development of new drug candidates. High throughput screening (HTS) is a well-established procedure and has been used widely in both industry and academia as a starting point for drug discovery.^{127–130} In the HTS approach, a library of small molecules is screened against a target protein to identify the best lead. Although target-based screening is powerful and cost-effective, it does not reflect the integrity and complexity of the biological system.

In contrast to target-based screening assays, scientists also turned to cell- or organism-based phenotype assays due to their ability to preserve the protein function and the integrity of cellular compartments.¹²⁵ Phenotypic screening aims to find out a protein target that alternates cellular functions or signalling pathways using a small molecule. Because there is no presumed target in this approach, a phenotype-based assay allows the discovery of initially unidentified or unknown targets that cause significant biological responses. The cost of using a phenotype-based assay is that target validation is required to identify the exact target and its mode of action, which is termed “target deconvolution”.¹³¹

Many techniques and methods have been developed for target deconvolution. Using small molecules is particularly attractive in this due to the ease in changing their chemical structure to systematically probe the biological spaces.¹³² There are various ways to identify the protein target using small molecules, some of which include the classic affinity-based approaches, phage and mRNA display technology, in silico target prediction, and a yeast-based approach.^{119,120} Herein, we will be focusing on the affinity-based approaches, which are used to label and isolate a protein target directly, as they set the foundation of this project.

The affinity-based approach remains the most widely used and direct method to identify the protein target of a small molecule of interest.^{126,133–135} Classic affinity-

based approaches include on-bead affinity matrix approach, biotin-tagged approach and trifunctional approach. Affinity purification typically works by chemically modifying the ligand with an affinity moiety, such as a biotin tag, or by directly conjugating to a resin like agarose beads. After incubation with live cells or cell extracts, followed by extensive washing and target elution, the isolated protein(s) are analyzed by sodium dodecyl sulfate–polyacrylamide gel electrophoresis (SDS-PAGE) and identified by mass spectroscopy (MS) or peptide sequencing.^{119,121–123,125}

The core of the affinity-based approach is the design of the small molecule probe. Typical affinity probes are composed of three parts: an affinity warhead (lead compound), a linker or a linker conjugated to a functional handle, and a matrix responsible for protein isolation. In order to purify the protein, the compound has to be immobilized directly onto the agarose beads or functionalized with a biotin tag through a linker. Polymethylene and polyethylene glycol (PEG) are popular options for the linker; the latter is preferred for its ability to increase hydrophilicity and decrease non-specific binding in biological settings.^{119,122,133}

The conventional biotin-tagged approach is when a biotin tag is attached directly to the affinity ligand for a pull-down assay. However, the increase in the size of the probe can potentially lead to loss in activity and binding affinity. This problem can be overcome by the application of photoaffinity labelling (PAL) technique and the incorporation of a bio-orthogonal functional group. The PAL technique utilizes a photo-crosslinker to label the interacting protein covalently. Photo-crosslinkers, sometimes called photoreactive groups, are functional groups sensitive to UV light and can form a covalent bond with the protein after irradiation.^{136–138} Installation of a bio-orthogonal tag, such as an alkyne or azide, can provide a point of structural derivatization via Cu(I)-catalyzed azide–alkyne cycloaddition (CuAAC).^{139–141} Combination of both reactions later emerged as the trifunctional approach and has become increasingly important in the field of drug discovery and development (Figure 1.12).^{142,143} Designing a multifunctional molecular probe based on the trifunctional approach potentially could minimize structural modification and maintain the efficiency of protein labelling.^{144,145}

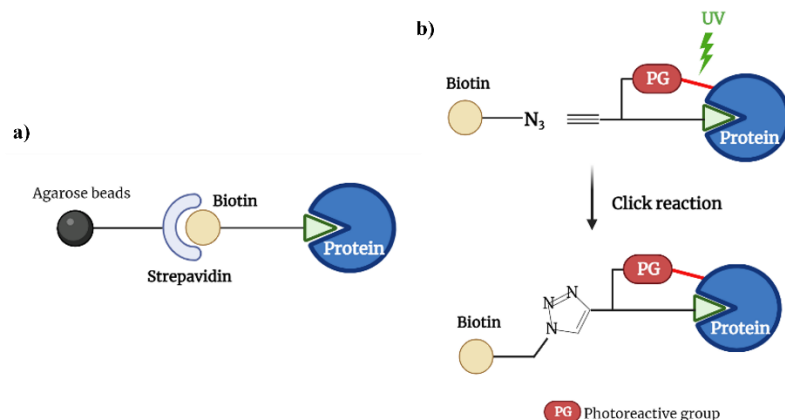


Figure 1.12. The biotin-tagged approach and the trifunctional approach.

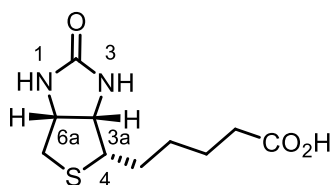
Although the affinity-based approach has been a useful technique, there are intrinsic drawbacks that need to be considered. First of all, the derivatization of the lead compound can be sensitive to the purification process. As the approach relies heavily on the activity of the compound toward the target, a slight modification on the molecule can lead to a drastic change in its biological activity and binding affinity. To overcome this problem, a structure–activity relationship (SAR) needs to be established prior to the modification of the molecule. Then, a non-essential site can be selected to install any linker or an affinity tag. Selection of small-size tags also can help in minimizing the structural perturbation to retain its activity. Secondly, non-specific binding or binding to multiple cellular components can result in the loss of binding affinity. Appropriate negative controls, for example, using similarly tagged but inactive derivatives, could be included to rule out any non-specific binders. Lastly, sensitivity and scale limitation have to be evaluated carefully. Isolation of an abundant protein with low affinity molecules is possible, but it can be very challenging to identify a low abundance protein if the molecular probe has weak affinity. The importance is to balance between binding affinity and protein abundance. More than one factor can come into play when the isolation of a target protein is not successful, especially when attempting to isolate an unknown protein target.^{122,123,133}

As new reactions and chemical biology methods have been developed to cope with these issues, the affinity-based approaches are becoming more sophisticated to

serve a better tool in protein identification. In this section, two different chemical biology applications (biotin-tagged approach and trifunctional approach) that are commonly used toward protein isolation will be introduced. These two methods form the basis of this project and will be discussed extensively in the following chapters.

1.5.1 Biotin-tagged Approach

Biotin, also known as vitamin B7, is a water-soluble vitamin that belongs to the B vitamin family (Figure 1.13).¹⁴⁶ It is a heterocyclic compound composed of fused ureido and tetrahydrothiophene rings with a C5 carboxylic acid side chain on the tetrahydrothiophene ring. The role of biotin in biology involves the digestion of carbohydrates, biotinylation/debiotinylation of histone, fatty acid synthesis, and gluconeogenesis.¹⁴⁶ Biotin binds to the protein streptavidin with a dissociation constant (K_d) of 10^{-15} M, which is considered one of the strongest known ligand–protein interactions.^{147,148} The strong binding has been applied in target validation, for example, in affinity-based approach.¹⁴⁹



(+)-Biotin

Figure 1.13. Structure of biotin.

The biotin-tagged approach is one of the most direct ways to accomplish protein purification. In this method, the ligand is modified structurally so that it is connected directly to a biotin tag.^{150,151} The synthesized molecular probe is treated to the cells over a period of time; then, they are lysed and washed before the targets are extracted (Figure 1.14). The target(s) that bind to the biotinylated ligand are subsequently purified via streptavidin-biotin interaction, which usually is done through an affinity column or streptavidin beads. Then, the isolated proteins are cleaved off from the matrix to be analyzed by SDS-PAGE and mass spectroscopy.

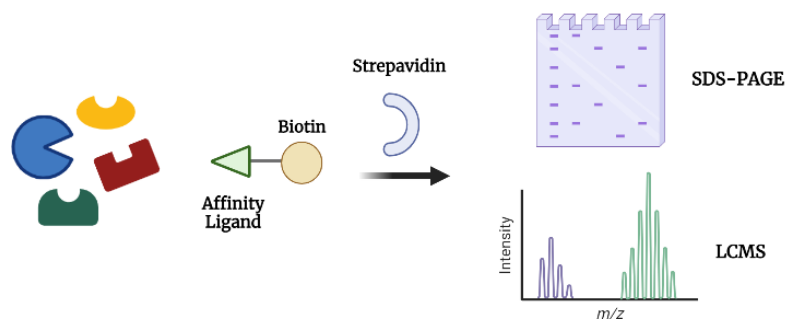


Figure 1.14. Biotin-tagged approach workflow.

One successful example of using the biotin-approach is the identification of NME2 as the target of stauprimide.¹⁵² In a high-content screening, stauprimide was found to inhibit NME2 nuclear localization, which in turn suppresses c-Myc expression. The decrease of c-Myc expression is able to induce the differentiation of mouse embryonic stem cells (ESCs). In this study, stauprimide was derivatized and conjugated to a biotin tag through a PEG linkage (Figure 1.15). The biotinylated stauprimide was treated to the mouse ESCs for 3 h, the cells were lysed, and the compound-target(s) complexes were isolated, using streptavidin immobilized agarose beads. The purified protein was analyzed by SDS-PAGE, and its identity was confirmed by mass spectroscopy as being NME2. A subsequent knockdown experiment also suggested that NME2 is the acting target of the small molecule stauprimide.

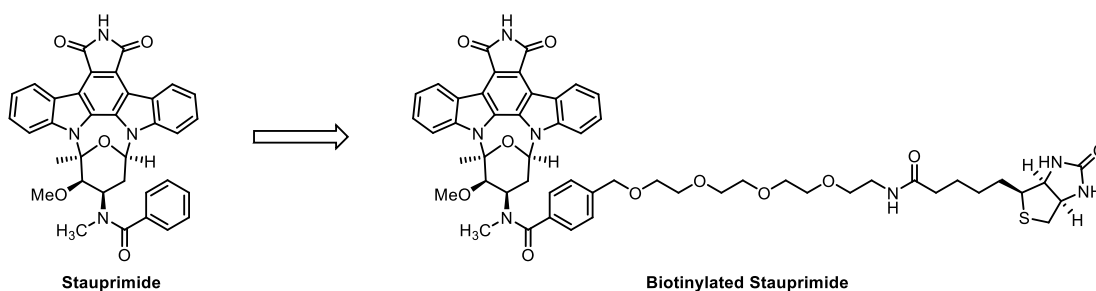


Figure 1.15. Molecular design of biotinylated stauprimide.

Due to the intrinsic property of biotin, off-target effect and non-specific binding is possible when a biotin tag is presented on the molecule. To overcome this issue, a SAR study or assessment of binding affinity can be carried out prior to the

actual assay. Another solution to circumvent this issue is by the installation of biotin using the trifunctional approach after the compound is bound to the protein counterpart.

1.5.2 Trifunctional Approach

The trifunctional approach is becoming a fruitful tool to study protein–ligand interactions and for target deconvolution.¹⁵³ This approach utilizes a small molecular probe composed of three parts: the affinity warhead, a photoreactive group, and a bio-orthogonal functional group. While the biotin-based affinity approach relies mostly on non-covalent interaction, PAL enables irreversible interaction with the target protein. Incorporation of photoreactive groups in the molecule makes PAL possible, otherwise, only non-covalent interaction would exist between the protein–ligand complex.^{154–157} Photoreactive groups are functional groups that generate highly reactive species, such as carbenes or radicals upon irradiation of UV light. The radical and carbene intermediates can react rapidly with a nearby molecule, presumably the protein target. Potentially, this could allow the protein–ligand complex to survive under harsh washing and elution conditions, thus increasing the chance of isolation.

The value of the trifunctional approach has evolved by merging PAL with bio-orthogonal reactions.^{158–162} Although PAL provides a covalent interaction between the ligand and the target protein, incorporation of a bio-orthogonal handle is still the key to the attachment of the isolation/visualization components. The bio-orthogonal tag can be an alkyne or an azide, and the reporter tag can be a biotin or a fluorescent dye.^{163–165} There are two reacting partners in the trifunctional approach: an affinity ligand–photo-crosslinker–alkyne and a reporter–azide counterpart. The bio-orthogonal functional groups, the alkynes or the azides, are exchangeable. During the process of the trifunctional approach, the ligand–photo-crosslinker–alkyne first enters the cell and interacts with its target, then a UV irradiation of appropriate wavelength is applied to capture the protein. The cells are lysed, and a click reaction is performed by the addition of a reporter–azide partner, a copper catalyst, and a reducing agent (Figure 1.16). PAL and bioconjugation methods will be elaborated with more detail in the following sections.

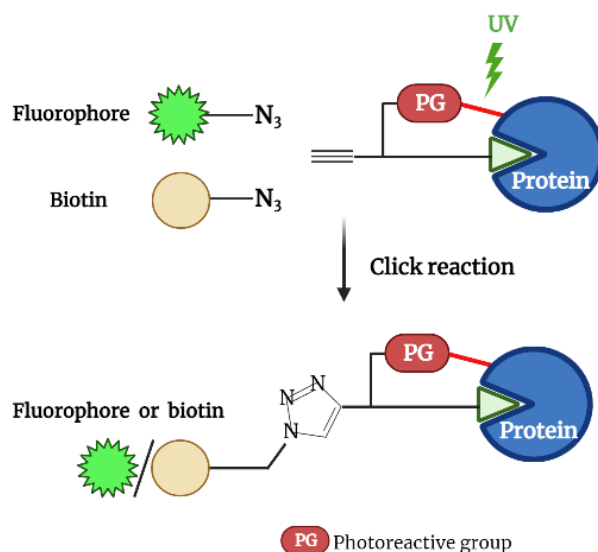
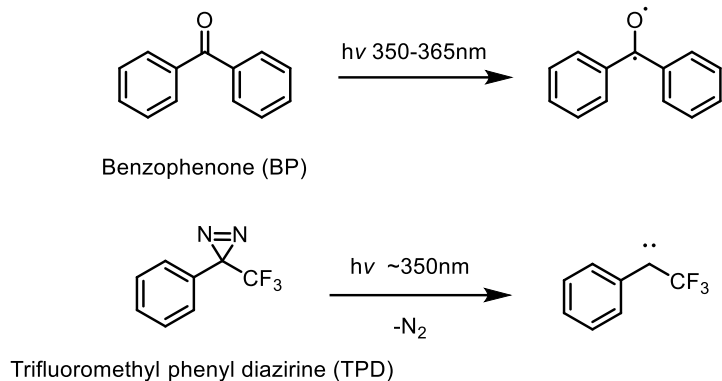


Figure 1.16. Trifunctional approach.

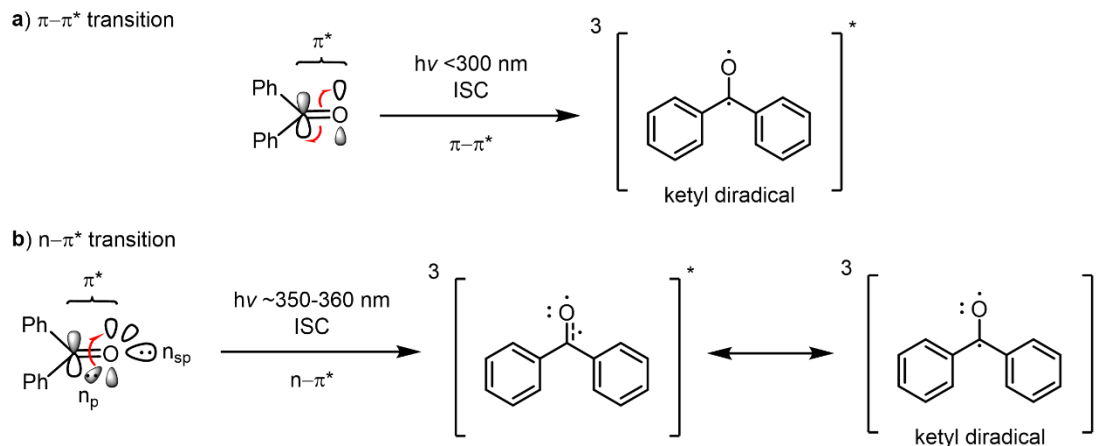
1.5.2.1 Photoaffinity Labelling

With the history of PAL, Frank Westheimer first demonstrated the concept by installing a diazo group onto chymotrypsin to undergo an intramolecular crosslink upon photolysis in 1962.¹⁶⁶ Following that, many photoaffinity probes have been developed and applied as tools to study protein–ligand interactions. In PAL, the pharmacophore–photo-crosslinker preassociates with the protein of interest before the UV irradiation is applied. A reactive intermediate, such as a carbene or a radical, is generated, which reacts to form a covalent linkage when in close proximity to the target protein. The wavelength used to activate photo-crosslinkers should avoid falling to around 200–280 nm, which are the wavelengths absorbed by peptide bonds and aromatic amino acids. Direct or indirect damages can be caused via singlet oxygen to amino acid residues, resulting in the fragmentation and aggregation of the proteins.¹⁶⁷ Ideally, the photo-crosslinkers should remain unreactive in the presence of incident visible light and only be activated when exposed to UV light. Until now, many photo-crosslinkers have been studied, and leading reviews are available for a detailed introduction of different photo-crosslinkers.^{154,157,168,169} Here, only benzophenone (BP) and trifluoromethyl phenyl diazirine (TPD) will be illustrated due to their vital role in this project (Scheme 1.1).¹⁷⁰



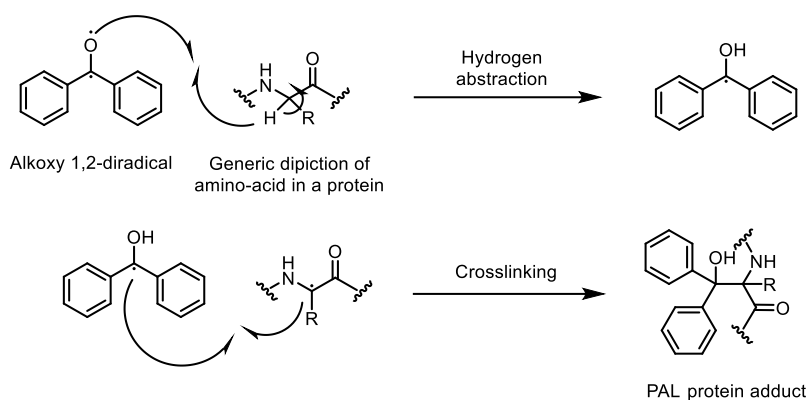
Scheme 1.1. Benzophenone (BP), trifluoromethyl phenyl diazirine (TPD), and the corresponding reactive intermediates.

The application of BPs was among one of the first demonstrations for target deconvolution.¹⁷¹ BPs are carbonyl-containing compounds, which makes them a robust photosensitizer due to efficient intersystem crossing (ISC). The excitation of BPs first reaches the (n, π^*) singlet excited state, which rapidly undergoes an ISC to the energetically close (π, π^*) triplet excited state, followed by a fast decay to the closest lower (n, π^*) triplet state. There are two transitions for the BPs: a high energy $\pi-\pi^*$ and a low energy $n-\pi^*$ transition (Scheme 1.2). The high energy $\pi-\pi^*$ excitation involves the breakage of the carbonyl π bond to form the diradical intermediates. This generation pathway requires irradiation with a shorter wavelength (<300 nm), which is more likely to cause damage to biological components. Another $n-\pi^*$ transition happens at a longer wavelength (around 350–360 nm), which is more compatible with the biological assays and living systems. This pathway promotes the non-bonding p-orbital electrons on the carbonyl oxygen to the orthogonal π^* orbital.^{170,172} Although the required irradiation poses less harm to proteins, the $n-\pi^*$ absorption is weaker than the $\pi-\pi^*$ excitation, indicated by the low molar absorptivity coefficient ($\epsilon_{\max} < 300$).¹⁷³



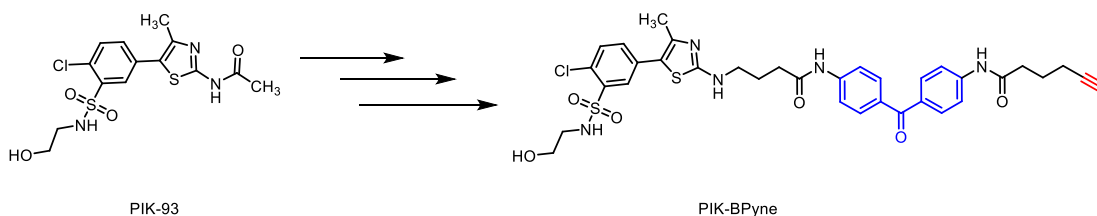
Scheme 1.2. Excitation pathways of BP.

When the alkoxy diradical species is generated after light exposure, the oxygen radical abstracts a hydrogen from the α -carbon of the nearby amino acids, or from a side-chain moiety. The resulting radical pair, consisting of the BP-centred radical and the protein radical, then collapses to form a covalent bond (Scheme 1.3).^{156,170} The advantages of using BPs in PAL includes the following: 1) benign photo-conditions, 2) stable in various solvents and reaction conditions, and 3) the BP building blocks are readily available from synthetic routes or commercially available sources. However, there are still some intrinsic downsides of BPs. Firstly, a long irradiation time usually is required due to the low quantum yield; this also gives rise to the increased possibility of non-specific binding with other proteins. When compared to carbenes, the BP excited state is a less reactive species, therefore is less likely to abstract a hydrogen. Secondly, the relatively large size of BPs can render the loss of bioactivity and binding affinity toward the target protein. During the photoactivation of BP, a possible side reaction may occur through the recombination of two molecules of oxyradical to form benzopinacol.



Scheme 1.3. Photoactivation mechanism of BP.

One successful example of applying BP in the trifunctional approach to study the protein–ligand interaction was demonstrated by Sherratt and co-workers.¹⁷⁴ They proposed an affinity probe, PIK-BPyne, to investigate the role of phosphatidylinositol kinases (PIKs) in live cells. The design and synthesis of PIL-BPyne was based on the structure of a reversible inhibitor, PIK-93 (Scheme 1.4). The presence of BP in the probe permitted the labelling of PIK-93-insensitive PI4K, which showed the characteristic nature to capture nearby protein covalently.

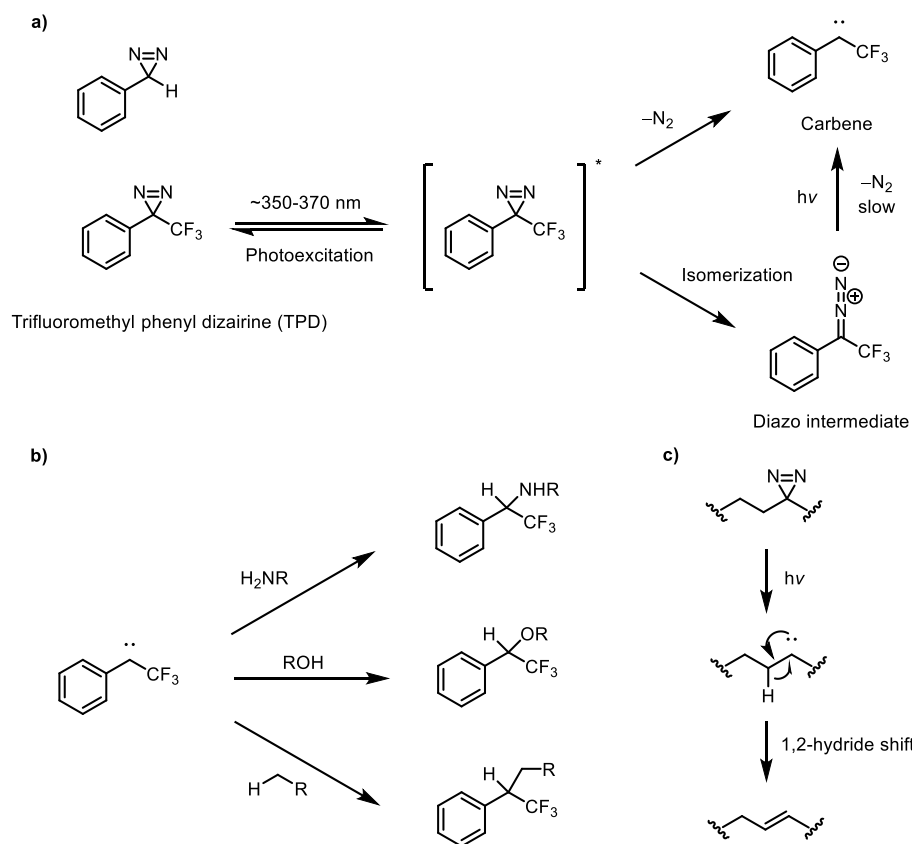


Scheme 1.4. Structural design of PIK-BPyne.

Like BPs, diazirines also can be activated with a biologically compatible UV light, typically with a wavelength around a 350–370 nm. The incorporation of diazirines has started to receive more attention because of their small size and capability to form highly reactive singlet carbene.^{154,170,175,176} Upon UV irradiation, carbenes are generated through two different pathways: direct photolysis from diazirine or from diazo compound after isomerization (Scheme 1.5a).¹⁷⁷ The generated carbenes have a very short half-life (in the range of nanoseconds), and insert very readily into neighbouring amino acid side chains. (Scheme 1.5b). The

isomerized diazo compound, a relatively long-lived intermediate, can diffuse out of the binding pocket, increasing the chance of non-specific binding or hydrolysis.

While aliphatic diazirines¹⁷⁸ have the advantage over aromatic diazirines in size, the latter still are favored for their photo-chemical properties. This is because aliphatic diazirines can isomerize to the less reactive diazo intermediates. Also, they have the tendency to undergo an unwanted 1,2-hydride shift to form alkene after photoexcitation, thus diminishing the efficiency of PAL (Scheme 1.5c).^{176,178,179}



Scheme 1.5. a) Photolysis of TPD and possible reactive intermediates. b) Bond insertion by a singlet carbene. c) Formation of alkene from aliphatic diazirine 1,2-hydride shift.

Diazirines were developed first to overcome the chemical instability and low reactivity of azide-derived nitrenes.¹⁸⁰ Smith et al. reported the first use of 3-aryl-3*H*-diazirine in PAL to be labeled in 1973.¹⁸¹ The proposed aryl diazirine underwent photoactivation with UV irradiation at 370 nm, which is characteristic of diazirine compounds. However, they observed the formation of an undesired side

product having similar spectroscopic properties with the azo-compound. It was speculated to be 7*aH*-indazole, likely yielded from the rearrangement of the linear diazo intermediate or directly from the ring expansion of diazirine.^{181,182} Although carbene still can be generated by prolonged irradiation of the diazo compound, the formation of diazo intermediates still hampered the efficacy of PAL by being labile in acidic environments and prone to nucleophilic attack.

Later in 1980, Brunner and colleagues published the synthesis of 3-trifluoromethyl-3-phenyldiazirine to tackle these problems.¹⁸³ The presence of the electron-withdrawing trifluoromethyl ($-\text{CF}_3$) group helps to stabilize the isomerized phenyl diazomethane and suppress the formation of carbocation under photolysis conditions. The nature of a strong C–F bond favors the existence of carbene by resisting the intramolecular rearrangement to give the unfavored trifluorostyrene side product. Overall, the phenyl and $-\text{CF}_3$ groups together improve the ratio of carbene/diazoisomer, giving approximately 30% of conversion to the diazoisomer. TPD demonstrated good stability under various conditions, including mild heat, acidic, basic, and reductive environments.^{170,176,183–185}

There are some points that need to be considered when using diazirines in PAL. The high reactivity of the generated singlet can be a double-edged sword. It can minimize non-specific binding, but at the same time, its high reactivity also makes it easily quenched by other molecules if not properly associated with the target. Also, the synthesis of TPD is more complicated and requires the use of hazardous materials, such as liquid ammonia.^{186–188}

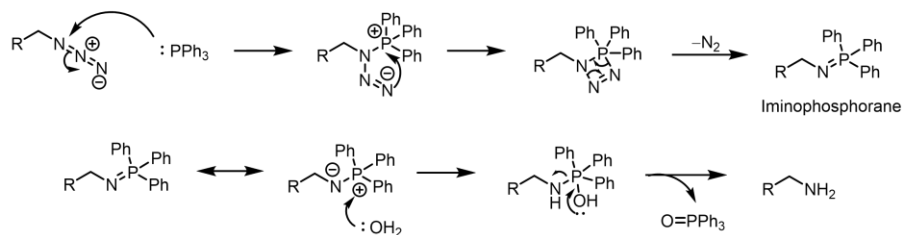
1.5.2.2 Bio-orthogonal Reactions

The added value of the trifunctional approach is realized in conjunction with the recently blooming field of bio-orthogonal chemistry.^{189–191} Bio-orthogonal chemistry refers to chemical reactions that can be performed in living systems and will not interfere with any biological processes. The concept originated from the Staudinger ligation in 1919, later made popular by Sharpless with the copper-catalyzed version in the 1990s then extensively adapted to the biological settings by Bertozzi in the 2000s.¹⁹² Since then, the field of bio-orthogonal chemistry has grown rapidly and has

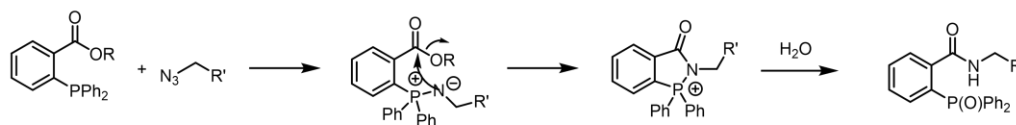
been applied in biological settings.^{158,162,193,194} The following are critical criteria of bio-orthogonal reactions: 1) the exogeneous functional groups should be absent from and inert to the innate biological system, 2) the reaction should be fast, high yielding, and selectively reactive with the introduced reacting partners, 3) the reactions must be able to be carried out under physiological pH and temperature, and 4) the reagents used should be compatible with the biological components. Some of the well-known bio-orthogonal reactions include Staudinger ligation, copper-catalyzed azide-alkyne cycloaddition (CuAAC), and strain-promoted azide-alkyne cycloaddition (SPAAC).

The Staudinger ligation is the earliest bio-orthogonal reaction derived from the Staudinger reaction,¹⁹⁵ which was discovered by Staudinger and Meyer in 1919, when they proposed a reaction between triphenylphosphine and azide to form iminophosphorane (Scheme 1.6).¹⁹⁶ The transformation proceeded swiftly with quantitative yield under mild conditions, setting a good basis to be performed in biological settings. Later, the reaction was modified by Carolyn Bertozzi and referred to as the non-traceless and traceless Staudinger ligation;^{197,198} it has been used extensively to label glycoproteins on cell surface in their works.

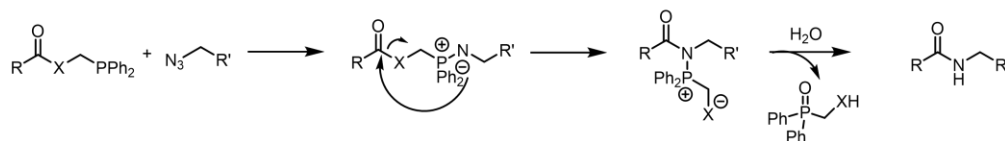
a) The Staudinger reaction



b) The non-traceless Staudinger ligation

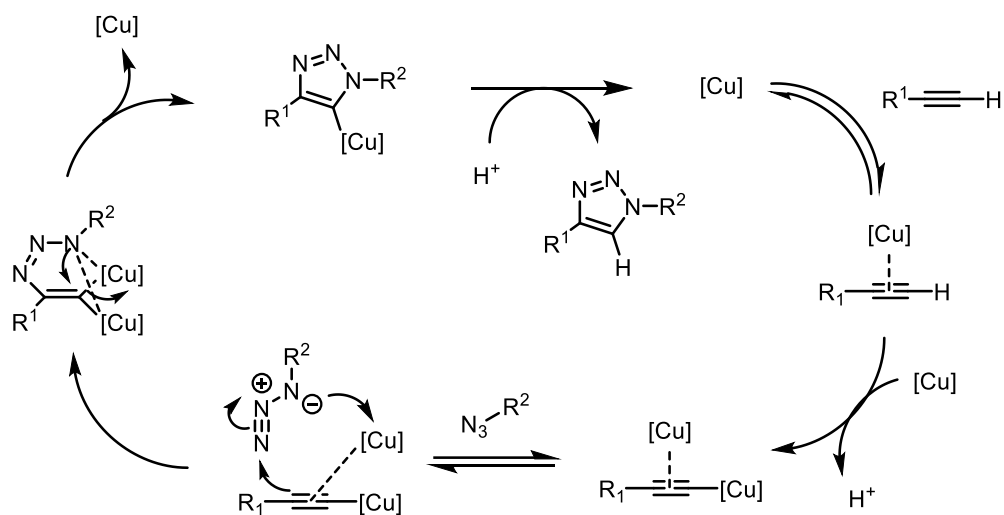


c) The traceless Staudinger ligation



Scheme 1.6. The Staudinger reaction and the Staudinger ligation.

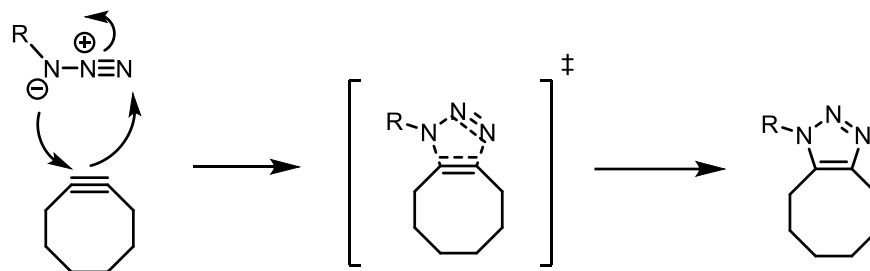
Copper-catalyzed azide–alkyne cycloaddition (CuAAC), later coined the term “click reaction” by Sharpless in 1998, was proposed first by Arthur Michael, while the kinetics and mechanism of 1,3-dipolar cycloaddition were studied carefully by Huisgen in the 1960s.¹⁹⁹ The reaction between alkynes and azides occurs through a 1,3-dipolar cycloaddition to give 1,2,3-triazoles. The reaction rate remained slow until the introduction of copper catalysts. The copper-catalyzed variation proposed by Sharpless²⁰⁰ and Meldal²⁰¹ greatly increases the reaction rate and regioselectivity. The incorporation of copper catalysts increases the reaction rate by around 100 million-fold and enables the exclusive formation of 1,4-substituted triazoles. Later, the mechanism of copper(I)-catalysis of the Huisgen 1,3-dipolar cycloaddition was proposed by Fokin and Sharpless (Scheme 1.7).^{200,202}



Scheme 1.7. Mechanism of Copper-catalyzed azide–alkyne cycloaddition (CuAAC).

The copper catalysts, especially the pre-catalysts Cu(II), however, can cause oxidative damage to live cells. Also, there are many copper-binding proteins and thiol-rich proteins in the system that potentially may deactivate the catalysts.²⁰³ Some systematic reviews of catalyst systems, ligands, and reductants proposed conditions that reduce oxidative damage are available.^{161,162,194,204} In order to solve this problem, strain-promoted azide–alkyne cycloaddition (SPAAC) is also used as an alternative.

SPAAC is a strain-promoted [3+2] cycloaddition proposed by the Bertozzi group to circumvent the use of toxic copper in living system (Scheme 1.8).²⁰⁵ This “copper-free click reaction” was developed based on the initial observation from Wittig and Kerb, who observed that cyclooctyne had remarkable reactivity with phenylazide.^{206,207} The ~18 kcal/mol ring strain was able to overcome the energy barrier of cycloaddition, therefore, avoiding the use of cytotoxic copper catalysts.



Scheme 1.8. Strain-promoted [3+2] cycloaddition.

1.6 Conclusion and Statement of Problem

Cancer is, with no doubt, one of the serious diseases that needs to be approached and tackled. Although surgery, chemotherapy, and radiotherapy provide a good chance for patients to recover from cancers, new therapeutics with less adverse effects, low cost, and good oral availability are still in urgent need.

In a systematic evaluation of small molecule immune checkpoint inhibitors, Barakat and co-workers found a small molecule (**Compound A**) able to promote immune response by promoting the proliferation of T cells and secretion of cytokine IL-2.¹¹⁵ During the target validation of **Compound A**, they found that **Compound A** did not act on the PD-1/PD-L1 immune checkpoint pathway but a currently unidentified protein target. The isolation and identification of the unknown protein target are the main objectives of this project. In this project, two main approaches were carried out through the biotin and the trifunctional modalities to find the protein of interest. The synthesized molecular probes first were evaluated for their ability to increase the production of IL-2 before the affinity pull-down assays were performed. Any cell-based assay performed in this project was carried out by our collaborator, Yasser Tabana, from the Barakat group at the University of Alberta. The

interdisciplinary collaboration between organic chemistry and chemical biology interface toward protein identification is the core value of this project.

In Chapter 2, we will discuss the use of **Compound A** as a reference compound for the structural modification and design for the probes. We considered several different possibilities and designed a biotin-tagged molecular probe. Later, the structure was optimized, and BP was incorporated according to the bioactivity of biotinylated probe molecule. The photoaffinity probe molecules were synthesized as for a proof-of-concept experiment to label a model protein. Results of the labelling experiments provided us insight for the design of the trifunctional probe molecules.

In Chapter 3, the synthesis of two different trifunctional probe molecules is described. Two different trifunctional probe molecules were proposed, with either BP or TPD embedded in the affinity ligand. The biological results of these probe molecules from the immunological assays were performed and served as an important guideline along the way. Moreover, the synthesis of the fluorescent probe molecules and the utilization of the trifunctional probes are described. After the trifunctional probe molecules were synthesized, another labelling experiment was conducted to evaluate the efficiency of the PAL reaction. Furthermore, a biotin tag was attached onto the trifunctional probe molecule via a click reaction prior to being administrated to the cells; this can simplify the biological workflow and reduce possible complications. Aside from the affinity pull-down of the protein of interest, we also were keen to know where the target protein distributes in the cells. Fluorescent compounds are good tools to probe the mechanism of the ligand and monitor the localization of the interacting protein. Therefore, the synthesis of fluorescent compounds and related microscopy experiments will be described herein.

In Chapter 4, another project aiming a different target with novel small molecules will be illustrated. A library of selective androgen receptor modulators (SARMs) was prepared through a robust synthetic route. SARMs are a class of performance enhancing drugs (PEDs) that along with steroids have benefited from their desired anabolic effects over the detrimental androgenic effects. The establishment of a broad structural database helps build a machine-learning algorithm

to detect existing PEDs in clinical samples by of gas chromatography–mass spectroscopy (GC-MS) analysis. This work will be done in collaboration with the Harynuk group in the Department of Chemistry. SARMs also possess potential clinical applications, like treating muscle wasting, osteoporosis, and diseases of the immobilized patients and the elderly; we will be screening the biological activity of these compounds in collaborations with Dr. Vickie Baracos.

Chapter 5 will provide a general conclusion for both projects on the development of small molecular immunomodulators and the derivatization of SARMs. Also, this chapter will suggest possible future directions for the identification of the immunological target.

1.7 References

- (1) World Health Organization: Regional Office for Europe. *World Cancer Report: Cancer Research for Cancer Development.*; IARC, 2020.
- (2) Sung, H.; Ferlay, J.; Siegel, R. L.; Laversanne, M.; Soerjomataram, I.; Jemal, A.; Bray, F. Global Cancer Statistics 2020: GLOBOCAN Estimates of Incidence and Mortality Worldwide for 36 Cancers in 185 Countries. *CA Cancer J Clin* **2021**, *71* (3), 209–249. <https://doi.org/10.3322/caac.21660>.
- (3) Schreiber, R. D.; Old, L. J.; Smyth, M. J. *Cancer Immunoediting: Integrating Immunity's Roles in Cancer Suppression and Promotion*; 2015. <http://science.sciencemag.org/>.
- (4) Dunn, G. P.; Bruce, A. T.; Ikeda, H.; Old, L. J.; Schreiber, R. D. Cancer Immunoediting: From Immuno-Surveillance to Tumor Escape. *Nat. Immunol.* **2002**, *3*, 991–998.
- (5) Janssen, L. M. E.; Ramsay, E. E.; Logsdon, C. D.; Overwijk, W. W. The Immune System in Cancer Metastasis: Friend or Foe? *J. Immunother. Cancer.* **2017**, *5* (1), 79. <https://doi.org/10.1186/s40425-017-0283-9>.
- (6) Bhatia, A.; Kumar, Y. Cellular and Molecular Mechanisms in Cancer Immune Escape: A Comprehensive Review. *Expert Review of Clinical Immunology*. January 2014, pp 41–62. <https://doi.org/10.1586/1744666X.2014.865519>.
- (7) American Cancer Society. *Cancer Treatment & Survivorship Facts & Figures 2019-2021*; 2019.
- (8) Schaeue, D.; McBride, W. H. Opportunities and Challenges of Radiotherapy for Treating Cancer. *Nat. Rev. Clin. Oncol.* **2015**, *12*, 527–540. <https://doi.org/10.1038/nrclinonc.2015.120>.
- (9) Huang, C. Y.; Ju, D. T.; Chang, C. F.; Muralidhar Reddy, P.; Velmurugan, B. K. A Review on the Effects of Current Chemotherapy Drugs and Natural Agents in Treating Non-Small Cell Lung Cancer. *Biomedicine* **2017**, *7* (4), 12–23. <https://doi.org/10.1051/bmdcn/2017070423>.
- (10) Malhotra, V.; Perry, M. C. Classical Chemotherapy: Mechanisms, Toxicities and the Therapeutic Window. *Cancer Biol. Ther.* **2003**, *2*, 1–3. <https://doi.org/10.4161/cbt.199>.

- (11) Makin, G.; Hickman, J. A. Apoptosis and Cancer Chemotherapy. *Cell Tissue Res.* **2000**, *301* (1), 143–152. <https://doi.org/10.1007/s004419900160>.
- (12) Dasari, S.; Bernard Tchounwou, P. Cisplatin in Cancer Therapy: Molecular Mechanisms of Action. *Eur. J. Pharmacol.* **2014**, *740*, 364–378. <https://doi.org/10.1016/j.ejphar.2014.07.025>.
- (13) Darvin, P.; Toor, S. M.; Sasidharan Nair, V.; Elkord, E. Immune Checkpoint Inhibitors: Recent Progress and Potential Biomarkers. *Exp. Mol. Med.* **2018**, *50* (12). <https://doi.org/10.1038/s12276-018-0191-1>.
- (14) Webster, R. M. The Immune Checkpoint Inhibitors: Where Are We Now? *Nat. Rev. Drug Discov.* **2014**, *13* (12), 883–884. <https://doi.org/10.1038/nrd4476>.
- (15) Hargadon, K. M.; Johnson, C. E.; Williams, C. J. Immune Checkpoint Blockade Therapy for Cancer: An Overview of FDA-Approved Immune Checkpoint Inhibitors. *Int. Immunopharmacol.* **2018**, *62*, 29–39. <https://doi.org/10.1016/j.intimp.2018.06.001>.
- (16) Seidel, J. A.; Otsuka, A.; Kabashima, K. Anti-PD-1 and Anti-CTLA-4 Therapies in Cancer: Mechanisms of Action, Efficacy, and Limitations. *Front. Oncol.* **2018**, *8*, 86. <https://doi.org/10.3389/fonc.2018.00086>.
- (17) Waldman, A. D.; Fritz, J. M.; Lenardo, M. J. A Guide to Cancer Immunotherapy: From T Cell Basic Science to Clinical Practice. *Nat. Rev. Immunol.* **2020**, *20* (11), 651–668. <https://doi.org/10.1038/s41577-020-0306-5>.
- (18) Savoia, P.; Astrua, C.; Fava, P. Ipilimumab (Anti-Ctla-4 Mab) in the Treatment of Metastatic Melanoma: Effectiveness and Toxicity Management. *Hum. Vaccines Immunother.* **2016**, *12* (5), 1092–1101. <https://doi.org/10.1080/21645515.2015.1129478>.
- (19) Lipson, E. J.; Drake, C. G. Ipilimumab: An Anti-CTLA-4 Antibody for Metastatic Melanoma. *Clin. Cancer Res.* **2011**, *17* (22), 6958–6962. <https://doi.org/10.1158/1078-0432.CCR-11-1595>.
- (20) Khoja, L.; Butler, M. O.; Kang, S. P.; Ebbinghaus, S.; Joshua, A. M. Pembrolizumab. *J. Immunother. Cancer.* **2015**, *3* (1), 36. <https://doi.org/10.1186/s40425-015-0078-9>.
- (21) Hegde, P. S.; Chen, D. S. Top 10 Challenges in Cancer Immunotherapy. *Immunity* **2020**, *52* (1), 17–35. <https://doi.org/10.1016/j.immuni.2019.12.011>.
- (22) Vasan, N.; Baselga, J.; Hyman, D. M. A View on Drug Resistance in Cancer. *Nature* **2019**, *575* (7782), 299–309. <https://doi.org/10.1038/s41586-019-1730-1>.
- (23) Holohan, C.; van Schaeybroeck, S.; Longley, D. B.; Johnston, P. G. Cancer Drug Resistance: An Evolving Paradigm. *Nat. Rev. Cancer.* **2013**, *13* (10), 714–726. <https://doi.org/10.1038/nrc3599>.
- (24) Gottesman, M. M. Mechanisms of Cancer Drug Resistance. *Annu. Rev. Med.* **2002**, *53*, 615–627.
- (25) Zugazagoitia, J.; Guedes, C.; Ponce, S.; Ferrer, I.; Molina-Pinelo, S.; Paz-Ares, L. Current Challenges in Cancer Treatment. *Clin. Ther.* **2016**, *38* (7), 1551–1566. <https://doi.org/10.1016/j.clinthera.2016.03.026>.
- (26) Marshall, J. S.; Warrington, R.; Watson, W.; Kim, H. L. An Introduction to Immunology and Immunopathology. *Allergy Asthma Clin. Immunol.* **2018**, *14*, 49. <https://doi.org/10.1186/s13223-018-0278-1>.

- (27) Vesely, M. D.; Kershaw, M. H.; Schreiber, R. D.; Smyth, M. J. Natural Innate and Adaptive Immunity to Cancer. *Annu. Rev. Immunol.* **2011**, *29*, 235–271. <https://doi.org/10.1146/annurev-immunol-031210-101324>.
- (28) Abbott, M.; Ustoyev, Y. Cancer and the Immune System: The History and Background of Immunotherapy. *Semin. Oncol. Nurs.* **2019**, *35* (5), 150923. <https://doi.org/10.1016/j.soncn.2019.08.002>.
- (29) Wolchok, J. D.; Saenger, Y. The Mechanism of Anti-CTLA-4 Activity and the Negative Regulation of T-Cell Activation. *Oncologist* **2008**, *13* (S4), 2–9. <https://doi.org/10.1634/theoncologist.13-s4-2>.
- (30) Meyer, M. A.; Baer, J. M.; Knolhoff, B. L.; Nywening, T. M.; Panni, R. Z.; Su, X.; Weilbaecher, K. N.; Hawkins, W. G.; Ma, C.; Fields, R. C.; Linehan, D. C.; Challen, G. A.; Faccio, R.; Aft, R. L.; Denardo, D. G. Breast and Pancreatic Cancer Interrupt IRF8-Dependent Dendritic Cell Development to Overcome Immune Surveillance. *Nat. Commun.* **2018**, *9*, 1250. <https://doi.org/10.1038/s41467-018-03600-6>.
- (31) Schaller, J.; Agudo, J. Metastatic Colonization: Escaping Immune Surveillance. *Cancers (Basel)* **2020**, *12* (11), 1–15. <https://doi.org/10.3390/cancers12113385>.
- (32) Oh, D. Y.; Fong, L. Cytotoxic CD4+ T Cells in Cancer: Expanding the Immune Effector Toolbox. *Immunity* **2021**, *54* (12), 2701–2711. <https://doi.org/10.1016/j.immuni.2021.11.015>.
- (33) Tay, R. E.; Richardson, E. K.; Toh, H. C. Revisiting the Role of CD4+ T Cells in Cancer Immunotherapy—New Insights into Old Paradigms. *Cancer Gene Ther.* **2021**, *28*, 5–17. <https://doi.org/10.1038/s41417-020-0183-x>.
- (34) Smyth, M. J.; Dunn, G. P.; Schreiber, R. D. Cancer Immunosurveillance and Immunoediting: The Roles of Immunity in Suppressing Tumor Development and Shaping Tumor Immunogenicity. *Adv. Immunol.* **2006**, *90*, 1–50. [https://doi.org/10.1016/S0065-2776\(06\)90001-7](https://doi.org/10.1016/S0065-2776(06)90001-7).
- (35) Alsaab, H. O.; Sau, S.; Alzhrani, R.; Tatiparti, K.; Bhise, K.; Kashaw, S. K.; Iyer, A. K. PD-1 and PD-L1 Checkpoint Signaling Inhibition for Cancer Immunotherapy: Mechanism, Combinations, and Clinical Outcome. *Front. Pharmacol.* **2017**, *8*, 561. <https://doi.org/10.3389/fphar.2017.00561>.
- (36) Han, Y.; Liu, D.; Li, L. PD-1/PD-L1 Pathway: Current Researches in Cancer. *Am J Cancer Res* **2020**, *10* (3), 727–742.
- (37) Pardoll, D. M. The Blockade of Immune Checkpoints in Cancer Immunotherapy. *Nat. Rev. Cancer.* **2012**, *12* (4), 252–264. <https://doi.org/10.1038/nrc3239>.
- (38) Chen, D. S.; Mellman, I. Oncology Meets Immunology: The Cancer-Immunity Cycle. *Immunity* **2013**, *39* (1), 1–10. <https://doi.org/10.1016/j.immuni.2013.07.012>.
- (39) Zou, W.; Chen, L. Inhibitory B7-Family Molecules in the Tumour Microenvironment. *Nat. Rev. Immunol.* **2008**, *8* (6), 467–477. <https://doi.org/10.1038/nri2326>.
- (40) Dong, H.; Strome, S. E.; Salomao, D. R.; Tamura, H.; Hirano, F.; Flies, D. B.; Roche, P. C.; Lu, J.; Zhu, G.; Tamada, K.; Lennon, V. A.; Cells, E.; Chen, L. Tumor-Associated B7-H1 Promotes T-Cell Apoptosis: A Potential Mechanism of Immune Evasion. *Nat. Med.* **2002**, *8* (8), 793–800. <https://doi.org/10.1038/nm730>.
- (41) Egen, J. G.; Kuhns, M. S.; Allison, J. P. CTLA-4: New Insights into Its Biological Function and Use in Tumor Immunotherapy. *Nat. Immunol.* **2002**, *3*, 611–618.

- (42) Zhang, Y.; Zhang, Z. The History and Advances in Cancer Immunotherapy: Understanding the Characteristics of Tumor-Infiltrating Immune Cells and Their Therapeutic Implications. *Cell. Mol. Immunol.* **2020**, *17* (8), 807–821. <https://doi.org/10.1038/s41423-020-0488-6>.
- (43) Dobosz, P.; Dzieciatkowski, T. The Intriguing History of Cancer Immunotherapy. *Front. Immunol.* **2019**, *10*, 2965. <https://doi.org/10.3389/fimmu.2019.02965>.
- (44) Mellman, I.; Coukos, G.; Dranoff, G. Cancer Immunotherapy Comes of Age. *Nature* **2011**, *480* (7378), 480–489. <https://doi.org/10.1038/nature10673>.
- (45) Couzin-Frankel, J. Cancer Immunotherapy. *Science*. 2013, pp 1432–1433. <https://doi.org/10.1126/science.342.6165.1432>.
- (46) Coley, M. D.; William, B. The Treatment Of Malignant Tumors By Repeated Inoculations of Erysipelas. *Am. J. Med. Sci.* **1893**, *105*, 487.
- (47) Esfahani, K.; Roudaia, L.; Buhlaiga, N.; del Rincon, S. v.; Papneja, N.; Miller, W. H. A Review of Cancer Immunotherapy: From the Past, to the Present, to the Future. *Curr. Oncol.* **2020**, *27* (S2), 87–97. <https://doi.org/10.3747/co.27.5223>.
- (48) Miller, J. F. A. P.; Mitchell, G. F.; Weiss, N. S. Cellular Basis of the Immunological Defects in Thymectomized Mice. *Nature* **1967**, *214* (5092), 992–997. <https://doi.org/10.1038/214992a0>.
- (49) Steinman, R. M.; Cohn, Z. A. Identification of a Novel Cell Type in Peripheral Lymphoid Organs of Mice. *J. Exp. Med.* **1973**, *137* (5), 1142–1162. <https://doi.org/10.1084/jem.137.5.1142>.
- (50) Kiessling, R.; Klein, E.; Pross, H.; Wigzell, H. “Natural” Killer Cells in the Mouse. II. Cytotoxic Cells with Specificity for Mouse Moloney Leukemia Cells. Characteristics of the Killer Cell. *Eur. J. Immunol.* **1975**, *5* (2), 117–121. <https://doi.org/10.1002/eji.1830050209>.
- (51) Kiessling, R.; Klein, E.; Wigzell, H. “Natural” Killer Cells in the Mouse. I. Cytotoxic Cells with Specificity for Mouse Moloney Leukemia Cells. Specificity and Distribution According to Genotype. *Eur. J. Immunol.* **1975**, *5* (2), 112–117. <https://doi.org/10.1002/eji.1830050208>.
- (52) Stutman, O. Delayed Tumour Appearance and Absence of Regression in Nude Mice Infected with Murine Sarcoma Virus. *Nature* **1975**, *253* (5487), 142–144. <https://doi.org/10.1038/253142a0>.
- (53) Stutman, O. Tumor Development after 3-Methylcholanthrene in Immunologically Deficient Athymic-Nude Mice. *Science* **1974**, *183* (4124), 534–536. <https://doi.org/10.1126/science.183.4124.534>.
- (54) van der Bruggen, P.; Traversari, C.; Chomez, P.; Lurquin, C.; de Plaen, E.; van den Eynde, B.; Knuth, A.; Boon, T. A Gene Encoding an Antigen Recognized by Cytolytic T Lymphocytes on a Human Melanoma. *Science* **1991**, *254* (5038), 1643–1647. <https://doi.org/10.1126/science.1840703>.
- (55) Rosenberg, S. A. IL-2: The First Effective Immunotherapy for Human Cancer. *J. Immunol.* **2014**, *192* (12), 5451–5458. <https://doi.org/10.4049/jimmunol.1490019>.
- (56) Ye, C.; Brand, D.; Zheng, S. G. Targeting IL-2: An Unexpected Effect in Treating Immunological Diseases. *Curr. Signal Transduct. Ther.* **2018**, *3* (1), 2. <https://doi.org/10.1038/s41392-017-0002-5>.

- (57) Jiang, T.; Zhou, C.; Ren, S. Role of IL-2 in Cancer Immunotherapy. *Oncoimmunology* **2016**, *5* (6), e1163462. <https://doi.org/10.1080/2162402X.2016.1163462>.
- (58) Brunet, J.-F.; Denizot, F.; Luciani, M.-F.; Roux-Dosseto, M.; Suzan, M.; Mattei, M.-G.; Golstein, P. A New Member of the Immunoglobulin Superfamily—CTLA-4. *Nature* **1987**, *328* (6127), 267–270. <https://doi.org/10.1038/328267a0>.
- (59) Krummel, M. F.; Allison, J. P. CD28 and CTLA-4 Have Opposing Effects on the Response of T Cells to Stimulation. *J. Exp. Med.* **1995**, *182* (2), 459–465. <https://doi.org/10.1084/jem.182.2.459>.
- (60) Leach, D. R.; Krummel, M. F.; Allison, J. P. Enhancement of Antitumor Immunity by CTLA-4 Blockade. *Science* **1996**, *271* (5256), 1734–1736. <https://doi.org/10.1126/science.271.5256.1734>.
- (61) Ishida, Y.; Agata, Y.; Shibahara, K.; Honjo, T. Induced Expression of PD-1, a Novel Member of the Immunoglobulin Gene Superfamily, upon Programmed Cell Death. *EMBO J.* **1992**, *11* (11), 3887–3895. <https://doi.org/10.1002/j.1460-2075.1992.tb05481.x>.
- (62) Nishimura, H.; Okazaki, T.; Tanaka, Y.; Nakatani, K.; Hara, M.; Matsumori, A.; Sasayama, S.; Mizoguchi, A.; Hiai, H.; Minato, N.; Honjo, T. Autoimmune Dilated Cardiomyopathy in PD-1 Receptor-Deficient Mice. *Science* **2001**, *291* (5502), 319–322. <https://doi.org/10.1126/science.291.5502.319>.
- (63) Agata, Y.; Kawasaki, A.; Nishimura, H.; Ishida, Y.; Tsubat, T.; Yagita, H.; Honjo, T. Expression of the PD-1 Antigen on the Surface of Stimulated Mouse T and B Lymphocytes. *Int. Immunopharmacol.* **1996**, *8* (5), 765–772. <https://doi.org/10.1093/intimm/8.5.765>.
- (64) Ishida, Y. PD-1: Its Discovery, Involvement in Cancer Immunotherapy, and Beyond. *Cells* **2020**, *9* (6). <https://doi.org/10.3390/cells9061376>.
- (65) Iwai, Y.; Ishida, M.; Tanaka, Y.; Okazaki, T.; Honjo, T.; Minato, N. Involvement of PD-L1 on Tumor Cells in the Escape from Host Immune System and Tumor Immunotherapy by PD-L1 Blockade. *Proc. Natl. Acad. Sci.* **2002**, *99* (19), 12293–12297. <https://doi.org/10.1073/pnas.192461099>.
- (66) Savoia, P.; Astrua, C.; Fava, P. Ipilimumab (Anti-Ctla-4 Mab) in the Treatment of Metastatic Melanoma: Effectiveness and Toxicity Management. *Hum. Vaccines Immunother.* **2016**, *12* (5), 1092–1101. <https://doi.org/10.1080/21645515.2015.1129478>.
- (67) *The Nobel Prize in Physiology or Medicine 2018*. <https://www.nobelprize.org/prizes/medicine/2018/press-release/> (accessed 2022-05-12).
- (68) Smyth, M. J.; Teng, M. W. 2018 Nobel Prize in Physiology or Medicine. *Clin Transl Immunology* **2018**, *7* (10), e1041. <https://doi.org/10.1002/cti2.1041>.
- (69) Darnell, E. P.; Mooradian, M. J.; Baruch, E. N.; Yilmaz, M.; Reynolds, K. L. Immune-Related Adverse Events (IrAEs): Diagnosis, Management, and Clinical Pearls. *Curr. Oncol. Rep.* **2020**, *22* (4), 39. <https://doi.org/10.1007/s11912-020-0897-9>.
- (70) Conroy, M.; Naidoo, J. Immune-Related Adverse Events and the Balancing Act of Immunotherapy. *Nat. Commun.* **2022**, *13* (1), 392. <https://doi.org/10.1038/s41467-022-27960-2>.
- (71) Spain, L.; Diem, S.; Larkin, J. Management of Toxicities of Immune Checkpoint Inhibitors. *Cancer Treat. Rev.* **2016**, *44*, 51–60. <https://doi.org/10.1016/j.ctrv.2016.02.001>.

- (72) Wang, D. Y.; Salem, J. E.; Cohen, J. v.; Chandra, S.; Menzer, C.; Ye, F.; Zhao, S.; Das, S.; Beckermann, K. E.; Ha, L.; Rathmell, W. K.; Ancell, K. K.; Balko, J. M.; Bowman, C.; Davis, E. J.; Chism, D. D.; Horn, L.; Long, G. v.; Carlino, M. S.; Lebrun-Vignes, B.; Eroglu, Z.; Hassel, J. C.; Menzies, A. M.; Sosman, J. A.; Sullivan, R. J.; Moslehi, J. J.; Johnson, D. B. Fatal Toxic Effects Associated With Immune Checkpoint Inhibitors: A Systematic Review and Meta-Analysis. *JAMA Oncol* **2018**, *4* (12), 1721–1728. <https://doi.org/10.1001/jamaoncol.2018.3923>.
- (73) Spain, L.; Diem, S.; Larkin, J. Management of Toxicities of Immune Checkpoint Inhibitors. *Cancer Treat. Rev.* **2016**, *44*, 51–60. <https://doi.org/10.1016/j.ctrv.2016.02.001>.
- (74) Curry, J. L.; Tetzlaff, M. T.; Nagarajan, P.; Drucker, C.; Diab, A.; Hymes, S. R.; Duvic, M.; Hwu, W.-J.; Wargo, J. A.; Torres-Cabala, C. A.; Rapini, R. P.; Prieto, V. G. Diverse Types of Dermatologic Toxicities from Immune Checkpoint Blockade Therapy. *J. Cutan. Pathol.* **2017**, *44* (2), 158–176. <https://doi.org/10.1111/cup.12858>.
- (75) Ernstoff, M.; Puzanov, I.; Robert, C.; Diab, A.; Hersey, P. *SITC's Guide to Managing Immunotherapy Toxicity*; Demos Medical Publishing, 2019.
- (76) Brahmer, J. R.; Lacchetti, C.; Schneider, B. J.; Atkins, M. B.; Brassil, K. J.; Caterino, J. M.; Chau, I.; Ernstoff, M. S.; Gardner, J. M.; Ginex, P.; Hallmeyer, S.; Holter Chakrabarty, J.; Leigh, N. B.; Mammen, J. S.; McDermott, D. F.; Naing, A.; Nastoupil, L. J.; Phillips, T.; Porter, L. D.; Puzanov, I.; Reichner, C. A.; Santomaso, B. D.; Seigel, C.; Spira, A.; Suarez-Almazor, M. E.; Wang, Y.; Weber, J. S.; Wolchok, J. D.; Thompson, J. A. Management of Immune-Related Adverse Events in Patients Treated With Immune Checkpoint Inhibitor Therapy: American Society of Clinical Oncology Clinical Practice Guideline. *J. Clin. Oncol.* **2018**, *36* (17), 1714–1768. <https://doi.org/10.1200/JCO.2017.77.6385>.
- (77) Haanen, J. B. A. G.; Carbone, F.; Robert, C.; Kerr, K. M.; Peters, S.; Larkin, J.; Jordan, K. Management of Toxicities from Immunotherapy: ESMO Clinical Practice Guidelines for Diagnosis, Treatment and Follow-Up. *Ann. Oncol.* **2017**, *28*, iv119–iv142. <https://doi.org/10.1093/annonc/mdx225>.
- (78) Maker, A. v.; Attia, P.; Rosenberg, S. A. Analysis of the Cellular Mechanism of Antitumor Responses and Autoimmunity in Patients Treated with CTLA-4 Blockade. *J. Immunol.* **2005**, *175* (11), 7746–7754. <https://doi.org/10.4049/jimmunol.175.11.7746>.
- (79) Peggs, K. S.; Quezada, S. A.; Korman, A. J.; Allison, J. P. Principles and Use of Anti-CTLA4 Antibody in Human Cancer Immunotherapy. *Curr. Opin. Immunol.* **2006**, *18* (2), 206–213. <https://doi.org/10.1016/j.coi.2006.01.011>.
- (80) Maker, A. v.; Phan, G. Q.; Attia, P.; Yang, J. C.; Sherry, R. M.; Topalian, S. L.; Kammula, U. S.; Royal, R. E.; Haworth, L. R.; Levy, C.; Kleiner, D.; Mavroukakis, S. A.; Yellin, M.; Rosenberg, S. A. Tumor Regression and Autoimmunity in Patients Treated with Cytotoxic T Lymphocyte-Associated Antigen 4 Blockade and Interleukin 2: A Phase I/II Study. *Ann. Surg. Oncol.* **2005**, *12* (12), 1005–1016. <https://doi.org/10.1245/ASO.2005.03.536>.
- (81) Robert, C.; Thomas, L.; Bondarenko, I.; O'Day, S.; Weber, J.; Garbe, C.; Lebbe, C.; Baurain, J.-F.; Testori, A.; Grob, J.-J.; Davidson, N.; Richards, J.; Maio, M.; Hauschild, A.; Miller, W. H.; Gascon, P.; Lotem, M.; Harmankaya, K.; Ibrahim, R.; Francis, S.; Chen, T.-T.; Humphrey, R.; Hoos, A.; Wolchok, J. D. Ipilimumab plus Dacarbazine for Previously Untreated Metastatic Melanoma. *N. Engl. J. Med.* **2011**, *364* (26), 2517–2526. <https://doi.org/10.1056/NEJMoa1104621>.

- (82) Hersh, E. M.; O'Day, S. J.; Powderly, J.; Khan, K. D.; Pavlick, A. C.; Cranmer, L. D.; Samlowski, W. E.; Nichol, G. M.; Yellin, M. J.; Weber, J. S. A Phase II Multicenter Study of Ipilimumab with or without Dacarbazine in Chemotherapy-Naïve Patients with Advanced Melanoma. *Investig. New Drugs* **2011**, *29* (3), 489–498. <https://doi.org/10.1007/s10637-009-9376-8>.
- (83) Reuben, J. M.; Lee, B. N.; Shen, D. Y.; Gutierrez, C.; Hernandez, I.; Parker, C. A.; Bozon, V. A.; Gomez-Navarro, J.; Lopez-Berestein, G.; Camacho, L. H. Therapy with Human Monoclonal Anti-CTLA-4 Antibody, CP-675,206, Reduces Regulatory T Cells and IL-10 Production in Patients with Advanced Malignant Melanoma (MM). *Journal of Clinical Oncology* **2005**, *23* (16_suppl), 7505–7505. https://doi.org/10.1200/jco.2005.23.16_suppl.7505.
- (84) Yang, J. C.; Beck, K. E.; Blansfield, J. A.; Tran, K. Q.; Lowy, I.; Rosenberg, S. A. Tumor Regression in Patients with Metastatic Renal Cancer Treated with a Monoclonal Antibody to CTLA4 (MDX-010). *J. Clin. Oncol.* **2005**, *23*, 2501. https://doi.org/10.1200/jco.2005.23.16_suppl.2501.
- (85) Bertrand, A.; Kostine, M.; Barnetche, T.; Truchetet, M. E.; Schaeferbeke, T. Immune Related Adverse Events Associated with Anti-CTLA-4 Antibodies: Systematic Review and Meta-Analysis. *BMC Med.* **2015**, *13* (1), 211. <https://doi.org/10.1186/s12916-015-0455-8>.
- (86) Jiang, Y.; Chen, M.; Nie, H.; Yuan, Y. PD-1 and PD-L1 in Cancer Immunotherapy: Clinical Implications and Future Considerations. *Hum. Vaccines Immunother.* **2019**, *15* (5), 1111–1122. <https://doi.org/10.1080/21645515.2019.1571892>.
- (87) Ohaegbulam, K. C.; Assal, A.; Lazar-Molnar, E.; Yao, Y.; Zang, X. Human Cancer Immunotherapy with Antibodies to the PD-1 and PD-L1 Pathway. *Trends. Mol. Med.* **2015**, *21* (1), 24–33. <https://doi.org/10.1016/j.molmed.2014.10.009>.
- (88) World Health Organization (2021). *World Health Organization Model List of Essential Medicines: 22nd List (2021)*; 2021. <https://apps.who.int/iris/handle/10665/345533> (accessed 2022-05-17).
- (89) Hamid, O.; Robert, C.; Daud, A.; Hodi, F. S.; Hwu, W.-J.; Kefford, R.; Wolchok, J. D.; Hersey, P.; Joseph, R. W.; Weber, J. S.; Dronca, R.; Gangadhar, T. C.; Patnaik, A.; Zarour, H.; Joshua, A. M.; Gergich, K.; Elassaiss-Schaap, J.; Algazi, A.; Mateus, C.; Boasberg, P.; Tume, P. C.; Chmielowski, B.; Ebbinghaus, S. W.; Li, X. N.; Kang, S. P.; Ribas, A. Safety and Tumor Responses with Lambrolizumab (Anti-PD-1) in Melanoma. *N. Engl. J. Med.* **2013**, *369* (2), 134–144. <https://doi.org/10.1056/NEJMoa1305133>.
- (90) Robert, C.; Schachter, J.; Long, G. v.; Arance, A.; Grob, J. J.; Mortier, L.; Daud, A.; Carlino, M. S.; McNeil, C.; Lotem, M.; Larkin, J.; Lorigan, P.; Neyns, B.; Blank, C. U.; Hamid, O.; Mateus, C.; Shapira-Frommer, R.; Kosh, M.; Zhou, H.; Ibrahim, N.; Ebbinghaus, S.; Ribas, A. Pembrolizumab versus Ipilimumab in Advanced Melanoma. *N. Engl. J. Med.* **2015**, *372* (26), 2521–2532. <https://doi.org/10.1056/nejmoa1503093>.
- (91) Naidoo, J.; Page, D. B.; Li, B. T.; Connell, L. C.; Schindler, K.; Lacouture, M. E.; Postow, M. A.; Wolchok, J. D. Toxicities of the Anti-PD-1 and Anti-PD-L1 Immune Checkpoint Antibodies. *Ann. Oncol.* **2015**, *26* (12), 2375–2391. <https://doi.org/10.1093/annonc/mdv383>.
- (92) Perez, H. L.; Cardarelli, P. M.; Deshpande, S.; Gangwar, S.; Schroeder, G. M.; Vite, G. D.; Borzilleri, R. M. Antibody–Drug Conjugates: Current Status and Future Directions. *Drug Discov. Today* **2014**, *19* (7), 869–881. <https://doi.org/10.1016/j.drudis.2013.11.004>.

- (93) Guzik, K.; Tomala, M.; Muszak, D.; Konieczny, M.; Hec, A.; Błaszkiwicz, U.; Pustuła, M.; Butera, R.; Dömling, A.; Holak, T. A. Development of the Inhibitors That Target the PD-1/PD-L1 Interaction—a Brief Look at Progress on Small Molecules, Peptides and Macrocycles. *Molecules* **2019**, *24* (11). <https://doi.org/10.3390/molecules24112071>.
- (94) Lin, X.; Lu, X.; Luo, G.; Xiang, H. Progress in PD-1/PD-L1 Pathway Inhibitors: From Biomacromolecules to Small Molecules. *Eur. J. Med. Chem.* **2020**, *186*, 111876. <https://doi.org/10.1016/j.ejmech.2019.111876>.
- (95) Skalniak, L.; Zak, K. M.; Guzik, K.; Magiera, K.; Musielak, B.; Pachota, M.; Szelazek, B.; Kocik, J.; Grudnik, P.; Tomala, M.; Krzanik, S.; Pyrc, K.; Dömling, A.; Dubin, G.; Holak, T. A. Small-Molecule Inhibitors of PD-1/PD-L1 Immune Checkpoint Alleviate the PD-L1-Induced Exhaustion of T-Cells. *Oncotarget* **2017**, *8* (42), 72167–72181.
- (96) Konieczny, M.; Musielak, B.; Kocik, J.; Skalniak, L.; Sala, D.; Czub, M.; Magiera-Mularz, K.; Rodriguez, I.; Myrcha, M.; Stec, M.; Siedlar, M.; Holak, T. A.; Plewka, J. Di-Bromo-Based Small-Molecule Inhibitors of the PD-1/PD-L1 Immune Checkpoint. *J. Med. Chem.* **2020**, *63* (19), 11271–11285. <https://doi.org/10.1021/acs.jmedchem.0c01260>.
- (97) Sasikumar, P. G.; Ramachandra, M. Small-Molecule Immune Checkpoint Inhibitors Targeting PD-1/PD-L1 and Other Emerging Checkpoint Pathways. *BioDrugs* **2018**, *32* (5), 481–497. <https://doi.org/10.1007/s40259-018-0303-4>.
- (98) Li, K.; Tian, H. Development of Small-Molecule Immune Checkpoint Inhibitors of PD-1/PD-L1 as a New Therapeutic Strategy for Tumour Immunotherapy. *J. Drug Target.* **2019**, *27* (3), 244–256. <https://doi.org/10.1080/1061186X.2018.1440400>.
- (99) Wu, Q.; Jiang, L.; Li, S. cheng; He, Q. jun; Yang, B.; Cao, J. Small Molecule Inhibitors Targeting the PD-1/PD-L1 Signaling Pathway. *Acta Pharmacol. Sin.* **2021**, *42* (1), 1–9. <https://doi.org/10.1038/s41401-020-0366-x>.
- (100) Zak, K. M.; Kitel, R.; Przetocka, S.; Golik, P.; Guzik, K.; Musielak, B.; Dömling, A.; Dubin, G.; Holak, T. A. Structure of the Complex of Human Programmed Death 1, PD-1, and Its Ligand PD-L1. *Structure* **2015**, *23* (12), 2341–2348. <https://doi.org/10.1016/j.str.2015.09.010>.
- (101) Sasikumar, P. G. N.; Ramachandra, M.; Vadlamani, S. K.; Vemula, K. R.; Satyam, L. K.; Subbarao, K.; Shrimali, R. K.; Kandepu, S. Immunosuppression Modulating Compounds. WO2011161699A2, 2011.
- (102) Wang, T.; Wu, X.; Guo, C.; Zhang, K.; Xu, J.; Li, Z.; Jiang, S. Development of Inhibitors of the Programmed Cell Death-1/Programmed Cell Death-Ligand 1 Signaling Pathway. *J. Med. Chem.* **2019**, *62* (4), 1715–1730. <https://doi.org/10.1021/acs.jmedchem.8b00990>.
- (103) Miller, M. M.; Mapelli, C.; Allen, M. P.; Bowsher, M. S.; Gillis, E. P.; Langley, D. R.; Mull, E.; Poirier, M. A.; Sanghvi, N.; Sun, L. Q. Macrocyclic Inhibitors of the PD-1/PD-L1 and CD80(B7-1)/PD-L1 Protein/Protein Interactions. WO2016039749, March 17, 2016.
- (104) Miller, M. M.; Mapelli, C.; Allen, M. P.; Bowsher, M. S.; Boy, K. M.; Gillis, E. P.; Langley, D. R.; Mull, E.; Poirier, M. A.; Sanghvi, N. Macrocyclic Inhibitors of the PD-1/PD-L1 and CD80(B7-1)/PD-L1 Protein/Protein Interactions. WO2014151634, September 25, 2014.
- (105) Magiera-Mularz, K.; Skalniak, L.; Zak, K. M.; Musielak, B.; Rudzinska-Szostak, E.; Berlicki, Ł.; Kocik, J.; Grudnik, P.; Sala, D.; Zarganes-Tzitzikas, T.; Shaabani, S.; Dömling, A.; Dubin, G.; Holak, T. A. Bioactive Macrocyclic Inhibitors of the PD-1/PD-L1 Immune Checkpoint. *Angew. Chem. Int. Ed.* **2017**, *56* (44), 13732–13735. <https://doi.org/10.1002/anie.201707707>.

- (106) Sasikumar, P. G.; Sudarshan, N. S.; Adurthi, S.; Ramachandra, R. K.; Samiulla, D. S.; Lakshminarasimhan, A.; Ramanathan, A.; Chandrasekhar, T.; Dhudashiya, A. A.; Talapati, S. R.; Gowda, N.; Palakolanu, S.; Mani, J.; Srinivasrao, B.; Joseph, D.; Kumar, N.; Nair, R.; Atreya, H. S.; Gowda, N.; Ramachandra, M. PD-1 Derived CA-170 Is an Oral Immune Checkpoint Inhibitor That Exhibits Preclinical Anti-Tumor Efficacy. *Commun. Biol.* **2021**, *4* (1), 699. <https://doi.org/10.1038/s42003-021-02191-1>.
- (107) Sasikumar, P. G. N.; Ramachandra, M.; Naremaddepalli, S. S. S. Dual Inhibitors of V-Domain Ig Suppressor of T-Cell Activation (VISTA) and PD-1 Pathways for Treatment of Cancer and Infectious Diseases. WO2018073754A1, 2018.
- (108) Lee, J. J.; Powderly, J. D.; Patel, M. R.; Brody, J.; Hamilton, E. P.; Infante, J. R.; Falchook, G. S.; Wang, H.; Adams, L.; Gong, L.; Ma, A. W.; Wyant, T.; Lazorchak, A.; Agarwal, S.; Tuck, D. P.; Daud, A. Phase 1 Trial of CA-170, a Novel Oral Small Molecule Dual Inhibitor of Immune Checkpoints PD-1 and VISTA, in Patients (Pts) with Advanced Solid Tumor or Lymphomas. *J. Clin. Oncol.* **2017**, *35*, TPS3099. https://doi.org/10.1200/JCO.2017.35.15_suppl.TPS3099.
- (109) Sasikumar, P. N. G.; Ramachandra, M.; Naremaddepalli, S. S. S. 1,3,4-Oxadiazole and 1,3,4-Thiadiazole Derivatives as Immunomodulators. WO2015033301, 2015.
- (110) Sasikumar, P. G. N.; Ramachandra, M.; Naremaddepalli, S. S. S. 1,2,4-Oxadiazole and Thiadiazole Compounds as Immunomodulators. US20180044303, 2018.
- (111) Gillman, K. W.; Goodrich, J.; Boy, K. M.; Zhang, Y.; Mapelli, C.; Poss, M. A.; Sun, L. Q.; Zhao, Q.; Mull, E.; Scola, P. M.; Langley, D. R. Macrocyclic Peptides Useful as Immunomodulators. WO2016077518A1, 2016.
- (112) Chupak, L. S.; Ding, M.; Martin, S. W.; Zheng, X.; Hewawasam, P.; Connolly, T. P.; Xu, N.; Yeung, K. S.; Zhu, J.; Langley, D. R.; Tenney, D. J.; Scola, P. M. Compounds Useful as Immunomodulators. WO2015160641A3, 2015.
- (113) Chupak, L. S.; Zheng, X. Compounds Useful as Immunomodulators. WO2015034820A1, 2015.
- (114) Zak, K. M.; Grudnik, P.; Guzik, K.; Zieba, B. J.; Musielak, B.; Dömling, A.; Dubin, G.; Holak, T. A. Structural Basis for Small Molecule Targeting of the Programmed Death Ligand 1 (PD-L1). *Oncotarget* **2016**, *7* (21), 30323–30335. <https://doi.org/10.18632/oncotarget.8730>.
- (115) Ganesan, A.; Ahmed, M.; Okoye, I.; Arutyunova, E.; Babu, D.; Turnbull, W. L.; Kundu, J. K.; Shields, J.; Agopsowicz, K. C.; Xu, L.; Tabana, Y.; Srivastava, N.; Zhang, G.; Moon, T. C.; Belovodskiy, A.; Hena, M.; Kandadai, A. S.; Hosseini, S. N.; Hitt, M.; Walker, J.; Smylie, M.; West, F. G.; Siraki, A. G.; Lemieux, M. J.; Elahi, S.; Nieman, J. A.; Tyrrell, D. L.; Houghton, M.; Barakat, K. Comprehensive in Vitro Characterization of PD-L1 Small Molecule Inhibitors. *Sci. Rep.* **2019**, *9* (1), 12392. <https://doi.org/10.1038/s41598-019-48826-6>.
- (116) McLeod, J. D.; Walker, L. S.; Patel, Y. I.; Boulougouris, G.; Sansom, D. M. Activation of Human T Cells with Superantigen (Staphylococcal Enterotoxin B) and CD28 Confers Resistance to Apoptosis via CD95. *J. Immun.* **1998**, *160* (5), 2072–2079.
- (117) William T Lee, D. K. J. Staphylococcal Enterotoxin B (SEB) Induces Memory CD4 T Cell Anergy in Vivo and Impairs Recall Immunity to Unrelated Antigens. *J. Clin. Cell. Immunol.* **2015**, *6* (4), 1–8. <https://doi.org/10.4172/2155-9899.1000346>.
- (118) Rödström, K. E. J.; Elbing, K.; Lindkvist-Petersson, K. Structure of the Superantigen Staphylococcal Enterotoxin B in Complex with TCR and Peptide–MHC Demonstrates

- Absence of TCR–Peptide Contacts. *J. Immunol.* **2014**, *193* (4), 1998–2004.
<https://doi.org/10.4049/jimmunol.1401268>.
- (119) Lee, H.; Lee, J. W. Target Identification for Biologically Active Small Molecules Using Chemical Biology Approaches. *Arch. Pharmacol. Res.* **2016**, *39* (9), 1193–1201.
<https://doi.org/10.1007/s12272-016-0791-z>.
- (120) Beckwith, R. E. J.; Jain, R. K. Recent Advances in Small Molecule Target Identification Methods. In *Annual Reports in Medicinal Chemistry*; Academic Press Inc., 2013; Vol. 48, pp 301–315. <https://doi.org/10.1016/B978-0-12-417150-3.00019-3>.
- (121) Lee, J.; Bogyo, M. Target Deconvolution Techniques in Modern Phenotypic Profiling. *Curr. Opin. Chem. Biol.* **2013**, *17* (1), 118–126. <https://doi.org/10.1016/j.cbpa.2012.12.022>.
- (122) Kawatani, M.; Osada, H. Affinity-Based Target Identification for Bioactive Small Molecules. *Medchemcomm* **2014**, *5* (3), 277–287. <https://doi.org/10.1039/c3md00276d>.
- (123) Lomenick, B.; Olsen, R. W.; Huang, J. Identification of Direct Protein Targets of Small Molecules. *ACS Chem. Biol.* **2011**, *6* (1), 34–46. <https://doi.org/10.1021/cb100294v>.
- (124) Stockwell, B. R. Chemical Genetics: Ligand-Based Discovery of Gene Function. *Nat. Rev. Genet.* **2000**, *1* (2), 116–125. <https://doi.org/10.1038/35038557>.
- (125) Kubota, K.; Funabashi, M.; Ogura, Y. Target Deconvolution from Phenotype-Based Drug Discovery by Using Chemical Proteomics Approaches. *Biochim. Biophys. Acta - Proteins Proteom.* **2019**, *1867* (1), 22–27. <https://doi.org/10.1016/j.bbapap.2018.08.002>.
- (126) Burdine, L.; Kodadek, T. Target Identification in Chemical Genetics. *Chem. Biol.* **2004**, *11* (5), 593–597. <https://doi.org/10.1016/j.chembiol.2004.05.001>.
- (127) Hertzberg, R. P.; Pope, A. J. High-Throughput Screening: New Technology for the 21st Century. *Curr. Opin. Chem. Biol.* **2000**, *4* (4), 445–451. [https://doi.org/10.1016/S1367-5931\(00\)00110-1](https://doi.org/10.1016/S1367-5931(00)00110-1).
- (128) Bajorath, J. Integration of Virtual and High-Throughput Screening. *Nat. Rev. Drug Discov.* **2002**, *1* (11), 882–894. <https://doi.org/10.1038/nrd941>.
- (129) Mayr, L. M.; Bojanic, D. Novel Trends in High-Throughput Screening. *Curr. Opin. Pharmacol.* **2009**, *9* (5), 580–588. <https://doi.org/10.1016/j.coph.2009.08.004>.
- (130) Swinney, D. C.; Anthony, J. How Were New Medicines Discovered? *Nat. Rev. Drug Discov.* **2011**, *10* (7), 507–519. <https://doi.org/10.1038/nrd3480>.
- (131) Schenone, M.; Dančik, V.; Wagner, B. K.; Clemons, P. A. Target Identification and Mechanism of Action in Chemical Biology and Drug Discovery. *Nat. Chem. Biol.* **2013**, *9* (4), 232–240. <https://doi.org/10.1038/nchembio.1199>.
- (132) Schreiber, S. L. The Small-Molecule Approach to Biology. *C&EN*. 2003, pp 51–61.
- (133) Sato, S.; Murata, A.; Shirakawa, T.; Uesugi, M. Biochemical Target Isolation for Novices: Affinity-Based Strategies. *Chem. Biol.* **2010**, *17* (6), 616–623.
<https://doi.org/10.1016/j.chembiol.2010.05.015>.
- (134) Leslie, B. J.; Hergenrother, P. J. Identification of the Cellular Targets of Bioactive Small Organic Molecules Using Affinity Reagents. *Chem. Soc. Rev.* **2008**, *37* (7), 1347.
<https://doi.org/10.1039/b702942j>.

- (135) Ziegler, S.; Pries, V.; Hedberg, C.; Waldmann, H. Target Identification for Small Bioactive Molecules: Finding the Needle in the Haystack. *Angew. Chem. Int. Ed.* **2013**, *52* (10), 2744–2792. <https://doi.org/10.1002/anie.201208749>.
- (136) Lapinsky, D. J. Tandem Photoaffinity Labeling-Bioorthogonal Conjugation in Medicinal Chemistry. *Bioorg. Med. Chem.* **2012**, *20* (21), 6237–6247. <https://doi.org/10.1016/j.bmc.2012.09.010>.
- (137) Grant, E. K.; Fallon, D. J.; Hann, M. M.; Fantom, K. G. M.; Quinn, C.; Zappacosta, F.; Annan, R. S.; Chung, C. wa; Bamborough, P.; Dixon, D. P.; Stacey, P.; House, D.; Patel, V. K.; Tomkinson, N. C. O.; Bush, J. T. A Photoaffinity-Based Fragment-Screening Platform for Efficient Identification of Protein Ligands. *Angew. Chem. Int. Ed.* **2020**, *59* (47), 21096–21105. <https://doi.org/10.1002/anie.202008361>.
- (138) Geurink, P. P.; Prely, L. M.; van der Marel, G. A.; Bischoff, R.; Overkleeft, H. S. Photoaffinity Labeling in Activity-Based Protein Profiling. *Top. Curr. Chem.* **2011**, 85–113. https://doi.org/10.1007/128_2011_286.
- (139) Hein, C. D.; Liu, X.-M.; Wang, D. Click Chemistry, A Powerful Tool for Pharmaceutical Sciences. *Pharm Res* **2008**, *25* (10), 2216–2230. <https://doi.org/10.1007/s11095-008-9616-1>.
- (140) Sletten, E. M.; Bertozzi, C. R. Bioorthogonal Chemistry: Fishing for Selectivity in a Sea of Functionality. *Angewandte Chemie International Edition* **2009**, *48* (38), 6974–6998. <https://doi.org/10.1002/anie.200900942>.
- (141) Best, M. D. Click Chemistry and Bioorthogonal Reactions: Unprecedented Selectivity in the Labeling of Biological Molecules. *Biochemistry* **2009**, *48* (28), 6571–6584. <https://doi.org/10.1021/bi9007726>.
- (142) Dormán, G.; Prestwich, G. D. Using Photolabile Ligands in Drug Discovery and Development. *Trends Biotechnol.* **2000**, *18* (2), 64–77. [https://doi.org/10.1016/S0167-7799\(99\)01402-X](https://doi.org/10.1016/S0167-7799(99)01402-X).
- (143) Hatanaka, Y.; Sadakane, Y. Photoaffinity Labeling in Drug Discovery and Developments: Chemical Gateway for Entering Proteomic Frontier. *Curr. Top. Med. Chem.* **2002**, *2*, 271–288.
- (144) Cisar, J. S.; Cravatt, B. F. Fully Functionalized Small-Molecule Probes for Integrated Phenotypic Screening and Target Identification. *J. Am. Chem. Soc.* **2012**, *134* (25), 10385–10388. <https://doi.org/10.1021/ja304213w>.
- (145) Kumar, N. S.; Young, R. N. Design and Synthesis of an All-in-One 3-(1,1-Difluoroprop-2-Ynyl)-3H-Diazirin-3-Yl Functional Group for Photo-Affinity Labeling. *Bioorg. Med. Chem.* **2009**, *17* (15), 5388–5395. <https://doi.org/10.1016/j.bmc.2009.06.048>.
- (146) Zempleni, J.; Wijeratne, S. S. K.; Hassan, Y. I. Biotin. *BioFactors* **2009**, *35* (1), 36–46. <https://doi.org/10.1002/biof.8>.
- (147) Weber, P. C.; Ohlendorf, D. H.; Wendoloski, J. J.; Salemme, F. R. Structural Origins of High-Affinity Biotin Binding to Streptavidin. *Science* **1989**, *243* (4887), 85–88. <https://doi.org/10.1126/science.2911722>.
- (148) Chaiet, L.; Wolf, F. J. The Properties of Streptavidin, a Biotin-Binding Protein Produced by Streptomyces. *Arch. Biochem. Biophys.* **1964**, *106*, 1–5. [https://doi.org/10.1016/0003-9861\(64\)90150-X](https://doi.org/10.1016/0003-9861(64)90150-X).

- (149) Dundas, C. M.; Demonte, D.; Park, S. Streptavidin–Biotin Technology: Improvements and Innovations in Chemical and Biological Applications. *Appl. Microbiol. Biotechnol.* **2013**, *97* (21), 9343–9353. <https://doi.org/10.1007/s00253-013-5232-z>.
- (150) Seki, M. Biological Significance and Development of Practical Synthesis of Biotin. *Med. Res. Rev.* **2006**, *26* (4), 434–482. <https://doi.org/10.1002/med.20058>.
- (151) Trippier, P. C. Synthetic Strategies for the Biotinylation of Bioactive Small Molecules. *ChemMedChem* **2013**, *8* (2), 190–203. <https://doi.org/10.1002/cmdc.201200498>.
- (152) Zhu, S.; Wurdak, H.; Wang, J.; Lyssiotis, C. A.; Peters, E. C.; Cho, C. Y.; Wu, X.; Schultz, P. G. A Small Molecule Primes Embryonic Stem Cells for Differentiation. *Cell Stem Cell* **2009**, *4* (5), 416–426. <https://doi.org/10.1016/j.stem.2009.04.001>.
- (153) Lapinsky, D. J. Tandem Photoaffinity Labeling–Bioorthogonal Conjugation in Medicinal Chemistry. *Bioorg. Med. Chem.* **2012**, *20* (21), 6237–6247. <https://doi.org/10.1016/j.bmc.2012.09.010>.
- (154) Holland, J. P.; Gut, M.; Klingler, S.; Fay, R.; Guillou, A. Photochemical Reactions in the Synthesis of Protein–Drug Conjugates. *Chemistry – A European Journal* **2020**, *26* (1), 33–48. <https://doi.org/10.1002/chem.201904059>.
- (155) Smith, E.; Collins, I. Photoaffinity Labeling in Target- and Binding-Site Identification. *Future Med Chem* **2015**, *7* (2), 159–183. <https://doi.org/10.4155/fmc.14.152>.
- (156) Sumranjit, J.; Chung, S. Recent Advances in Target Characterization and Identification by Photoaffinity Probes. *Molecules* **2013**, *18* (9), 10425–10451. <https://doi.org/10.3390/molecules180910425>.
- (157) Murale, D. P.; Hong, S. C.; Haque, M. M.; Lee, J. S. Photo-Affinity Labeling (PAL) in Chemical Proteomics: A Handy Tool to Investigate Protein-Protein Interactions (PPIs). *Proteome Sci.* **2017**, *15* (1), 14. <https://doi.org/10.1186/s12953-017-0123-3>.
- (158) Kolb, H. C.; Sharpless, K. B. The Growing Impact of Click Chemistry on Drug Discovery. *Drug Discov Today* **2003**, *8* (24), 1128–1137. [https://doi.org/10.1016/S1359-6446\(03\)02933-7](https://doi.org/10.1016/S1359-6446(03)02933-7).
- (159) Presolski, S. I.; Hong, V. P.; Finn, M. G. Copper-Catalyzed Azide–Alkyne Click Chemistry for Bioconjugation. *Curr Protoc Chem Biol* **2011**, *3* (4), 153–162. <https://doi.org/10.1002/9780470559277.ch110148>.
- (160) Sletten, E. M.; Bertozzi, C. R. Bioorthogonal Chemistry: Fishing for Selectivity in a Sea of Functionality. *Angew. Chem. Int. Ed.* **2009**, *48* (38), 6974–6998. <https://doi.org/10.1002/anie.200900942>.
- (161) Hong, V.; Presolski, S. I.; Ma, C.; Finn, M. G. Analysis and Optimization of Copper-Catalyzed Azide-Alkyne Cycloaddition for Bioconjugation. *Angewandte Chemie - International Edition* **2009**, *48* (52), 9879–9883. <https://doi.org/10.1002/anie.200905087>.
- (162) Li, S.; Wang, L.; Yu, F.; Zhu, Z.; Shobaki, D.; Chen, H.; Wang, M.; Wang, J.; Qin, G.; Erasquin, U. J.; Ren, L.; Wang, Y.; Cai, C. Copper-Catalyzed Click Reaction on/in Live Cells. *Chem Sci* **2017**, *8* (3), 2107–2114. <https://doi.org/10.1039/c6sc02297a>.
- (163) Cañeque, T.; Müller, S.; Rodriguez, R. Visualizing Biologically Active Small Molecules in Cells Using Click Chemistry. *Nat. Rev. Chem.* **2018**, *2* (9), 202–215. <https://doi.org/10.1038/s41570-018-0030-x>.

- (164) Ghosh, B.; Jones, L. H. Target Validation Using In-Cell Small Molecule Clickable Imaging Probes. *Medchemcomm* **2014**, *5* (3), 247–254. <https://doi.org/10.1039/c3md00277b>.
- (165) le Droumaguet, C.; Wang, C.; Wang, Q. Fluorogenic Click Reaction. *Chem. Soc. Rev.* **2010**, *39* (4), 1233–1239. <https://doi.org/10.1039/b901975h>.
- (166) Singh, A.; Thronton, E. R.; Westheimer, F. H. The Photolysis of Diazoacetylchymotrypsin. *J. Biol. Chem.* **1962**, *237*, 3006–3008.
- (167) Pattison, D. I.; Rahmanto, A. S.; Davies, M. J. Photo-Oxidation of Proteins. *Photochem. Photobiol. Sci.* **2012**, *11* (1), 38–53. <https://doi.org/10.1039/C1PP05164D>.
- (168) Sakurai, K.; Ozawa, S.; Yamada, R.; Yasui, T.; Mizuno, S. Comparison of the Reactivity of Carbohydrate Photoaffinity Probes with Different Photoreactive Groups. *ChemBioChem* **2014**, *15* (10), 1399–1403. <https://doi.org/10.1002/cbic.201402051>.
- (169) Fleming, S. A. Chemical Reagents in Photoaffinity Labeling. *Tetrahedron* **1995**, *51*, 12419–12520. [https://doi.org/10.1016/0040-4020\(95\)00598-3](https://doi.org/10.1016/0040-4020(95)00598-3).
- (170) Hassan, M. M.; Olaoye, O. O. Recent Advances in Chemical Biology Using Benzophenones and Diazirines as Radical Precursors. *Molecules* **2020**, *25* (10), 2285. <https://doi.org/10.3390/molecules25102285>.
- (171) Galardy, R. E.; Craig, L. C.; Printz, M. P. Benzophenone Triplet: A New Photochemical Probe of Biological Ligand-Receptor Interactions. *Nature New Biol.* **1973**, *242* (117), 127–128. <https://doi.org/10.1038/newbio242127a0>.
- (172) Dormán, G.; Nakamura, H.; Pulsipher, A.; Prestwich, G. D. The Life of Pi Star: Exploring the Exciting and Forbidden Worlds of the Benzophenone Photophore. *Chem. Rev.* **2016**, *116* (24), 15284–15398. <https://doi.org/10.1021/acs.chemrev.6b00342>.
- (173) Prestwich, G. D.; Dormán, G.; Elliott, J. T.; Marecak, D. M.; Chaudhary, A. Benzophenone Photoprobes for Phosphoinositides, Peptides and Drugs. *Photochem. Photobiol.* **1997**, *65* (2), 222–234. <https://doi.org/10.1111/j.1751-1097.1997.tb08548.x>.
- (174) Sherratt, A. R.; Nasheri, N.; McKay, C. S.; O'Hara, S.; Hunt, A.; Ning, Z.; Figeys, D.; Goto, N. K.; Pezacki, J. P. A New Chemical Probe for Phosphatidylinositol Kinase Activity. *ChemBioChem* **2014**, *15* (9), 1253–1256. <https://doi.org/10.1002/cbic.201402155>.
- (175) Hashimoto, M.; Hatanaka, Y. Recent Progress in Diazirine-Based Photoaffinity Labeling. *Eur. J. Org. Chem.* **2008**, *15*, 2513–2523. <https://doi.org/10.1002/ejoc.200701069>.
- (176) Geurink, P. P.; Prely, L. M.; van der Marel, G. A.; Bischoff, R.; Overkleeft, H. S. Photoaffinity Labeling in Activity-Based Protein Profiling. *Top. Curr. Chem.* **2011**, *324*, 85–113. https://doi.org/10.1007/128_2011_286.
- (177) Korneev, S. M. Valence Isomerization between Diazo Compounds and Diazirines. *Eur. J. Org. Chem.* **2011**, *31*, 6153–6175. <https://doi.org/10.1002/ejoc.201100224>.
- (178) Das, J. Aliphatic Diazirines as Photoaffinity Probes for Proteins: Recent Developments. *Chem. Rev.* **2011**, *111* (8), 4405–4417. <https://doi.org/10.1021/cr1002722>.
- (179) Bonneau, R.; Liu, M. T. H.; Kim, K. C.; Goodman, J. L. Rearrangement of Alkylchlorocarbenes: 1,2-H Shift in Free Carbene, Carbene–Olefin Complex, and Excited States of Carbene Precursors. *J. Am. Chem. Soc.* **1996**, *118* (16), 3829–3837. <https://doi.org/10.1021/ja952700n>.

- (180) Bayley, H.; Knowles, J. R. Photogenerated Reagents for Membrane Labeling. 2. Phenylcarbene and Adamantylidene Formed within the Lipid Bilayer. *Biochemistry* **1978**, *17* (12), 2420–2423. <https://doi.org/10.1021/bi00605a026>.
- (181) Smith, R. A. G.; Knowles, J. R. Aryldiazirines. Potential Reagents for Photolabeling of Biological Receptor Sites. *J. Am. Chem. Soc.* **1973**, *95* (15), 5072–5073. <https://doi.org/10.1021/ja00796a062>.
- (182) Smith, R. A. G.; Knowles, J. R. The Preparation and Photolysis of 3-Aryl-3H-Diazirines. *J. Chem. Soc., Perkin trans. II* **1975**, *7*, 686. <https://doi.org/10.1039/p29750000686>.
- (183) Brunner, J.; Serin, H.; Richards, F. M. 3-Trifluoromethyl-3-Phenyldiazirine. A New Carbene Generating Group for Photolabeling Reagents. *J. Biol. Chem.* **1980**, *255* (8), 3313–3318.
- (184) Djordjevic, I.; Wicaksono, G.; Solic, I.; Steele, T. W. J. Diazoalkane Decay Kinetics from UVA-Active Protein Labelling Molecules: Trifluoromethyl Phenyl Diazirines. *Results Chem.* **2020**, *2*, 100066. <https://doi.org/10.1016/j.rechem.2020.100066>.
- (185) Zhang, Y.; Burdzinski, G.; Kubicki, J.; Platz, M. S. Direct Observation of Carbene and Diazo Formation from Aryldiazirines by Ultrafast Infrared Spectroscopy. *J. Am. Chem. Soc.* **2008**, *130* (48), 16134–16135. <https://doi.org/10.1021/ja805922b>.
- (186) Hill, J. R.; Robertson, A. A. B. Fishing for Drug Targets: A Focus on Diazirine Photoaffinity Probe Synthesis. *J. Med. Chem.* **2018**, *61* (16), 6945–6963. <https://doi.org/10.1021/acs.jmedchem.7b01561>.
- (187) Mayer, T.; Maier, M. E. Design and Synthesis of a Tag-Free Chemical Probe for Photoaffinity Labeling. *Eur. J. Org. Chem.* **2007**, No. 28, 4711–4720. <https://doi.org/10.1002/ejoc.200700188>.
- (188) Wixe, T.; Almqvist, F. An Improved Synthesis of 3-[3-(Trifluoromethyl)-3H-1,2-Diazirin-3-Yl]Aniline: A Key Intermediate in the Synthesis of Photoaffinity Probes. *Tetrahedron Lett.* **2017**, *58* (34), 3350–3352. <https://doi.org/10.1016/j.tetlet.2017.07.031>.
- (189) Scinto, S. L.; Bilodeau, D. A.; Hincapie, R.; Lee, W.; Nguyen, S. S.; Xu, M.; am Ende, C. W.; Finn, M. G.; Lang, K.; Lin, Q.; Pezacki, J. P.; Prescher, J. A.; Robillard, M. S.; Fox, J. M. Bioorthogonal Chemistry. *Nat. Rev. Methods. Primers.* **2021**, *1* (1), 30. <https://doi.org/10.1038/s43586-021-00028-z>.
- (190) Bird, R. E.; Lemmel, S. A.; Yu, X.; Zhou, Q. A. Bioorthogonal Chemistry and Its Applications. *Bioconjug. Chem.* **2021**, *32* (12), 2457–2479. <https://doi.org/10.1021/acs.bioconjchem.1c00461>.
- (191) Bertozzi, C. R. A Decade of Bioorthogonal Chemistry. *Acc. Chem. Res.* **2011**, *44* (9), 651–653. <https://doi.org/10.1021/ar200193f>.
- (192) Hang, H. C.; Yu, C.; Kato, D. L.; Bertozzi, C. R. A Metabolic Labeling Approach toward Proteomic Analysis of Mucin-Type O-Linked Glycosylation. *Proc. Natl. Acad. Sci.* **2003**, *100* (25), 14846–14851. <https://doi.org/10.1073/pnas.2335201100>.
- (193) Rudolf, G. C.; Sieber, S. A. Copper-Assisted Click Reactions for Activity-Based Proteomics: Fine-Tuned Ligands and Refined Conditions Extend the Scope of Application. *ChemBioChem* **2013**, *14* (18), 2447–2455. <https://doi.org/10.1002/cbic.201300551>.
- (194) Lallana, E.; Riguera, R.; Fernandez-Megia, E. Reliable and Efficient Procedures for the Conjugation of Biomolecules through Huisgen Azide-Alkyne Cycloadditions. *Angew. Chem. Int. Ed.* **2011**, *50* (38), 8794–8804. <https://doi.org/10.1002/anie.201101019>.

- (195) Köhn, M.; Breinbauer, R. The Staudinger Ligation - A Gift to Chemical Biology. *Angew. Chem. Int. Ed.* **2004**, *43* (24), 3106–3116. <https://doi.org/10.1002/anie.200401744>.
- (196) Staudinger, von H.; Meyer, J. Über Neue Organische Phosphorverbindungen III. Phosphinmethylenderivate Und Phosphinimine. *Helv. Chim. Acta.* **1919**, *2*, 635–646.
- (197) Saxon, E.; Armstrong, J. I.; Bertozzi, C. R. A “Traceless” Staudinger Ligation for the Chemoselective Synthesis of Amide Bonds. *Org. Lett.* **2000**, *2* (14), 2141–2143. <https://doi.org/10.1021/ol006054v>.
- (198) Saxon, E.; Bertozzi, C. R. Cell Surface Engineering by a Modified Staudinger Reaction. *Science* **2000**, *287* (5460), 2007–2010. <https://doi.org/10.1126/science.287.5460.2007>.
- (199) Huisgen, R. Kinetics and Mechanism of 1,3-Dipolar Cycloadditions. *Angew. Chem. Int. Ed.* **1963**, *2* (11), 633–645. <https://doi.org/10.1002/anie.196306331>.
- (200) Rostovtsev, V. v.; Green, L. G.; Fokin, V. v.; Sharpless, K. B. A Stepwise Huisgen Cycloaddition Process: Copper(I)-Catalyzed Regioselective “Ligation” of Azides and Terminal Alkynes. *Angew. Chem. Int. Ed.* **2002**, *41* (14), 2596–2599. [https://doi.org/10.1002/1521-3773\(20020715\)41:14<2596::AID-ANIE2596>3.0.CO;2-4](https://doi.org/10.1002/1521-3773(20020715)41:14<2596::AID-ANIE2596>3.0.CO;2-4).
- (201) Tornøe, C. W.; Christensen, C.; Meldal, M. Peptidotriazoles on Solid Phase: [1,2,3]-Triazoles by Regiospecific Copper(I)-Catalyzed 1,3-Dipolar Cycloadditions of Terminal Alkynes to Azides. *J. Org. Chem.* **2002**, *67* (9), 3057–3064. <https://doi.org/10.1021/jo011148j>.
- (202) Worrell, B. T.; Malik, J. A.; Fokin, V. v. Direct Evidence of a Dinuclear Copper Intermediate in Cu(I)-Catalyzed Azide-Alkyne Cycloadditions. *Science* **2013**, *340* (6131), 457–460. <https://doi.org/10.1126/science.1229506>.
- (203) Kennedy, D. C.; McKay, C. S.; Legault, M. C. B.; Danielson, D. C.; Blake, J. A.; Pegoraro, A. F.; Stollow, A.; Mester, Z.; Pezacki, J. P. Cellular Consequences of Copper Complexes Used To Catalyze Bioorthogonal Click Reactions. *J. Am. Chem. Soc.* **2011**, *133* (44), 17993–18001. <https://doi.org/10.1021/ja2083027>.
- (204) Haldón, E.; Nicasio, M. C.; Pérez, P. J. Copper-Catalysed Azide-Alkyne Cycloadditions (CuAAC): An Update. *Org. Biomol. Chem.* **2015**, *13* (37), 9528–9550. <https://doi.org/10.1039/c5ob01457c>.
- (205) Agard, N. J.; Prescher, J. A.; Bertozzi, C. R. A Strain-Promoted [3 + 2] Azide–Alkyne Cycloaddition for Covalent Modification of Biomolecules in Living Systems. *J. Am. Chem. Soc.* **2004**, *126* (46), 15046–15047. <https://doi.org/10.1021/ja044996f>.
- (206) Wittig, G.; Krebs, A. Zur Existenz Niedergliedriger Cycloalkyne, I. *Chem. Ber.* **1961**, *94* (12), 3260–3275. <https://doi.org/10.1002/cber.19610941213>.
- (207) Sletten, E. M.; Bertozzi, C. R. From Mechanism to Mouse: A Tale of Two Bioorthogonal Reactions. *Acc. Chem. Res.* **2011**, *44* (9), 666–676. <https://doi.org/10.1021/ar200148z>.

CHAPTER 2

Design and Synthesis of Small-molecule Probes Based on The Biotin-tagged Approach and The Photoaffinity Labelling Technique

2.1 Introduction

2.1.1 Biotinylation of Small Molecules

The biotin-tagged approach remains a direct and non-covalent method to ascertain the cellular protein target of a biologically active small molecule. This method relies on the strong interaction between biotin and streptavidin. This interaction is by far one of the strongest protein–ligand interactions found in nature, with an estimated K_d of 10^{-15} M.¹ Such a strong binding affinity has found widespread applications in the field of protein identification and drug discovery. Multiple amino acids from the streptavidin provide binding affinity with biotin, mostly by interacting with its unique bicyclic structure of the molecule, containing an imidazolidinone fused to a tetrahydrothiophene. This includes a number of non-covalent interactions, such as hydrogen bonds, Van der Waals interactions, and electrostatic interactions.^{2–4} Due to the necessary interactions between the bicyclic structure and streptavidin, the valeric acid side chain has been used widely to chemically derivatize biotin.

Biotinylation of small molecules is the key to the biotin-tagged approach.^{5,6} One of the most common ways to synthesize biotinylated molecules is through amide bond formation, which can be done by using coupling reagents, such as 1-(3-dimethylaminopropyl)-3-ethylcarbodiimide hydrochloride (EDCI).⁷ Even so, the low reactivity of the acid significantly decreases the rate of the reaction. Consequently, a variety of activated biotin esters have been developed over time to accelerate the reaction. For example, both *p*-nitrophenyl ester and *N*-hydroxysuccinimide ester (NHS) have been used commonly as activated biotin esters. The *p*-nitrophenyl group is an excellent leaving group, favoring the formation of the amide bond. Using NHS ester can help increase the solubility of the compound

in various organic solvents. With a sulfonate group added to the NHS ester, this can increase its solubility in aqueous media (Figure 2.1).

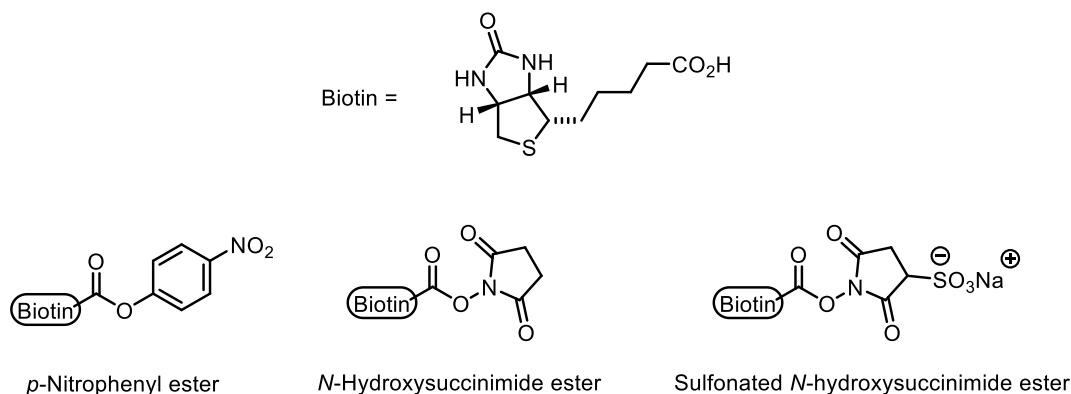
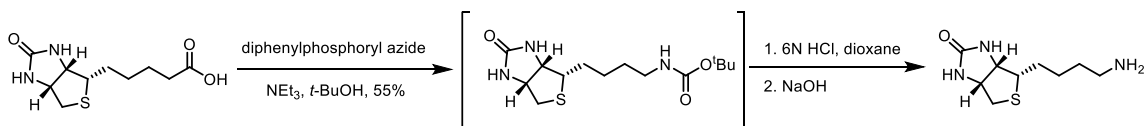


Figure 2.1. The biotin and activated biotin esters for amide bond formation.

The conversion of biotin to norbiotinamine provides another way to couple the biotin moiety to the molecule directly. Szalecki proposed the synthesis of norbiotinamide via an one-pot procedure based on a modified Curtius rearrangement, using diphenylphosphoryl azide⁸ in *t*-BuOH followed by the hydrolysis of the tert-butoxycarbamate intermediate (Scheme 2.1).^{9,10}



Scheme 2.1. Synthesis of norbiotinamine from naturally occurring biotin.

Although the use of amide coupling agents and activated biotin ester represents the vast majority of the direct biotinylation of small molecules, problems have been encountered due to the steric effect caused by the bulkiness of the biotin. This drawback can be circumvented by the incorporation of a spacer between the biotin moiety and the affinity ligand. Polyethylene glycol or a polymethylene linker are common options for spacers for their easy accessibility, especially the former for its ability to increase solubility.

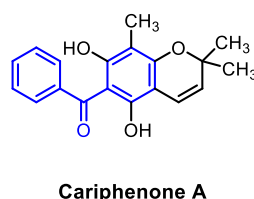
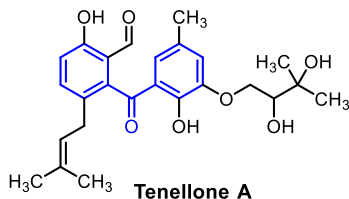
The spacer can extend the valeric acid side sidechain with a terminal amine, alkyl halide, or a bio-orthogonal tag. An amine-bearing biotin could couple with an

acid in the presence of a coupling reagent and base.³ The bromine-bearing biotin is particularly useful in connecting the biotin to an alcohol-containing molecule. Also, a biotin can be installed to the molecule of interest via a click reaction if a bio-orthogonal tag is presented on the molecule. The 1,2,3-triazole formed by CuAAC has been considered as a stable bioisostere for amide and represents a safe alternative for different connectivities.¹¹

2.1.2 Synthetic Strategies of Benzophenones

Benzophenones are important scaffolds, not only because they are used frequently toward photoaffinity labelling in protein identification but also because they themselves possess pharmacologically relevant activities. Many naturally occurring benzophenones show a wide range of activities, such as antiparasitic and antioxidant activity (Figure 2.2a). Benzophenone is also found in commercially available drugs. For example, ketoprofen exhibits nonsteroidal anti-inflammatory activity and fenofibrate is used to maintain the cholesterol level in patients with cardiovascular diseases (Figure 2.2b). For these reasons, the synthesis of benzophenones has become increasingly attractive to organic chemists. There are numerous ways to access these building blocks, and several synthetic strategies will be discussed here for their significance.¹²

a) Natural products containing benzophenone.



b) Commercially available drugs bearing benzophenone scaffold.

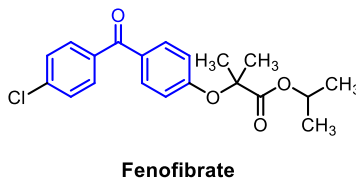
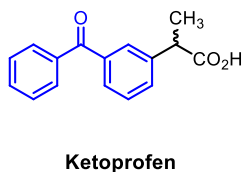
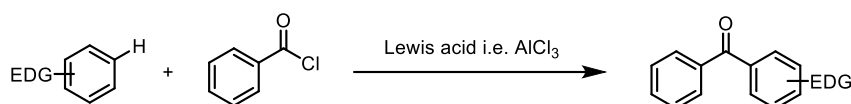


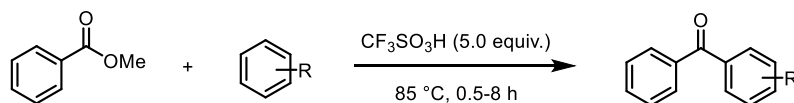
Figure 2.2. a) Naturally occurring compounds containing benzophenone. b) Commercial drugs with benzophenone scaffold.

The Friedel–Crafts acylation offers a direct and inexpensive access to aromatic ketones. This synthetic approach employs a Lewis acid, such as aluminum trichloride (AlCl₃) (Scheme 2.2a).¹³ Hwang and co-workers demonstrated a variation of the conventional Friedel–Crafts acylation to synthesize benzophenone derivatives (Scheme 2.2b).¹⁴ Instead of using highly reactive benzoyl chlorides, the reaction was carried out between methyl benzoate and aryl groups containing different substitution patterns in the presence of five equivalents of trifluoromethanesulfonic acid (TfOH).

a) Friedel–Crafts acylation



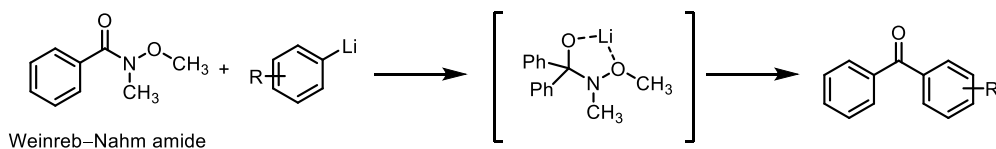
b) Variation of Friedel–Crafts acylation



R = H, F, Cl, Me, OMe, CF₃, NO₂ etc.

Hwang et al. *Tetrahedron*. **2000**, 56, 7199–7203.

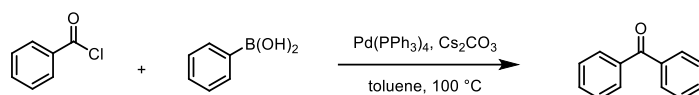
c) Weinreb–Nahm ketone synthesis



Scheme 2.2. a) The Friedel–Crafts acylation to benzophenones catalyzed by a Lewis acid. b) the variation of Friedel–Crafts proposed by Hwang et al. in the presence of TfOH. c) The Weinreb–Nahm ketone synthesis to benzophenone.

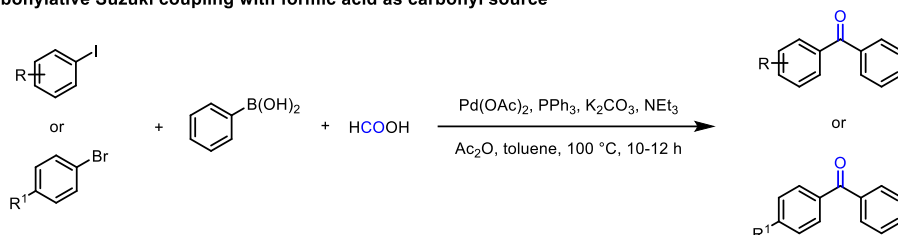
Similar to the Friedel–Crafts reaction, the Weinreb–Nahm ketone synthesis can be used to synthesize aromatic ketones. This strategy relies on the characteristic reactivity of the Weinreb–Nahm amide, which reacts with only one equivalent of organolithium reagent (Scheme 2.2c). For example, Yamazaki and co-workers synthesized the derivatives of an anti-microtubule compound bearing benzophenone, using the Weinreb–Nahm ketone synthesis. During the preparation, a benzoic acid was converted first to the corresponding Weinreb–Nahm amide with

a) The palladium-catalyzed cross-coupling of acid chlorides



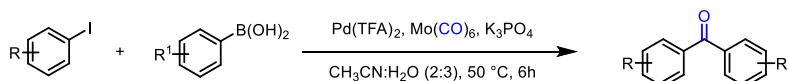
Haddach et al. *Tetrahedron*. **1999**, *40*, 3109–3112.

b) Carbonylative Suzuki coupling with formic acid as carbonyl source



Qi et al. *Chem. Eur. J.* **2015**, *21*, 17650–17656.

c) Carbonylative Suzuki coupling with Mo(CO)₆ as carbonyl source

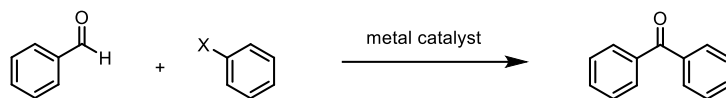


Sun et al. *Adv. Synth. Catal.* **2019**, *361*, 2117–2123.

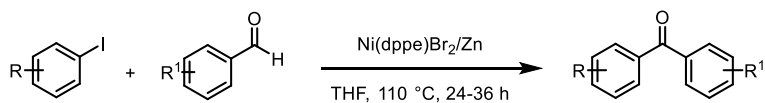
Scheme 2.4. Carbon monoxide-free syntheses to benzophenone.

Beside Pd-catalyzed cross-coupling, transition metal-catalyzed C–H bond functionalization of aldehydes provides another route to benzophenones (Scheme 2.5a). For instance, Huang and co-workers reported the synthesis of benzophenone via a carbonyl-Heck reaction between aldehydes and aryl iodides, employing Ni(dppe)Br₂ and Zn as catalyst system (Scheme 2.5b).²¹ In addition, a palladium-catalyzed carbonyl-Heck reaction of aldehydes to synthesize asymmetrical diaryl ketones was introduced by Wakaki and colleagues (Scheme 2.5c).²² This transformation, which dismisses the use of an external reducing agent and tolerates aldehydes and aryl bromides with different substitution patterns, also could be used to synthesize heteroaryl ketones.

a) Aldehyde C–H coupling to benzophenone

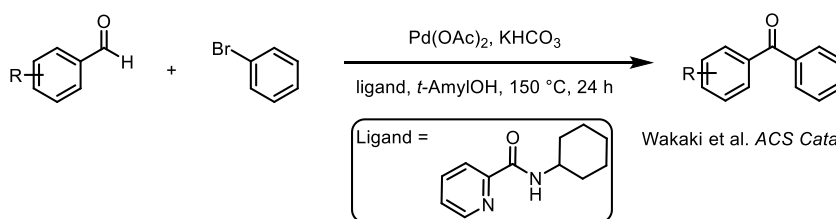


b) Ni/Zn-catalyzed coupling between aryl iodides and aryl aldehydes



Huang et al. *J. Org. Chem.* **2002**, *67*, 1682–1684.

c) Pd-catalyzed C–H activation of aldehyde to diaryl ketones



Wakaki et al. *ACS Catal.* **2018**, *8*, 3123–3128.

Scheme 2.5. Metal-catalyzed C–H activation of aryl aldehyde to diaryl ketone.

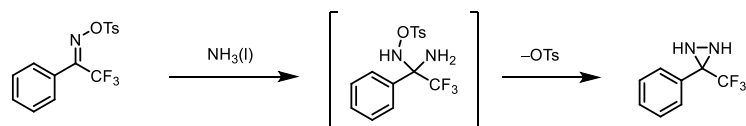
2.1.3 Synthetic Strategies of Trifluoromethyl Phenyl Diazirines

The diazirines have found useful applications in the identification of unknown protein targets, probing the binding sites of small molecules, and studying protein–protein interactions. Their syntheses are, therefore, an important research area for organic chemists and can be categorized into two variations, with or without the use of liquid ammonia.²³

The syntheses of trifluoromethyl phenyl diazirine (TPD) utilizing liquid ammonia mostly follow the classical sequence proposed by Zeifman and co-workers.²⁴ In their study, liquid ammonia was used to test the electrophilicity of trifluoroacetophenone *O*-tosyl oxime (Scheme 2.6a). The geminal intermediate originated from the nucleophilic attack of the ammonia to the electrophilic oxide C=N bond and undergoes a cyclization reaction, providing the diaziridine product. Later in 1980, Brunner and colleagues extended this transformation to synthesize the first example of TPD (Scheme 2.6b).²⁵ The synthesis started with 2,2,2-trifluoroacetophenone, which was treated with hydroxylamine to form the oxime intermediate. The oxime was transformed to the corresponding diaziridine according

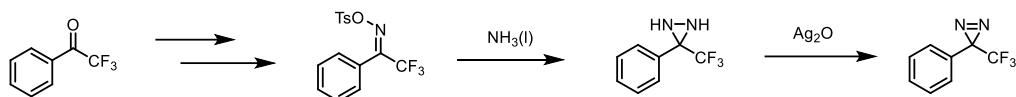
to the sequence set by Zeifman et al. Finally, the trifluoromethyl phenyl diaziridine was oxidized into TPD with silver oxide (Ag_2O). Since then, reaction in liquid ammonia has been employed in the vast majority of TPD synthesis.^{26–28}

a) The derivatization of trifluoroacetophenone *O*-tosyl oxime with liquid ammonia



Zeifman et al. *Izv. Akad. Nauk. SSSSR Ser. Khim.* **1972**, 12,2737-2741.

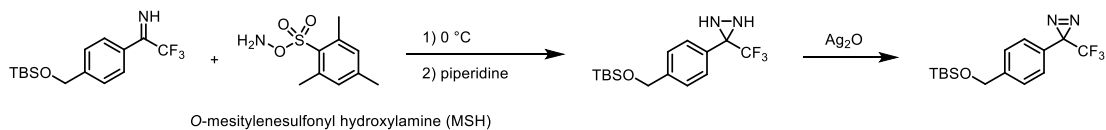
b) The first synthesis of TPD utilizing liquid ammonia.



Brunner et al. *J. Biol. Chem.* **1980**, 255, 3313-3318

Scheme 2.6. Synthetic routes utilizing liquid ammonia. a) Zeifmann and co-workers established the key transformation from trifluoroacetophenone *O*-tosyl oxime to trifluoromethyl phenyl diaziridine. b) Brunner et al. later proposed the first synthesis of TPD with this transformation.

Liquid ammonia employed in the reaction is extremely volatile, toxic, and corrosive to various organs of the human body. In order to handle liquid ammonia, the reaction has to be conducted at a very low temperature, which usually requires the use of a dry ice/acetone cooling bath. Recently, Kumar et al. came up with a method to avoid the use of liquid ammonia to synthesize TPD.²⁹ In the study, *O*-mesitylenesulfonyl hydroxylamine (MSH) was used to substitute anhydrous liquid ammonia in the main reaction step to react with *N*-TMS-ketimine (Scheme 2.7). The formed diaziridine can subsequently be oxidized into diazirine with Ag_2O .



Scheme 2.7. Ammonia-free synthesis to the TPD.

This work offers an option to synthesize TPDs from phenyl trifluoromethyl ketones in an ammonia-free manner. However, it is important to consider that the

aminating reagent, MSH, is notorious for its instability. MSH has been reported to undergo rapid exothermic decomposition when stored as a dry sample in an amber glass container.³⁰ Therefore, MSH should be made freshly only when needed and stored at temperature below 0 °C as a solution in dichloromethane.³¹ Also, the excess MSH needs to be quenched by piperidine to avoid the decomposition of the product.

To derivatize TPDs further, a better understanding of their stability under different reaction conditions is desired. TPDs are known to tolerate a wide variety of reaction conditions, and some will be laid out here.²³ TPDs are able to withstand various acidic and basic conditions but should be kept at low temperatures. For example, the formylation of unsubstituted TPD on the *para*-position can be reached in 80% yield with titanium chloride (TiCl₄), TfOH, and dichloromethyl methyl ether at 0 °C.³² Unfortunately, TPDs are not compatible with strong organometallic reagents, such as organomagnesium (Grignard reagents) and organolithium because of their high nucleophilicity, both of which are known to attack the diazirinyl ring, causing the degradation of diazirine.³³

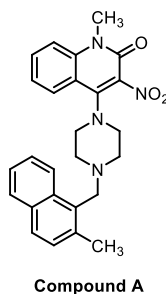
TPD-containing compounds are able to survive under mild oxidative conditions, including potassium permanganate (KMnO₄), but a prolonged reaction time usually leads to diminished yields, likely from the decomposition of diazirine.³⁴ Also, hydrogenation of TPD derivatives containing alkenes was reported to proceed with the use of a rhodium catalyst (Wilkinson's catalyst)³⁵ but using palladium on activated carbon (Pd/C) caused the hydrogenation of N–N double bond.³⁶ It demonstrates that transition metal-catalyzed reactions involving TPDs need to be screened carefully for compatibility. For example, only copper(I) catalyst afforded the desired product in the work from Rennhack et al. after extensive screening of different metal catalysts.³⁷

In general, the handling of TPDs should avoid elevated temperature, strong light, long reaction time, and multistep syntheses. Due to the thermal instability of TPDs, reactions under these conditions often result in low yields or in the deconstruction of diazirine moiety. To tackle the sensitivity issue of TPD, the

synthesis of TPD-bearing compounds should be planned accordingly or TPD should be installed closer to the final stage of the synthesis.

2.1.4 Project Objectives

A preliminary in vitro screening result led to the discovery of a series of newly identified small molecules with promising biological activities.³⁸ This series of small molecules was found to be able to promote the proliferation of CD8+ T cells and the secretion of immunity related cytokines, IL-2 and interferon gamma (IFN γ) (Figure 1.11). Both CD8+ T cells and IL-2 concentration are important indices that represent the host's immunity. The population of CD8+ T cell is related directly to the immune response for their cytotoxic activity. IL-2 is a vital factor for the growth and survival of T cells, therefore, it is recognized as an important indication of host immunity.³⁹ Among all tested derivatives, **Compound A** demonstrated the best results in both assays (Figure 2.3).



Compound A

Figure 2.3. The chemical structure of the lead compound, **Compound A**.

In the process of target deconvolution of **Compound A**, Barakat and co-workers confirmed that the observed immune responses were not mediated through a PD-1/PD-L1 pathway but an unidentified protein. Therefore, our objective has been to identify and isolate the protein of interest using the biotin-tagged approach and the trifunctional approach. Since **Compound A** was able to provoke the desired immune responses, it was used as the lead compound and as the structural basis of the synthesized molecular probes. From there, several generations of molecules were developed and served as probes for different purposes. It is important to mention that after the designed molecular probes were synthesized, their ability to promote IL-2

production were evaluated by an ELISA before further application, for example, affinity pull-down assay or microscopic experiments. We are pleased to collaborate with a graduate student from the Barakat group, Yasser Tabana, who contributed to all the biological work.

In this project, we designed molecular probes mainly based on two protein identification approaches, the biotin-tagged and the trifunctional approach (Figure 2.4).

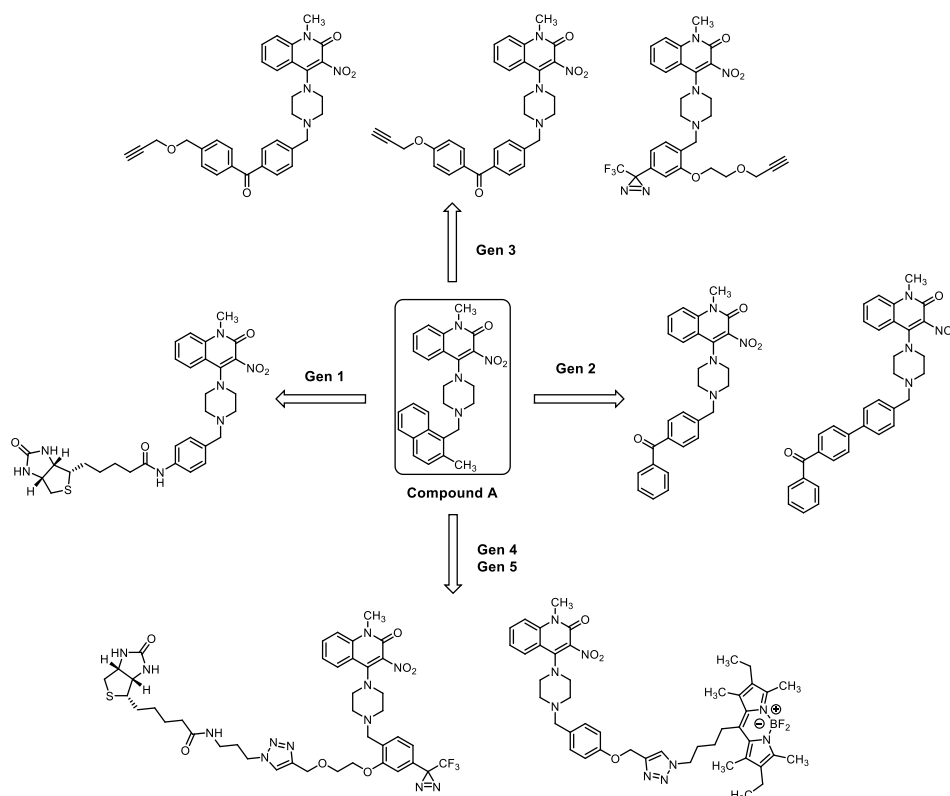


Figure 2.4. Overview and design of different generations of molecules.

The first generation probe molecule was proposed for an affinity pull-down purification. Therefore, a biotin tag was embedded in the molecule. The second generation of probe molecules was synthesized for a proof-of-concept labelling experiment, utilizing the photoaffinity labelling technique. The benzophenones were chosen as the photo-crosslinker and incorporated into the trial molecules. Then, we proposed two different kinds of trifunctional probe molecules as the third generation probe molecules to address problems encountered with the previously mentioned

biotinylated and photoaffinity compounds. The fourth generation fluorescent probe molecule was synthesized for related microscopy experiments. Last but not least, the fifth generation probe molecule was suggested in order to simplify the biological workflow. To do that, a biotin tag was attached to the trifunctional probe molecule through CuAAC prior to the pull-down assay.

The work of this project will be divided into two chapters. In this chapter, the molecular design and synthesis of the first and the second generation probe molecules will be elaborated first. Following that, the biological results of the synthesized probe molecules will be shown (Figure 2.5). Lastly, a proof-of-concept experiment will be described in order to examine the efficacy of two photoaffinity labelling probe molecules.

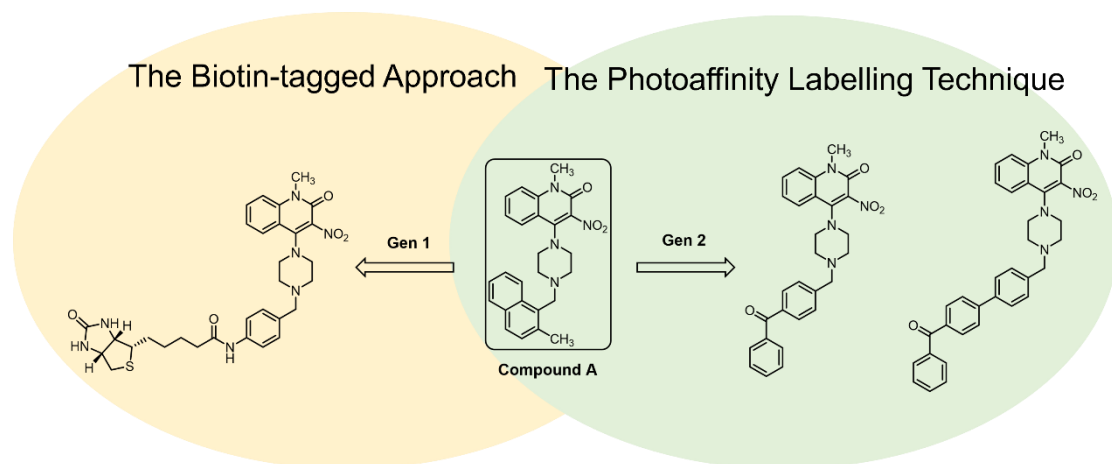


Figure 2.5. The first and the second generation probe molecules.

2.2 Result and Discussion

2.2.1 Synthesis of The First-Generation Biotinylated Probe Molecules

The first step of the project was the structural modification of the lead **Compound A**. We envisioned the installation of a biotin functionality as a handle for a streptavidin–biotin affinity pull-down assay to isolate the unknown protein. To do that, we proposed three candidates for the biotinylated molecules: two biotinylated compounds with an amide linkage and one with an ester linkage (Figure 2.6).

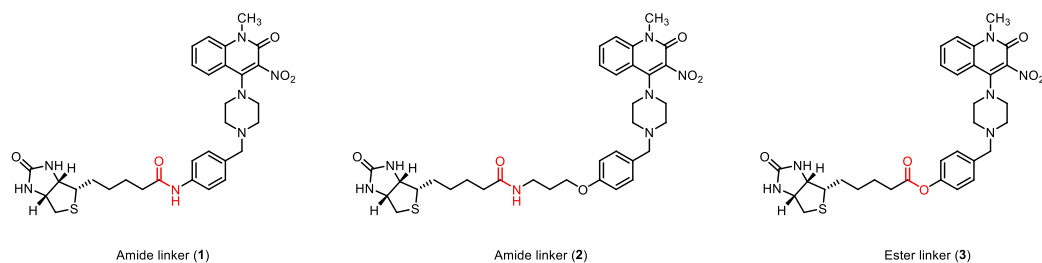


Figure 2.6. Proposed biotinylated molecules with an amide or an ester linker.

The proposed probe **3** with an ester linkage was ruled out due to the lability of ester functionalities under various conditions, such as acidic conditions, or in the presence of esterases. Therefore, we focused on the synthesis of probes **1** and **2**. The synthesis of probe **2** was proposed to start from the amide formation between a biotin and 3-bromopropyl amine, followed by an S_N2 reaction to displace the bromine with a phenol group. The synthesis of probe **1** followed a similar fashion as probe **2**. It started from the amide formation to construct the biotin building block then the reductive amination to the final product, as shown in Figure 2.7.

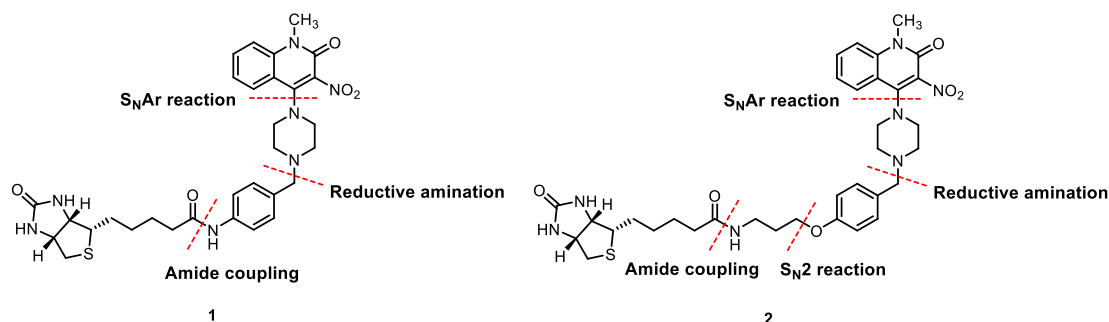
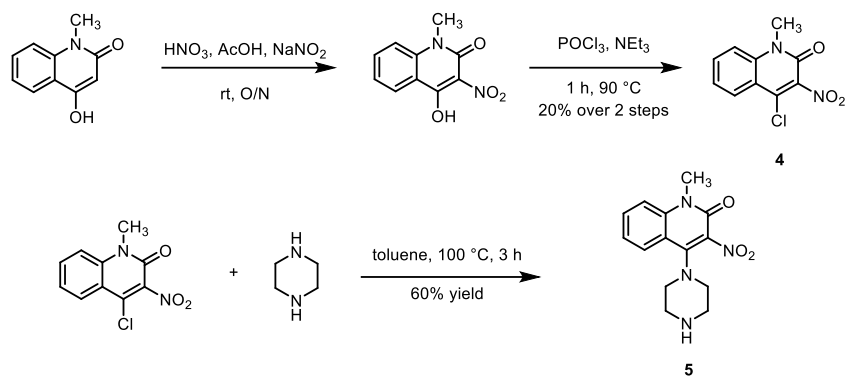


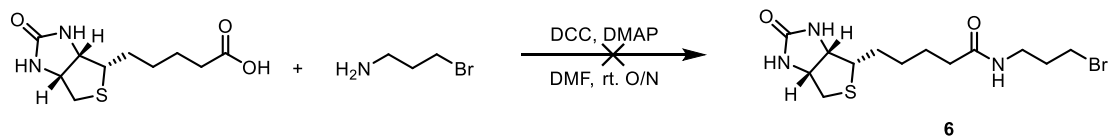
Figure 2.7. The proposed retrosynthetic strategies of biotinylated probes **1** and **2**.

The 3-nitroquinolinone scaffold **4** had been purchased initially from a commercially available source, but later it was synthesized in the lab. The synthesis started with the nitration of the enol of 4-hydroxy-1-methylquinolin-2(1*H*)-one with nitric acid, followed by the substitution of the hydroxyl group of the beta-carbonyl position by a chlorine, using phosphorus(V) oxychloride ($POCl_3$) (Scheme 2.8).⁴⁰ From the intermediate **4**, the piperazine-containing affinity warhead **5** was synthesized through an S_NAr reaction in toluene at 100 °C.



Scheme 2.8. The synthesis of building block **5**.

We planned to construct the biotin counterpart **6** from the amide formation before the attachment to the rest of the molecule. Thus, an amide coupling involving the classic coupling condition (dicyclohexylcarbodiimide (DCC) along with 4-dimethylaminopyridine (DMAP)) was evaluated (Scheme 2.9). However, the reaction did not provide the desired product **6**, as the presence of bromine was not seen in high-resolution mass spectroscopy (HRMS). We postulated that the bromine was displaced by other nucleophiles in the reaction medium.

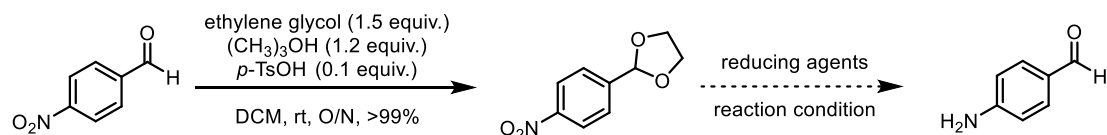


Scheme 2.9. The amide coupling of compound **6**.

In parallel to making **6**, I also attempted the synthesis of 4-aminobenzaldehyde from 4-nitrobenzaldehyde for the construction of biotinylated molecule probe **1**. To prevent the undesired reduction of aldehyde function, it was transformed firstly to the corresponding acetal by the reaction with ethylene glycol. Different loading of palladium on activated carbon, reaction time, and solvent were applied in the hope to achieve the desired reduction product (Table 2.1 entry 1–6). Unfortunately, we observed only trace amounts of the desired 4-aminobenzaldehyde in the crude NMR spectrum when the reaction times were shortened to less than 6 h (Table 2.1 entry 3–5). We postulated that the acetal protecting group was deprotected in the acidic silica gel during flash column chromatography. However, the reaction

failed to afford the desired product when performed on a larger scale (Table 2.1 entry 6). Therefore, we adjusted the strategy and started the reduction using 4-nitrobenzaldehyde as the starting material (Table 2-1 entry 7–10). Among all the conditions used, only iron (0) gave the desired 4-aminobenzaldehyde, albeit in very low yield (Table 2.1).⁴¹

Table 2.1. Reduction of 4-Nitrobenzaldehyde with Various Reductive Agents



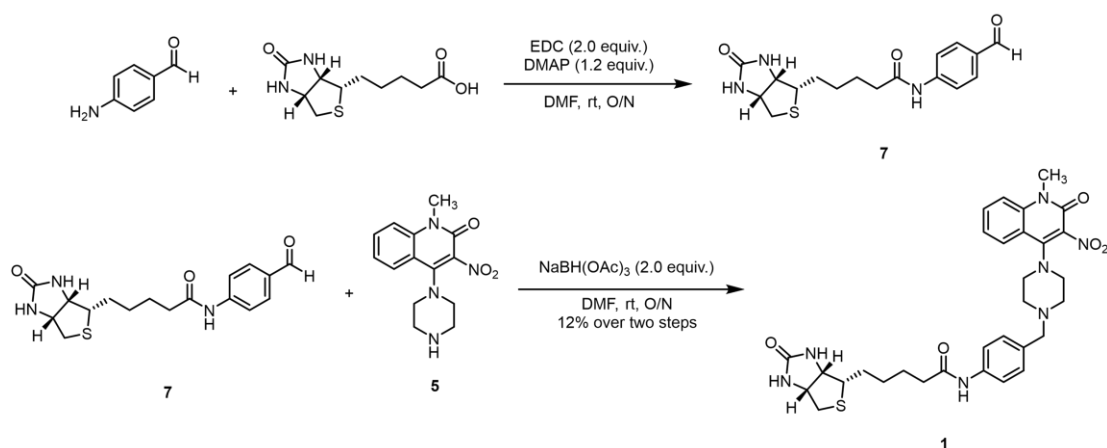
	Reducing agent	Condition	Time	Observations
1	5% Pd/C (10 wt. %), H ₂	EtOAc, r.t. then silica gel	16 h	No conversion
2 ^a	5% Pd/C (10 wt. %), H ₂	CH ₂ Cl ₂ , r.t. then silica gel	16 h	Decomposition
3 ^a	5% Pd/C (10 wt. %), H ₂	CH ₂ Cl ₂ , r.t. then silica gel	5.5 h	Trace
4 ^a	5% Pd/C (20 wt. %), H ₂	CH ₂ Cl ₂ , r.t. then silica gel	4 h	Trace
5 ^a	5% Pd/C (30 wt. %), H ₂	CH ₂ Cl ₂ , r.t. then silica gel	3.5 h	Trace
6 ^b	5% Pd/C (10 wt. %), H ₂	CH ₂ Cl ₂ , r.t. then silica gel	8 h to 24 h	Decomposition
7 ^c	Zn/ MeOH	CH ₂ Cl ₂ , r.t.	16 h to 2 days	No conversion
8 ^c	Zn/ NH ₄ HCO ₂	CH ₂ Cl ₂ , r.t.	16 h to 2 days	Trace
9 ^c	Raney nickel/ NH ₄ HCO ₂	MeOH, r.t.	16 h	No conversion
10 ^c	Fe/ AcOH/ HCl	EtOH, 80 °C	16 h	11% yield

a) With 100 mg of starting material. b) With 200 mg of starting material. c) 4-nitrobenzaldehyde was used as the starting material.

However, I noticed that an orange solid was formed during the synthesis of 4-aminobenzaldehyde. Precipitation occurred spontaneously within a very short period of time upon concentration. The crystalline solid was not soluble in any organic solvent or aqueous solution, including dimethyl sulfoxide (DMSO), dichloromethane (CH₂Cl₂), ethyl acetate (EtOAc), and water. This observation is supported by several literature precedents that 4-aminobenzaldehyde can self-condense into a number of products, including bisanhydro trimer and/or trisanhydro

tetramer.⁴²⁻⁴⁴ These self-condensed products can interconvert readily, and are therefore difficult to characterize. These polymers were reported to possess high thermal stability and low solubility in organic solvents. Therefore, the structural characterizations of these polymers were made mostly with spectroscopic analyses or the X-ray crystallography of their metal complexes.^{45,46}

Later, **7** was made by the amide bond formation, using the coupling reagent EDC, employing DMAP in DMF. The final biotinylated probe **1** was synthesized via the reductive amination between the secondary amine of **5** and the aldehyde counterpart of **7** (Scheme 2.10).



Scheme 2.10. The synthesis to the final biotinylated probe **1**.

Concomitantly, another group member of ours also accomplished the synthesis of **1** using a different reaction sequence.⁴⁷ He first performed the reductive amination between 4-aminobenzaldehyde and **5**, followed by the amide bond formation with biotin to provide the final biotinylated probe **1**. Both synthetic routes were able to afford **1**, but the latter method resulted in **1** with an inseparable undesired impurity.

2.2.2 Immunological Evaluation of Biotinylated Probe **1**

The first biotinylated probe **1** was evaluated by our collaborator Yasser Tabana, at the Faculty of Pharmacy & Pharmaceutical Sciences. The ability of the synthesized compound to stimulate the secretion of IL-2 was accessed with human peripheral

blood mononuclear cells (PBMCs) from healthy donors, using an ELISA. PBMCs were selected as they are composed of lymphocytes, which are important indicators of immune response. According to the biological result, we concluded that biotinylated probe **1** was able to promote certain level of IL-2 production, but without obvious dose-dependent responses (Figure 2.8). Its activity decreased as the concentration dropped below 32 nM.

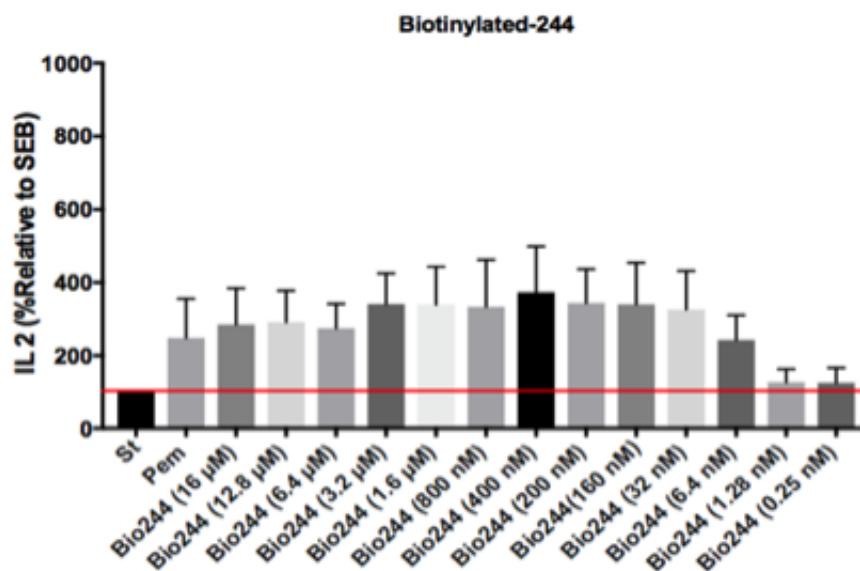


Figure 2.8. The immunological result of the biotinylated probe **1**. St: PBMCs stimulated with SEB without treatment of probe **1**. Pem: PBMCs stimulated with SEB treated with 34nM of pembrolizumab. The result was plotted by the IL-2 concentration of each control relative to control stimulated with SEB.

We postulated that the lack of dose-dependent response could be the consequence of having a molecule of relatively large size. Substrates with pronounced steric demand might cause difficulties to be trafficked through the cell membrane or interfere with its binding to the protein target. These factors potentially could result in less potent activity. Also, the biotin incorporated on the molecule can bind to other endogenous proteins, causing non-specific bindings. Therefore, we concluded that the biotin reporter tag should be installed after the probe molecule associates with the target protein. This also could solve the problem of having to introduce a biotin-containing molecule into the cells. To achieve the proposed direction, we then decided to make use of the photoaffinity labelling technique^{12,48}

which allows the formation of a covalent bond between the affinity ligand and the interacting protein. In this approach, a biotin tag can be attached to the protein–ligand complex after the exposure of UV light. In the next section, the design and synthesis of two different probe molecules with a photo-crosslinker will be elaborated.

2.2.3. Design and Synthesis of Two Second Generation Photoaffinity Labelling Probe Molecules

In order to tackle the previously mentioned issues, we designed two new probe molecules. The core of these second generation molecules was the inclusion of a photo-crosslinker into the probes. We reasoned that this would allow covalent modification of the target protein with the application of UV light. Then, other reporter tags could be installed after the covalent interaction is built. Here, BP was chosen as the photo-crosslinker for several reasons. Firstly, it can be activated at a wavelength friendly to other biological components of the live cells. Also, BPs are more synthetically accessible from commercially available starting materials. Therefore, we proposed three different photoaffinity labelling probe molecules to fulfill the goal (Figure 2.9). Probe **9** and **10** differ in a phenyl group, and we would like to evaluate if this extra phenyl group could cause any difference in protein labelling and biological results.

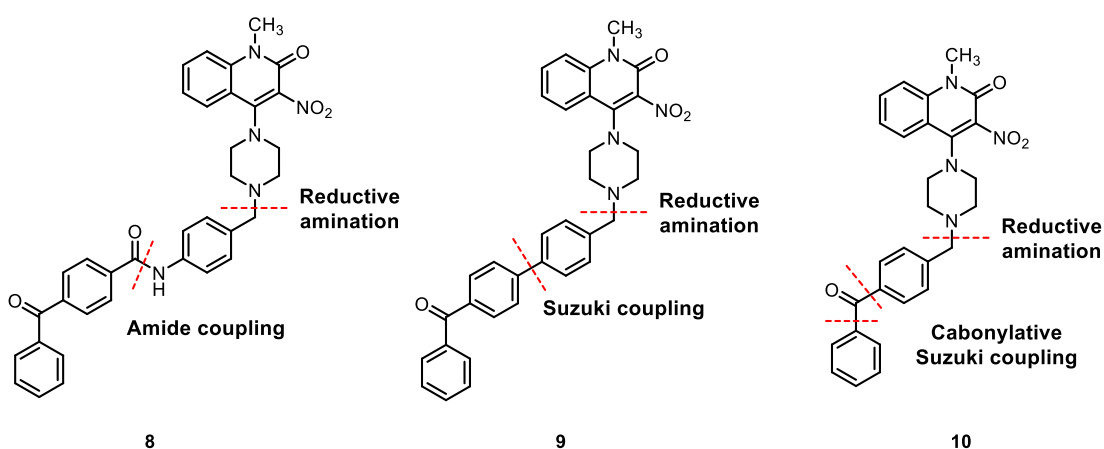
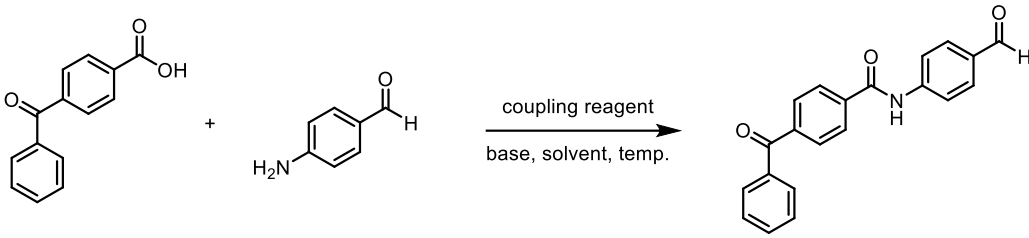


Figure 2.9. Proposed photoaffinity probe molecules **8**, **9**, and **10**.

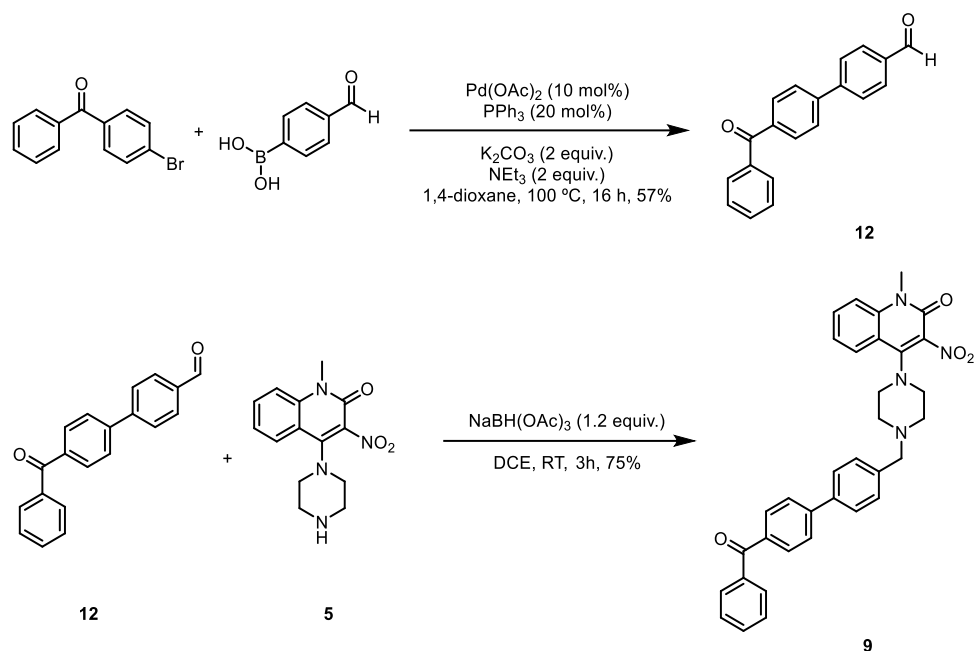
I intended to perform the synthesis of the benzophenone-containing probe **8** starting from the aldehyde **11**. The synthetic attempts were carried out, using two coupling reagents, EDC and hexafluorophosphate benzotriazole tetramethyluronium (HBTU), under different reaction conditions (Table 2.2). Unfortunately, none of the strategies were able to provide the desired amide product. I assumed that this was the result of the self-condensation of 4-aminobenzaldehyde.

Table 2.2. The Amide Coupling to the Corresponding Aldehyde **11**



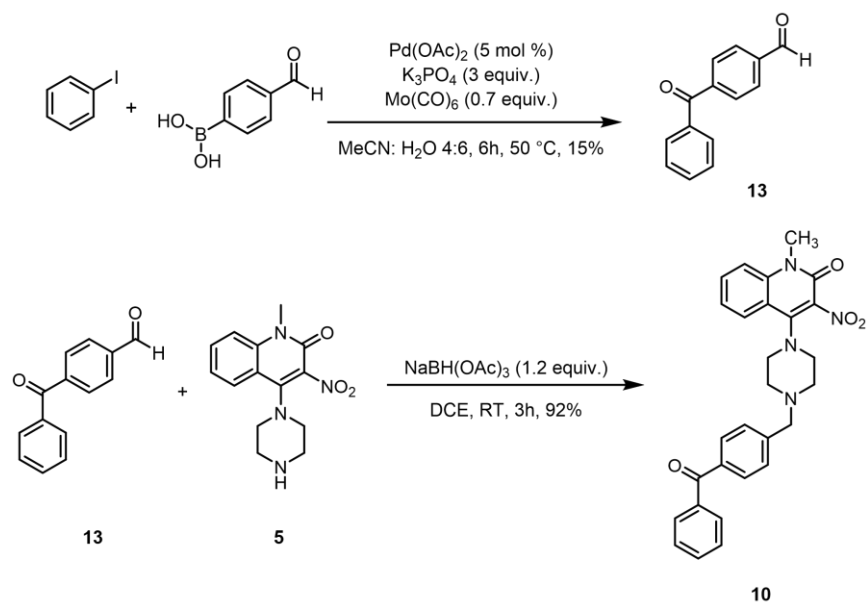
	Coupling reagent	Base	Solvent	Time and temperature	Observations
1	EDC	DMAP	DCM/DMF	r.t., 2 days	No conversion
2	EDC	DMAP	DCE	55 °C, O/N	No conversion
3	EDC	DMAP	DMF	60 °C, O/N	No conversion
4	EDC	DMAP	DMF	r.t., O/N	No conversion
5	HBTU	NEt ₃	DMF	r.t., O/N	No conversion

After the unsuccessful synthesis of compound **11**, we switched our attention to making probes **9** and **10**. The synthesis of probe **9** started with the Suzuki–Miyaura cross-coupling reaction between 4-bromobenzophenone and 4-formylphenylboronic acid to afford intermediate **12**.⁴⁹ The product was confirmed by the NMR data with the literature reports.^{49,50} Subsequently, this intermediate **12** was submitted to a reductive amination with the intermediate **5** to afford the desired probe **9** in 75% of isolated yield (Scheme 2.11).



Scheme 2.11. The synthesis of photoaffinity probe **9**.

Following that, we performed the synthesis of the photoaffinity probe **10**. The first step was the synthesis of 4-formylbenzophenone **13** via the carbonylative Suzuki coupling. In this reaction, molybdenum hexacarbonyl ($\text{Mo}(\text{CO})_6$) was used as the carbonyl source.²⁰ The product was confirmed by comparison of the NMR data with the literature reports. Then, the reductive amination between compound **5** and the synthesized **13** gave the final photoaffinity probe **10** in good yield (Scheme 2.12).



Scheme 2.12. The synthesis of photoaffinity probe **10**.

2.2.4 Immunological Results of Photoaffinity Labelling Probe **9** and **10**

After probe **9** and probe **10** were synthesized, their biological activities were evaluated. To our delight, both probes exhibited comparable or greater activity to pembrolizumab at low nanomolar concentration (Figure 2.10). When the cells were treated with either probe at the micromolar range, the concentrations of IL-2 could be promoted two to three times higher than when treated with pembrolizumab. More importantly, dose-dependent responses were observed in the immunological results. This suggests that the size and structure of benzophenone is tolerable upon treatments to the PBMCs.

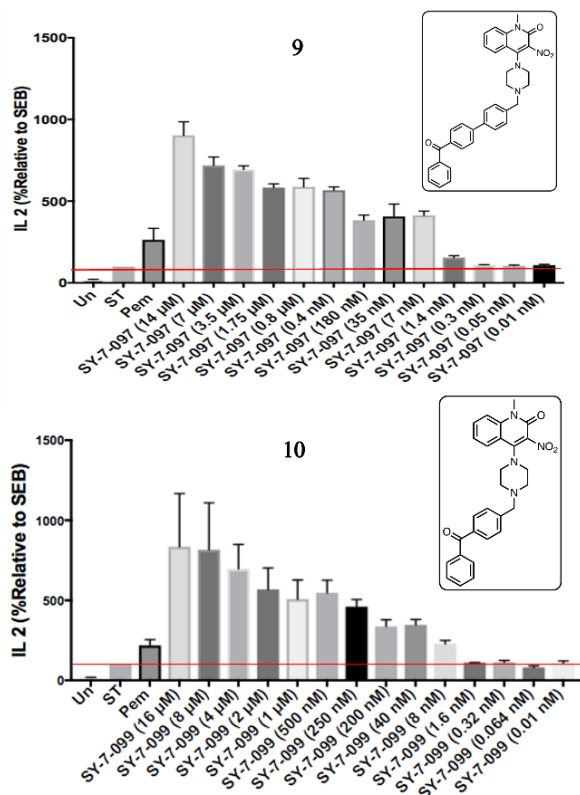


Figure 2.10. The immunological result of the photoaffinity labelling probe **9** and **10**. St: PBMCs stimulated with SEB without treatment of probe **9** or **10**. Pem: PBMCs stimulated with SEB treated with 34nM of pembrolizumab.

It is important to note that this generation of molecules was proposed for a proof-of-concept experiment. We aimed to examine the efficacy of photoaffinity labelling and the ability of these probe molecules to covalently label a protein. To test that, we designed a labelling experiment using the synthesized probes and a model protein.

2.2.5 Photoaffinity Labelling Experiment Using Bovine Serum Albumin (BSA)

To test out the viability of photoaffinity labelling, we had to choose a protein for the labelling experiment. We settled on using bovine serum albumin (BSA) as the model protein due to its ability to bind small, nonpolar drug-like molecules.⁵¹

In the experiment, samples of BSA (10 μM) in water or Roswell Park Memorial Institute (RPMI) media were incubated with either probe **9** (10 μM) or probe **10** (10 μM) for 1 h. The percentage of DMSO in each sample was kept at 0.5%

to mimic the conditions of the biological assay. A UV lamp equipped with an uranium sleeve was used as the light source. The prepared samples were exposed to UV irradiation over various time points. Samples were taken out and properly labelled after they were irradiated for 15, 30, 60, or 120 min. One sample was kept in the dark to serve as a negative control. The irradiated samples were analyzed by matrix-assisted laser desorption/ionization (MALDI) without purification.

After data interpretation, we found that it was impossible to draw a clear conclusion from the MALDI results. We could not tell a clear difference between the negative control (Figure 2.11a) and the positive controls (Figure 2.11b and c).

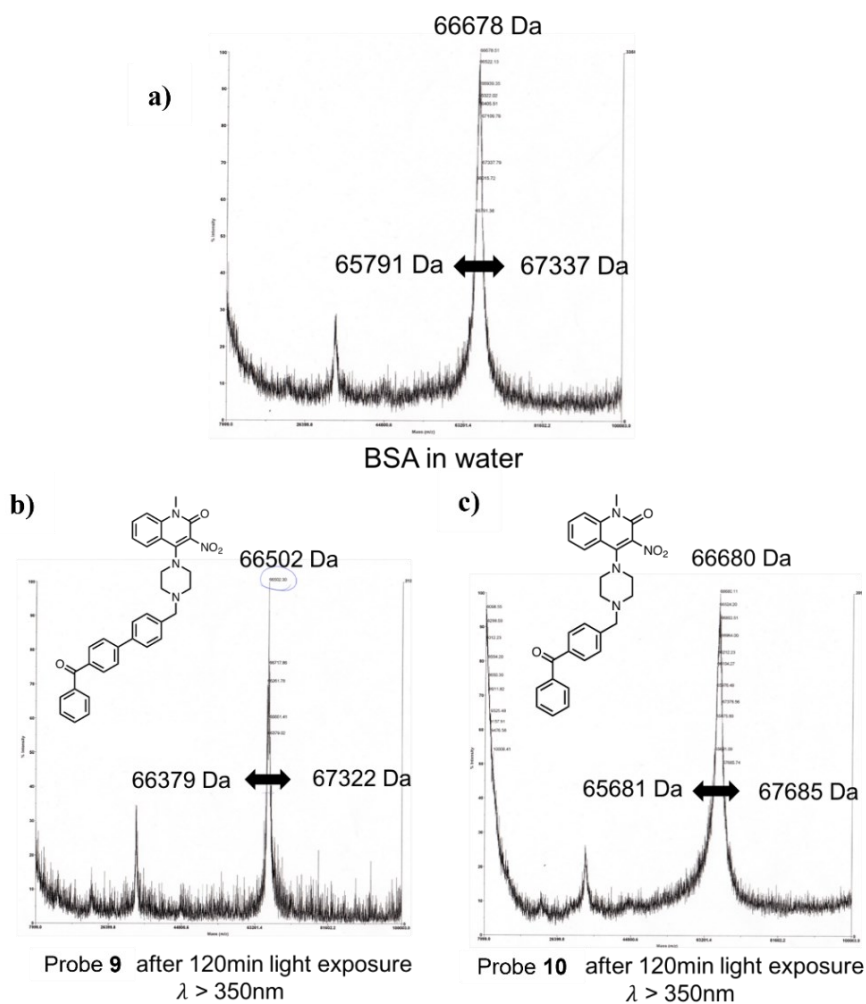


Figure 2.11. MALDI results of the photoaffinity labelling model experiments. a) Only BSA in water. b) BSA incubated with probe **9** and irradiated with UV light for 2 h. c) BSA incubated with probe **10** and irradiated with UV light for 2 h.

Due to the low molecular weight of the probes and the low loading of probes being used during the labelling experiments, the conclusion on whether the labelling had occurred could not be established.

2.3 Conclusion

The biotin-tagged approach and the photoaffinity labelling techniques composed an essential part of this project. In this chapter, an effort made to isolate and label a protein using the biotinylated probe molecule and two photoaffinity labelling probe molecules was described. The biotinylated probe molecule **1** would offer a chance to isolate the interacting protein by streptavidin–biotin affinity purification. The photoaffinity labelling probes **9** and **10**, on the other hand, enabled the reinforcement of the interaction between the affinity ligand and the target. A covalent bond could be built prior to the attachment of a biotin tag under UV irradiation.

Our first step was to synthesize the biotinylated probe molecule **1** (Figure 2.12). Its synthesis includes nitro-reduction, amide bond formation, and reductive amination. We postulated that due to the steric demand of biotin and its non-specific binding to other proteins, the immunological results were confounded. Therefore, we thought to decrease the size of the probe, hoping to enhance its activity. The biotin functionality should be introduced to the system after the probe associates with the protein.

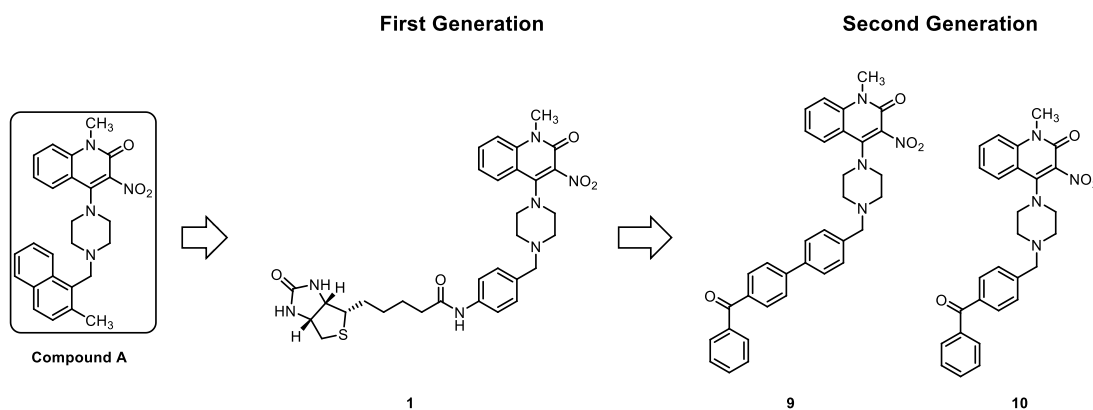


Figure 2.12. Molecular design of the first and the second-generation probe molecules.

With these in mind, we decided to utilize the photoaffinity labelling technique and synthesized two photoaffinity labelling probes, **9** and **10** (Figure 2.12). The probes **9** and **10** were synthesized via a modified Suzuki–Miyaura cross-coupling and reductive amination. Then, they were used in a proof-of-concept protein labelling experiment. However, the change in mass of protein was not observed in the model protein, BSA. Here, we suggested several reasons that might lead to the unsuccessful labelling result. Firstly, the BSA:probe ratio should be at least 1:10 to ensure that more than one molecule binds to the protein. Secondly, the concentration of BSA should be increased to the millimolar range for a clear readout from the mass spectroscopy. Lastly, the irradiated samples should be purified in order to remove the salts present in the buffer. Any salt remaining in the sample can influence the result of the MALDI analysis.

In the next chapter, the synthesis of several trifunctional probe molecules and their applications will be described. The trifunctional probes are an inevitable part of the work, as a point for structural extension is required to install a reporter tag further. Compared to the second-generation probe molecules, the trifunctional probe molecules possess a bio-orthogonal functionality. With the presence of an alkyne, a reporter tag, such as a fluorophore or a biotin, can be linked to the molecule via CuAAC (Figure 2.13). Then, the functionalized molecules can be used in various applications, for instance, confocal microscopy and affinity pull-down purification.

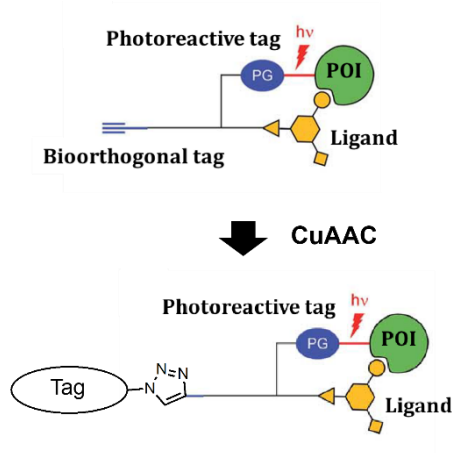
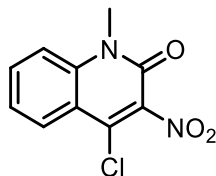


Figure 2.13. The schematic representation depicting the design of the trifunctional probe molecules.

2.4 Experimental

2.4.1 Synthesis of 1-Methyl-3-nitro-4-(piperazin-1-yl)quinolin-2(1H)-one **5**

4-Chloro-1-methyl-3-nitroquinolin-2(1H)-one (**4**)



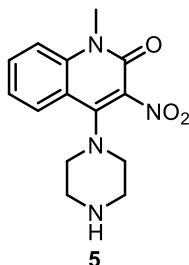
4

In a 25 mL round bottom flask, a catalytic amount of NaNO_2 was added to a stirring solution of 4-hydroxy-1-methylquinolin-2(1H)-one (2.9 mmol, 0.50 g) in glacial acetic acid (5.0 mL) and concentrated nitric acid (0.50 mL). The flask was capped with a septum, and a needle was applied to serve as a vent. The reaction was kept under room temperature and magnetically stirred for 16 h. The reaction mixture was filtered, and the solid was dried in an oven for 30 min to provide a yellow solid (0.43 g, yield 68%), which was used in the next step without further purification.

An oven dried round bottom flask, equipped with a stir bar and a rubber septum, was charged with the nitro intermediate (1.1 mmol, 0.25 g). The system was sealed, evacuated, and backfilled with an inert atmosphere. Then, phosphorus oxychloride (2.0 mL) and triethylamine (0.10 mL) were added. The reaction mixture was heated and stirred at 90 °C for 2 h and then cooled down to room temperature. The reaction mixture was mixed with ice-cold water (20 mL) and extracted with ethyl acetate (20 mL). The organic layer was separated, dried over MgSO_4 , filtered, and concentrated under reduced pressure. The crude mixture was purified by flash column chromatography, employing 1:1 ethyl acetate: hexanes as eluent to give **4** (0.13 g, yield 20%): R_f 0.49 (1:1 ethyl acetate:hexanes); IR (cast film): 3049, 2922, 2852, 1730, 1664, 1597, 1538, 1457, 1354, 1191, 1088, 767, 756 cm^{-1} ; ^1H NMR (500 MHz, CDCl_3) δ 8.13 (dd, $J = 8.0, 1.5$ Hz, 1H), 7.81–7.78 (m, 1H), 7.51–7.43 (m, 2H), 3.80 (s, 3H). ^{13}C $\{^1\text{H}\}$ NMR (125 MHz, CDCl_3) δ 153.8, 138.7, 135.9, 134.1, 127.6, 124.2, 116.8, 114.9, 30.5, one of the carbons signal was not observed likely due to

spectral overlap; HRMS (ESI, $[M+H]^+$) calcd for $C_{10}H_7ClN_2O_3$ 239.0218; found: m/z 239.0218.

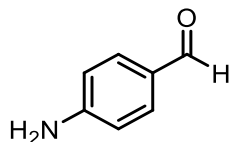
1-Methyl-3-nitro-4-(piperazin-1-yl)quinolin-2(1H)-one (5)



In a 25 mL round bottom flask was added **4** (1.3 mmol, 0.30 g), piperazine (3.8 mmol, 0.33 g) and toluene (2 mL). The flask was capped with a septum, and a needle was applied to serve as a vent. The reaction was heated to 100 °C and magnetically stirred for 3 h. The reaction progress was monitored by thin layer chromatography and LC-MS. The reaction mixture was diluted with ethyl acetate (20 mL) and washed with saturated aqueous Na_2CO_3 (10 mL) and H_2O (10 mL). The organic layer was dried over $MgSO_4$, filtered, and concentrated under reduced pressure. The crude was purified by flash column chromatography, employing 1:9 methanol:ethyl acetate solution as eluent to afford **5** as light yellow sticky oil (0.22 g, yield 60%). R_f 0.19 (1:4 methanol:ethyl acetate); IR (cast film): 3333, 3053, 2951, 2916, 1849, 1650, 1613, 1593, 1527, 1460, 1398, 1327, 1189, 1084, 1025, 763 cm^{-1} ; 1H NMR (500 MHz, $CDCl_3$) δ 7.96 (dd, $J = 8.5, 1.5$ Hz, 1H), 7.65 (ddd, $J = 8.5, 7.0, 1.5$ Hz, 1H), 7.39 (d, $J = 8.0$ Hz, 1H), 7.31 (ddd, $J = 8.0, 7.0, 1.5$ Hz, 1H), 3.71 (s, 3H), 3.25–3.19 (m, 4H), 3.11–3.05 (m, 4H), 1.70 (br s, 1H); ^{13}C $\{^1H\}$ NMR (125 MHz, $CDCl_3$) δ 156.2, 149.2, 139.7, 134.9, 132.6, 126.6, 122.7, 117.5, 115.1, 51.7, 46.1, 30.0.; HRMS (ESI, $[M+H]^+$) calcd for $C_{14}H_{17}N_4O_3$ 289.1295; found: m/z 289.1295.

2.4.2 Reduction of 4-Nitrobenzaldehyde to 4-Aminobenzaldehyde

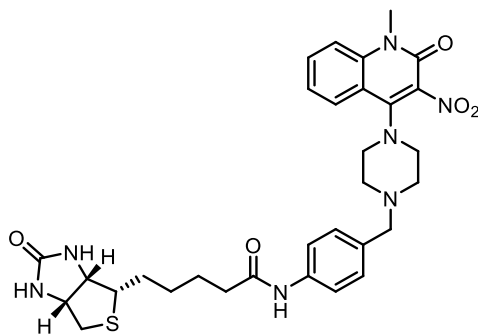
4-Aminobenzaldehyde



To an oven-dried 250 mL round bottom flask equipped with a magnetic stir bar was added 4-nitrobenzaldehyde (19 mmol, 3.0 g), acetic acid (5.0 mL), conc. HCl (1 drop), and ethanol (20 mL). The solution was stirred at room temperature, and Fe(0) (36 mmol, 2.0 g) was added portion-wise under magnetic stirring. Then, the reaction system was connected to a reflux condenser, immersed in an oil bath at 80 °C, and stirred for 16 h.

The reaction mixture was filtered through a pad of celite with vacuum suction, then the pad was wined with EtOAc (20 mL). The filtrate was basified with NaOH(aq) to pH = 10 and diluted with EtOAc (200 mL). Then, the solution was washed with saturated aqueous Na₂CO₃ solution and water. The organic layer was dried over MgSO₄, the solvent was removed, and the product was purified by flash column chromatography, employing 3:1 hexane:ethyl acetate as eluent to afford the 4-aminobenzaldehyde (0.30 g, yield 11%). The spectral data were in agreement with the literature report.⁵² ¹H NMR (400 MHz, CDCl₃) δ 9.72 (s, 1H), 7.70–7.62 (m, 2H), 6.72–6.64 (m, 2H), 4.38 (br s, 2H); HRMS (EI, M⁺) calcd for C₇H₇NO 121.0528; found: *m/z* 121.0526.

2.4.3 Synthesis of Biotinylated Probe 1



1

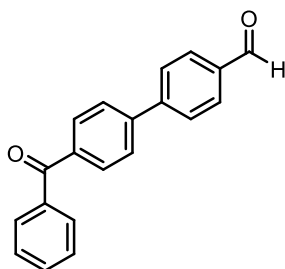
To an oven-dried 25 mL round bottom flask with a magnetic stir bar was added biotin (0.20 mmol, 0.050 g) and DMF (1 mL). Then, EDC (0.4 mmol, 78 mg) and DAMP (0.25 mmol, 0.030 g) were added to the stirring solution. The system was evacuated and backfilled with argon and magnetically stirred at room temperature for 30 min. Then, 4-aminobenzaldehyde (0.24 mmol, 33 mg) was added to the system, and the reaction was stirred at room temperature under inert atmosphere for 18 h, with progress monitored by thin layer chromatography (TLC). The crude reaction mixture was filtered through a short pad of silica gel, which was rinsed additionally with a solution of 5% MeOH/EtOAc (10–15 mL) to remove the excess DMAP and any unreacted biotin. Then, the resulting solution was concentrated under reduced pressure, and the crude mixture was employed in the next step without further purification.

An oven dried round bottom flask equipped with a stir bar and a rubber septum was charged with **7** (0.043 mmol, 15 mg) and **5** (0.052 mmol, 15 mg). The system was evacuated and backfilled with argon. DMF (1.0 mL) and NaBH(OAc)₃ (0.086 mmol, 18 mg) were added to the reaction mixture, which was then stirred at room temperature for 16 h. After the reaction went to completion, the solvent was removed under reduced pressure. The reaction residue was re-dissolved in CH₂Cl₂ (10 mL), and it was washed with H₂O (10 mL x 2) and brine (10 mL). The organic layer was dried over MgSO₄, filtered, and the solvent removed under reduced pressure. The crude mixture was purified by flash column chromatography, employing 9:1 ethyl acetate:methanol as eluent to afford **1** (15 mg, yield 12%): R_f 0.21 (1:4 methanol:ethyl acetate); IR (cast film): 3295, 3117, 3061, 2919, 2850, 1698, 1650, 1529, 1461, 1409, 1331, 1269, 1192, 763 cm⁻¹; ¹H NMR (500 MHz, CD₃OD) δ 8.03 (dd, *J* = 8.5, 1.5 Hz, 1H), 7.74 (ddd, *J* = 8.5, 7.0, 1.5 Hz, 1H), 7.63 (d, *J* = 8.5 Hz, 1H), 7.53 (app. d, *J* = 8.0 Hz, 2H), 7.40 (app. d, *J* = 8.0 Hz, 1H), 7.32 (d, *J* = 8.5 Hz, 2H), 4.48 (dd, *J* = 8.0, 4.5 Hz, 1H), 4.30 (dd, *J* = 8.0, 4.5 Hz, 1H), 3.72 (s, 3H), 3.60 (s, 2H), 3.28–3.27 (m, 4H), 3.26–3.15 (m, 2H), 2.92 (dd, *J* = 13.0, 5.0 Hz, 1H), 2.73–2.66 (m, 4H), 2.40–2.36 (m, 2H), 1.81–1.59 (m, 4H), 1.50 (p, *J* = 7.5 Hz, 2H). NH protons were not observed; ¹³C {¹H} NMR (125 MHz,

CD₃OD) δ 174.4, 166.1, 157.8, 150.9, 140.8, 139.2, 135.8, 134.1, 134.1, 131.0, 127.8, 124.3, 121.2, 118.6, 116.9, 63.4, 61.7, 57.0, 54.0, 51.4, 49.6, 41.0, 37.6, 30.5, 29.8, 29.5, 26.8; HRMS (ESI, [M+H]⁺) calcd for C₃₁H₃₈N₇O₅S 620.2650; found: m/z 620.2651.

2.4.4 Synthesis of Photoaffinity Probe 9

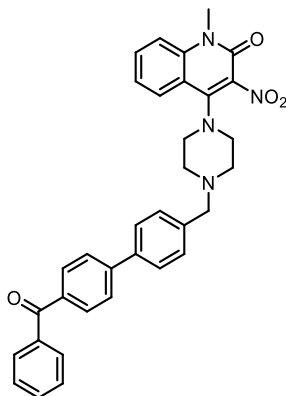
4'-Benzoyl-[1,1'-biphenyl]-4-carbaldehyde (**12**)



12

An oven dried tube equipped with a stir bar and a rubber septum was charged with 4-bromobenzophenone (0.50 mmol, 0.13 g), 4-formylboronic acid (0.50 mmol, 75 mg) and 1,4-dioxane (2.0 mL). The system was evacuated and backfilled with argon. K₂CO₃ (1.0 mmol, 0.14 g), NEt₃ (1.0 mmol, 0.14 mL), and Pd(OAc)₂ (10 mol%, 11 mg) were added to the reaction system. The system was carried out under nitrogen and stirred at 100 °C for 16 h. Upon reaction completion, the solvent was removed under reduced pressure. The resulting residue was purified by flash column chromatography, employing 1:1 ethyl acetate:hexane to give **12** (0.050 g, yield 15%) The obtained spectral data were in agreement with the literature.^{49,50} ¹H NMR (500 MHz, CDCl₃) δ 10.09 (s, 1H), 8.00 (d, J = 8.5 Hz, 2H), 7.93 (d, J = 8.5 Hz, 2H), 7.87–7.79 (m, 4H), 7.76 (d, J = 8.0 Hz, 2H), 7.62 (t, J = 7.5 Hz, 1H), 7.52 (dd, J = 8.0, 7.5 Hz, 2H). HRMS (EI, M⁺) calcd for C₂₀H₁₄O₂ 286.0094; found: m/z 286.0093.

4-(4-((4'-Benzoyl-[1,1'-biphenyl]-4-yl)methyl)piperazin-1-yl)-1-methyl-3-nitroquinolin-2(1H)-one (9)

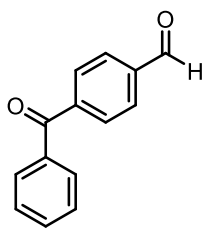


9

The previously described reductive amination procedure employed in the synthesis of **1** was carried out using 4'-benzoyl-[1,1'-biphenyl]-4-carbaldehyde **12** (0.090 mmol, 26 mg), **5** (0.080 mmol, 23 mg), NaBH(OAc)₃ (0.090 mmol, 19 mg) and dichloroethane (DCE) (0.30 mL) to give **9** as a yellow sticky oil (33 mg, yield 75%); IR (cast film): 3052, 2911, 2854, 2816, 2771, 1652, 1611, 1595 cm⁻¹; ¹H NMR (500 MHz, CD₃OD) δ 8.08–8.02 (dd, *J* = 8.5, 1.0 Hz, 1H), 7.87–7.85 (m, 2H), 7.82–7.79 (m, 4H), 7.77–7.71 (m, 3H), 7.65–7.62 (m, 2H), 7.56–7.53 (m, 4H), 7.41 (ddd, *J* = 8.0, 7.0, 1.0 Hz, 1H), 3.72 (s, 3H), 3.71 (s, 2H), 3.32 (s, 4H), 2.74 (s, 4H); ¹³C NMR (125 MHz, CD₃OD) δ 198.2, 157.8, 150.9, 146.5, 140.9, 140.2, 139.0, 138.9, 137.4, 135.8, 134.1, 133.8, 131.8, 131.2, 130.9, 129.5, 128.3, 127.9, 127.8, 124.3, 118.6, 116.9, 63.5, 54.1, 51.5, 30.5; HRMS (ESI, [M+H]⁺) calcd for C₃₄H₃₁N₄O₄ 559.2338, found: *m/z* 559.2340.

2.4.5 Synthesis of Photoaffinity Probe 10

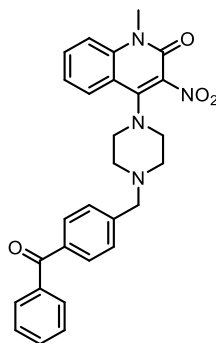
4-Benzoylbenzaldehyde (13)



13

4-benzoylbenzaldehyde **13** was prepared according to a previously reported procedure, using iodobenzene (1.6 mmol, 0.32 g), 4-formylboronic acid (2.4 mmol, 0.12 g), Mo(CO)₆ (0.79 mmol, 0.21 g), K₃PO₄ (4.7 mmol, 1.0 g), Pd(OAc)₂ (0.16 mmol, 35 mg), acetonitrile CH₃CN (1.2 mL), and H₂O (1.8 mL), affording 4-benzoylbenzaldehyde as a white solid (0.050 g, yield 15%), and the spectral data was in agreement with the literature.²⁰ ¹H NMR (500 MHz, CDCl₃) δ 10.14 (s, 1H), 8.01 (d, *J* = 8.5 Hz, 2H), 7.93 (d, *J* = 8.5 Hz, 2H), 7.81 (d, *J* = 8.0 Hz, 2H), 7.64 (t, *J* = 7.5 Hz, 1H), 7.52 (dd, *J* = 8.0, 7.5 Hz, 2H). HRMS (EI, M⁺) calcd for C₁₄H₁₀O₂ 210.0681; found: *m/z* 210.0682.

4-(4-(4-Benzoylbenzyl)piperazin-1-yl)-1-methyl-3-nitroquinolin-2(1H)-one (10)



10

The previously described reductive amination procedure employed in the synthesis of **1** was carried out 4-benzoylbenzaldehyde **13** (0.071 mmol, 15 mg), **5** (0.059 mmol, 17 mg), NaBH(OAc)₃ (0.071 mmol, 15 mg) and dichloroethane (DCE) (0.2 mL). **10** was achieved as an yellow sticky oil (26 mg, yield 92%); IR (cast film): 3055, 2944, 2895, 2812, 2769, 1652, 1603, 1561, 1528 cm⁻¹; ¹H NMR (500 MHz, CDCl₃) δ 7.96 (dd, *J* = 8.0, 1.5 Hz, 1H), 7.80 (m, 4H), 7.66 (ddd, *J* = 8.5, 7.0, 1.5 Hz, 1H), 7.60–7.58 (m, 1H), 7.51–47 (m, 4H), 7.40 (d, *J* = 9.0 Hz, 1H), 7.31 (t, *J* = 7.5 Hz, 1H), 3.72 (s, 3H), 3.70 (s, 2H), 3.32 (app. t, *J* = 5.0 Hz, 4H), 2.70 (br s, 4H); ¹³C {¹H} NMR (125 MHz, CDCl₃) δ 196.4, 156.2, 149.0, 142.8, 139.7, 137.7, 136.8, 135.0, 132.6, 132.4, 130.3, 130.1, 128.8, 128.3, 126.6, 122.7, 117.4, 115.2, 62.6, 53.2, 50.4, 30.1; HRMS (ESI, [M+H]⁺) calcd for C₂₈H₂₇N₄O₄ 483.2029, found: *m/z* 483.2027.

2.4.6 Photoaffinity Labelling Experiment With BSA

The experimental procedure described herein took probe **9** as an example, and probe **10** followed the same procedure. The BSA used was purchased from Sigma-Aldrich. All samples were prepared in glass vials. The RPMI 1640 media buffer was used in this experiment and was provided by our collaborators from the Faculty of Pharmacy and Pharmaceutical Science.

A 1.0 mg sample of probe **9** was measured and dissolved in 1 mL of DMSO. Then, 5 μ L of solution were taken out and added to a solution of 10 μ M of BSA to make up a sample of 1 mL. The final concentrations were 10 μ M BSA and 10 μ M **9**. The percentage of DMSO in each sample was controlled at 0.5%.

The prepared samples were placed in the dark before irradiation. A UV lamp equipped with a uranium sleeve and four samples was placed inside a wooden box. The samples were irradiated for 15, 30, 60, or 120 min. One sample was covered with aluminum foil and kept in the dark to serve as the negative control. The samples were removed from the wooden box and labelled properly after irradiation. Then, they were analyzed by MALDI equipped in the Department of Chemistry Spectrometry Facility (see detailed description below).

MALDI sample preparation

The MALDI samples of the above-mentioned experiments were prepared by using two-layer sample preparation method. The required solutions were prepared in prior to sample preparation.

Solution A: 10 mg/mL sinapinic acid (SA) in 4:1 acetone:methanol

Solution B: 10 mg/mL SA solution in 1:1 acetonitrile:0.1% trifluoroacetic acetic (TFA)

1. Before loading any solution, rinse the metal plate with acetone, methanol, and water. Wipe dry with KimWipe and let dry under air for 30 seconds.
2. Deposit 0.6-0.7 μ L of solution A to the sample plate with a clean micropipette, wait until dry. (Layer 1)
3. Dissolve the analyte with 0.1% TFA solution.

4. In a clean micropipette, mix 1 μL of solution B and 1 μL of sample properly with a micropipette.
5. Deposit 0.5 μL onto layer 1 with a micropipette tip and let dry. (Layer 2)
6. Rinse the dry sample spot(s) with 0.1% TFA (2.0 $\mu\text{L} \times 3$) with a micropipette, let stand for 5-10 seconds before blowing off with air.
7. The sample is now ready for MALDI analysis.

2.5 References

- (1) Weber, P. C.; Ohlendorf, D. H.; Wendoloski, J. J.; Salemme, F. R. Structural Origins of High-Affinity Biotin Binding to Streptavidin. *Science* **1989**, *243* (4887), 85–88. <https://doi.org/10.1126/science.2911722>.
- (2) Green, N. M. Avidin. In *Advances in Protein Chemistry*; New York, 1975; pp 85–133. [https://doi.org/10.1016/S0065-3233\(08\)60411-8](https://doi.org/10.1016/S0065-3233(08)60411-8).
- (3) Bayer, E. A.; Meir, W. The Avidin-Biotin Complex in Bioanalytical Applications. *Anal. Biochem.* **1988**, *171*, 1–32.
- (4) Sano, T.; Vajda, S.; Reznik, G. O.; Smith, C. L.; Cantor, C. R. Molecular Engineering of Streptavidin. *Ann. N. Y. Acad. Sci.* **1996**, *799* (1), 383–390. <https://doi.org/10.1111/j.1749-6632.1996.tb33229.x>.
- (5) Trippier, P. C. Synthetic Strategies for the Biotinylation of Bioactive Small Molecules. *ChemMedChem* **2013**, *8* (2), 190–203. <https://doi.org/10.1002/cmdc.201200498>.
- (6) Wilchek, M.; Bayer, E. A. [13] Biotin-Containing Reagents. In *Methods in Enzymology*; 1990; Vol. 184, pp 123–138. [https://doi.org/10.1016/0076-6879\(90\)84267-K](https://doi.org/10.1016/0076-6879(90)84267-K).
- (7) Murakami, N.; Ye, Y.; Kawanishi, M.; Aoki, S.; Kudo, N.; Yoshida, M.; Nakayama, E. E.; Shioda, T.; Kobayashi, M. New Rev-Transport Inhibitor with Anti-HIV Activity from Valerianae Radix. *Bioorganic Med. Chem. Lett.* **2002**, *12* (20), 2807–2810. [https://doi.org/10.1016/S0960-894X\(02\)00624-8](https://doi.org/10.1016/S0960-894X(02)00624-8).
- (8) Shioiri, T.; Ninomiya, K.; Yamada, S. Diphenylphosphoryl Azide. New Convenient Reagent for a Modified Curtius Reaction and for Peptide Synthesis. *J. Am. Chem. Soc.* **1972**, *94* (17), 6203–6205. <https://doi.org/10.1021/ja00772a052>.
- (9) Szalecki, W. Synthesis of Norbiotinamine and Its Derivatives. *Bioconjug. Chem.* **1996**, *7* (2), 271–273. <https://doi.org/10.1021/bc950094f>.
- (10) Foulon, C. F.; Alston, K. L.; Zalutsky, M. R. Synthesis and Preliminary Biological Evaluation of (3-Iodobenzoyl)Norbiotinamide and ((5-Iodo-3-Pyridinyl)Carbonyl)Norbiotinamide: Two Radioiodinated Biotin Conjugates with Improved Stability. *Bioconjug. Chem.* **1997**, *8* (2), 179–186. <https://doi.org/10.1021/bc970006m>.
- (11) Malik, M. S.; Ahmed, S. A.; Althagafi, I. I.; Ansari, M. A.; Kamal, A. Application of Triazoles as Bioisosteres and Linkers in the Development of Microtubule Targeting Agents. *RSC Med. Chem.* **2020**, *11* (3), 327–348. <https://doi.org/10.1039/C9MD00458K>.
- (12) Surana, K.; Chaudhary, B.; Diwaker, M.; Sharma, S. Benzophenone: A Ubiquitous Scaffold in Medicinal Chemistry. *Medchemcomm* **2018**, *9* (11), 1803–1817. <https://doi.org/10.1039/C8MD00300A>.
- (13) Sartori, G.; Maggi, R. Update 1 of: Use of Solid Catalysts in Friedel–Crafts Acylation Reactions. *Chem. Rev.* **2011**, *111* (5), PR181–PR214. <https://doi.org/10.1021/cr100375z>.

- (14) Hwang, J. P.; Surya Prakash, G. K.; Olah, G. A. Trifluoromethanesulfonic Acid Catalyzed Novel Friedel–Crafts Acylation of Aromatics with Methyl Benzoate. *Tetrahedron Lett.* **2000**, *56* (37), 7199–7203. [https://doi.org/10.1016/S0040-4020\(00\)00633-5](https://doi.org/10.1016/S0040-4020(00)00633-5).
- (15) Yamazaki, Y.; Sumikura, M.; Masuda, Y.; Hayashi, Y.; Yasui, H.; Kiso, Y.; Chinen, T.; Usui, T.; Yakushiji, F.; Potts, B.; Neuteboom, S.; Palladino, M.; Lloyd, G. K.; Hayashi, Y. Synthesis and Structure–Activity Relationships of Benzophenone-Bearing Diketopiperazine-Type Anti-Microtubule Agents. *Bioorg. Med. Chem.* **2012**, *20* (14), 4279–4289. <https://doi.org/10.1016/j.bmc.2012.05.059>.
- (16) Ishiyama, T.; Kizaki, H.; Miyaura, N.; Suzuki, A. Synthesis of Unsymmetrical Biaryl Ketones via Palladium-Catalyzed Carbonylative Cross-Coupling Reaction of Arylboronic Acids with Iodoarenes. *Tetrahedron Lett.* **1993**, *34* (47), 7595–7598. [https://doi.org/10.1016/S0040-4039\(00\)60409-4](https://doi.org/10.1016/S0040-4039(00)60409-4).
- (17) Ishiyama, T.; Kizaki, H.; Hayashi, T.; Suzuki, A.; Miyaura, N. Palladium-Catalyzed Carbonylative Cross-Coupling Reaction of Arylboronic Acids with Aryl Electrophiles: Synthesis of Biaryl Ketones. *J. Org. Chem.* **1998**, *63* (14), 4726–4731. <https://doi.org/10.1021/jo980417b>.
- (18) Haddach, M.; McCarthy, J. R. A New Method for the Synthesis of Ketones: The Palladium-Catalyzed Cross-Coupling of Acid Chlorides with Arylboronic Acids. *Tetrahedron Lett.* **1999**, *40* (16), 3109–3112. [https://doi.org/10.1016/S0040-4039\(99\)00476-1](https://doi.org/10.1016/S0040-4039(99)00476-1).
- (19) Qi, X.; Jiang, L.-B.; Li, H.-P.; Wu, X.-F. A Convenient Palladium-Catalyzed Carbonylative Suzuki Coupling of Aryl Halides with Formic Acid as the Carbon Monoxide Source. *Eur. J. Chem.* **2015**, *21* (49), 17650–17656. <https://doi.org/10.1002/chem.201502943>.
- (20) Sun, N.; Sun, Q.; Zhao, W.; Jin, L.; Hu, B.; Shen, Z.; Hu, X. Ligand-free Palladium-Catalyzed Carbonylative Suzuki Coupling of Aryl Iodides in Aqueous CH₃CN with Sub-stoichiometric Amount of Mo(CO)₆ as CO Source. *Adv. Synth. Catal.* **2019**, *361* (9), 2117–2123. <https://doi.org/10.1002/adsc.201900011>.
- (21) Huang, Y.-C.; Majumdar, K. K.; Cheng, C.-H. Nickel-Catalyzed Coupling of Aryl Iodides with Aromatic Aldehydes: Chemoselective Synthesis of Ketones. *J. Org. Chem.* **2002**, *67* (5), 1682–1684. <https://doi.org/10.1021/jo010289i>.
- (22) Wakaki, T.; Togo, T.; Yoshidome, D.; Kuninobu, Y.; Kanai, M. Palladium-Catalyzed Synthesis of Diaryl Ketones from Aldehydes and (Hetero)Aryl Halides via C–H Bond Activation. *ACS Catal.* **2018**, *8* (4), 3123–3128. <https://doi.org/10.1021/acscatal.8b00440>.
- (23) Hill, J. R.; Robertson, A. A. B. Fishing for Drug Targets: A Focus on Diazirine Photoaffinity Probe Synthesis. *J. Med. Chem.* **2018**, *61* (16), 6945–6963. <https://doi.org/10.1021/acs.jmedchem.7b01561>.
- (24) Zeifman, Yu. v.; Abduganiev, E. G.; Rokhlin, E. M.; Knunyants, I. L. Derivatives of Hexafluoroacetone Oxime. *Russ. Chem. Bull.* **1972**, *21* (12), 2667–2671. <https://doi.org/10.1007/BF00849836>.
- (25) Brunner, J.; Serin, H.; Richards, F. M. 3-Trifluoromethyl-3-Phenyldiazirine. A New Carbene Generating Group for Photolabeling Reagents. *J. Biol. Chem.* **1980**, *255* (8), 3313–3318.
- (26) Mayer, T.; Maier, M. E. Design and Synthesis of a Tag-Free Chemical Probe for Photoaffinity Labeling. *Eur. J. Org. Chem.* **2007**, No. 28, 4711–4720. <https://doi.org/10.1002/ejoc.200700188>.
- (27) Geurink, P. P.; Klein, T.; Prèly, L.; Paal, K.; Leeuwenburgh, M. A.; van der Mare, G. A.; Kauffman, H. F.; Overkleeft, H. S.; Bischoff, R. Design of Peptide Hydroxamate-Based Photoreactive Activity-Based Probes of Zinc-Dependent Metalloproteases. *Eur. J. Org. Chem.* **2010**, *2010* (11), 2100–2112. <https://doi.org/10.1002/ejoc.200901385>.
- (28) Wixe, T.; Almqvist, F. An Improved Synthesis of 3-[3-(Trifluoromethyl)-3H-1,2-Diazirin-3-Yl]Aniline: A Key Intermediate in the Synthesis of Photoaffinity Probes. *Tetrahedron Lett.* **2017**, *58* (34), 3350–3352. <https://doi.org/10.1016/j.tetlet.2017.07.031>.

- (29) Kumar, A. B.; Manetsch, R. Ammonia-Free Synthesis of 3-Trifluoromethyl-3-Phenyldiaziridine. *Synth. Commun.* **2018**, *48* (6), 626–631. <https://doi.org/10.1080/00397911.2017.1354026>.
- (30) Ning, R. Y. Employment Ad Information. *Chem. Eng. News Archive* **1973**, *51* (51), 36–37. <https://doi.org/10.1021/cen-v051n051.p028>.
- (31) Mendiola, J.; Rincón, J. A.; Mateos, C.; Soriano, J. F.; de Frutos, Ó.; Niemeier, J. K.; Davis, E. M. Preparation, Use, and Safety of *O*-Mesitylenesulfonylhydroxylamine. *Org. Process Res. Dev.* **2009**, *13* (2), 263–267. <https://doi.org/10.1021/op800264p>.
- (32) Nakashima, H.; Hashimoto, M.; Sadakane, Y.; Tomohiro, T.; Hatanaka, Y. Simple and Versatile Method for Tagging Phenyldiazirine Photophores. *J. Am. Chem. Soc.* **2006**, *128* (47), 15092–15093. <https://doi.org/10.1021/ja066479y>.
- (33) Paget, C. J.; Davis, C. S. Synthesis and in Vitro Activity of Some Aryl Diaziridines as Potential Monoamine Oxidase Inhibitors. *J. Med. Chem.* **1964**, *7* (5), 626–628. <https://doi.org/10.1021/jm00335a012>.
- (34) Mchedlidze, M. T.; Sumbatyan, N. v.; Bondar', D. A.; Taranenko, M. v.; Korshunova, G. A. New Photoreactive Cleavable Reagents with Trifluoromethyldiazirine Group. *Russ. J. Bioorg. Chem.* **2003**, *29* (2), 177–184. <https://doi.org/10.1023/A:1023268617727>.
- (35) Hashimoto, M.; Kato, Y.; Hatanaka, Y. Selective Hydrogenation of Alkene in (3-Trifluoromethyl) Phenyldiazirine Photophore with Wilkinson's Catalyst for Photoaffinity Labeling. *Chem Pharm Bull (Tokyo)* **2007**, *55* (10), 1540–1543. <https://doi.org/10.1248/cpb.55.1540>.
- (36) Ambroise, Y.; Mioskowski, C.; Djéga-Mariadassou, G.; Rousseau, B. Consequences of Affinity in Heterogeneous Catalytic Reactions: Highly Chemoselective Hydrogenolysis of Iodoarenes. *J. Org. Chem.* **2000**, *65* (21), 7183–7186. <https://doi.org/10.1021/jo0012243>.
- (37) Rennhack, A.; Jumpertz, T.; Ness, J.; Baches, S.; Pietrzik, C. U.; Weggen, S.; Bulic, B. Synthesis of a Potent Photoreactive Acidic γ -Secretase Modulator for Target Identification in Cells. *Bioorg. Med. Chem.* **2012**, *20* (21), 6523–6532. <https://doi.org/10.1016/j.bmc.2012.08.034>.
- (38) Ganesan, A.; Ahmed, M.; Okoye, I.; Arutyunova, E.; Babu, D.; Turnbull, W. L.; Kundu, J. K.; Shields, J.; Agopsowicz, K. C.; Xu, L.; Tabana, Y.; Srivastava, N.; Zhang, G.; Moon, T. C.; Belovodskiy, A.; Hena, M.; Kandadai, A. S.; Hosseini, S. N.; Hitt, M.; Walker, J.; Smylie, M.; West, F. G.; Siraki, A. G.; Lemieux, M. J.; Elahi, S.; Nieman, J. A.; Tyrrell, D. L.; Houghton, M.; Barakat, K. Comprehensive in Vitro Characterization of PD-L1 Small Molecule Inhibitors. *Sci. Rep.* **2019**, *9* (1), 12392. <https://doi.org/10.1038/s41598-019-48826-6>.
- (39) Bachmann, M. F.; Oxenius, A. Interleukin 2: From Immunostimulation to Immunoregulation and Back Again. *EMBO Rep.* **2007**, *8* (12), 1142–1148. <https://doi.org/10.1038/sj.embor.7401099>.
- (40) Hur, W.; Sun, Z.; Jiang, T.; Mason, D. E.; Peters, E. C.; Zhang, D. D.; Luesch, H.; Schultz, P. G.; Gray, N. S. A Small-Molecule Inducer of the Antioxidant Response Element. *Chem. Biol.* **2010**, *17* (5), 537–547. <https://doi.org/10.1016/j.chembiol.2010.03.013>.
- (41) Ramurthy, S.; Lin, X.; Subramanian, S.; Rico, A. Quinazolines For PDK1 Inhibition. WO 2007/117607 A2, October 18, 2007.
- (42) McGeachin, S. G. The Structures Of Two Self-Condensation Products From *o*-Aminobenzaldehyde. *Can. J. Chem.* **1966**, *44* (19), 2323–2328. <https://doi.org/10.1139/v66-348>.
- (43) Kimura, K.; Zhuang, J.-H.; Kida, M.; Yamashita, Y.; Sakaguchi, Y. Self-Assembling Polycondensation of 4-Aminobenzaldehyde. Preparation of Star-Like Aggregates of Cone-Shaped Poly(Azomethine) Crystals. *Polym. J.* **2003**, *35* (5), 455–459. <https://doi.org/10.1295/polymj.35.455>.

- (44) Fleischer, E. B.; Klem, E. The Structure of a Self-Condensation Product of *o*-Aminobenzaldehyde in the Presence of Nickel Ions. *Inorg. Chem.* **1965**, *4* (5), 637–642. <https://doi.org/10.1021/ic50027a008>.
- (45) Owston, P. G.; Shaw (née Gözen), L. S.; Tasker, P. A. The Self-Condensation of *o*-Aminobenzaldehyde: The Polycyclic Structure of the Picrate Salt of the Diprotonated Tetra-Anhydro Tetramer, 4b,5,15b,16-Tetrahydrodibenzo[3,4:7,8][1,5]Diazocino-[2,1-b:6,5-b]Diquinazoline-11,22-Di-ium Picrate: X-Ray Crystal Structure. *J. Chem. Soc., Chem. Commun.* **1982**, *1*, 17–19. <https://doi.org/10.1039/C39820000017>.
- (46) Jircitano, A. J.; Sommerer, S. O.; Shelley, J. J.; Westcott Jnr, B. L.; Suh, I. H. The Self-Condensation of a Derivative of *o*-Aminobenzaldehyde. Structure of the Polycyclic Bisanhydro Trimer of 2-Amino-5-Bromobenzaldehyde. *Acta Crystallogr. C Struct.* **1994**, *50* (3), 445–447. <https://doi.org/10.1107/S0108270193006894>.
- (47) Yu, S. Unpublished Results. *University of Alberta*.
- (48) Smith, E.; Collins, I. Photoaffinity Labeling in Target- and Binding-Site Identification. *Future Med Chem* **2015**, *7* (2), 159–183. <https://doi.org/10.4155/fmc.14.152>.
- (49) Rej, S.; Chatani, N. Transient Imine as a Directing Group for the Metal-Free *o*-C–H Borylation of Benzaldehydes. *J. Am. Chem. Soc.* **2021**, *143* (7), 2920–2929. <https://doi.org/10.1021/jacs.0c13013>.
- (50) Li, Z.; Li, X.; Yang, Y. Conjugated Macrocyclic Polymer Nanoparticles with Alternating Pillarenes and Porphyrins as Struts and Cyclic Nodes. *Small* **2019**, *15* (12), 1805509. <https://doi.org/10.1002/smll.201805509>.
- (51) Tang, H.; Huang, L.; Zhao, D.; Sun, C.; Song, P. Interaction Mechanism of Flavonoids on Bovine Serum Albumin: Insights from Molecular Property-Binding Affinity Relationship. *Spectrochim. Acta A Mol. Biomol. Spectrosc.* **2020**, *239*, 118519. <https://doi.org/10.1016/j.saa.2020.118519>.
- (52) Cai, S.; Duan, H.; Rong, H.; Wang, D.; Li, L.; He, W.; Li, Y. Highly Active and Selective Catalysis of Bimetallic Rh₃ Ni₁ Nanoparticles in the Hydrogenation of Nitroarenes. *ACS Catal.* **2013**, *3* (4), 608–612. <https://doi.org/10.1021/cs300689w>.

CHAPTER 3

Design, Synthesis, and Applications of the Trifunctional Probe Molecules and the Fluorescent Probe Molecules

3.1 Introduction

Chapter 2 described approaches to isolate the protein of interest via the biotin-tagged approach or photoaffinity labelling using a tethered benzophenone. However, the biotinylated probe molecule only showed moderate activity to stimulate the production of IL-2, possibly as a result of non-specific binding. Therefore, two photoaffinity probe molecules were proposed for their ability to establish covalent bond with the interacting protein. After carrying out a labelling experiment with the benzophenone probes, we realized that the photoaffinity probe molecules were not able to provide a solid result of being able to label the BSA. Based on the result of the BSA labelling experiment, we envisioned that increasing the molecular weight of the probe and optimizing the procedure would help to improve the readout of the labelling experiment.

The intrinsic drawback of target deconvolution is that the molecular target remains unknown, therefore, structure optimization for a lead compound is required. The classic affinity chromatography approach using small molecules constantly experiences loss of binding affinity as a result of structure modification, non-specific binding due to the presence of the biotin handle, and the isolation of endogenous proteins that contain biotin. Additionally, if the isolated protein of interest is of low amount, it will pose difficulties to be detected or analyzed by the mass spectroscopy.

Due to the challenging process of target deconvolution, we decided to utilize different techniques to obtain more information about the unknown target. In addition to protein isolation, the visualization of the protein target in the system and monitoring its distribution remains a crucial direction of the project. In this regard, different molecular probes, such as trifunctional probe molecules, fluorescent probe molecules, and a biotin-TPD probe molecule, were proposed for various purposes

(Figure 3.1). These include microscopic experiments and the photoaffinity labelling on top of the streptavidin–biotin affinity purification.

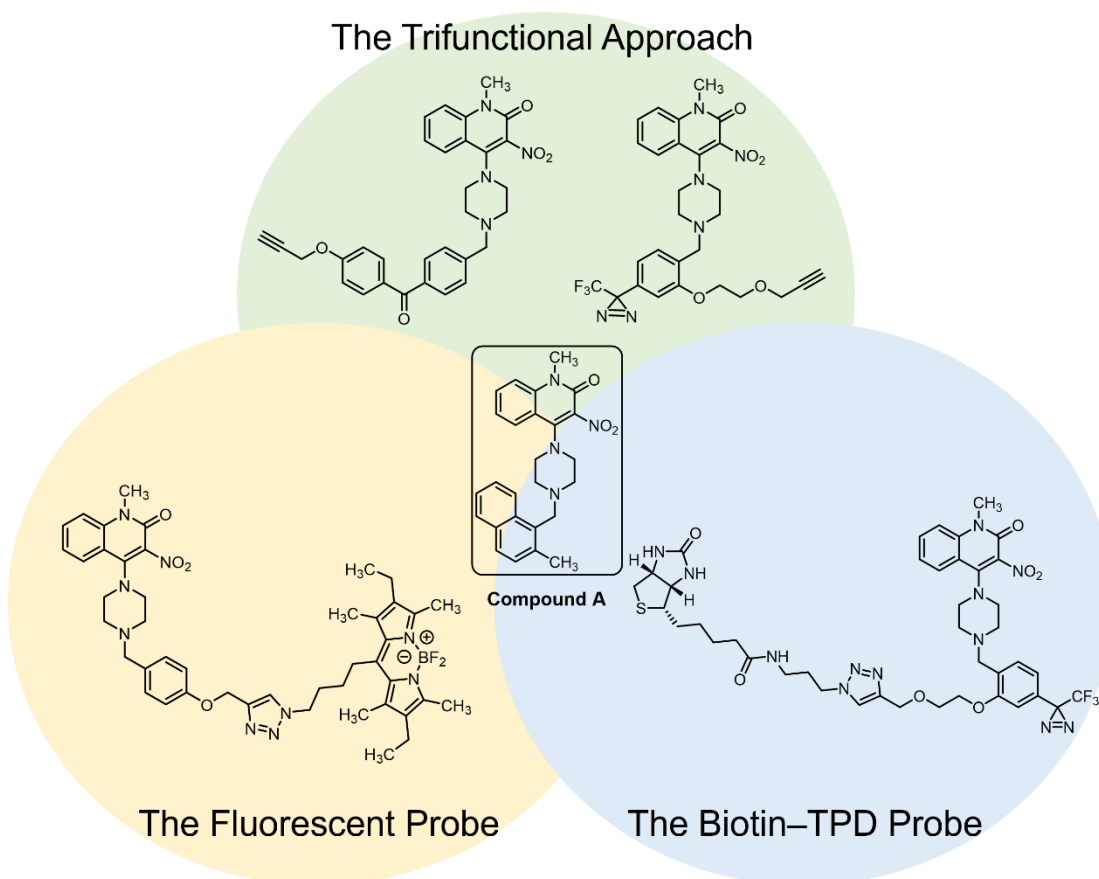


Figure 3.1. The molecular design of the trifunctional, fluorescent, and biotin-TPD probe molecules.

3.1.1 The Trifunctional Probe Molecules

The trifunctional approach makes use of molecular probes featuring an affinity ligand, a photo-crosslinker, and a bio-orthogonal functionality to fish out the protein target from a biological system. The workflow of the trifunctional approach includes three key steps. Firstly, the trifunctional probe is introduced to the biological system, such as live cells, followed by the application of UV irradiation to fix the probe–target interaction. Then, a CuAAC is performed to ensure a reporter tag, for instance, a fluorophore or a biotin is present on the ligand–protein complex for microscopic profiling or affinity capture. Finally, the streptavidin–biotin pull-down purification is

used to isolate the protein target(s), which subsequently can be analyzed and identified by LC-MS.

There are literature precedents describing the use of trifunctional probe molecules that lead to successful protein identification. One of these examples is the work by Shi and co-workers, who designed two trifunctional probe molecules, DA-1 and DA-2, to profile the potential cellular targets of Dasatinib (Figure 3.2).¹ Live cell imaging and in vitro pull-down experiments were made possible by attaching a rhodamine-azide or a biotin-azide via a CuAAC. Among two molecular probes, DA-2 demonstrated a better membrane permeability and helped the identification of 50 potential protein targets of Dasatinib.

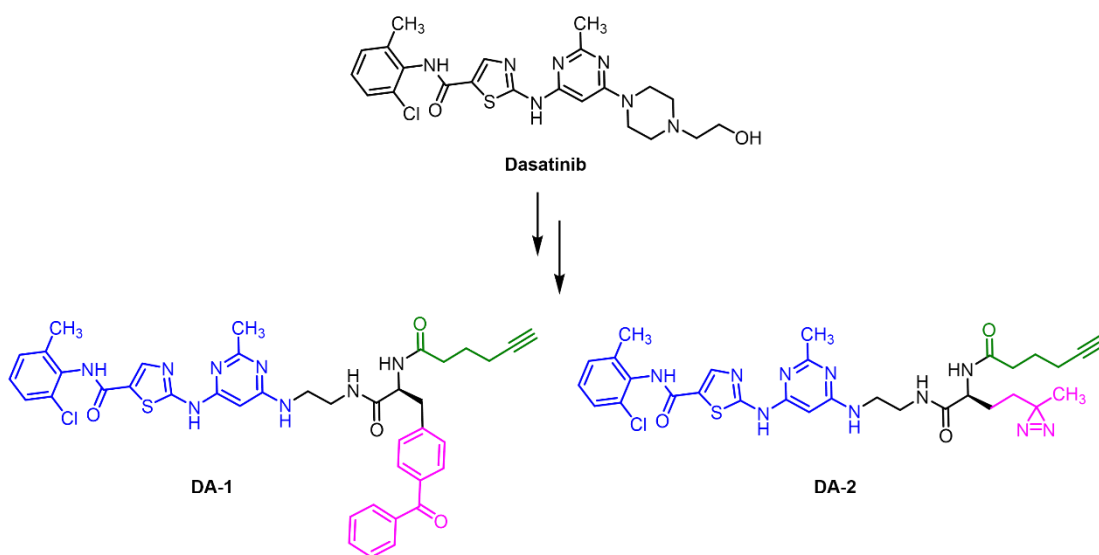


Figure 3.2. The molecular design of DA-1 and DA-2 based on the trifunctional approach.

3.1.2 The Fluorescent Small-molecule Probe

Fluorescent microscopy is a powerful technique that helps provide insight on complex cellular events, including protein–ligand interactions, protein distribution, and enzyme activities.^{2–5} The fundamental principle of fluorescent imaging makes use of a fluorescent protein or naturally occurring fluorescent molecules, such as tryptophan, NAD(P)H, and flavins, but more often by an introduced exogenous fluorescent compound. The luminescence emitted by the fluorophore is detected after absorbing energy near its excitation wavelength, giving the “colors” of the images.⁶

More recently, near infrared (NIR) fluorescence has been opening up the opportunity to visualize deeper tissues, as NIR light can penetrate further into the tissues without scattering.

3.1.2.1. The Selection of Fluorophores

The fluorophore that is incorporated in the compound must be selected carefully because the fluorescent imaging depends heavily on the properties of the fluorescent compound. Organic small-molecule fluorophores are of particular interest because they are easier to handle, inexpensive, and their excitation and emission properties can be fine-tuned through structural modifications.^{7,8} Some of the representative fluorophores that have been used commonly in bioimaging include coumarin, fluorescein, rhodamine, BODIPY, and cyanine dyes (Figure 3.3).^{9,10}

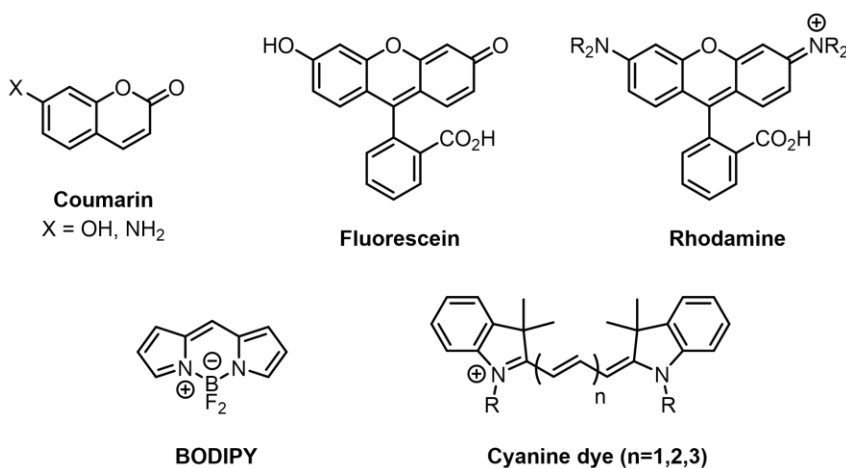


Figure 3.3. Fluorophores that have been used commonly in bioimaging.

7-Hydroxycoumarin absorbs light at the ultraviolet region, which makes it a common ingredient in sunscreens. Other derivatives of coumarin display a broad spectrum of excitation wavelengths; for example, 3-phenyl-7-hydroxycoumarin has an ex/em of 420/481 nm.¹¹ Fluorescein becomes negatively charged under physiological pH, making it difficult to travel through the cell membrane. Conversely, rhodamine, a cationic molecule, can penetrate through the cell membrane easily. It has the tendency to accumulate in the membrane of mitochondria, therefore, has been used to measure the membrane polarization of mitochondria.¹² The key features of

BODIPY derivatives include small Stokes shift, high quantum yield, and good lipophilicity.^{13–16} Cyanine dyes demonstrated widespread applications in animals or in vivo imaging for their ability to absorb NIR energy.

3.2 Results and Discussion

3.2.1 The Trifunctional Probe Molecules

In light of the previously encountered problems and the reported successful examples, a decision was made to design trifunctional probe molecules. We rationalized that the incorporation of a photo-crosslinker could help improve the efficiency of labelling the protein by establishing a covalent bond. The alkyne functionality provides a point of extension for the installation of different reporter tags through CuAAC. This led us to design different trifunctional probe molecules that contain either a TPD or a BP as the photo-crosslinker and an alkyne as the bio-orthogonal tag. Two BP-containing trifunctional probe molecules and one TPD-containing trifunctional probe molecule were proposed as our third generation probe molecules (Figure 3.4).

The TPD was preferred over the aliphatic diazirines due to its reported stability under various chemical conditions.¹⁷ The two proposed BP-bearing trifunctional probes differ by the presence or absence of one methylene group, which would allow for modulating the optical properties of the benzophenone moiety.¹⁸ It is expected that direct substitution of a propargyl ether oxygen atom para to the benzophenone C=O as in the case of **1** was anticipated to affect absorption maxima and/or molar absorptivity.

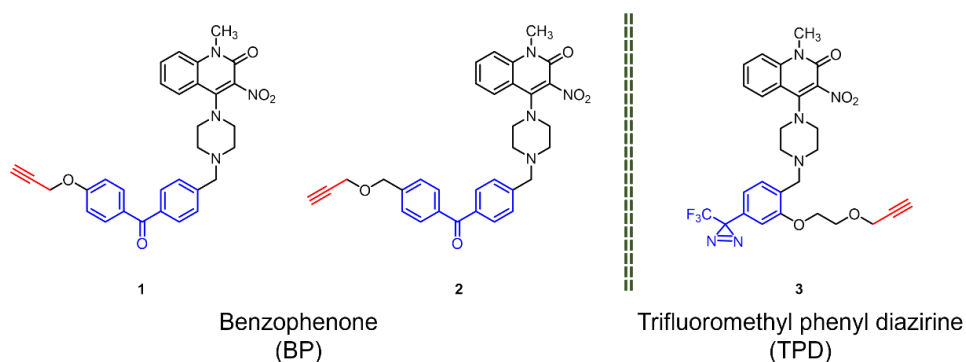
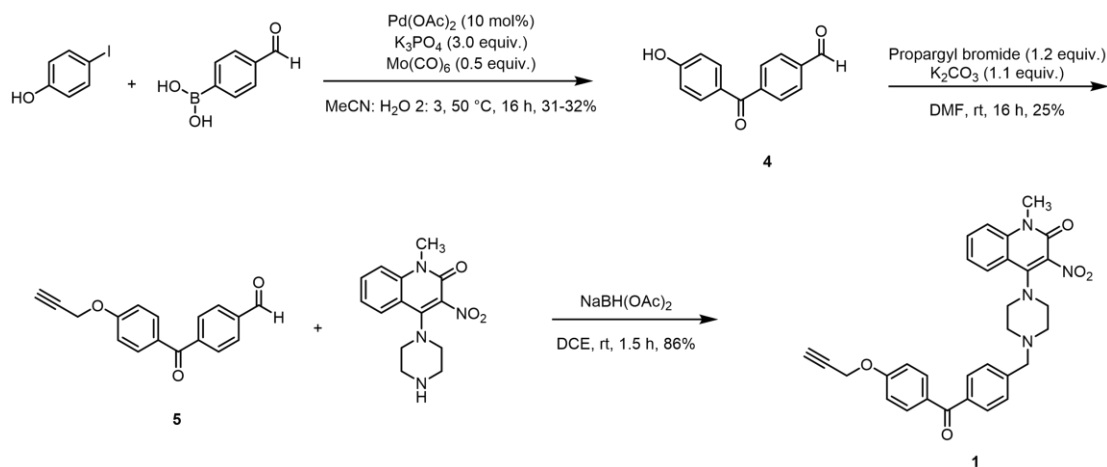


Figure 3.4. The proposed trifunctional probe molecules.

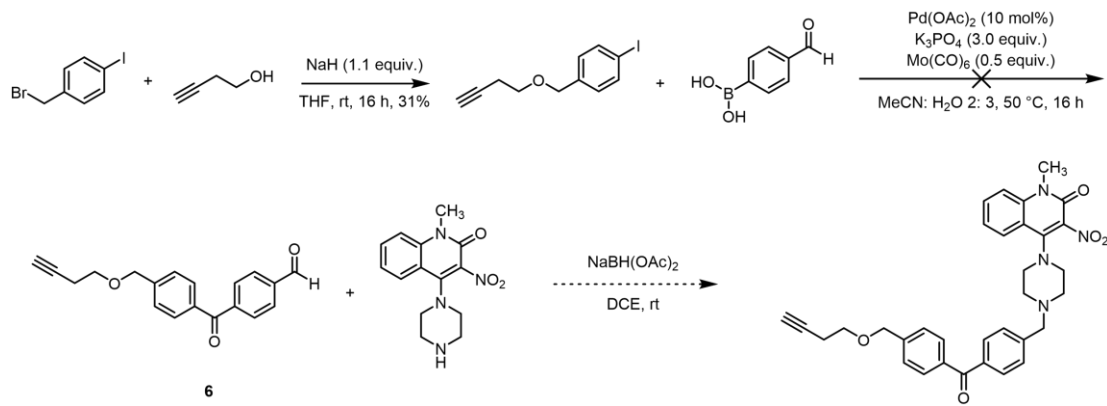
3.2.1.1 Synthesis of BP Probe Molecules 1 and 2

To initiate the synthesis of these probes, I started with the synthesis of the BP building blocks. The intermediate **4** was synthesized through the carbonylative Suzuki–Miyaura coupling between 4-iodophenol and 4-formylphenylboronic acid in 32% yield. Then, the synthesized intermediate **4** underwent an S_N2 reaction and reductive amination to afford the final BP-bearing trifunctional probe **1** (Scheme 3.1).



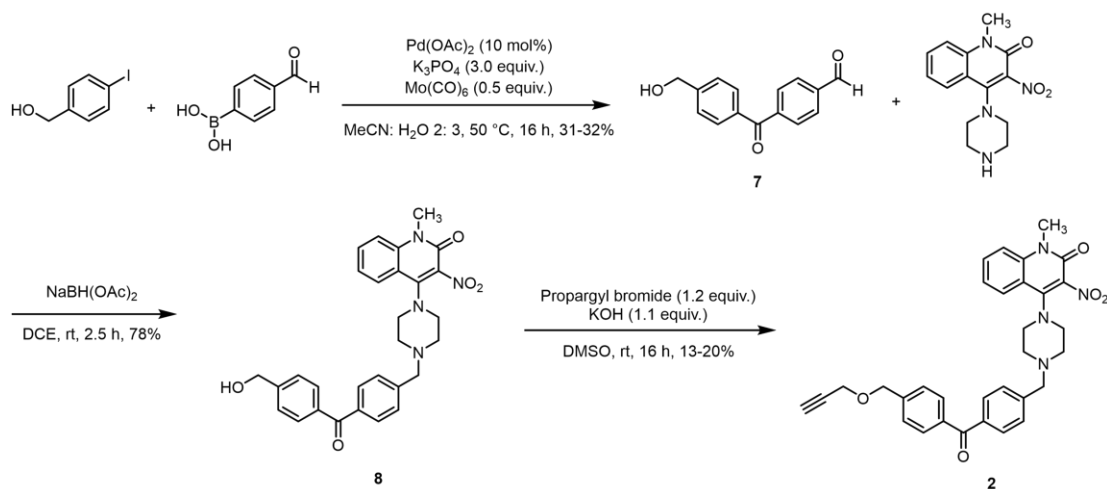
Scheme 3.1. The synthetic strategy of the BP-bearing trifunctional probe **1**.

In order to obtain probe **2**, I intended to synthesize the BP building block **6**. However, I did not see any appreciable conversion from the starting materials to the expected product **6**. The reason behind this might be that the terminal alkyne group is not tolerated during the carbonylative Suzuki–Miyaura coupling reaction (Scheme 3.2).



Scheme 3.2. The proposed synthetic strategy for a BP-bearing trifunctional probe.

Therefore, the strategy was revised, and a slightly modified BP building block **7** was obtained first via a carbonylative Suzuki coupling. Later, the final probe **2** was prepared by reductive amination, followed by an S_N2 reaction to install the terminal alkyne. However, the subsequent S_N2 reaction to introduce the propargyl group occurred only in low yields despite the examination of various reaction conditions, perhaps due to the reduced acidity of the benzylic alcohol relative to the phenolic hydroxyl found in intermediate **4** (Scheme 3.3). Due to the limited amount of probe **2** acquired, related experiments elaborated hereafter, including immunological assay and pull-down purification, were carried out using only probe **1**.



Scheme 3.3. The synthetic strategy of the BP-bearing trifunctional probe **2**.

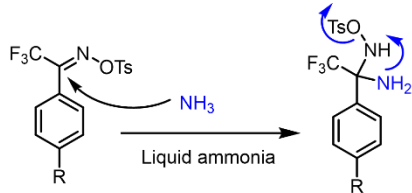
3.2.1.2 Synthesis of TPD Probe Molecule **3**

Aside from the two BP-bearing trifunctional probes **1** and **2**, we proposed a TPD-containing trifunctional probe (**3**) as another candidate (Figure 3.4). TPD was chosen as the photo-crosslinker because of its high reactivity after irradiation as well as its improved stability under chemical and photochemical conditions.¹⁷ Also, its relatively small size makes it an ideal option, as there is less chance of negatively impacting binding to the protein of interest.¹⁹

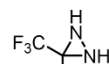
Initially, we wanted to circumvent the use of liquid ammonia in the laboratory to prevent potential safety hazards.²⁰ We found a literature precedent, describing the synthesis of TPD without applying liquid ammonia.²¹ In this article,

O-mesitylenesulfonyl hydroxylamine (MSH) was used as a liquid ammonia surrogate to introduce the second nitrogen of the diazirine functionality (Scheme 3.4).

TPD synthesis with liquid ammonia



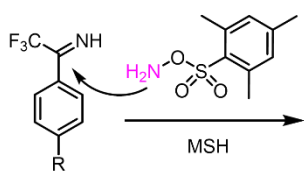
Ring closure



[O]



TPD synthesis with MSH



Ring closure

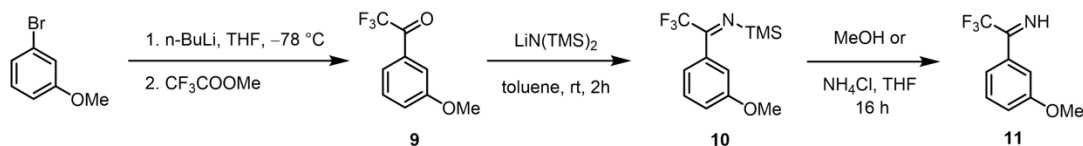
diaziridine

diazirine

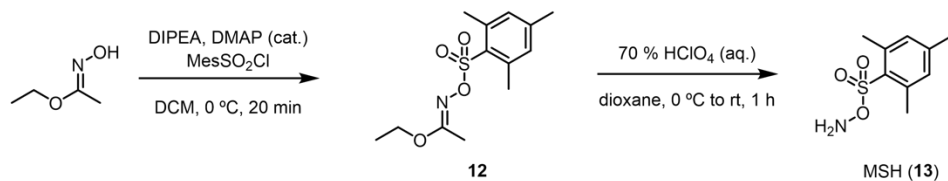
Scheme 3.4. TPD synthesis utilizing liquid ammonia or the nitrogen surrogate, MSH.

The synthesis of the imine counterpart **11** started from the metal–halogen exchange reaction between 3-bromoanisole and *n*-BuLi, followed by the trifluoroacetylation of the aryl lithium intermediate generated to yield the trifluoromethyl phenyl ketone **9** (Scheme 3.5). Then, this ketone **9** was subjected to treatment with lithium bis(trimethylsilyl)amide to provide the *N*-TMS-ketimine **10**, which subsequently underwent TMS deprotection in methanol or ammonium chloride in tetrahydrofuran (THF) to provide the corresponding imine **11** (Scheme 3.5a). On the other hand, MSH **13** was synthesized from the procedure reported by Tamura et al.²² The mesitylation reaction of the oxime gave the intermediate **12**, which later was hydrolyzed to give MSH **13** (Scheme 3.5b). After the two starting materials **11** and **13** were prepared, we intended to synthesize the diaziridine scaffold **14**. The imine **11** was treated with MSH **13** in THF at 0 °C, then, piperidine was used to quench the excess amount of MSH that was still present in the reaction (Scheme 3.5c). Unfortunately, we did not observe the formation of the desired diaziridine **14**. We speculated that the possible reasons behind this unsuccessful reaction might be the incomplete desilylation of **10**, the lability of the moisture-sensitive imine **11**, or the poor stability of MSH **13**.^{23,24}

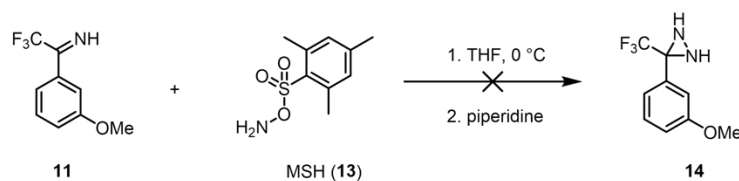
a) Synthesis of trifluoromethyl imine



b) MSH Synthesis

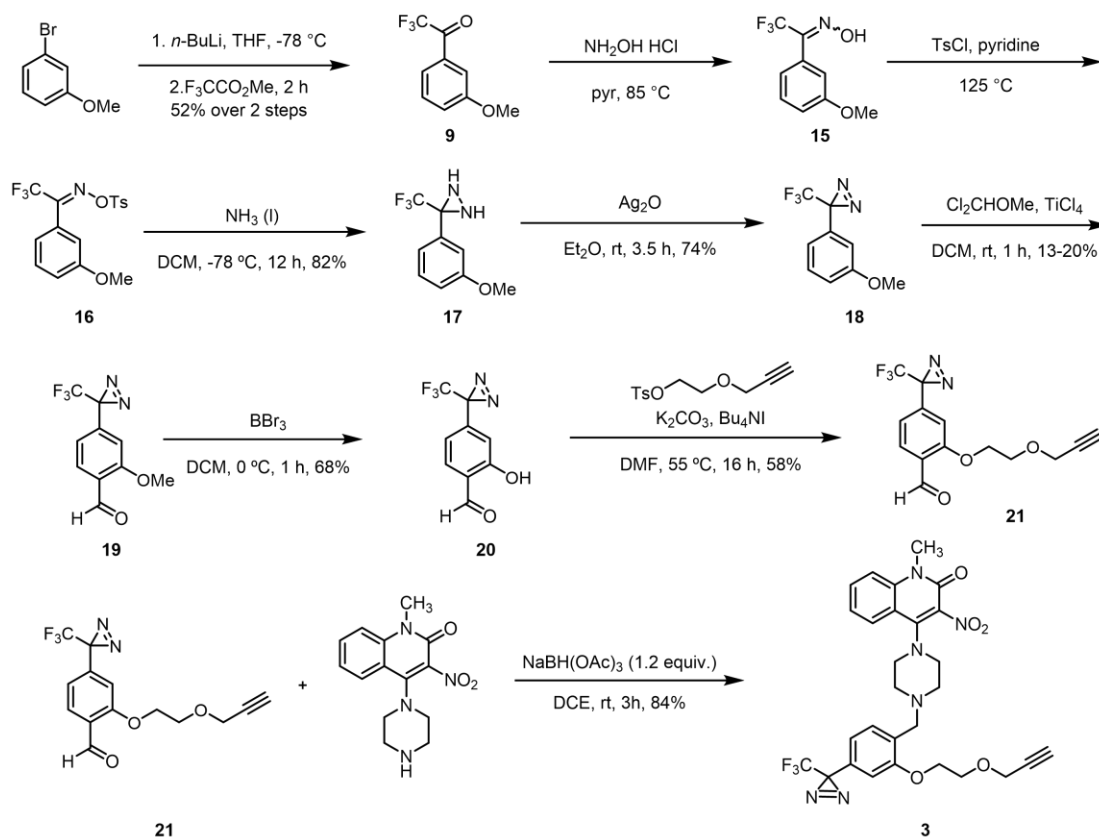


c) Diaziridine formation with MSH



Scheme 3.5. The synthesis of the imine **11**, MSH **13**, and the attempted synthesis of diaziridine **14**.

Thus, use of liquid ammonia in the preparation of our target TPD probe became inevitable. The synthesis of the trifunctional probe **3** followed a procedure published by Mayer and co-workers.²⁵ The trifluoromethyl phenyl ketone **9** was converted to the oxime **15** with hydroxylamine hydrochloride, which was tosylated to the corresponding *O*-tosyl imine **16**. Then, liquid ammonia was introduced to the reaction at $-78\text{ }^{\circ}\text{C}$ to afford the diaziridine **17** in good yield. The diaziridine **17** was oxidized to the diazine **18**, using silver oxide. The formyl group *para* to the diazine was installed via the Friedel–Crafts alkylation to give the TPD–aldehyde **19**, which underwent demethylation, employing boron tribromide (BBr_3) and an $\text{S}_{\text{N}}2$ reaction with a terminal alkyne to provide the TPD–alkyne precursor **21**. Finally, the trifunctional probe **3** was synthesized smoothly via reductive amination between the TPD–alkyne precursor **21** and the affinity ligand (Scheme 3.6).



Scheme 3.6. The synthesis of the trifunctional probe **3** using liquid ammonia.

3.2.1.3 The Immunological Result of the Synthesized Probes **1** and **3**

After the probes were prepared successfully, their biological activity was evaluated. To our delight, both **1** and **3** showed moderate to good activity to stimulate the production of IL-2 (Figure 3.5). Of the two probes, the TPD-containing compound **3** demonstrated superior ability to induce IL-2 production in a dose-dependent manner (Figure 3.5b). Therefore, we decided to carry out most of the future experiments using the TPD trifunctional probe **3**.

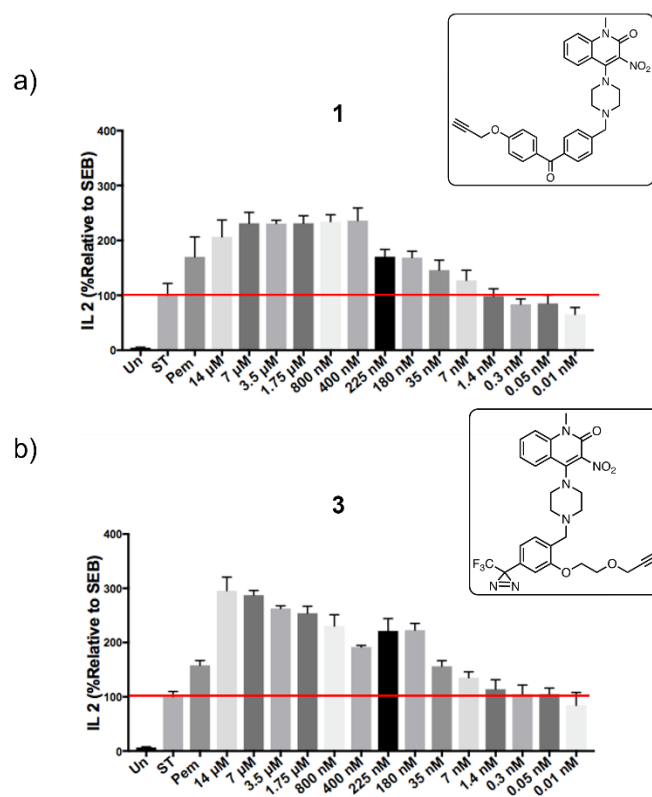


Figure 3.5. The immunological result of trifunctional probes **1** (panel a) and probe **3** (panel b). Un: PBMCs without SEB activation. ST: PBMCs activated with SEB without treatment with small molecule. Pem: PBMCs activated with SEB treated with pembrolizumab. Cell culture supernatant was acquired after SEB-stimulated PBMCs treated with antibody or small molecule. IL-2 production was measured using an ELISA.

3.2.2 Optimization of the Click Reaction and Photoaffinity Labelling

3.2.2.1 Stability Test of Diazirine in Click Reaction Conditions

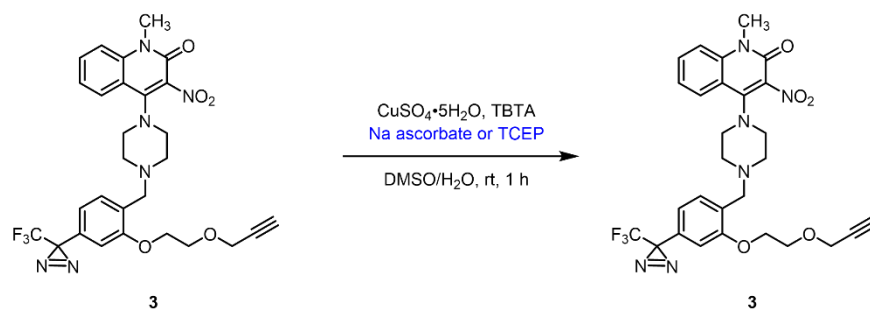
Before performing any “click chemistry” with the synthesized probe **3**, we sought to assess the stability and compatibility of TPD with the selected reagents for the CuAAC. We settled on copper sulfate pentahydrate ($\text{CuSO}_4 \cdot 5\text{H}_2\text{O}$) as the catalyst, as it remains the most classic and widely used catalyst for the CuAAC. The catalytically active species, Cu(I), can be generated in situ by the presence of a reducing agent.²⁶

As reducing reagents, we decided to evaluate sodium ascorbate and tris(2-carboxyethyl)phosphine (TCEP) for the proposed reaction. Reported by Sharpless and Fokin, the combination of $\text{CuSO}_4 \cdot 5\text{H}_2\text{O}$ and sodium ascorbate as the reducing agent possesses the advantage of tolerating aqueous and aerobic

conditions.^{27,28} Another common choice of reducing agent, TCEP, is used often to prevent the oxidation of sensitive protein residues presented in the system.^{29–31}

Also, Sharpless and colleagues pointed out that the incorporation of ligands can accelerate the cycloaddition process.²⁹ These ligands, usually polydentate *N*-donor chelators bearing a central tris(triazolylmethyl)amine scaffold, coordinate to the copper atom, enhancing both the stability and catalytic activity of the transition metal. Tris((1-benzyl-4-triazolyl)methyl)amine (TBTA) has been shown to be a potent promoter that enhances the reaction rate; therefore, it was chosen to be employed in our experiment.

To examine the stability of trifunctional probe **3** in the presence of reagents, it was mixed with the chosen CuAAC reagents without adding the azide counterpart (Scheme 3.7). The reactions were kept in the dark for an hour and were monitored and analyzed by LC-MS. Fortunately, LC-MS strongly indicated that intact probe **3** still was present in the reaction media, and no sign of decomposition was seen. Therefore, we concluded that TPD is stable enough to undergo click reactions under the set conditions.

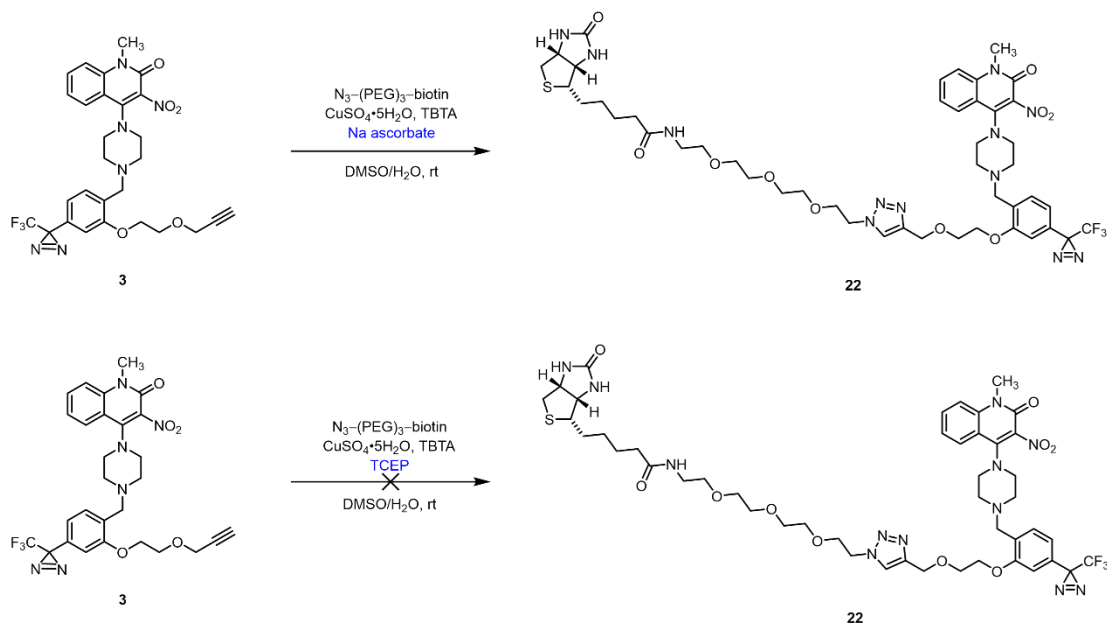


Scheme 3.7. The stability test of TPD under the selected reaction conditions.

3.2.2.2 Comparison of Two Reducing Agents

Later, we proceeded to examine the efficacy of two reducing reagents, sodium ascorbate and TCEP. Two click reactions were carried out in parallel, utilizing different reducing agents and biotin–(PEG)₃–azide (Scheme 3.8). Both reactions were monitored via LC-MS after one hour and three hours. The formation of the product **22** was confirmed by LC-MS and high-resolution ESI only when sodium ascorbate was employed as the reducing agent. We assumed that the failure of the reaction

when using TCEP was due to the reduction of the biotin-(PEG)₃-azide to the corresponding amine by TCEP via the Staudinger reduction.^{32–36} Based on the observations, we decided to carry out the CuAAC using sodium ascorbate as the reducing agent in the future.

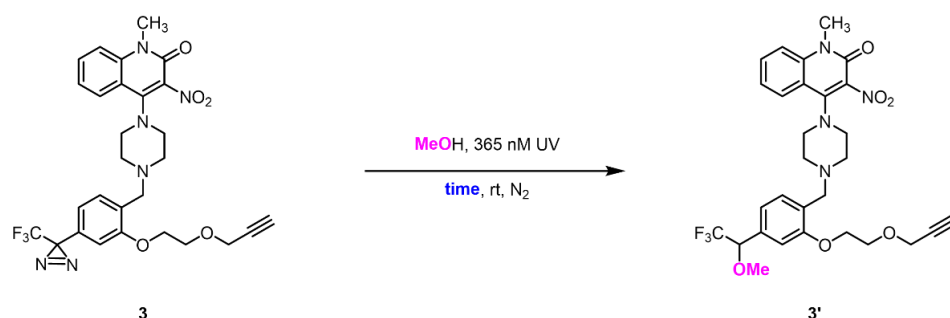


Scheme 3.8. The comparison between sodium ascorbate and TCEP as the reducing agent.

3.2.2.3 Photoaffinity Labeling Experiment With Probe **3** in Methanol

After the suitable condition for the CuAAC was established, we started to look for an appropriate irradiation time for the photoaffinity labelling experiment. Prior to the labelling experiment with BSA, we decided to use methanol trapping off the carbene intermediate as a measure for consumption of the diazirine (Scheme 3.9).²⁵ The probe **3** was dissolved with methanol in glass vials, which were kept under a UV lamp over variable periods of time, including 30, 60, 90, and 120 min, while one vial was kept in the dark as the negative control. The samples were monitored and analyzed by LC-MS after each specific irradiation time. The methanol adduct **3'** was observed through LC-MS analysis after 30 min of light exposure, suggesting that the photoaffinity labelling had occurred between probe **3** and methanol. Also, significantly more complex by-products were observed once the irradiation time

exceeded 60 min. Therefore, we selected a 60 min irradiation time for the proof-of-concept BSA labelling experiment.



Scheme 3.9. Photoaffinity labelling using methanol as the substrate.

3.2.3 Proof-of-concept BSA Labelling Experiment Using the Probe **3**

With the optimized conditions in hand, I decided to attempt another labelling experiment, using BSA as a model protein. I tried to perform the photoaffinity labelling on the BSA sample that was pre-incubated with **3**, followed by a CuAAC of the irradiated sample (Figure 3.6). The sample was desalted with a C18 reverse phase column before it was analyzed by MALDI.

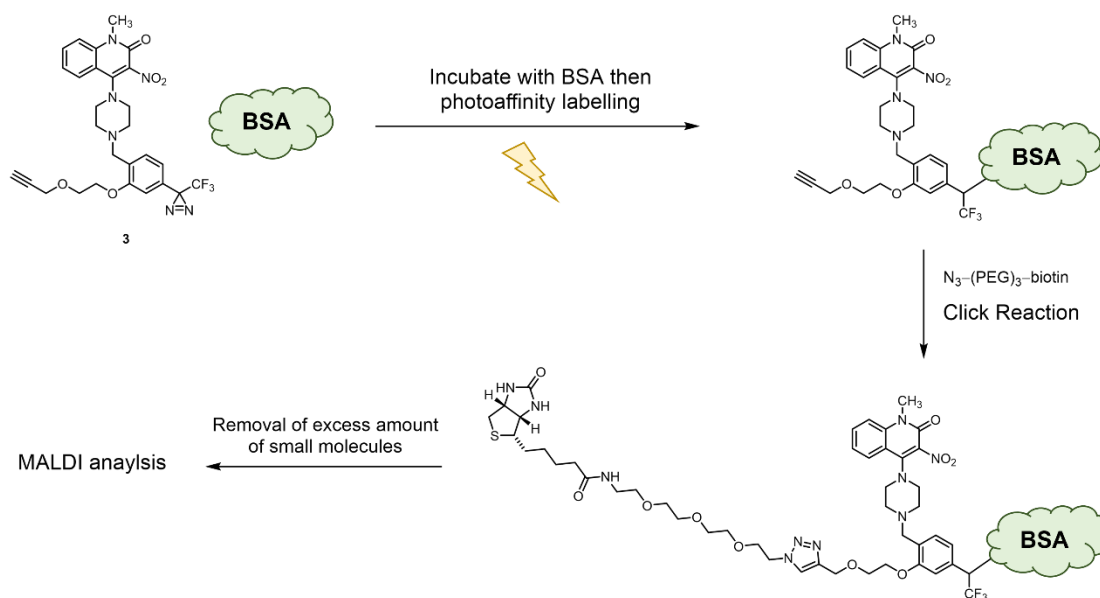


Figure 3.6. The workflow of the proof-of-concept BSA labelling experiment.

However, no obvious increase in molecular weight of the labelled BSA was observed (Figure 3.7). Also, the concentration of the labelled BSA was too low to draw a clear conclusion on the result of the labelling experiment. An alternative strategy of conducting the click reaction prior to photoaffinity labelling was brought up to improve the readout of the experiment. This could ensure the full conversion of probe **3** to the desired compound **22** as well as help prevent storing BSA under room temperature for prolonged time.

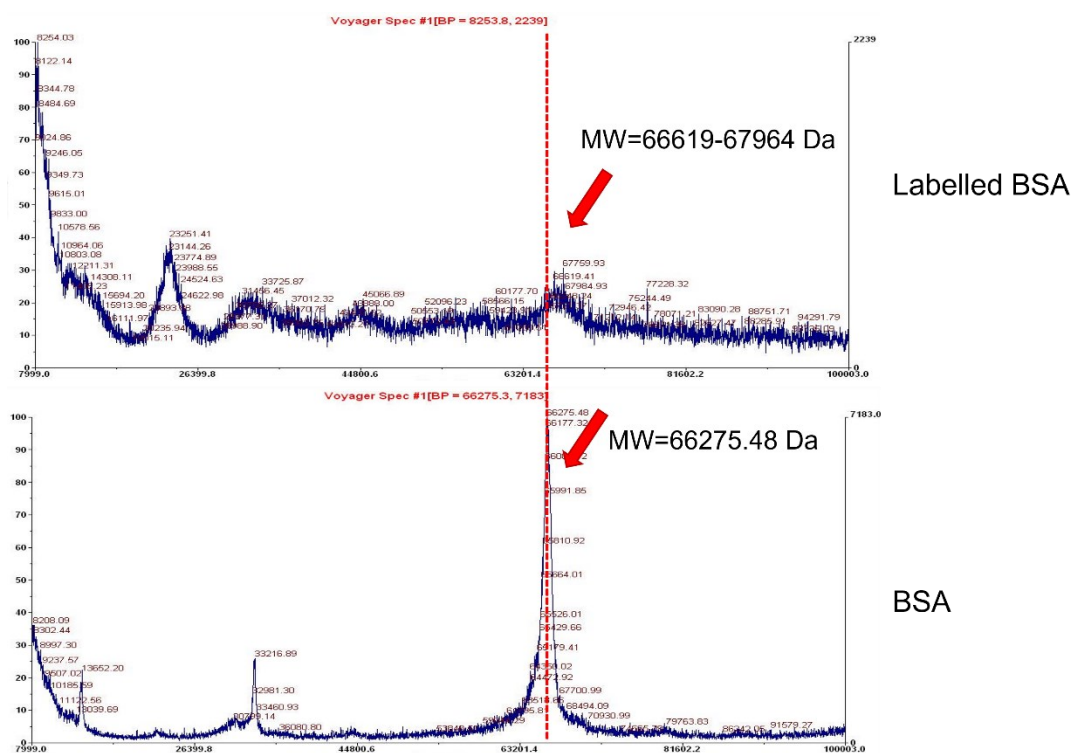


Figure 3.7. The MALDI result of the first photoaffinity labelling experiment.

Based on the abovementioned result, we began another labelling experiment by performing the click reaction first (Figure 3.7). The formation of **22** and the consumption of **3** were monitored by LC-MS. Next, the reaction mixture was added directly to the solution of BSA and incubated for 20 min. Then, the sample was exposed to UV light for 1 h. The reaction was designed in such a way that the ratio of **22**:BSA was greater than 10:1, which could help to ensure the sufficient binding of **22** to the protein. Finally, the irradiated sample was desalted with a C18 reverse-phase

column to remove any salt present in the sample that could affect the result of the MALDI analysis.

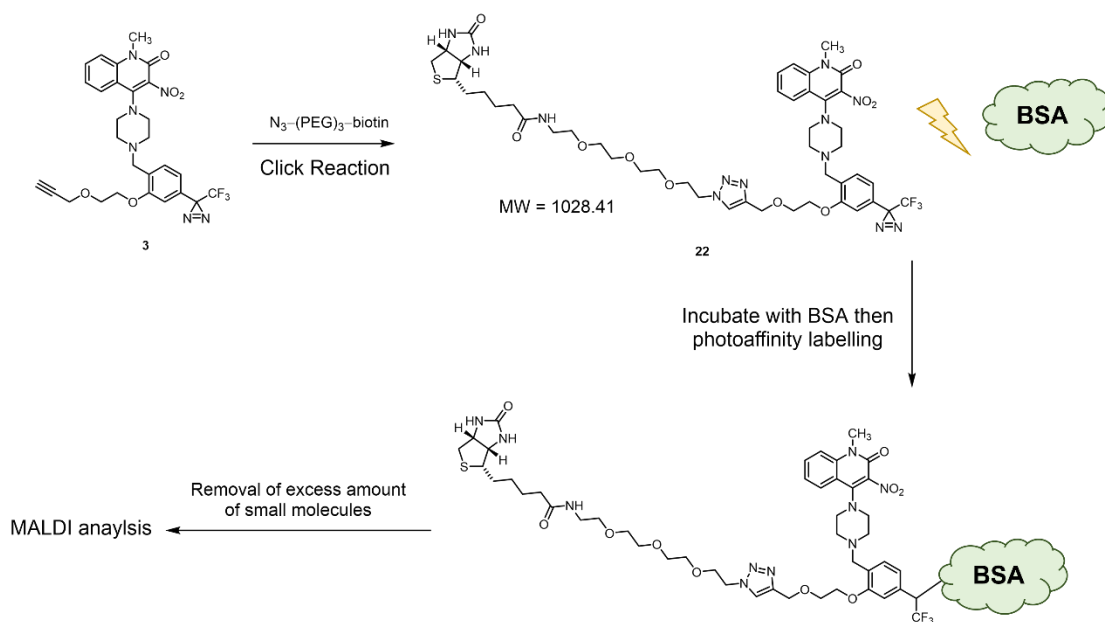


Figure 3.8. The revised workflow of the proof-of-concept BSA labelling experiment.

By these actions, we were pleased to see an obvious increase in the molecular weight of the labelled BSA (Figure 3.9). The broadening of the peak implied the formation of a heterogeneous mixture of labelling products due to reaction at more than one site, and some degree of reaction with more than one molecule of probe **22**. On the basis of this result, we concluded that TPD-based probe **3** would be suitable for efforts to identify the unknown protein target of **Compound A**.

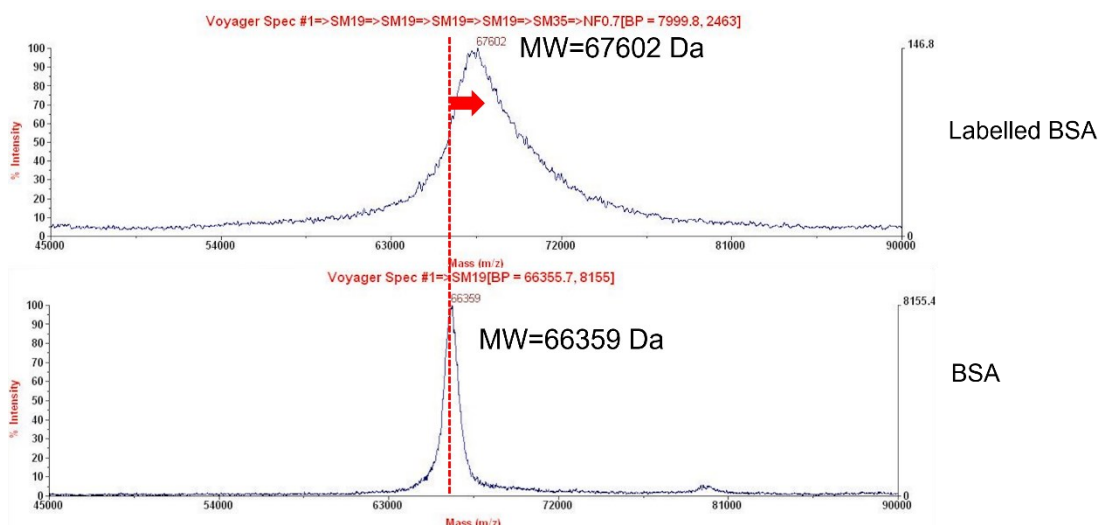


Figure 3.9. The MALDI result of the labelling experiment utilizing the TPD-containing probe **3**.

3.2.4 The Biological Workflow Using Probe **3**

With the successful photoaffinity labelling result obtained, we submitted the TPD-containing probe **3** to our collaborators for the affinity pull-down purification. The workflow of the pull-down purification, using the probe **3**, is outlined briefly here (Figure 3.10). In the beginning, the probe **3** was treated to the peripheral blood mononuclear cell (PBMCs) and incubated for six hours. The cells later were exposed under UV light for an hour, lysed, followed by the measurement of the protein concentration. Then, the CuAAC was carried out in the cell lysate to introduce a biotin tag. Finally, the labelled proteins were purified using streptavidin, and were subsequently analyzed by the Western blot and LC-MS.

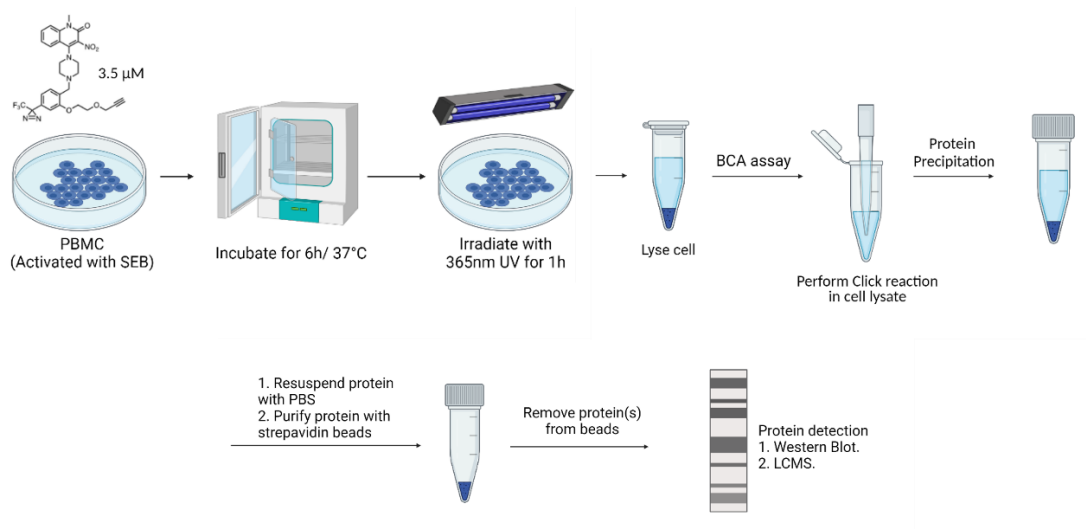


Figure 3.10. The biological workflow utilizing probe **3** in attempts to isolate the protein of interest.

3.2.4.1 The Result of Immunoblotting

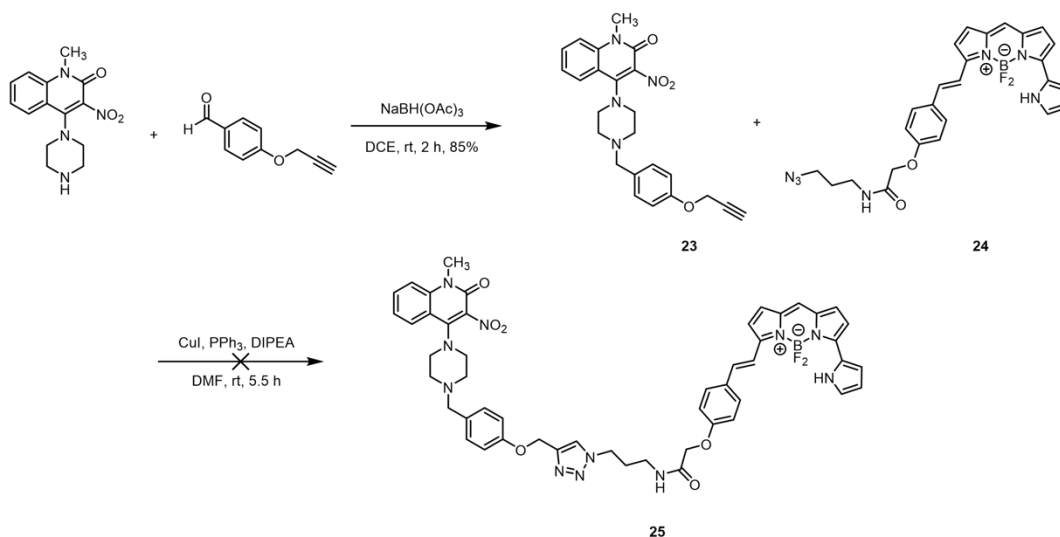
During the experiments, we suffered constantly from inconsistent and irreproducible results of the immunoblotting (result not shown). The main concern was that the efficacy of the CuAAC could not be confirmed when it was performed in cells. Another speculation was that the amount of protein acquired was too low to produce a valid result. This might have originated from the fact that the PBMCs are heterogenous cells, which are composed of multiple cell types.

3.2.5 The Fluorescent Probe Molecules

Applying fluorescent probe molecules in the project can provide additional information on the whereabouts of the protein target. To design the fluorescent probe that will be utilized in confocal microscopy, an appropriate fluorophore needs to be decided first. The fluorophore that is chosen should fulfill several criteria. First, the excitation wavelength for fluorescent compounds should fall outside the wavelength used for photoaffinity labelling, which is around 350 nm to 365 nm, Next, the ex/em window of the selected fluorophore should not overlap with commonly used biomarkers, such as 4',6-diamidino-2-phenylindole (DAPI, ex/em: 358/461). Also, a longer excitation wavelength is desired, which is more compatible with the biological systems. After considering these criteria, we settled on using a BODIPY scaffold as the fluorophore to be incorporated into the probe molecule.

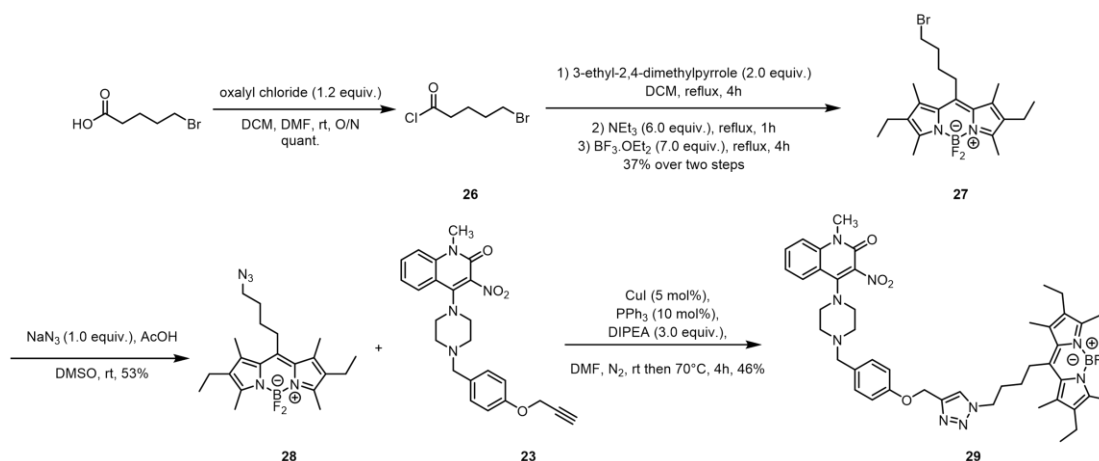
3.2.5.1 Synthesis of the Fluorescent Molecules

First, I worked on the synthesis of the fluorescent probe molecule **25**. The alkyne **23** was synthesized by reductive amination, then later was subjected to a CuAAC with the commercially available BODIPY fluorophore **24** (Scheme 3.10). However, the expected fluorescent probe **25** was not observed due mainly to the limited material available and the difficult purification and characterization process of the product.



Scheme 3.10. The synthesis of the BODIPY-containing fluorescent probe **25**.

Later, a decision was made to synthesize the BODIPY scaffold in the laboratory.^{37,38} The BODIPY scaffold was synthesized in three reaction steps. Firstly, 5-bromovaleric acid was treated with oxalyl chloride in the presence of catalytic amounts of DMF to generate the corresponding acyl chloride. Secondly, it was reacted with two equivalents of the substituted pyrrole to provide the substituted 2,2'-dipyrromethene. Lastly, the complexation with boron trifluoride provided the desired BODIPY **27**. Subsequently, the nucleophilic substitution reaction, employing sodium azide, led to the desired BODIPY-azide **28** in moderate yield.³⁹ The synthesized BODIPY-azide **28** and the alkyne **23** underwent a CuAAC, employing the previously established reaction conditions, to yield the final fluorescent probe **29** in 46% yield (Scheme 3.11).



Scheme 3.11. The synthesis of the fluorescent probe molecule **29**.

3.2.5.2 The Immunological Result of the Fluorescent Probe Molecules

We found that although the synthesized fluorescent probe **29** only demonstrated moderate activity toward the production of IL-2, its activity is comparable to pembrolizumab at μM concentrations (Figure 3.11). We considered that probe **29** still possessed adequate activity to be applied in the microscopic experiments.

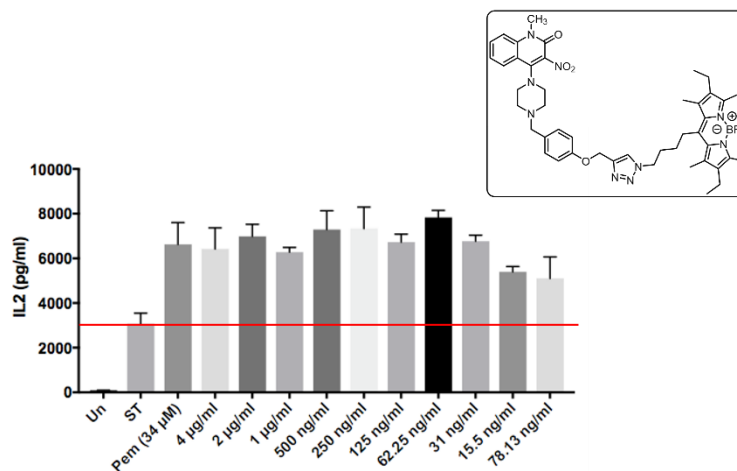


Figure 3.11. The immunological result of the fluorescent probe **29**. Un: PBMCs without SEB activation. ST: PBMCs activated with SEB without treatment with small molecule. Pem: PBMCs activated with SEB treated with pembrolizumab. Cell culture supernatant was acquired after SEB-stimulated PBMCs treated with antibody or small molecule. IL-2 production was measured using an ELISA.

3.2.5.3 Fluorescent Analysis

In order to find the optimal excitation wavelength for the microscopic experiments, the fluorescent analysis of probe **29** was performed. The fluorescent probe **29** has two

excitation wavelength, 385 nm and 495 nm, and emits at 548 nm (Figure 3.12a). The result showed that the probe **29** meets the criteria of having long excitation wavelength and does not overlap with other commonly used biomarkers. We also conducted the concentration-dependent fluorescent analysis of probe **29** to see under what concentration the strongest fluorescence would be observed. According to the results, when the irradiation at 490 nm wavelength was applied, the highest fluorescent signal was recorded at 0.09 μM concentration and dropped as the concentration decreased (Figure 3.12b). The strongest signal was recorded at 0.18 μM concentration when a 400 nm excitation was applied; this gradually decreased with the concentration (Figure 3.12c).

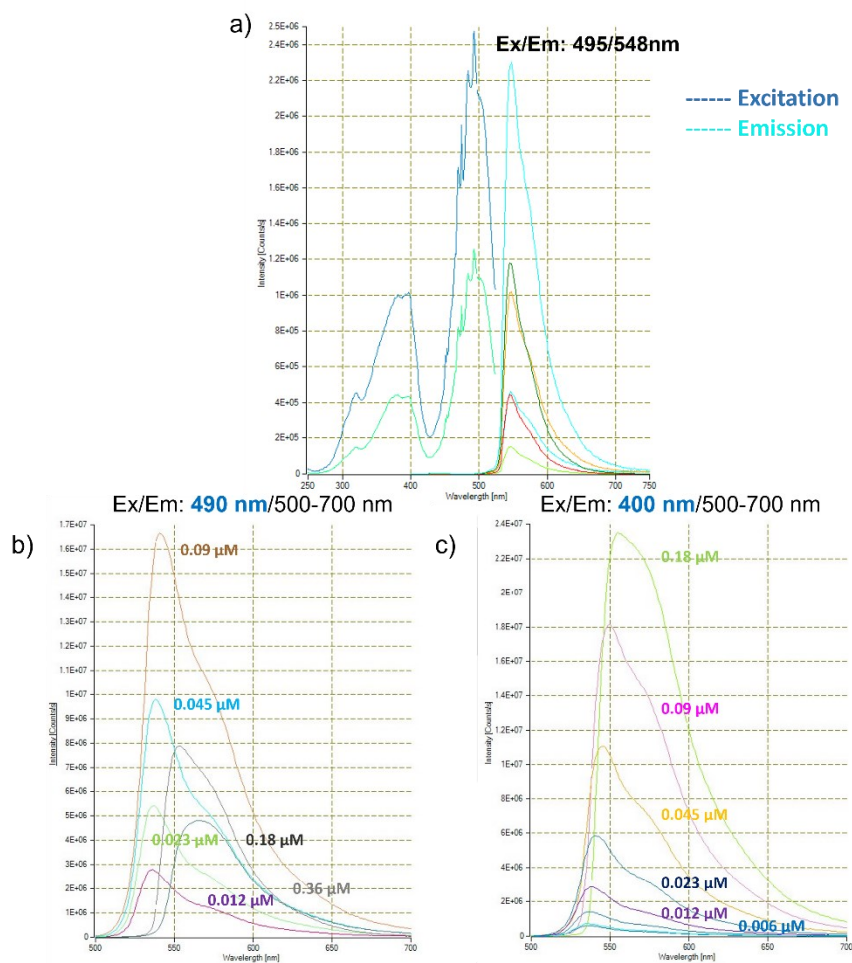


Figure 3.12. a) The fluorescence analysis of probe **29** and the concentration-dependent fluorescent analyses when b) 490 nm or c) 400 nm excitation was applied.

3.2.5.4 Confocal Microscopy and High-content Live Cell Imaging

We were fortunate to receive help from a graduate student in the Campbell group at the University of Alberta to lead the microscopic experiments. First, we performed a real-time high content imaging to study the kinetic uptake of probe **29** by the PBMCs. This experiment takes advantage of the ImageXpress high-content imager, which is capable of automatically acquiring images at different time points and different conditions. Images were taken at zero hour, two hours, four hours, and six hours with various concentrations ranging from 4.8 μM to 0.02 μM (Figure 3.13). Results showed that the uptake of the molecule by the cells increased with concentration and time, which suggested that the molecule exhibited good membrane permeability.

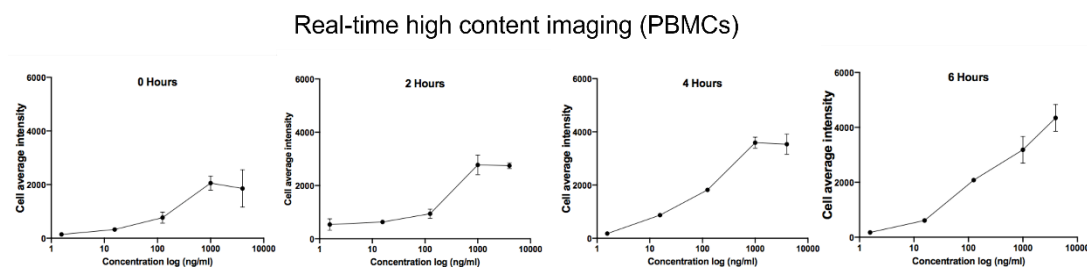


Figure 3.13. The real-time high content imaging of probe **29** with PBMCs.

Then, we moved forward to the confocal microscopy experiments. The PBMCs were incubated with the probe **29** over variable time periods, including 10 minutes, one hour, three hours, and six hours. The cells were washed to remove any unbound **29**, fixed, and harvested for imaging. The results were captured by the Leica Falcon SP8 STED System equipped in the cell imaging facilities at the Department of Oncology, University of Alberta.

In the confocal microscopy, we observed that the probe **29** possessed good membrane permeability and traveled through the membrane within a short period of time, which agreed with the result from the real-time high content imaging (Figure 3.14). The probe **29** distributed evenly throughout the cytoplasm but was not seen on the membrane nor in the nucleus. However, there was no specific pattern of accumulation found to indicate in which cytosolic compartment the probe may reside. Another imaging experiment, using HEK239 cells, further indicated that the

distribution of probe **29** lacked cell specificity, as a similar result was seen (data not shown).

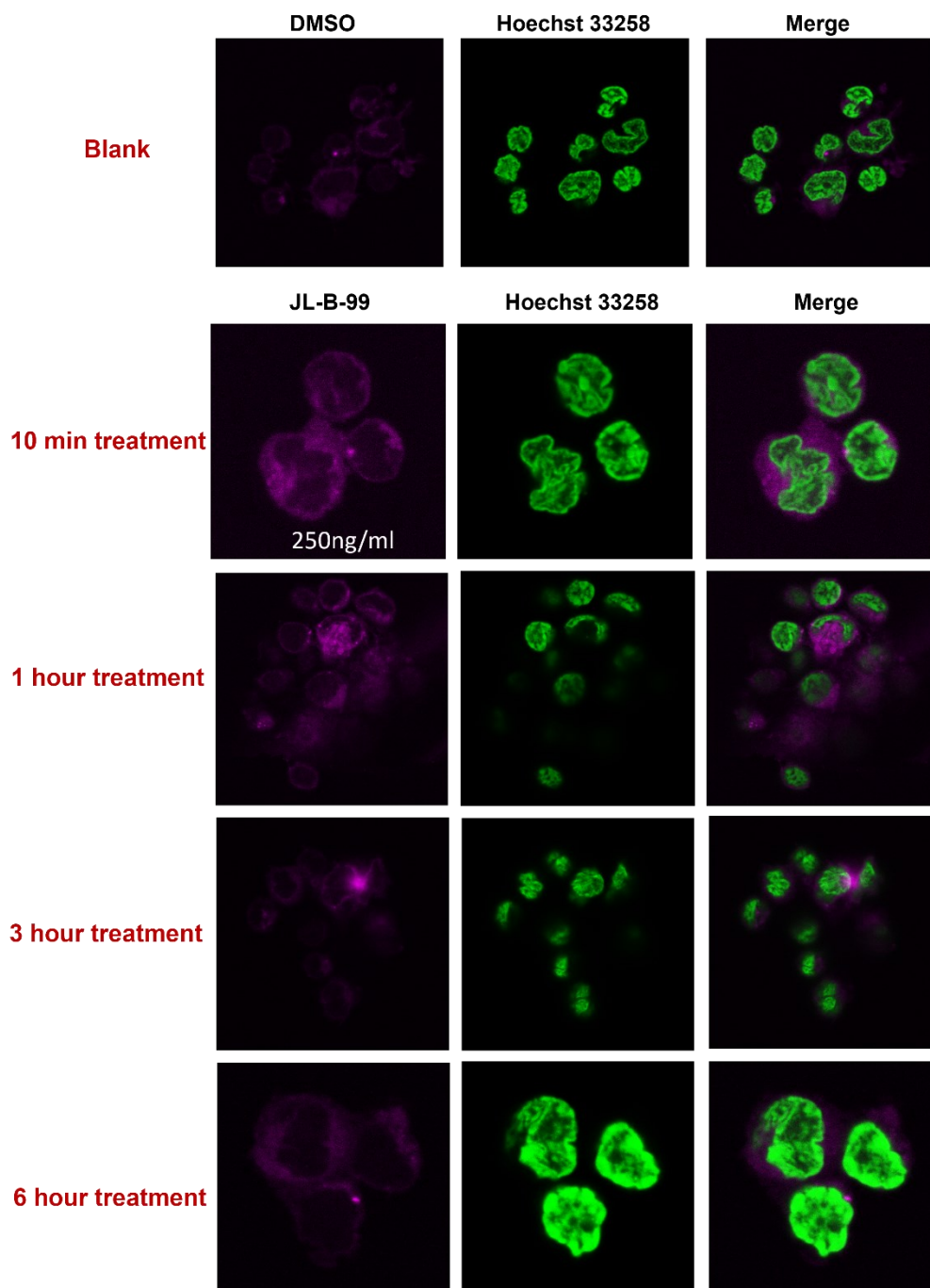


Figure 3.14. Confocal microscopy using the probe **29**. The nuclei were stained with Hoechst 33258. The left panel shows the fluorescent after PBMCs were treated with probe **29** and the right panel shows the merged images.

3.2.6 The Biotin–TPD Probe Molecule

The inconclusive results from the confocal microscopy and the real-time high content imaging made us prioritize the pull-down purification for protein isolation. The biotin–TPD probe molecules were proposed because we were not able to ascertain the efficiency of the CuAAC when it was carried out in the cell lysate (Figure 3.15). The pre-installation of the biotin functionality could help to circumvent the need of performing the CuAAC in the biological system and, at the same time, clinch the formation of the desired click product. Another risk is potential sequestration of the probe by biotin-binding proteins present in the cells or the media.

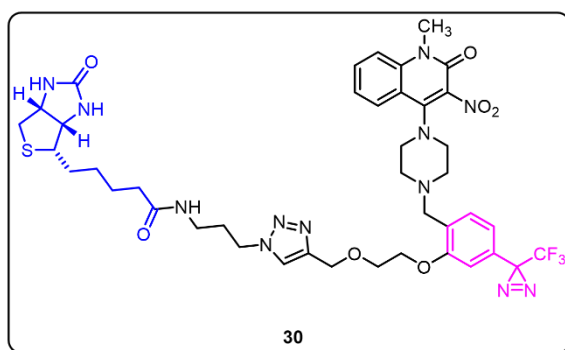
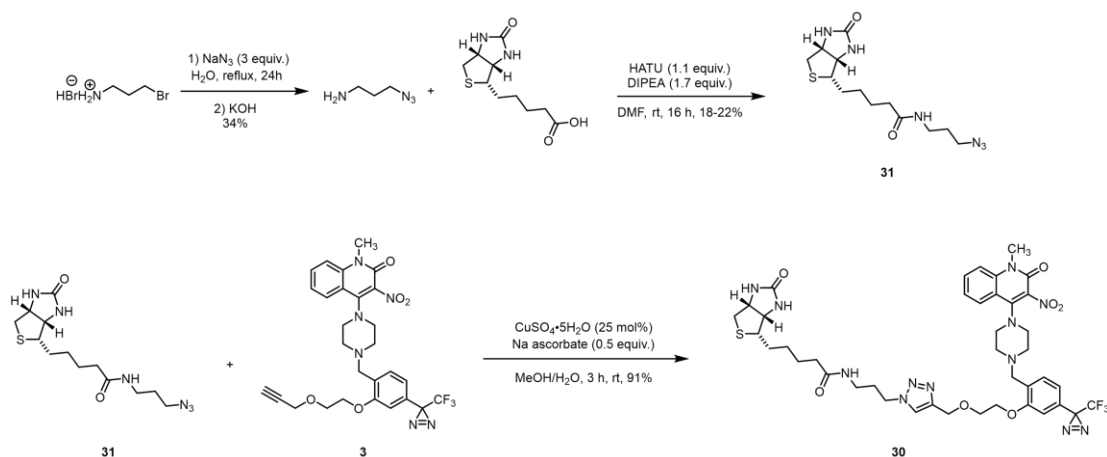


Figure 3.15. The proposed biotin–TPD probe **30**.

3.2.6.1 Synthesis of the Biotin–TPD Probe Molecule **30**

We designed the biotin–azide **31** as the building block for the biotin–TPD probe **30** (Scheme 3.12). First, 3-bromopropylamine hydrobromide was transformed in 3-azidopropylamine, using sodium azide and basified with potassium hydroxide (KOH) to free the amine. Then, the amide bond formation was carried out between biotin and 3-azidopropylamine with the coupling reagent HATU. The last step involved the CuAAC, utilizing the classic click chemistry reagents, the combination of CuSO₄ and sodium ascorbate, to afford the biotin–TPD in satisfying yield.



Scheme 3.12. The synthesis of the biotin-TPD probe **30**.

3.2.6.2 The Immunological Result of the Biotin-TPD Probe Molecule

It is not surprising that increasing the size of the biotin-TPD showed an adverse effect on the biological activity of the compound. The prepared biotin-TPD molecule **30** exerted the lowest activity compared to other generations of probe molecules, including the TPD-containing trifunctional probe molecule **3** and the BODIPY fluorescent probe molecule **29** (Figure 3.16). Despite its low activity, we still considered the compound active and proceeded the pull-down purification with the biotin-TPD probe **30**.

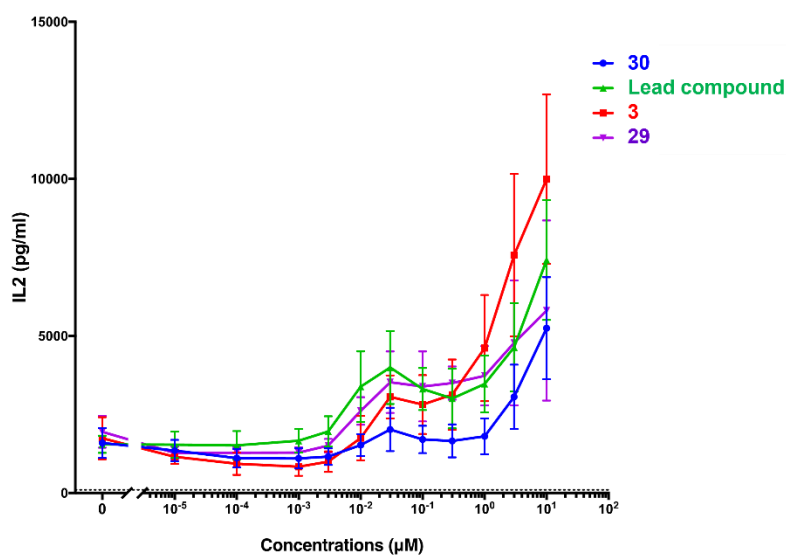


Figure 3.16. The comparison between the biological activity of probe **30** and other probe molecules.

3.2.6.3 The Pull-down Purification Using the Biotin–TPD probe 30

The biotin–TPD molecule **30** was employed in the pull-down assay after its biological activity was examined. Before the actual pull-down experiment was conducted, our collaborators designed a control experiment to test the efficacy of the TPD for photoaffinity labeling. In this experiment, the PBMCs were incubated with probe **30** for six hours. Then, the cells were divided into two controls: one was kept in the dark as the negative control and another one was exposed to UV light. (Figure 3.17).

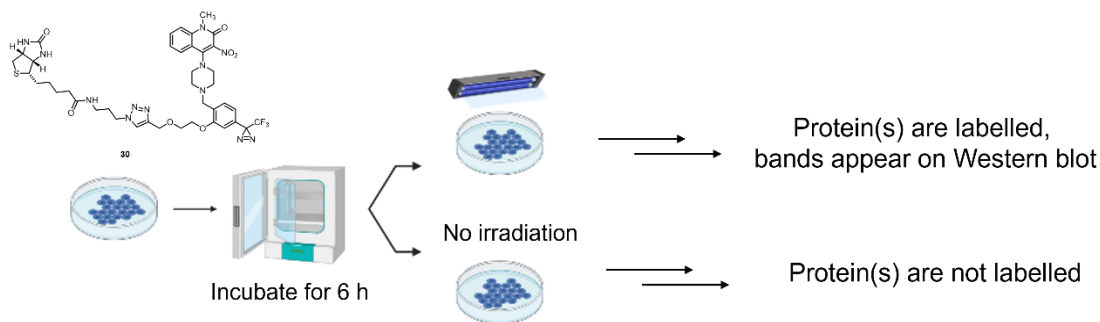


Figure 3.17. The control experiment with or without UV irradiation.

Less or no band should be found in the immunoblotting result for the negative control, as the absence of light prohibits the formation of the covalent connection between protein(s) and probe **30**. To our delight, we identified significantly more bands in the positive control, suggesting that the TPD functionality was able to modify proteins covalently through photoaffinity labelling (Figure 3.18). We postulated that the band at around 63 kDa was one of the endogenous biotinylated proteins, however, were not able to determine its identity.

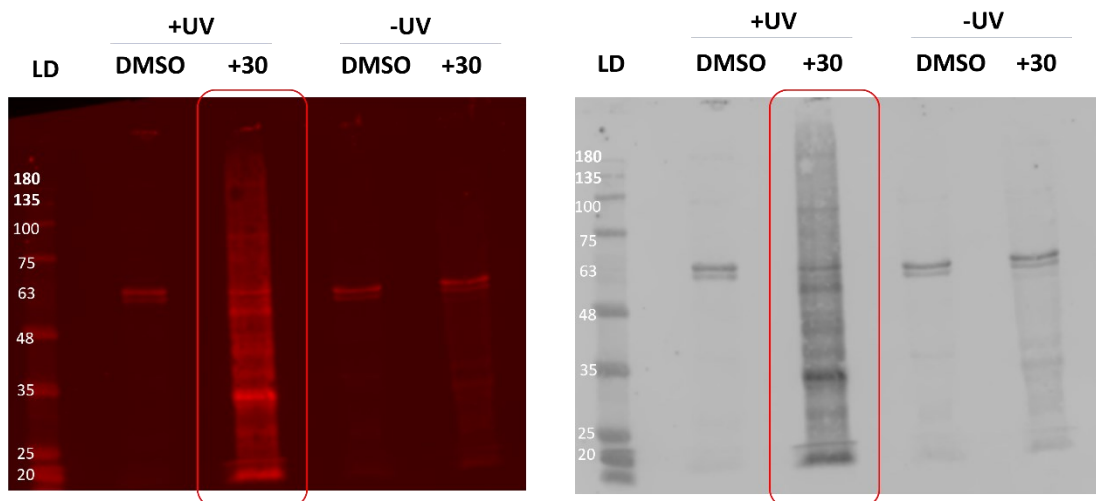


Figure 3.18. The result of the UV irradiation control experiment. The molecular probe **30** was incubated with PBMCs for 6 h after activation with SEB. The cells are then divided into two controls, with or without UV irradiation. After irradiation, the cells were lysed, proteins were precipitated and subsequently analyzed by Western blot.

After the effectiveness of the photoaffinity labelling was confirmed, we implemented the pull-down assay, using the biotin-TPD probe **3** (Figure 3.19). The pull-down procedure using **30** differed little from that using probe **3** (Figure 3.10). Here, the probe **30** was treated to the PBMCs and incubated for six hours. Next, the cells were exposed to UV light and irradiated for an hour. The cells were lysed, and the protein concentration was measured. Following that, the proteins were resuspended, labelled as “resuspended protein”, and used towards the Western blot. Then, any protein that contained biotin in the resuspended sample was isolated by streptavidin beads, which later were cleaved off from the beads for LC-MS analyses. On the other hand, the supernatant that presumably did not contain any biotinylated protein was saved and used as a comparison with the “resuspended protein”.

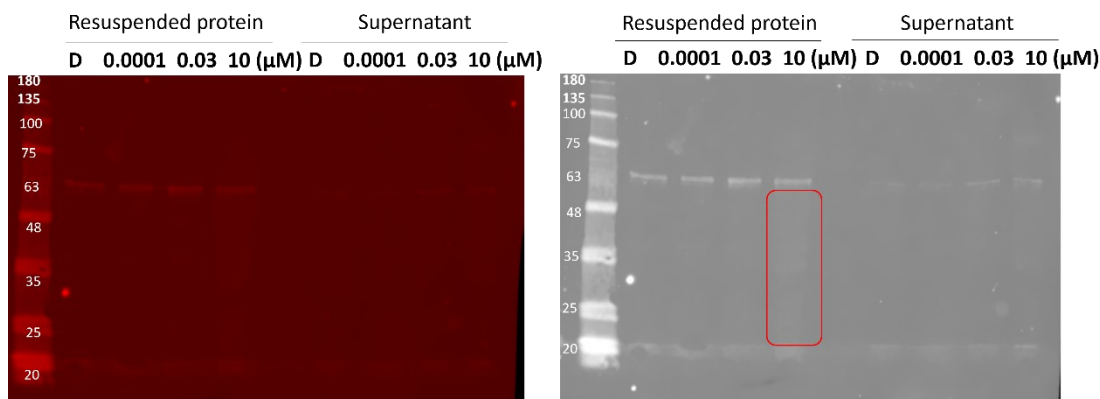


Figure 3.20. One of the Western blot results from utilizing probe **30** and the PBMCs.

3.2.6.4 Preliminary LC-MS Result

From the pull-down assay, we were able to isolate some proteins, despite the low protein concentration obtained. With the appreciable contribution from Yasser Tabana and several other collaborators, we received feedback after the proteins were analyzed by LC-MS. According to the result, several dozens of proteins were isolated, but we were able to narrow down the possible targets to around 20 proteins. It is important to point out that the proteomic result suffered from a high background signal due to the limited amount of sample. Therefore, repetitions of the experiment with optimized protocols and detailed analyses need to be conducted in the future to validate the results.

3.3 Conclusion

In this chapter, we designed and synthesized several probe molecules for various purposes (Figure 3.21). Firstly, two different trifunctional probe molecules, **1** and **3**, were synthesized for the BSA labelling experiment and the protein pull-down purification. Probe **3** demonstrated its capability of covalently modifying a protein and successfully labelled BSA. However, attempts to isolate the protein target from the PBMCs were in vain. The pull-down assay suffered from various uncertainties, including limited protein available and undetermined click reaction efficiency.

Next, we turned to design a fluorescent molecule for confocal microscopy, hoping that we could pinpoint where the protein might reside. The synthesized BODIPY-bearing molecule **29** showed excellent cell membrane permeability but

failed to provide useful information about the location of the protein target. Then, the idea of pre-installing the biotin tag was proposed to achieve the best outcome of the CuAAC. Several pull-down assays were carried out with the synthesized biotin-TPD probe molecule **30**. The proteomic result from the assays currently awaits for validation.

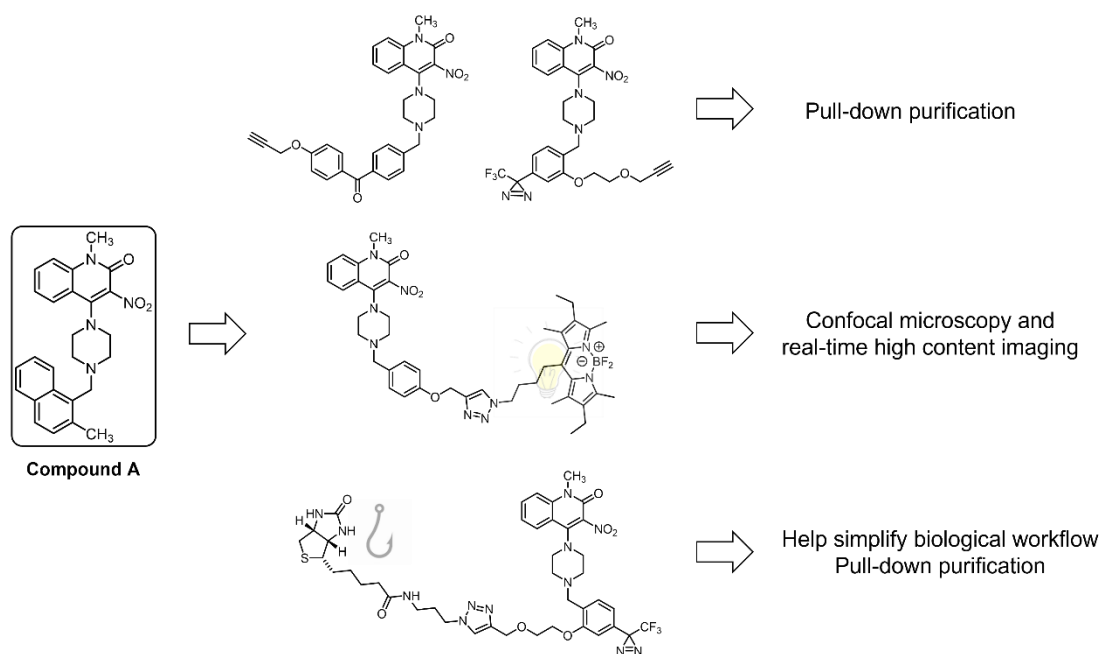


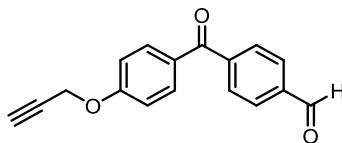
Figure 3.21. Overview of the synthesized probe molecules.

3.4 Experimental

I was responsible for all the synthetic work of the molecules reported. Ashley Ponich, an NSERC USRA summer undergraduate researcher, carried out significant portions of the synthesis of probe **3**. Yasser Tabana, a collaborator of ours, was responsible for all the biological related work described in the project. Shuce Zhang, a graduate student in the Campbell group in the Department of Chemistry, led the microscopic experiment, using the fluorescent compound **29**.

3.4.1 Synthesis of the Trifunctional Probe Molecule 1

4-(4-(Prop-2-yn-1-yloxy)benzoyl)benzaldehyde (**5**)

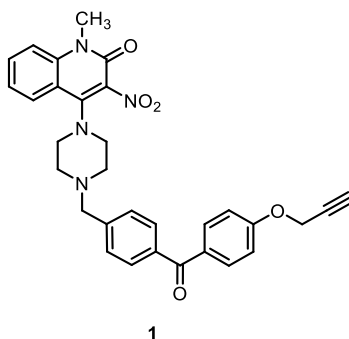


5

In a 10 mL round bottom flask with a magnetic stir bar, 4-iodophenol (1.4 mmol, 0.30 g) and formylphenylboronic acid (1.5 mmol, 0.23 g) were dissolved in 2 mL of acetonitrile/H₂O (4:6 v/v). Pd(OAc)₂ (5 mol%, 1.5 mg), K₃PO₄ (4.1 mmol, 0.87 g), and Mo(CO)₆ (0.82 mmol, 0.25 g) were added to the solution.⁴⁰ The system was sealed, purged with N₂, immersed in a oil bath at 50 °C, and the reaction mixture was stirred under this condition for 3 h. Upon cooling to rt, the reaction mixture was poured over H₂O, acidified with 0.5M HCl, and extracted with ethyl acetate (20 mL). The organic layer was separated, dried over MgSO₄, filtered, and the solvent was evaporated under reduced pressure. The resulting crude reaction mixture was filtered through a short pad of silica gel and concentrated under reduced pressure to give the diaryl ketone intermediate. The intermediate (0.44 mmol, 0.10 g) was dissolved in DMF (2.0 mL), followed by the addition of K₂CO₃ (0.48 mmol, 67 mg). After 20 minutes of stirring at rt, propargyl bromide (0.53 mmol, 59 μL) was added to the solution, and the reaction was stirred additionally under these conditions for 24 h. Later, H₂O (15 mL) was added, and the solution was extracted with ethyl acetate (10 mL x 2). The combined organic layers were dried over MgSO₄, filtered, and concentrated under reduced pressure. The crude reaction mixture was purified further by flash column chromatography (1:6 ethyl acetate:hexanes) to give **5** (92 mg, yield 25%); R_f 0.74 (1:1 ethyl acetate:hexane); IR (cast film) 3289, 3069, 2919, 2848, 2778, 2739, 1703, 1653, 1596, 1010, 1304, 1205, 1019, 929, 762 cm⁻¹; ¹H NMR (500 MHz, CDCl₃) δ 10.12 (s, 1H), 7.99 (d, *J* = 8.0 Hz, 2H), 7.87 (d, *J* = 8.0 Hz, 2H), 7.82 (d, *J* = 8.5 Hz, 2H), 7.06 (d, *J* = 8.5 Hz, 2H), 4.79 (d, *J* = 2.5 Hz, 2H), 2.57 (t, *J* = 2.5 Hz, 1H); ¹³C {¹H} NMR (125 MHz, CDCl₃) δ 194.4, 191.6, 161.5, 143.2, 138.2,

132.5, 130.2, 130.0, 129.5, 114.7, 77.7, 76.4, 56.0; HRMS (EI, M⁺) calcd for C₁₇H₁₂O₃ 264.0786; found: *m/z* 264.0783.

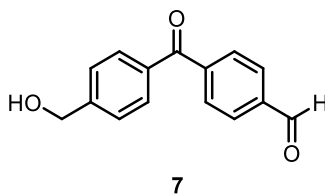
The BP Trifunctional Probe 1



A 10 mL round bottom flask, equipped with a magnetic stir bar and a rubber septum, was charged with **5** (0.17 mmol, 46 mg), DCE (2.0 mL), and 1-methyl-3-nitro-4-(piperazin-1-yl)quinolin-2(1*H*)-one (0.19 mmol, 55 mg) in that order. Subsequently, under stirring at rt, NaBH(OAc)₃ (0.39 mmol, 74 mg) was added to the reaction solution in one portion. The reaction was purged with N₂ and stirred at room temperature for 3 h. Dichloroethane (DCE) was added to the reaction (15 mL), and the solution was extracted with H₂O (10 mL x 2) and brine (10 mL). The organic layer was dried over MgSO₄, filtered, and concentrated under reduced pressure. The crude reaction mixture was purified by flash column chromatography, employing 1:1 ethyl acetate:hexane as eluent, to afford **1** (0.080 g, yield 86%): R_f 0.2 (1:1 ethyl acetate:hexane); IR (cast film) 3358, 2921, 2851, 1650, 1695, 1528, 1459, 1284, 1171, 1006, 762 cm⁻¹; ¹H NMR (500 MHz, CDCl₃) δ 7.95 (d, *J* = 8.0 Hz, 1H), 7.83 (d, *J* = 8.5 Hz, 2H), 7.73 (d, *J* = 8.5 Hz, 2H), 7.65 (app. t, *J* = 8.0 Hz, 1H), 7.46 (d, *J* = 8.0 Hz, 2H), 7.39 (d, *J* = 8.0 Hz, 1H), 7.31 (app. t, *J* = 8.0 Hz, 1H), 7.04 (d, *J* = 8.4 Hz, 2H), 4.77 (s, 2H), 3.70 (s, 3H), 3.68 (s, 2H), 3.30 (s, 4H), 2.69 (s, 4H), 2.57 (s, 1H); ¹³C {¹H} NMR (125 MHz, CDCl₃) δ 195.1, 161.0, 156.1, 149.0, 142.3, 139.7, 137.2, 134.9, 132.6, 132.4, 131.0, 130.0, 128.7, 126.6, 122.7, 117.4, 115.2, 114.5, 77.8, 76.2, 62.6, 55.9, 53.1, 50.4, 30.0; HRMS (ESI, [M+H]⁺) calcd for C₃₁H₂₉N₄O₅ 537.2132; found: *m/z* 537.2140.

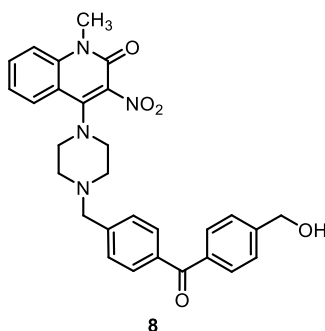
3.4.2 Synthesis of the Trifunctional Probe Molecule 2

4-(4-(Hydroxymethyl)benzoyl)benzaldehyde (7)



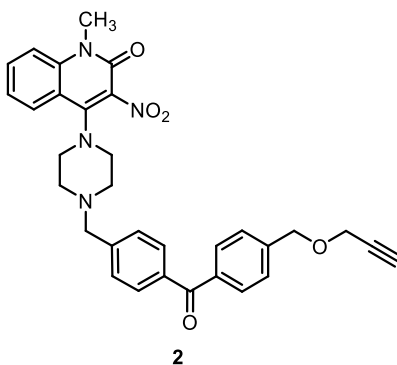
A 10 mL round bottom flask, equipped with a stir bar and a rubber septum, was charged with 4-iodobenzyl alcohol (1.3 mmol, 0.30 g), formylphenylboronic acid (1.4 mmol, 0.21 g), and 2 mL of a solution of acetonitrile/H₂O (4:6 v/v). After the starting materials were dissolved fully, K₃PO₄ (3.8 mmol, 0.82 mg), Mo(CO)₆ (0.90 mmol, 0.24 g), and Pd(OAc)₂ (1 mol %, 0.29 mg) were added to the reaction solution, respectively. The system was sealed, purged with N₂, immersed in an oil bath at 50 °C, and stirred for 3 h.⁴⁰ Upon cooling to rt, the reaction mixture was poured over H₂O, acidified with 1M HCl (30 mL), and extracted with ethyl acetate (10 mL x 2). The organic layers were combined, dried over MgSO₄, filtered, and concentrated under reduced pressure. The crude reaction mixture was purified by flash column chromatography, employing 1:2 ethyl acetate:hexanes as eluent, to afford **7** (0.10 g, yield 33%): R_f 0.16 (1:2 ethyl acetate:hexane); IR (cast film) 3344 (broad), 3059, 2919, 2849, 1704, 1650, 1609, 1412, 1302, 1206, 1042, 854, 752 cm⁻¹; ¹H NMR (500 MHz, CDCl₃) δ 10.13 (s, 1H), 8.00 (d, *J* = 8.0 Hz, 2H), 7.91 (d, *J* = 8.0 Hz, 2H), 7.81 (d, *J* = 8.5 Hz, 2H), 7.51 (d, *J* = 8.5 Hz, 2H), 4.82 (d, *J* = 2.5 Hz, 2H), 1.99 (br s, 1H); ¹³C {¹H} NMR (125 MHz, CDCl₃) δ 195.5, 191.6, 146.3, 142.7, 138.5, 135.9, 130.5, 130.3, 129.5, 126.6, 64.6; HRMS (EI, M⁺) calcd for C₁₅H₁₂O₃ 240.0786; found: *m/z* 240.0786.

The BP Intermediate (8)



The compound was synthesized according to previous procedure of **1**, using **7** (0.16 mmol, 39 mg), 1-methyl-3-nitro-4-(piperazin-1-yl)quinolin-2(1H)-one (0.18 mmol, 52 mg), and NaBH(OAc)₃ (0.33 mmol, 0.070 g) in DCE (1.5 mL), to afford **8** (66 mg, yield 79%): *R_f* 0.48 (ethyl acetate); IR (cast film) 3447 (broad), 3053, 2916, 2820, 1650, 1610, 1593, 1528, 1460, 1401, 1311, 1280, 1193, 1005, 929, 762, 735 cm⁻¹; ¹H NMR (500 MHz, CDCl₃) δ 7.95 (d, *J* = 8.0 Hz, 1H), 7.81 (d, *J* = 8.0 Hz, 2H), 7.78 (d, *J* = 8.0 Hz, 2H), 7.66 (t, *J* = 8.0 Hz, 1H), 7.50–7.57 (m, 4H), 7.40 (d, *J* = 8.0 Hz, 1H), 7.31 (t, *J* = 8.0 Hz, 1H), 4.82 (s, 2H), 3.71 (s, 3H), 3.69 (s, 2H), 3.32 (app. t, *J* = 5.0 Hz, 4H), 2.70 (br s, 4H), 1.91 (s, 1H); ¹³C {1H} NMR (125 MHz, CDCl₃) δ 196.1, 156.1, 148.9, 145.5, 142.7, 139.7, 136.9, 136.8, 135.0, 132.6, 130.4, 130.3, 128.8, 126.6, 126.5, 122.7, 117.4, 115.1, 64.8, 62.6, 53.2, 50.4, 30.0; HRMS (ESI, [M+H]⁺) calcd for C₂₉H₂₉N₄O₅ 513.2130; found: *m/z* 513.2140.

The BP Trifunctional Probe (2)

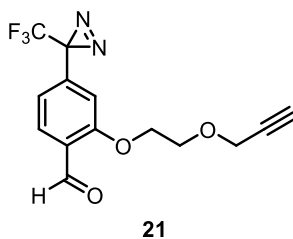


To a 10 mL round bottom flask with the solution of **8** (0.049 mmol, 25 mg) in DMSO (1.0 mL), was added potassium hydroxide (0.059 mmol, 3.3 mg). After it was stirred

at rt for 30 minutes, propargyl bromide (0.074 mmol, 5.6 μ L) was added, the system was sealed, purged with N₂, and the reaction mixture was stirred at rt for 24 h. Subsequently, the reaction was poured over H₂O (10 mL) and extracted with ethyl acetate (10 mL x 2). The organic layers were combined, washed with brine (10 mL), separated, dried over MgSO₄, filtered, and concentrated under reduced pressure. The reaction crude was purified by flash column chromatography, employing 1:2 ethyl acetate:hexanes as eluent, to afford **2** (5.3 mg, yield 20%) as a yellow oil: R_f 0.75 (2:1 ethyl acetate:hexane); ¹H NMR (400 MHz, CDCl₃) δ 7.96 (dd, *J* = 8.4, 1.6 Hz, 1H), 7.86–7.75 (m, 4H), 7.66 (ddd, *J* = 8.8, 7.2, 1.6 Hz, 1H), 7.50–7.47 (m, 4H), 7.40 (d, *J* = 8.4 Hz, 1H), 7.31 (t, *J* = 7.6 Hz, 1H), 4.71 (s, 2H), 4.25 (d, *J* = 2.4 Hz, 2H), 3.72 (s, 3H), 3.70 (s, 2H), 3.32 (app. t, *J* = 4.8 Hz, 4H), 2.70 (br s, 4H), 2.50 (t, *J* = 2.4 Hz, 1H); ¹³C {¹H} NMR (125 MHz, CDCl₃) δ 196.0, 156.1, 148.9, 142.8, 142.1, 139.7, 137.2, 136.8, 135.0, 132.6, 130.27, 130.25, 128.8, 127.6, 126.6, 122.7, 117.4, 115.1, 79.3, 75.0, 71.0, 62.6, 57.6, 53.2, 50.4, 30.0; HRMS (ESI, [M+Na]⁺) calcd for C₃₂H₃₀N₄NaO₅ 573.2108; found: *m/z* 573.2103.

3.4.3 Synthesis of the Trifunctional Probe Molecule **3**

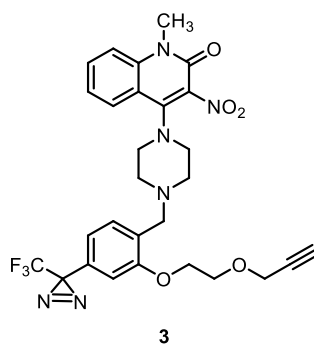
2-(2-(Prop-2-yn-1-yloxy)ethoxy)-4-(3-(trifluoromethyl)-3*H*-diazirin-3-yl)benzaldehyde (**21**)



The compound was synthesized according to a previously reported literature procedure,²⁴ employing 2-hydroxy-4-(3-(trifluoromethyl)-3*H*-diazirin-3-yl)benzaldehyde (0.75 mmol, 0.17 g) the tosylated alkyne (0.84 mmol, 0.21 g), tetrabutylammonium iodide (Bu₄NI) (0.083 mmol, 31 mg), K₂CO₃ (1.3 mmol, 0.18 mg), and DMF (18 mL) to give **21** (0.14 g, yield 58%) as a pale yellow solid. R_f 0.25 (1:6 petroleum ether: diethyl ether); ¹H NMR (500 MHz, CDCl₃)

δ 10.49 (s, 1H), 7.85 (d, $J = 8.0$ Hz, 1H), 6.85 (d, $J = 8.0$ Hz, 1H), 6.75 (s, 1H), 4.33–4.21 (m, 4H), 3.99–3.94 (m, 2H), 2.48 (t, $J = 2.4$ Hz, 1H); ^{13}C $\{^1\text{H}\}$ NMR (125 MHz, CDCl_3) δ 188.8, 160.9, 136.6, 128.9, 125.7, 121.8 (q, $^1J_{\text{C-F}} = 274$ Hz, CF_3), 119.0, 110.9, 79.1, 75.1, 68.4, 67.8, 58.6, 28.6 (q, $^2J_{\text{C-F}} = 41$ Hz, CCF_3); HRMS (ESI, $[\text{M}+\text{Na}]^+$) calcd for $\text{C}_{14}\text{H}_{11}\text{F}_3\text{N}_2\text{NaO}_3$ 335.0614, found: m/z 335.0606.

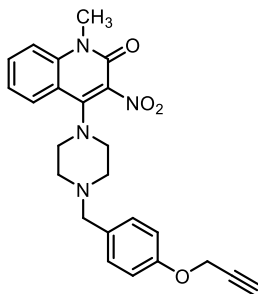
The TPD Trifunctional Probe 3



The compound was synthesized according to the previous procedure of preparing **1**, using **21** (0.16 mmol, 51 mg), 1-methyl-3-nitro-4-(piperazin-1-yl)quinolin-2(1H)-one (0.16 mmol, 48 mg), $\text{NaBH}(\text{OAc})_3$ (0.32 mmol, 68 mg), and DCE (1.5 mL) to give pure **3** (79 mg, yield 85%) as a yellow solid: R_f 0.22 (1:1 ethyl acetate:hexane); ^1H NMR (500 MHz, CDCl_3) δ 7.94 (d, $J = 7.5$ Hz, 1H), 7.66–7.63 (m, 1H), 7.42 (d, $J = 7.5$ Hz, 1H), 7.39 (d, $J = 8.5$ Hz, 1H), 7.30 (t, $J = 7.5$ Hz, 1H), 6.80 (d, $J = 7.5$ Hz, 1H), 6.65 (s, 1H), 4.28 (d, $J = 2.5$ Hz, 2H), 4.19–4.14 (m, 2H), 3.96–3.90 (m, 2H), 3.70 (s, 3H), 3.67 (s, 2H), 3.28 (app. t, $J = 4.5$ Hz, 4H), 2.70 (br s, 4H), 2.47 (t, $J = 2.5$ Hz, 1H). ^{13}C $\{^1\text{H}\}$ NMR (125 MHz, CDCl_3) δ 157.1, 156.1, 149.0, 139.7, 134.8, 132.5, 130.8, 129.1, 128.4, 126.7, 122.6, 122.1 (q, $^1J_{\text{C-F}} = 274$ Hz), 119.13, 117.4, 115.1, 109.8, 79.4, 74.9, 68.1, 68.0, 58.6, 55.7, 53.0, 50.5, 30.0, 28.5 (q, $^2J_{\text{C-F}} = 40$ Hz); HRMS (ESI, $[\text{M}+\text{H}]^+$) calcd for $\text{C}_{28}\text{H}_{28}\text{F}_3\text{N}_6\text{O}_5$ 585.2068; found: m/z 585.2070.

3.4.4 Synthesis of the Fluorescent Probe Molecule 29

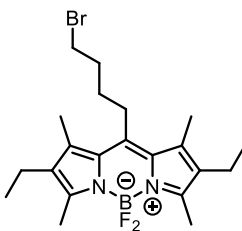
1-Methyl-3-nitro-4-(4-(4-(prop-2-yn-1-yloxy)benzyl)piperazin-1-yl)quinolin-2(1H)-one (23)



23

The compound was prepared according to the previously reported procedure of **1**, using 1-methyl-3-nitro-4-(piperazin-1-yl)quinolin-2(1H)-one (0.17 mmol, 0.050 g), 4-(prop-2-yn-1-yloxy)benzaldehyde (0.21 mmol, 33 mg), and NaBH(OAc)₃ (0.35 mmol, 74 mg) in DCE (3.0 mL), to afford **23** as a yellow sticky oil (64 mg, yield 85%): *R_f* 0.35 (1:1 ethyl acetate:hexane); IR (cast film) 3299, 3052, 2919, 2850, 1734, 1649, 1613, 1594, 1529, 1460, 1399, 1266, 1216, 1030, 1004, 763, 737 cm⁻¹; ¹H NMR (500 MHz, CDCl₃) δ 7.94 (dd, *J* = 8.5, 1.5 Hz, 1H), 7.65 (ddd, *J* = 8.5, 7.0, 1.5 Hz, 1H), 7.38 (d, *J* = 8.0 Hz, 1H), 7.33–7.26 (m, 3H), 6.94 (d, *J* = 9.0 Hz, 2H), 4.68 (d, *J* = 2.5 Hz, 2H), 3.70 (s, 3H), 3.55 (s, 2H), 3.28 (t, *J* = 5.0 Hz, 4H), 2.64 (br s, 4H), 2.52 (t, *J* = 2.5 Hz, 1H); ¹³C {¹H} NMR (125 MHz, CDCl₃) δ 156.9, 156.1, 149.0, 139.7, 134.8, 132.6, 130.7, 130.2, 126.7, 122.6, 117.4, 115.1, 114.8, 78.6, 75.5, 62.3, 55.9, 53.0, 50.4, 30.0; HRMS (ESI, [M+H]⁺) calcd for C₂₄H₂₅N₄O₄ 433.1870; found: *m/z* 433.1866.

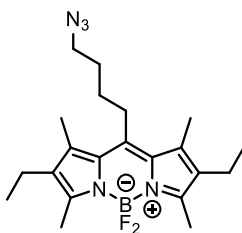
The BODIPY–bromide (27)



27

To a 25 mL round bottom flask was added 5-bromovaleric acid (1.4 mmol, 0.25 g) CH₂Cl₂ (5.0 mL) and a catalytic amount of DMF. Then, oxalyl chloride (1.7 mmol, 0.14 mL) was added dropwise to the stirring solution. The reaction was stirred under room temperature for 24 h, and the solvent was removed carefully under reduced pressure over a short period of time. The intermediate was carried on to the next step without further purification. The 5-bromovaleryl chloride (assuming 100% yield, 1.4 mmol, 0.27 g) was added dropwise into a stirring solution of 3-ethyl-2,4-dimethylpyrrole (2.8 mmol, 0.37 mL) in CH₂Cl₂ (12 mL) under an inert atmosphere (N₂). A reflux condenser was connected to the round bottom flask, the reaction system was immersed in an oil bath at 50°C, and magnetically stirred for 2h. Upon cooling to rt, the solvent was removed under reduced pressure to yield a red-brown solid, which was used directly in the next step. The red-brown solid was dissolved in a mixture of toluene (10 mL) and CH₂Cl₂ (2.0 mL), and, under stirring, triethylamine (1.2 mL) was added dropwise over 10 minutes to the solution, using a syringe pump. The system was sealed, purged with N₂, and the reaction mixture was stirred at rt for 1h. Subsequently, boron trifluoride diethyl etherate (1.2 mL) was added dropwise to the reaction over 10 min with a syringe pump under N₂. The system was immersed in an oil bath at 50 °C and stirred for 2 h. Upon cooling to rt, the solvent was removed by rotary evaporation under reduced pressure, and the crude reaction mixture was purified by flash column chromatography, employing 1:40 ethyl acetate:hexane as an eluent to give **27** as a red solid (0.22 mg, yield 37%). The characterization data were in agreement with literature values. ³⁹R_f 0.40 (1:9 ethyl acetate:hexane); IR (cast film) 2963, 2922, 2851, 1737, 1547, 1479, 1197, 981, 740 cm⁻¹; ¹H NMR (500 MHz, CDCl₃) δ 3.44 (t, *J* = 6.5 Hz, 2H), 2.99–2.96 (m, 2H), 2.50 (s, 6H), 2.40 (q, *J* = 7.5 Hz, 4H), 2.32 (s, 6H), 2.07–2.02 (m, 2H), 1.81–1.75 (m, 2H), 1.05 (t, *J* = 7.5 Hz, 6H); ¹³C {¹H} NMR (125 MHz, CDCl₃) δ 152.3, 143.7, 135.6, 132.7, 130.9, 33.1, 32.8, 30.1, 27.5, 17.2, 14.8, 13.3, 12.4; HRMS (ESI, [M–F]⁺) calcd for C₂₁H₃₀[¹¹B]BrFN₂ 419.1664; found: *m/z* 419.1665.

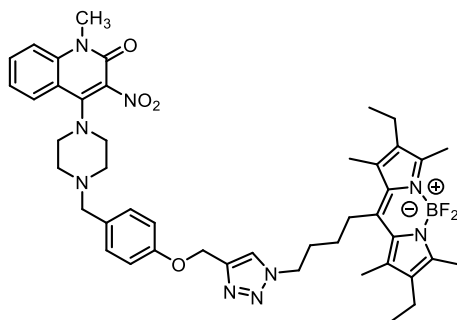
The BODIPY–azide (28)



28

To a 10 mL round bottom flask, **27** (0.23 mmol, 0.10 g), sodium azide (0.23 mmol, 75 mg), DMSO (1.5 mL), and a catalytic amount of acetic acid were added. The reaction was kept under ambient atmosphere and stirred at rt for 3 h. The resulting reaction mixture was poured over H₂O (20 mL) and extracted with CH₂Cl₂ (15 mL x 2). The organic layers were combined, dried over MgSO₄, filtered, and concentrated under reduced pressure. The crude reaction mixture was purified with flash column chromatography, employing 1:40 ethyl acetate:hexanes, to afford **28** as a dark red oil (67 mg, yield 73%). The characterization data were in agreement with literature values³⁹. *R_f* 0.30 (1:5 ethyl acetate:hexanes); ¹H NMR (500 MHz, CDCl₃) δ 3.36 (t, *J* = 6.5 Hz, 2H), 3.02–2.99 (m, 2H), 2.50 (s, 6H), 2.40 (q, *J* = 7.5 Hz, 4H), 2.33 (s, 6H), 1.79–1.70 (m, 4H), 1.05 (t, *J* = 7.5 Hz, 6H); ¹³C {¹H} NMR (125 MHz, CDCl₃) δ 152.4, 143.7, 135.5, 132.8, 130.9, 51.0, 29.2, 28.8, 27.8, 17.2, 14.8, 13.3, 12.4; HRMS (ESI, [M+Na]⁺) calcd for C₂₁H₃₀[¹¹B]BrF₂N₂Na 424.2455; found: *m/z* 424.2459.

The Fluorescent Probe (29)

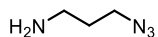


29

To a solution of **23** (0.040 mmol, 18 mg) in DMF (0.50 mL), triphenylphosphine (4.0 μ mol, 1.0 mg), CuI (5 mol %, 0.39 mg), diethylpropylamine (0.12 mmol, 44 μ L), and **28** (0.040 mmol, 17 mg) were added. The reaction was purged with N₂ and stirred at 70° C for 3 h. The solvent was removed under reduced pressure, the resulting residue was re-dissolved in DCM (15 mL), and extracted with H₂O (10 mL x 2). The organic layer was dried over MgSO₄, filtered, and concentrated under reduced pressure. The crude reaction mixture was purified by flash column chromatography, employing 2:1 ethyl acetate:hexanes as eluent, to afford **29** as a red sticky oil (16 mg, yield 46%): *R_f* 0.11 (1:1 ethyl acetate:hexane); IR (cast film) 3143, 3052, 2962, 2930, 1649, 1594, 1478, 1403, 1196, 1064, 981, 736 cm⁻¹; ¹H NMR (500 MHz, CDCl₃) δ 7.94 (dd, *J* = 8.5, 1.5 Hz, 1H), 7.65 (ddd, *J* = 8.5, 7.0, 1.5 Hz, 1H), 7.58 (s, 1H), 7.39 (d, *J* = 8.5 Hz, 1H), 7.30 (d, *J* = 7.5 Hz, 2H), 7.24 (d, *J* = 8.5 Hz, 2H), 6.94 (d, *J* = 8.5 Hz, 2H), 5.20 (s, 2H), 4.40 (t, *J* = 7.0 Hz, 2H), 3.71 (s, 3H), 3.53 (s, 2H), 3.28 (t, *J* = 5.0 Hz, 4H), 3.04–3.00 (m, 2H), 2.63 (br s, 4H), 2.48 (s, 6H), 2.38 (q, *J* = 7.5 Hz, 4H), 2.27 (s, 6H), 2.15 (p, *J* = 7.5 Hz, 2H), 1.70–1.64 (m, 2H), 1.03 (t, *J* = 7.5 Hz, 6H); ¹³C {¹H} NMR (125 MHz, CDCl₃) δ 156.1, 152.6, 149.0, 144.3, 143.1, 139.7, 135.4, 132.9, 132.5, 130.8, 130.3, 126.7, 122.8, 122.6, 117.4, 115.1, 114.7, 62.3, 62.2, 53.0, 50.1, 30.4, 30.0, 28.7, 27.7, 17.2, 14.8, 13.4, 12.5; HRMS (ESI, [M+H]⁺) calcd for C₄₅H₅₅[¹¹B]F₂N₂O₄ 834.4433; found: *m/z* 834.4429.

3.4.5 Synthesis of the Biotin–TPD Probe Molecule **30**

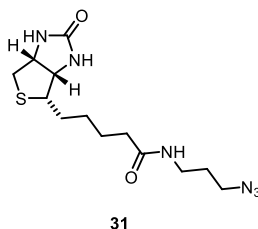
3-Azidopropylamine



In a 50 mL round bottom flask, 3-bromopropylamine hydrobromide (4.6 mmol, 1.0 g) was dissolved in H₂O (3.0 mL). A solution of sodium azide (15 mmol, 0.99 g) in H₂O (9.0 mL) was added to the reaction, and the resulting solution was stirred under reflux for 24 h. Upon the specified time, the system was immersed in an ice-bath, and the reaction mixture was basified to pH = 14 with KOH powder. After the solution reached pH = 14, the aqueous phase was extracted with ether (20 mL x 2), the organic layers were combined, dried over MgSO₄ filtered, and concentrated under reduced

pressure to give pure 3-azidopropylamine as a yellow oil (0.16 g, yield 34%): IR (cast film): 3306, 2930, 2102, 1576, 1484, 1306 cm^{-1} ; ^1H NMR (500 MHz, CDCl_3) δ 3.37 (t, $J = 7.0$ Hz, 2H), 2.80 (t, $J = 7.0$ Hz, 2H), 1.72 (p, $J = 7.0$ Hz, 2H), 1.10 (br s, 2H); ^{13}C $\{^1\text{H}\}$ NMR (125 MHz, CDCl_3) δ 49.2, 39.4, 32.6; HRMS (ESI, $[\text{M}+\text{H}]^+$) calcd for $\text{C}_3\text{H}_9\text{N}_4$ 101.0822, found: m/z 101.0825.

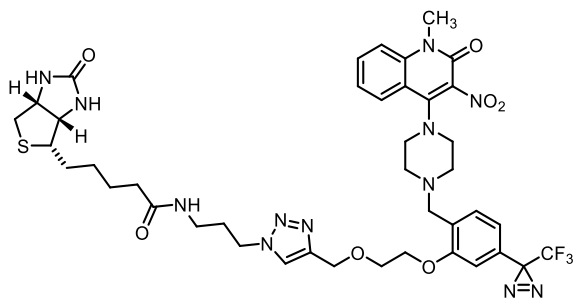
***N*-(3-azidopropyl)-5-(2-oxohexahydro-1*H*-thieno[3,4-*d*]imidazol-4-yl)pentanamide (31)**



In a 25 mL round bottom flask, DIPEA (0.70 mmol, 0.12 mL) and HATU (0.44 mmol, 0.17 g) were added to a solution of biotin (0.41 mmol, 0.10 g) in DMF (1.0 mL). The system was sealed with a rubber septum, purged with N_2 , and the reaction mixture was stirred at rt for 30 min. Then, the system was immersed in an ice bath, and, under magnetic stirring, 3-azidopropylamine (0.49 mmol, 47 μL) was added to it dropwise. After the addition of 3-azidopropylamine, the system was allowed to return to rt, and the resulting mixture was stirred for 16 h under this condition. Upon reaction completion, the solvent was removed under reduced pressure, and the residue was re-dissolved in CH_2Cl_2 (15 mL). The organic phase was washed with 1M HCl (10 mL x 2), saturated aqueous NaHCO_3 (10 mL), and brine (10 mL). The organic layer was separated, dried over MgSO_4 , filtered, and concentrated under reduced pressure. The reaction crude was purified with flash column chromatography, employing 1:8 methanol: CH_2Cl_2 as eluent to give pure **31** as a pale-yellow waxy solid (0.030 g, yield 22%): R_f 0.45 (1:5 methanol: CH_2Cl_2); IR (cast film) 3295 (sharp), 3089, 2928, 2857, 2099 (sharp), 1702, 1645, 1550, 1463, 1265, 1205, 728 cm^{-1} ; ^1H NMR (500 MHz, CD_3OD) δ 4.48 (dd, $J = 7.5, 4.5$ Hz, 1H), 4.29 (dd, $J = 8.0, 4.5$ Hz, 1H), 3.34 (t, $J = 7.0$ Hz, 2H), 3.28–3.16 (m, 3H), 2.92 (dd, $J = 13.0, 5.0$ Hz, 1H), 2.70 (d, $J = 13.0$ Hz, 1H), 2.20 (d, $J = 7.0$ Hz, 2H),

1.78–1.55 (m, 6H), 1.48–1.40 (m, 2H), three exchangeable NH protons were not observed; ^{13}C $\{^1\text{H}\}$ NMR (125 MHz, CD_3OD) δ 176.0, 165.9, 63.2, 61.5, 56.8, 49.9, 40.9, 37.5, 36.6, 29.6, 29.6, 29.3, 26.7; HRMS (ESI, $[\text{M}+\text{Na}]^+$) calcd for $\text{C}_{13}\text{H}_{22}\text{N}_6\text{NaO}_2\text{S}$ 349.1417, found: m/z 349.1411.

The Biotin–TPD Probe Molecule **30**



30

In a 5 mL round bottom flask, **3** (0.014 mmol, 8.3 mg) and **31** (0.018 mmol, 6.0 mg) were added and dissolved in 0.4 mL methanol/ H_2O (1:1 v/v) solution. $\text{CuSO}_4 \cdot 5\text{H}_2\text{O}$ (3.5 μmol , 0.88 mg) and sodium ascorbate (7.0 μmol , 1.4 mg) were added, and the reaction mixture was stirred at rt under inert atmosphere (N_2) for 3 h. After the reaction had gone to completion, the solvent was removed under reduced pressure, and the crude reaction mixture was purified by flash column chromatography, employing 1:9 methanol: CH_2Cl_2 as eluent to give a pure **30** as pale-yellow oil (12 mg, yield 91%): R_f 0.29 (1:9 methanol: CH_2Cl_2); IR (cast film) 3227, 3085, 2926, 2856, 1700, 1646, 1528, 1460, 1263, 1192, 1156, 1050, 1004, 763, 734 cm^{-1} ; ^1H NMR (500 MHz, CD_3OD) δ 8.00–7.94 (m, 2H), 7.74 (ddd, $J = 8.5, 7.0, 1.5$ Hz, 1H), 7.61 (d, $J = 8.0$ Hz, 1H), 7.46 (d, $J = 7.5$ Hz, 1H), 7.38 (t, $J = 7.5$ Hz, 1H), 6.89 (d, $J = 7.5$ Hz, 1H), 6.74 (s, 1H), 4.71 (s, 2H), 4.46 (dd, $J = 7.5, 4.5$ Hz, 1H), 4.37 (t, $J = 7.0$ Hz, 2H), 4.27 (dd, $J = 8.0, 4.5$ Hz, 1H), 4.20–4.18 (m, 2H), 3.93–3.92 (m, 2H), 3.73 (s, 2H), 3.71 (s, 3H), 3.22 (t, $J = 5.0$ Hz, 4H), 3.18–3.14 (m, 3H), 2.89 (dd, $J = 12.5, 4.5$ Hz, 1H), 2.74 (br s, 4H), 2.67 (d, $J = 12.5$ Hz, 1H), 2.17 (t, $J = 7.5$ Hz, 2H), 2.04 (p, $J = 7.0$ Hz, 2H), 1.79–1.49 (m, 4H), 1.44–1.37 (m, 2H), three exchangeable NH protons were not observed; ^{13}C $\{^1\text{H}\}$ NMR (125 MHz, CD_3OD) δ 176.2, 166.1, 159.1, 157.7, 150.9, 145.9, 140.9, 135.8, 134.2, 133.0, 130.6, 129.0,

127.9, 125.2, 124.7 (CF₃), 124.4, 120.1, 118.6, 117.0, 110.9, 70.0, 69.4, 65.2, 63.4, 61.6, 57.0, 56.6, 54.0, 51.4, 41.0, 37.4, 36.8, 31.2, 30.8, 30.6, 29.8, 29.7 (CCF₃), 29.5, 26.8, ¹J_{C-F} and ²J_{C-F} were not observed in ¹³C NMR; however, ¹⁹F NMR and C-F HSQC supported the presence of -CF₃. HRMS (ESI, [M+H]⁺) calcd for C₄₁H₄₉F₃N₁₂O₇S 911.3593, found: *m/z* 911.3691.

3.4.6 The Stability Test of The TPD Trifunctional Probe 3

1. The stock solutions of the TPD probe **3** in DMSO (1 mM), CuSO₄·5H₂O in water (20 mM), sodium ascorbate in water (200 mM), TCEP·HCl in NaOH solution (200 mM), and TBTA in DMSO (10 mM) were prepared prior to the experiment.
2. To one chromatography vial was added sequentially with the stock solutions of probe **3** (20 μL), CuSO₄·5H₂O (25 μL), TCEP·HCl (25 μL), TBTA (25 μL), and water (400 μL). To another new chromatography vial was added with the stock solutions of probe **3** (20 μL), CuSO₄·5H₂O (25 μL), sodium ascorbate (25 μL), TBTA (25 μL), and water (400 μL).
3. The vials were vortexed and sealed properly with a plastic cap.
4. The vials were covered with aluminum foil and kept in the dark for an hour.
5. After one hour, the vials were directly submitted to LC-MS for analysis.

3.3.7. The Selection of Reducing Agent for the Click Reaction Condition

1. The same stock solutions indicated in 3.3.6 along with the stock solution of biotin-(PEG)₃-azide in DMSO (2 mM) were prepared.
2. To one chromatography vial was added sequentially with the stock solutions of probe **3** (20 μL), water (375 μL), azide (20 μL), CuSO₄·5H₂O (25 μL), TBTA (25 μL), and sodium ascorbate (25 μL). To another new chromatography vial was added with the stock solutions of probe **3** (20 μL), water (375 μL), azide (20 μL), CuSO₄·5H₂O (25 μL), TBTA (25 μL), and TCEP·HCl (25 μL).
3. The vials were vortexed and sealed properly with a plastic cap.
4. The vials were covered with aluminum foil and kept in the dark for an hour.

5. After one hour and three hours, 100 μ L of sample was taken out each time and submitted for LC-MS analyses.

3.3.8. The Optimization of Photoaffinity Labelling Reaction

1. A stock solution of probe **3** in methanol (1 mM) was prepared.
2. In five 5 mL glass vials were added 100 μ L of the prepared stock solution.
3. The reaction solutions were purged with N₂ and properly sealed with a plastic cap and parafilm.
4. One vial was wrapped with aluminum foil and kept in the dark to serve as the negative control. The other four vials were placed 3 cm underneath a UV lamp that was pre-warmed for 30 min.
5. After 30, 60, 90, and 120 min, one vial was removed from the light each time and submitted for LC-MS analysis immediately.

3.3.9. The BSA Labelling Experiment

1. The stock solutions of the TPD probe **3** in DMSO (3 mM), biotin-(PEG)₃-azide in DMSO (12 mM), CuSO₄·5H₂O in water (20 mM), sodium ascorbate in water (200 mM), and TBTA in DMSO (100 mM) were prepared prior to the experiment.
2. In 5 mL glass vials was added sequentially with the stock solutions of probe **3** (20 μ L), water (375 μ L), azide (20 μ L), CuSO₄·5H₂O (25 μ L), TBTA (25 μ L), and sodium ascorbate (25 μ L).
3. The reaction was vortexed, sealed with a plastic cap, and wrapped with aluminum foil overnight.
4. The reaction progress was accessed by LC-MS after 24 h. LC-MS indicated that the diazirine starting material almost was consumed after 24 h, and the signal corresponding to the triazole product with correct molecular weight was observed.
5. Assuming that the click reaction went to completion, 350 μ L of the reaction mixture was added to 250 μ L of BSA solution (1mg/mL in PBS).
6. The sample was vortexed for three times and kept under room temperature in the dark for 20 min to ensure proper mixture of BSA and the compound.

7. The sample was placed 3 cm underneath a UV lamp and irradiated for an hour.
8. The irradiated sample was desalted with a C18 column according to the procedure provided by the manufacturer.
9. The purified protein sample was subjected to MALDI analyses.

3.5 References

- (1) Shi, H.; Zhang, C.-J.; Chen, G. Y. J.; Yao, S. Q. Cell-Based Proteome Profiling of Potential Dasatinib Targets by Use of Affinity-Based Probes. *J. Am. Chem. Soc.* **2012**, *134* (6), 3001–3014. <https://doi.org/10.1021/ja208518u>.
- (2) Stephens, D. J.; Allan, V. J. Light Microscopy Techniques for Live Cell Imaging. *Science* (1979) **203**, *300*, 82–86. <https://doi.org/10.1126/science.1082160>.
- (3) Rao, J.; Dragulescu-Andrasi, A.; Yao, H. Fluorescence Imaging in Vivo: Recent Advances. *Curr. Opin. Biotech.* **2007**, *18* (1), 17–25. <https://doi.org/10.1016/j.copbio.2007.01.003>.
- (4) Vendrell, M.; Zhai, D.; Er, J. C.; Chang, Y.-T. Combinatorial Strategies in Fluorescent Probe Development. *Chem. Rev.* **2012**, *112* (8), 4391–4420. <https://doi.org/10.1021/cr200355j>.
- (5) Liu, H.-W.; Chen, L.; Xu, C.; Li, Z.; Zhang, H.; Zhang, X.-B.; Tan, W. Recent Progresses in Small-Molecule Enzymatic Fluorescent Probes for Cancer Imaging. *Chem. Soc. Rev.* **2018**, *47* (18), 7140–7180. <https://doi.org/10.1039/C7CS00862G>.
- (6) Lichtman, J. W.; Conchello, J.-A. Fluorescence Microscopy. *Nat. Methods.* **2005**, *2* (12), 910–919. <https://doi.org/10.1038/nmeth817>.
- (7) Kobayashi, H.; Ogawa, M.; Alford, R.; Choyke, P. L.; Urano, Y. New Strategies for Fluorescent Probe Design in Medical Diagnostic Imaging. *Chem. Rev.* **2010**, *110* (5), 2620–2640. <https://doi.org/10.1021/cr900263j>.
- (8) Terai, T.; Nagano, T. Small-Molecule Fluorophores and Fluorescent Probes for Bioimaging. *Pflügers Arch.* **2013**, *465*, 347–359. <https://doi.org/10.1007/s00424-013-1234-z>.
- (9) Lavis, L. D.; Raines, R. T. Bright Ideas for Chemical Biology. *ACS Chem Biol* **2008**, *3* (3), 142–155. <https://doi.org/10.1021/cb700248m>.
- (10) Wysocki, L. M.; Lavis, L. D. Advances in the Chemistry of Small Molecule Fluorescent Probes. *Curr. Opin. Chem. Biol.* **2011**, *15* (6), 752–759. <https://doi.org/10.1016/j.cbpa.2011.10.013>.
- (11) Sherman, W. R.; Robins, Eli. Fluorescence of Substituted 7-Hydroxycoumarins. *Anal. Chem.* **1968**, *40*, 803–805. <https://doi.org/10.1021/ac60260a045>.
- (12) Baracca, A.; Sgarbi, G.; Solaini, G.; Lenaz, G. Rhodamine 123 as a Probe of Mitochondrial Membrane Potential: Evaluation of Proton Flux through F₀ during ATP Synthesis. *Biochim. Biophys. Acta* **2003**, *1606* (1–3), 137–146. [https://doi.org/10.1016/S0005-2728\(03\)00110-5](https://doi.org/10.1016/S0005-2728(03)00110-5).
- (13) Kowada, T.; Maeda, H.; Kikuchi, K. BODIPY-Based Probes for the Fluorescence Imaging of Biomolecules in Living Cells. *Chem. Soc. Rev.* **2015**, *44* (14), 4953–4972. <https://doi.org/10.1039/C5CS00030K>.
- (14) Gupta, M.; Mula, S.; Ghanty, T. K.; Naik, D. B.; Ray, A. K.; Sharma, A.; Chattopadhyay, S. Structure and Solvent-Induced Tuning of Laser Property and Photostability of a Boradiazaindacene (BODIPY) Dye. *J. Photochem. Photobiol. A* **2017**, *349*, 162–170. <https://doi.org/10.1016/j.jphotochem.2017.09.033>.

- (15) Guseva, Galina. B.; Antina, E. v.; Berezin, M. B.; Pavelyev, R. S.; Kayumov, A. R.; Sharafutdinov, I. S.; Lisovskaya, S. A.; Lodochnikova, O. A.; Islamov, D. R.; Usachev, K. S.; Boichuk, S. v.; Nikitina, L. E. Meso-Substituted-BODIPY Based Fluorescent Biomarker: Spectral Characteristics, Photostability and Possibilities for Practical Application. *J. Photochem. Photobiol. A* **2020**, *401*, 112783. <https://doi.org/10.1016/j.jphotochem.2020.112783>.
- (16) Rybczynski, P.; Smolarkiewicz-Wyczachowski, A.; Piskorz, J.; Bocian, S.; Ziegler-Borowska, M.; Kędziera, D.; Kaczmarek-Kędziera, A. Photochemical Properties and Stability of BODIPY Dyes. *Int. J. Mol. Sci.* **2021**, *22* (13), 6735. <https://doi.org/10.3390/ijms22136735>.
- (17) Hill, J. R.; Robertson, A. A. B. Fishing for Drug Targets: A Focus on Diazirine Photoaffinity Probe Synthesis. *J. Med. Chem.* **2018**, *61* (16), 6945–6963. <https://doi.org/10.1021/acs.jmedchem.7b01561>.
- (18) Beckett, A.; Porter, G. Primary Photochemical Processes in Aromatic Molecules. Part 10.—Photochemistry of Substituted Benzophenones. *Trans. Faraday Soc.* **1963**, *59* (0), 2051–2057. <https://doi.org/10.1039/TF9635902051>.
- (19) Hassan, M. M.; Olaoye, O. O. Recent Advances in Chemical Biology Using Benzophenones and Diazirines as Radical Precursors. *Molecules*. MDPI AG May 1, 2020. <https://doi.org/10.3390/molecules25102285>.
- (20) Joshi, D. K.; Sutton, J. W.; Carver, S.; Blanchard, J. P. Experiences with Commercial Production Scale Operation of Dissolving Metal Reduction Using Lithium Metal and Liquid Ammonia. *Org. Process Res. Dev.* **2005**, *9* (6), 997–1002. <https://doi.org/10.1021/op050155x>.
- (21) Kumar, A. B.; Manetsch, R. Ammonia-Free Synthesis of 3-Trifluoromethyl-3-Phenyldiaziridine. *Synth. Commun.* **2018**, *48* (6), 626–631. <https://doi.org/10.1080/00397911.2017.1354026>.
- (22) Tamura, Y.; Minamikawa, J.; Sumoto, K.; Fujii, S.; Ikeda, M. Synthesis and Some Properties of O-Acyl- and O-Nitrophenylhydroxylamines. *J. Org. Chem.* **1973**, *38* (6), 1239–1241. <https://doi.org/10.1021/jo00946a045>.
- (23) Ning, R. Y. Employment Ad Information. *Chem. Eng. News Archive* **1973**, *51* (51), 36–37. <https://doi.org/10.1021/cen-v051n051.p028>.
- (24) Mendiola, J.; Rincón, J. A.; Mateos, C.; Soriano, J. F.; de Frutos, Ó.; Niemeier, J. K.; Davis, E. M. Preparation, Use, and Safety of O-Mesitylenesulfonylhydroxylamine. *Org. Process Res. Dev.* **2009**, *13* (2), 263–267. <https://doi.org/10.1021/op800264p>.
- (25) Mayer, T.; Maier, M. E. Design and Synthesis of a Tag-Free Chemical Probe for Photoaffinity Labeling. *Eur. J. Org. Chem.* **2007**, No. 28, 4711–4720. <https://doi.org/10.1002/ejoc.200700188>.
- (26) Haldón, E.; Nicasio, M. C.; Pérez, P. J. Copper-Catalysed Azide–Alkyne Cycloadditions (CuAAC): An Update. *Org. Biomol. Chem.* **2015**, *13* (37), 9528–9550. <https://doi.org/10.1039/C5OB01457C>.
- (27) Rostovtsev, V. v.; Green, L. G.; Fokin, V. v.; Sharpless, K. B. A Stepwise Huisgen Cycloaddition Process: Copper(I)-Catalyzed Regioselective “Ligation” of Azides and Terminal Alkynes. *Angew. Chem.* **2002**, *114*, 2708–2711. [https://doi.org/10.1002/1521-3757\(20020715\)114:14<2708::AID-ANGE2708>3.0.CO;2-0](https://doi.org/10.1002/1521-3757(20020715)114:14<2708::AID-ANGE2708>3.0.CO;2-0).
- (28) Tron, G. C.; Piralì, T.; Billington, R. A.; Canonico, P. L.; Sorba, G.; Genazzani, A. A. Click Chemistry Reactions in Medicinal Chemistry: Applications of the 1,3-Dipolar Cycloaddition between Azides and Alkynes. *Med. Res. Rev.* **2008**, *28* (2), 278–308. <https://doi.org/10.1002/med.20107>.
- (29) Wang, Q.; Chan, T. R.; Hilgraf, R.; Fokin, V. v.; Sharpless, K. B.; Finn, M. G. Bioconjugation by Copper(I)-Catalyzed Azide-Alkyne [3 + 2] Cycloaddition. *J. Am. Chem. Soc.* **2003**, *125* (11), 3192–3193. <https://doi.org/10.1021/ja021381e>.

- (30) Pujari, S. S.; Seela, F. Parallel Stranded DNA Stabilized with Internal Sugar Cross-Links: Synthesis and Click Ligation of Oligonucleotides Containing 2'-Propargylated Isoguanosine. *J. Org. Chem.* **2013**, *78* (17), 8545–8561. <https://doi.org/10.1021/jo4012706>.
- (31) Pujari, S. S.; Ingale, S. A.; Seela, F. High-Density Functionalization and Cross-Linking of DNA: “Click” and “Bis-Click” Cycloadditions Performed on Alkynylated Oligonucleotides with Fluorogenic Anthracene Azides. *Bioconjugate Chem.* **2014**, *25* (10), 1855–1870. <https://doi.org/10.1021/bc5003532>.
- (32) Staudinger, von H.; Meyer, J. Über Neue Organische Phosphorverbindungen III. Phosphinmethylenderivate Und Phosphinimine. *Helv. Chim. Acta.* **1919**, *2*, 635–646.
- (33) Faucher, A.-M.; Grand-Maître, C. *Tris* (2-Carboxyethyl)Phosphine (TCEP) for the Reduction of Sulfoxides, Sulfonylchlorides, *N*-Oxides, and Azides. *Synth. Commun.* **2003**, *33* (20), 3503–3511. <https://doi.org/10.1081/SCC-120024730>.
- (34) Saneyoshi, H.; Ochikubo, T.; Mashimo, T.; Hatano, K.; Ito, Y.; Abe, H. Triphenylphosphinecarboxamide: An Effective Reagent for the Reduction of Azides and Its Application to Nucleic Acid Detection. *Org. Lett.* **2014**, *16* (1), 30–33. <https://doi.org/10.1021/ol402832w>.
- (35) Lenstra, D. C.; Wolf, J. J.; Mecinović, J. Catalytic Staudinger Reduction at Room Temperature. *J. Org. Chem.* **2019**, *84* (10), 6536–6545. <https://doi.org/10.1021/acs.joc.9b00831>.
- (36) Bednarek, C.; Wehl, I.; Jung, N.; Schepers, U.; Bräse, S. The Staudinger Ligation. *Chem. Rev.* **2020**, *120* (10), 4301–4354. <https://doi.org/10.1021/acs.chemrev.9b00665>.
- (37) Loudet, A.; Burgess, K. BODIPY Dyes and Their Derivatives: Syntheses and Spectroscopic Properties. *Chem. Rev.* **2007**, *107* (11), 4891–4932. <https://doi.org/10.1021/cr078381n>.
- (38) Ulrich, G.; Ziessel, R.; Harriman, A. The Chemistry of Fluorescent Bodipy Dyes: Versatility Unsurpassed. *Angew. Chem. Int. Ed.* **2008**, *47* (7), 1184–1201. <https://doi.org/10.1002/anie.200702070>.
- (39) Bacsa, I.; Konc, C.; Orosz, A.; Kecskeméti, G.; Rigó, R.; Özvegy-Laczka, C.; Mernyák, E. Synthesis of Novel C-2- or C-15-Labeled BODIPY—Estrone Conjugates. *Molecules* **2018**, *23* (4), 821. <https://doi.org/10.3390/molecules23040821>.
- (40) Sun, N.; Sun, Q.; Zhao, W.; Jin, L.; Hu, B.; Shen, Z.; Hu, X. Ligand-free Palladium-Catalyzed Carbonylative Suzuki Coupling of Aryl Iodides in Aqueous CH₃CN with Sub-stoichiometric Amount of Mo(CO)₆ as CO Source. *Adv. Synth. Catal.* **2019**, *361* (9), 2117–2123. <https://doi.org/10.1002/adsc.201900011>.

CHAPTER 4

Synthesis and Characterization of Aryl Propionamide Derivatives as Potential Selective Androgen Receptor Modulators

4.1 Introduction

4.1.1 Androgen and Androgen Receptor (AR)

The androgen receptor (AR) is a member of the steroid hormone nuclear receptor class, which plays a vital role in the expression of the male phenotype.^{1,2} Real-time PCR determined that AR exists mainly in male sexual organs but is found also in muscle, neuronal, renal tissues, and female reproductive organs.³ Some important functions of AR include the maintenance of spermatogenesis, the development of reproductive organs, and male puberty.^{4,5} Aside from its androgenic effects, AR also regulates a wide range of anabolic influences on various organs and tissues such as skin, bone, muscle, and the hematopoiesis system.⁴ These processes are initiated after its native ligands, androgens, bind to the AR.

Testosterone (T) and 5 α -dihydrotestosterone (DHT) are two primary endogenous ligands that activate AR upon binding (Figure 4.1).⁶ Testosterone is secreted by the Leydig cells in the testes, under the regulation of the luteinizing hormone (LH). Once synthesized, testosterone circulates in the body through the blood system and eventually enters the target cells by simple or facilitated diffusion. Testosterone can be converted to the more potent metabolite, DHT, by the enzyme 5 α -reductase in the presence of NADPH.^{7,8} It is found that the binding affinity of DHT to AR is four times higher than that of T, and DHT dissociates from AR three times more slowly than T.⁹ Although collective results suggested that DHT is a more potent endogenous ligand than T, DHT is produced mainly in the organs and tissues that express 5 α -reductase, such as the prostate gland, skin, and liver.^{10,11}

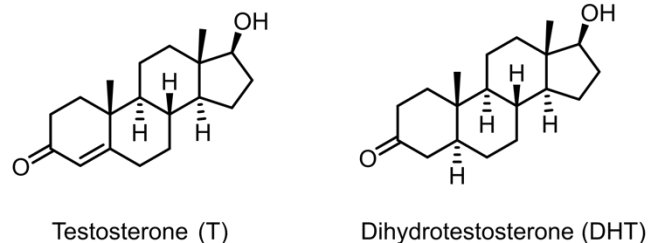


Figure 4.1. Chemical structure of testosterone and dihydrotestosterone.

4.1.1.1 The Structure of AR

The AR is a 110 kDa protein encoded by the AR gene composed of 919 amino acids. The AR contains three functionally distinct domains: the N-terminal domain (NTD), the DNA binding domain (DBD or D-box), and the ligand binding domain (LBD). Between DBD and LBD exists a flexible hinge region, connecting the two domains (Figure 4.2).^{6,12-15} The NTD, residues 1–555, makes up the majority of AR but is the least conserved domain. It contains the activation function-1 (AF-1) domain and is pivotal in maintaining the stability of AR. The AF-1 domain is an intrinsically disordered domain, which allows folding and the formation of protein–protein interactions to maintain the structural integrity.¹⁶ The FQNLF motif that resides within AF-1 is important in providing intra- and intermolecular NTD–LBD interdomain interactions, which could help stabilize the ARs upon dimerization after entering the nucleus and reduce dissociation.¹⁷ It has been shown that the deletion of AF-1 resulted in significant loss in its transcriptional activity.¹⁸⁻²⁰

The DBD (residues 556–623) is conserved highly in the family of steroid hormone receptors.¹³ It is a cysteine-rich region with two zinc-finger motifs, which are responsible for the homodimerization of AR. The zinc-finger motifs also interact with the androgen responsive elements (AREs) in the major groove of DNA to facilitate DNA recognition. The hinge region (residues 624–665) is a lysine-rich region and contains part of the nuclear localization signal (NLS). NLS (residues 617–633), which resides partially in the DBD and the hinge region, is necessary for the import of the receptor to the nucleus.^{21,22} Near the C-terminus, the LBD (residues 666–919) contains a ligand-binding pocket that binds to androgens and the AF-2

domain, which is essential for the transcriptional activity of AR. Unlike NTD, the crystal structure of LBD was well determined by the X-ray crystallography in 2000.²³

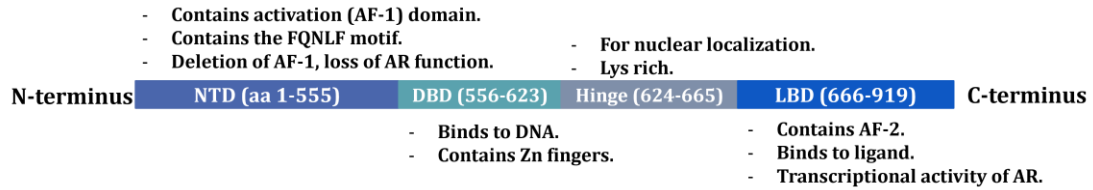


Figure 4.2. The schematic representation of AR structure.

4.1.1.2 Mechanism of Action of Androgens

In the cytoplasm, the AR initially is held inactive by the heat shock proteins, such as Hsp40 and Hsp70, through interacting with the FQNLF motif in the NTD. When the AR is bound to the heat shock protein, it is kept in a stable and soluble conformation ready for ligand binding.²⁴ Upon ligand binding, the heat shock protein is displaced by the ligand, and the intramolecular N/C interaction between the FQNLF motif in the NTD and the AF-2 in the LBD is initiated.^{25,26} Then, the agonist-bound AR is translocated to the nucleus. In the nucleus, the intramolecular N/C interaction is shifted mostly to the intermolecular N/C interaction to form the homodimer of AR.¹⁷ The transcription is regulated after the binding of dimerized AR to the androgen response elements (AREs) and the recruitment of coactivators (Figure 4.3).

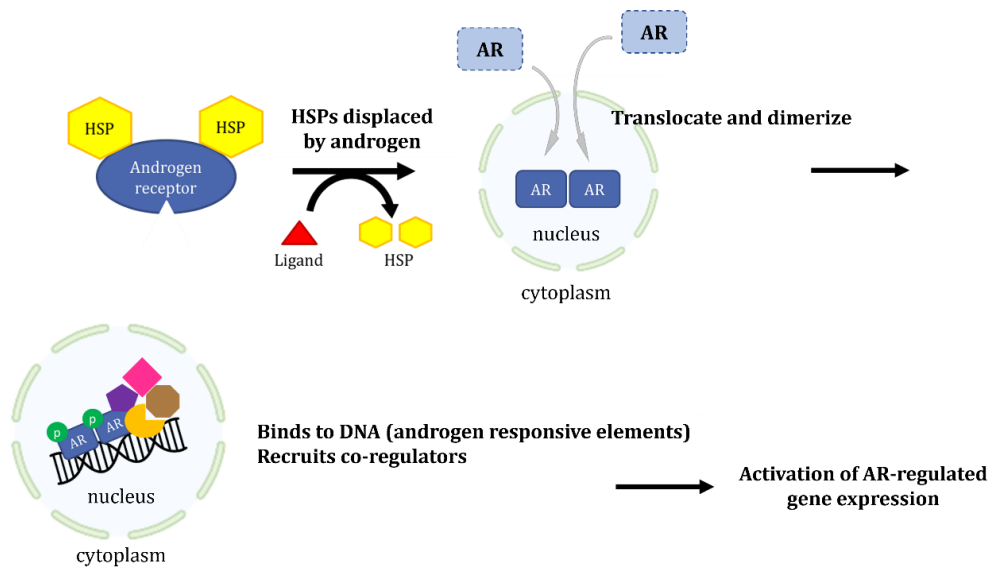


Figure 4.3. The schematic representation of AR mechanism.

4.1.1.3 Clinical Applications of Androgen

Androgens are the endogenous ligands of the AR. Endogenous androgens include testosterone (T) and its reduced metabolite, dihydrotestosterone (DHT). The most obvious therapeutic indication of androgens is hormone replacement therapy (HRT) for symptomatic hypogonadism.²⁷ Hypogonadism is the decreased level of sex hormones, such as testosterone for men, produced by the sex gland. It occurs commonly in aging men and often is accompanied with loss of body mass and reducing muscle strength, which result in immobility and poor quality of life. The administration of testosterone helps make up the deficient testosterone level and maintains related sexual functions.^{28,29} Aside from its androgenic effects, testosterone also possesses the ability to promote anabolism. Patients with testosterone in HRT were reported to have increased body mass and stronger muscle strength, which offers a chance to improve the quality of life.^{30,31}

Although a testosterone supplement in the HRT has shown to be able to increase body mass and muscle strength, adverse events also have been reported. In a Testosterone in Older Men with Mobility Limitations (TOM) trial conducted in 2010, participants were monitored for any adverse events associated with the treatment.³² The result suggested that participants who received transdermal testosterone gel developed a greater frequency of cardiovascular-related adverse events than the placebo group. In other randomized, placebo-controlled trials, testosterone-treated participants were more likely to develop erythrocytosis³³ compared to the placebo-treated men. Other reported adverse events associated with HRT include hepatotoxicity, benign prostate hyperplasia, risk of prostate cancer, lower urinary tract symptoms, and obstructive sleep apnea.³⁴

Most of the undesired adverse events of HRT originate from the intrinsic androgenic activities of androgens, which precluded the use of steroids.^{35,36} Aside from the undesired androgenic side effects, steroid-based therapies are usually given by injection or patches due to their poor bioavailability. To overcome the drawbacks of using steroids in HRT, attention has been drawn to investigate a class of small molecules, selective androgen receptor modulators (SARMs).

4.1.2 Selective Androgen Receptor Modulators (SARMs)

Selective androgen receptor modulators (SARMs) are classes of small molecules that act as androgen surrogates to target the AR selectively. Negro-Vilar coined the term selective androgen receptor modulators for their analogous activities with selective estrogen receptor modulators (SERMs), a class of molecules targeting estrogen receptors.³⁷ Ideal SARMs are described to be partial-agonists of the AR, which are capable of enhancing muscle mass/strength, bone growth, and libido, but with minimal stimulatory effects on the reproductive organs. Other advantages of non-steroidal SARMs include ease of structural modification and the potential to improve bioavailability.^{38–40} Benefiting from these advantages, SARMs have found clinical potential in treating diseases like cancer-related cachexia, sarcopenia, and osteoporosis.⁴¹ Although the clinical development of SARMs falls far behind that of SERMs, progress has been made in the past two decades.

SARMs are mostly non-steroidal small molecules, consisting of compounds with various chemical structures, which include aryl propionamide, hydantoin, *N*-aryl tropine, and quinolinone scaffolds (Figure 4.4).^{42–44} Aryl propionamide derivatives are one of the earliest classes of compounds investigated as SARMs. During the early stage of SARMs discovery, the Hershberger assay was the main approach to access their anabolic ability and tissue selectivity. In the assay, it was shown that several aryl propionamides were able to increase the weight of levator ani muscle, a muscular sheet that located in the pelvic floor. On the other hand, the aryl propionamide derivatives caused less increase in the weight of sexual-related organs, such as the prostate and seminal vesicle.^{45,46} Among the investigated aryl propionamide SARMs, enobosarm (GTx-024, S-22) has made its way into several phase II and phase III clinical trials for treating muscle wasting in patients who received chemotherapy previously.^{41,47,48}

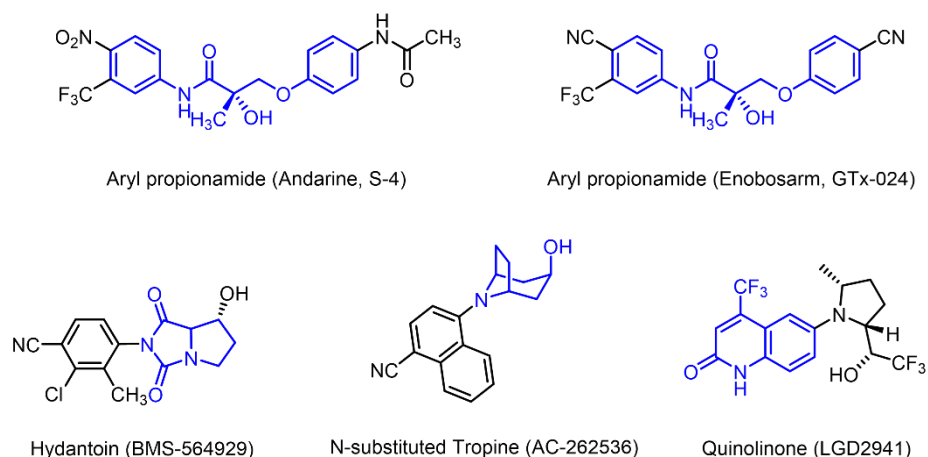


Figure 4.4. SARMs with different chemical structures.

Other pharmaceutical companies are devoted in the development of SARMs for age-related functional decline, such as muscle-wasting conditions and osteoporosis. Merck, Ligand Pharmaceuticals, Bristol-Myers Squibb, Johnson and Johnson, GSK, and several other pharmaceutical companies are also part of the race to discover potent SARM drug candidates for eventual commercialization.

4.1.2.1 Tissue Selectivity of SARMs

The mechanism of SARMs to selectively increase muscle mass and reach the desired anabolic effects in certain tissue remains poorly understood. However, several possible molecular mechanisms, such as the expression of enzyme in different tissues and the coactivator–corepressor ratio, were proposed to explain the tissue-selectivity of SARMs.^{39,44} One mechanism was proposed, based on the different distribution of 5 α -reductase, which is responsible for converting T to the more potent DHT. The enzyme is expressed mainly in skin and male accessory sex glands, which amplifies the cascade signal initiated by endogenous androgen but not by non-steroidal SARMs.^{49,50}

Another molecular mechanism concerns the recruitment or tissue-specific expression of co-regulators. To elaborate, the AR undergoes conformational changes in LBD after binding to the ligand, which leads to the expression of the downstream gene. Non-steroidal SARMs possess the ability to initiate a unique conformational

change compared to the endogenous androgens, which leads to the recruitment of different co-regulators and expression of related genes.⁵¹ The recruitment of co-regulators depends also on the availability of co-activators/co-repressors; therefore, the interaction between the AR and co-regulators may differ from organ to organ.⁵²

4.1.2.2 Potential Abuse of SARMs

Although the beneficial anabolic effects of non-steroidal SARMs indicate useful therapeutic applications towards muscle-wasting conditions, problems have emerged due to their performance-enhancing activity. Pioneered by Dalton et al., non-steroidal SARMs containing aryl propionamide scaffolds have made significant progress in the clinical trial; however, they have not received official approval by the Food and Drug Administration (FDA) yet. The performance-enhancing activity of SARMs makes them appealing to specific communities, for example, athletes and body builders. Despite not being approved by the FDA, many of the SARMs can be purchased online.⁵³ Thus, unapproved and forbidden SARMs could be accessed easily by athletes to boost their physical performance within a short period. For example, Andarine (S-4) and its metabolite were detected in the clinical samples of an athlete by liquid chromatography-tandem mass spectrometry (LC-MS/MS) analyses (Figure 4.4).⁵⁴ Due to their performance-enhancing properties, the SARMs were banned by the World Anti-Doping Agency (WADA) in 2008.

As increasing incidents of performance-enhancing drugs (PEDs) doping in the sports community occur, new means to detect possible PEDs in blood samples are in urgent need. Although existing PEDs can be detected by liquid chromatography with tandem mass spectrometry (LC-MS/MS), limitations still exist. Current methods rely on the comparison of the samples with the existing compounds and their metabolites, therefore, pose a challenge to detect newly emerged PEDs, including non-steroidal SARMs.⁵⁵

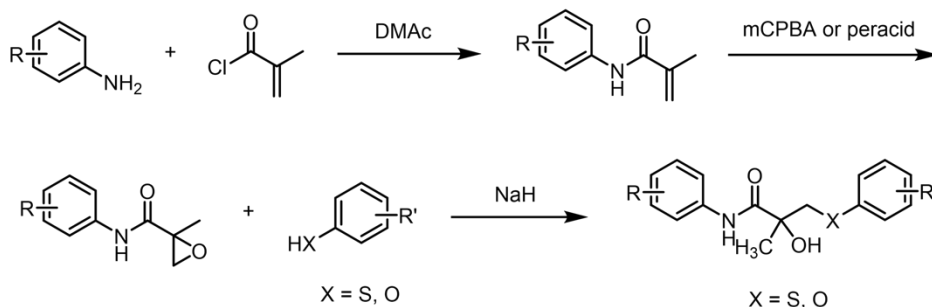
4.1.3 Different Categories of SARMs

SARMs are non-steroidal small molecules with different chemical structures, which comprise common scaffolds, including aryl propionamide, hydantoin, quinolinone,

and *N*-aryl tropine (Figure 4.4). In this section, the synthesis of prevalent SARMs will be described.

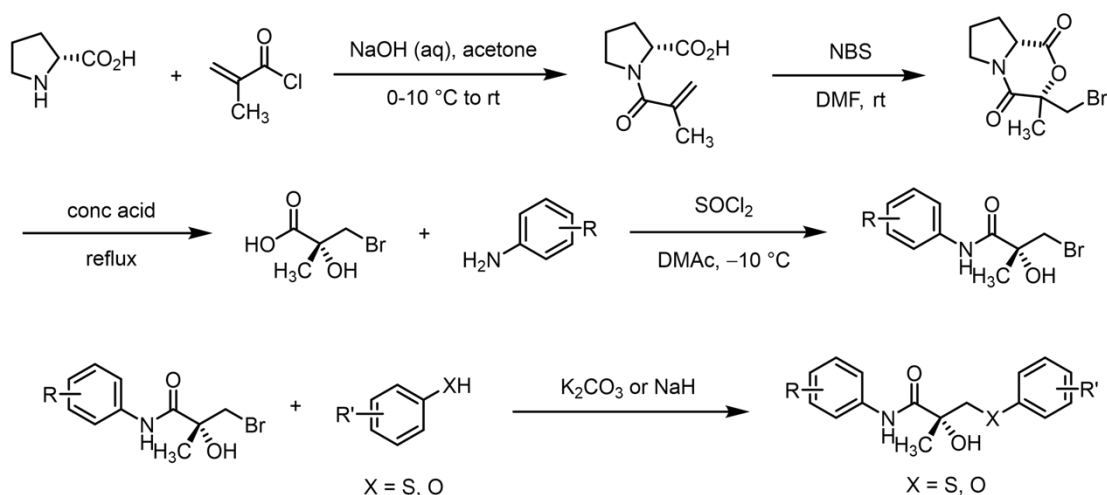
4.1.3.1 Aryl Propionamides

The synthesis of aryl propionamide derivatives can be accomplished by a robust synthetic route, involving three main steps (Scheme 4.1).⁵⁶ First, the construction of the α,β -unsaturated amide can be achieved by the coupling between a substituted aniline and methacryloyl chloride. Then, the α,β -unsaturated amide undergoes epoxidation to the corresponding epoxide with *m*-chloroperoxybenzoic acid (mCPBA) or other peroxide. Finally, the ring opening of epoxide with substituted aniline or thiophenol gives the aryl propionamide derivatives.



Scheme 4.1. General synthetic procedure of aryl propionamide derivatives.

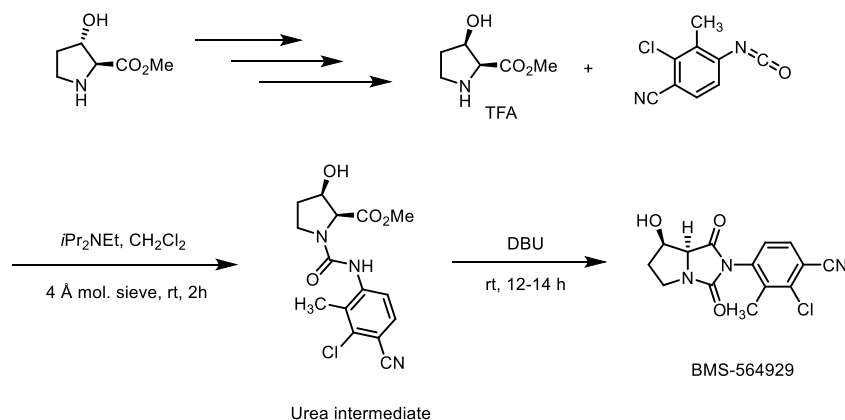
Enantiomerically-pure aryl propionamide can be prepared by using commercially accessible chiral auxiliary, (S)- or (R)-proline (Scheme 4.2). The synthesis began with the coupling between the chiral proline and methacryloyl chloride in aqueous acetone at low temperature. Next, the (S)- or (R)-prolineamide was converted to the bromolactone, according to an asymmetric bromolactonization reported by Jew and co-workers.^{57,58} The bromohydrin acid was furnished after the hydrolysis of bromolactone. The bromohydrin acid was converted to the corresponding acyl chloride, which was coupled with a substituted aniline. An S_N2 reaction was used to attach the other ring and provide the final aryl propionamide.



Scheme 4.2. Enantioselective route to aryl propionamides.

4.1.3.2 Hydantoin

One general synthetic route to the hydantoin is depicted in Scheme 4.3. The urea compound is the key intermediate to the hydantoin scaffold, which can be obtained by reaction between isocyanates and amino esters.^{59,60} Bristol-Myers Squibb established the synthesis of enantiomerically pure hydantoin SARMS, BMS-564929 (Scheme 4.3).⁶¹ The synthesis of the molecule involved the key urea intermediate, which was obtained from *trans*-3-hydroxy-L-proline methyl ester and 2-chloro-4-isocyanato-3 methylbenzonitrile at room temperature. The final step of the ring formation was carried out in the presence of DBU and purified by recrystallization to afford BMS-564929, whose stereochemistry was determined by the X-ray crystallography.⁶²



Scheme 4.3. Synthesis of BMS-564929 reported by Bristol-Myers Squibb.

4.1.3.3 Quinolinones

Quinolinones, especially the 6-*N*-alkyl or the 6-*N*-aryl quinolinones, were discovered recently to be potent and orally available SARMs. Ligand Pharmaceutical pioneered the discovery of these molecules as SARMs. LGD2226 and LGD2941 are two promising clinical candidates proposed by the company (Figure 4.5). The former is their first pre-clinical lead but later discontinued, as it is on the prohibited list by WADA. Although discontinued, the company reported that LGD2226 could bind to AR selectively and demonstrated the ability to modulate transcriptional activity.⁶³ On the other hand, LGD2941 is the compound that is in Phase I clinical trials for osteoporosis.⁶⁴

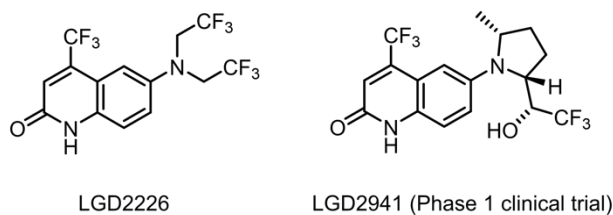
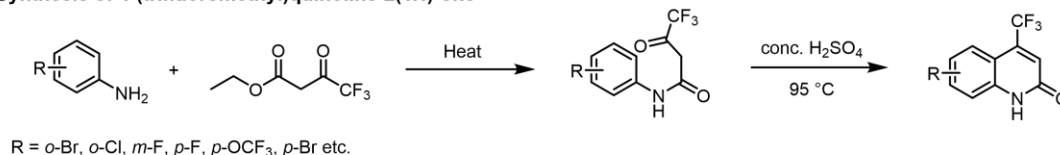


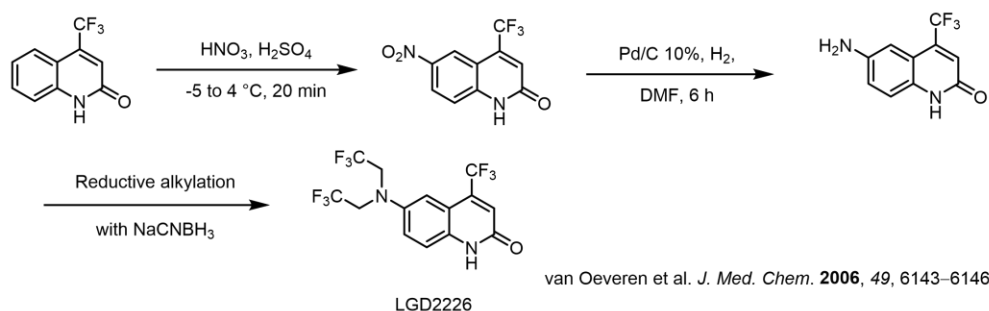
Figure 4.5. LGD2226 and LGD2941 by Ligand Pharmaceuticals.

They also demonstrated the synthetic procedures of the 6-substituted quinolinones.^{64,65} The reported SARMs shared the common 4-(trifluoromethyl)quinoline-2(1*H*)-one moiety, which could be synthesized from the condensation between ethyl 4,4,4-trifluoromethylacetoacetate and aniline, followed by cyclization promoted by concentrated sulfuric acid and heat (Scheme 4.4a).^{66,67} From there, the 6-*N,N*-dialkylamino substitution of LGD2226 was installed by nitration, using nitric acid, reduction of the nitro group to an amine group, followed by reductive alkylation (Scheme 4.4b).⁶⁵ The 6-pyrrolidine of LGD2941 was installed via the Buchwald–Hartwig reaction (Scheme 4.4c).⁶⁴

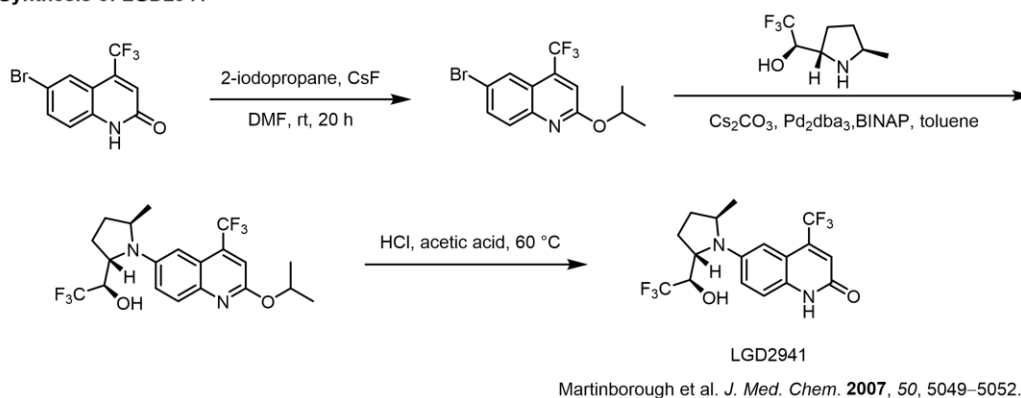
a) Synthesis of 4-(trifluoromethyl)quinoline-2(1H)-one



b) Synthesis of LGD2226



c) Synthesis of LGD2941



Scheme 4.4. Synthesis of quinolinone-containing SARMs.

4.1.3.4 N-Aryl Tropine

AC262536, an example of an N-aryl tropine, was discovered by Acadia Pharmaceuticals as the hit to lead compound during the development of SARMs. Along the SAR study of AC262536, they discovered another compound, ACP-105, as a potent SARMs with improved bioavailability (Figure 4.6).

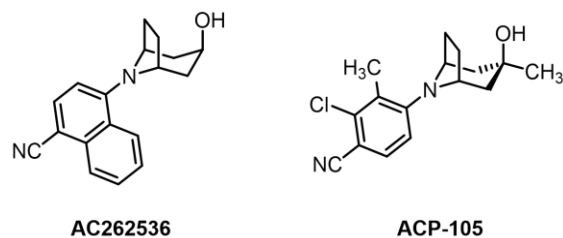
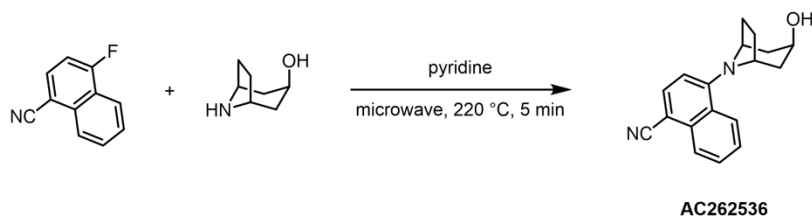


Figure 4.6. The chemical structures of AC262536 and ACP-105.

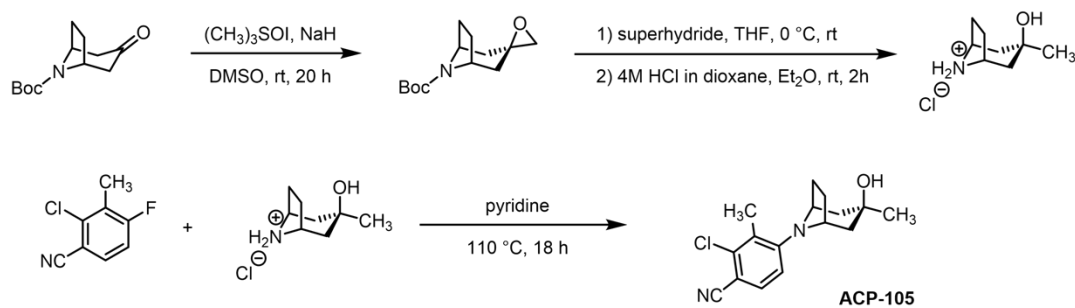
AC262536 could be accessed by a microwave assisted S_NAr reaction between the commercially available nortropine and 4-fluoro-1-naphthonitrile (Scheme 4.5a). Similarly, ACP-105 was synthesized through a S_NAr reaction, using the HCl salt of the nortropine intermediate and multi-substituted aniline (Scheme 4.5b).⁶⁸ The nortropine HCl salt was prepared from the Boc-protected tropinone in three steps: a diastereoselective Corey–Chaykovsky epoxidation, ring-opening with superhydride, followed by Boc deprotection with HCl.

a) Synthesis of AC262536



Schlienger et al. *J. Med. Chem.* **2009**, *52*, 7186–7191.

b) Synthesis of ACP-105



Schlienger et al. *J. Med. Chem.* **2009**, *52*, 7186–7191.

Scheme 4.5. Synthesis of N-aryl tropane SARMs.

4.1.3 Project Objectives

As mentioned earlier, the detection of PEDs relies currently on the comparison of known compounds and the samples; this makes the detection of new PEDs difficult, as no references are available. In consultation with collaborators, we hypothesized that building a library of SARMS-based PEDs, containing distinct chemical structures, offers a better chance to flag possible PEDs in clinical samples. Working with the research group of Professor James Harynuk in the Department of Chemistry at the University of Alberta, we set out to measure the physical properties and study their fragmentation patterns, using two dimensional gas chromatography (GC×GC).⁶⁹ When the GC×GC dataset is established, it can be used towards building a machine-learning algorithms and a predictive model to help flag any SARMS-based PEDs in blood or urine samples.

Along the way, we recognized the clinical significance of SARMS to treat cancer-related cachexia for their potentially beneficial muscle-building properties. However, we encountered difficulty in securing a collaborator to design and perform the screening of the compounds. In light of the delays around the evaluation of these compounds, our attention refocused on the molecular probe studies described in Chapters 2 and 3.

In this project, a library of SARMS with diverse scaffolds was assembled. This chapter mainly concerns the preparation and characterization of the aryl propionamide analogues. Although not yet tested, the bioactivity of the synthesized compounds will be evaluated when a suitable collaborator is secured.

4.2 Result and Discussion

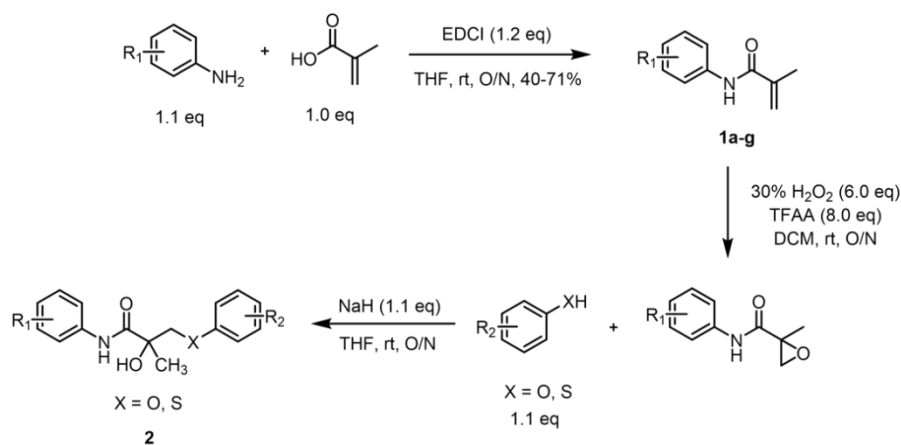
We were able to build a library of molecules with common non-steroidal SARMS structures, including aryl propionamide, hydantoin, quinolinone, and tropine. My contribution to this project focuses solely on the synthesis of the aryl propionamides, therefore, only the preparation and characterization of this class of molecules will be discussed in the following section.

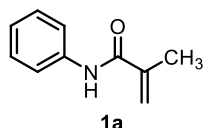
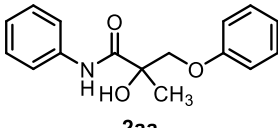
4.2.1 Synthesis of Aryl Propionamide Analogues

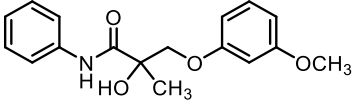
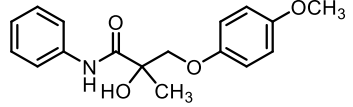
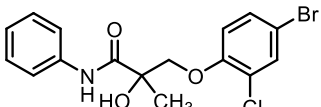
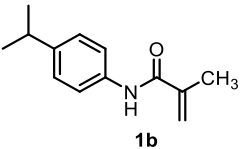
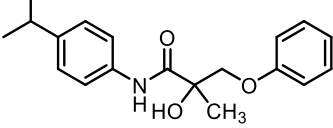
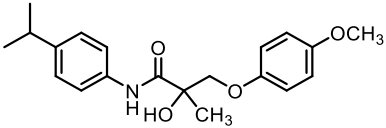
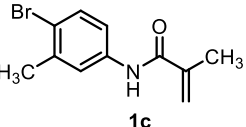
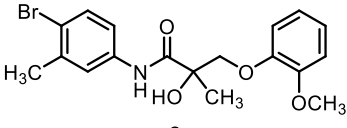
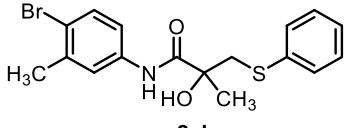
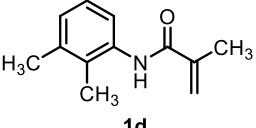
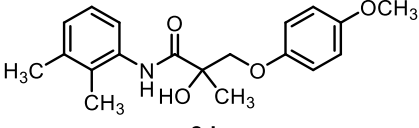
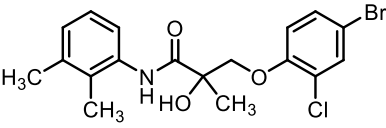
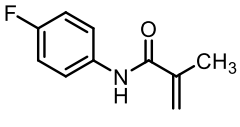
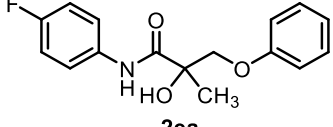
Library synthesis began with the preparation of anilide intermediates **1a-g**, which were synthesized via the amide bond formation with coupling reagent EDCI. Then, an epoxidation was carried out, using 30% hydrogen peroxide and trifluoroacetic anhydride (TFAA) in CH₂Cl₂ to give the corresponding epoxide, which could be employed in the next reaction without further purification. To derivatize the molecules, the epoxides underwent a ring opening with a substituted phenol or thiophenol as the nucleophile in the presence of sodium hydride to furnish the final aryl propionamide derivatives **2** (Table 4.1).

To build a reliable database to predict and flag any suspicious substances in a clinical sample, synthesizing molecules with various substitutions in the library remains an important objective of the project. I was able to synthesize a total of 19 derivatives with various substitutions. The library includes substrates with an electron-donating group, an electron-withdrawing group, and a halogen on both the aromatic rings. Derivatives with multiple substitutions, **2fc**, **2ga**, and **2gb**, were proposed and synthesized in order to obtain a better knowledge about the fragmentation patterns of the aryl propionamide analogs.

Table 4.1. Synthesis of the Anilide Intermediate **1a-g** and Aryl Propionamide Derivatives **2**



	1a-g	Yield	2	Yield
1	 1a	61%	 2aa	21%

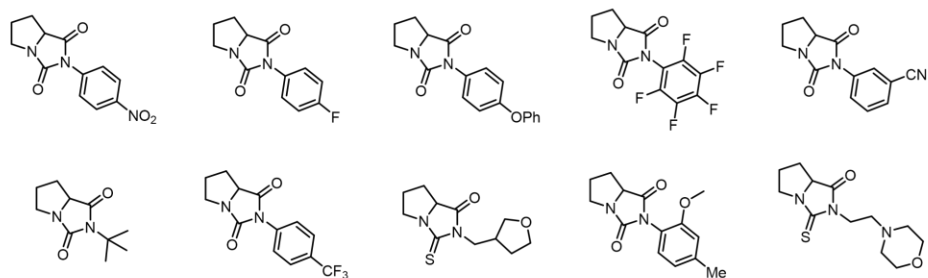
2			 2ab	40%
3			 2ac	42%
4			 2ad	38%
5	 1b	45%	 2ba	58%
6			 2bb	44%
7	 1c	61%	 2ca	33%
8			 2cb	45%
9	 1d	41%	 2da	24%
10			 2db	30%
11	 1e	71%	 2ea	34%

12			 2eb	28%
13			 2ec	22%
14			 2ed	25%
15			 2fa	54%
16	 1f	43%	 2fb	76%
17			 2fc	29%
18	 1g	70%	 2ga	32%
19			 2gb	39%

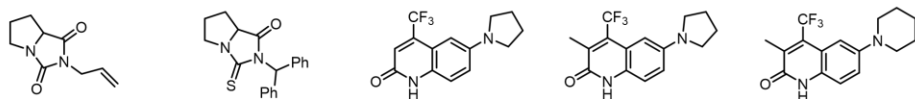
4.2.1. Compound Library

The construction of the full SARM library was carried out together by me and one of our colleagues, Dr. Tom Scully. The complete library has 67 compounds, including 36 aryl propionamide analogs, 12 hydantoin analogs, 3 quinolinone analogs, and 16 tropine/tropinone analogs. The complete library is laid out in Figure 4.7, and the compounds contributed by me are highlighted in blue.

b) Hydantoin analogues



c) Quinolinone analogues



d) N-alkyl/N-aryl tropine or tropinone analogues

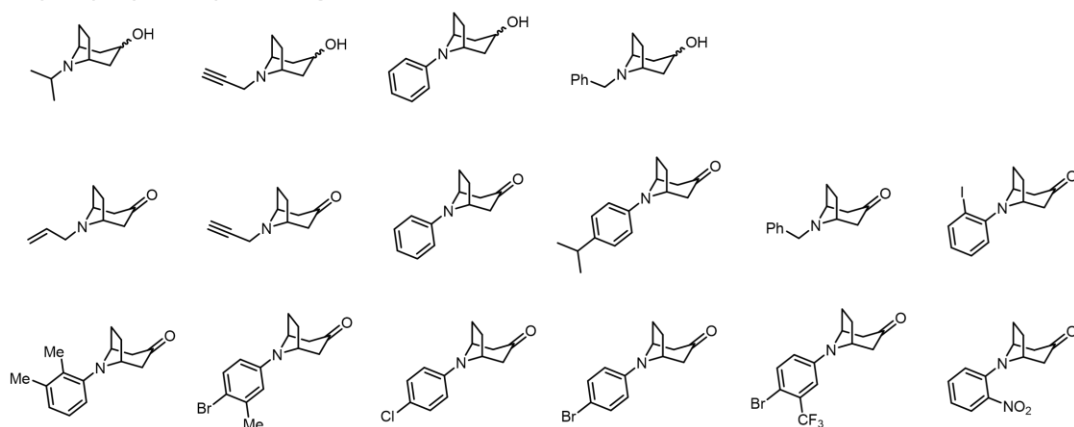


Figure 4.7. Library of the synthesized SARMs (cont.).

4.3 Conclusion

Selective androgen receptor modulators (SARMs) are molecules with diverse chemical structures that mimic the function of endogenous androgens. They are able to bind to the AR and trigger the downstream transcriptional activities. Unlike androgens, SARMs show stimulatory effects on muscle and bone, with minimal influence on the reproductive organs, such as the prostate gland. The desired anabolic effects of SARMs make them valuable candidates in treating muscle wasting disorders, for example, cancer-related cachexia, osteoporosis, and sarcopenia. However, their performance-enhancing property is a double-edged sword, as abuse of these un-approved drugs has been reported in athletes. In this project, we aim to synthesize a library of SARMs, which will be used towards building a machine learning algorithm to help detect newly emerged SARMs in clinical samples.

The prepared compounds will be analyzed by GC×GC for their fragmentation pattern, which will become useful information for anti-doping.

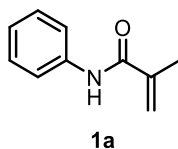
Along the development of the library, we came to realize that these compounds could point towards new therapeutics for muscle-wasting conditions. We envisioned testing the compounds in a cachexia model would provide insight on the potency of the compounds. Currently, effort is being made to find a suitable collaborator, and the biological activity of the synthesized compounds will be evaluated once the collaboration is established.

In this chapter, the synthesis and characterization of the aryl propionamides analogs were described. I was able to synthesize 19 compounds with various substitutions. Three multi-substituted compounds were made to obtain more information on the fragmentation patterns of the aryl propionamide derivatives. Together with one of my colleagues, we were able to construct a library of 67 compounds, including aryl propionamides, hydantoins, quinolinones, and *N*-aryl tropines/tropinones.

4.4 Experimental

General procedure for 1a-g

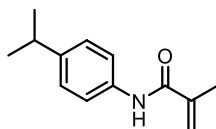
N-phenylmethacrylamide (1a)



To a 25 mL round bottom flask, equipped with a magnetic stir bar, was added methacrylic acid (2.3 mmol, 0.20 g, 0.20 mL) and tetrahydrofuran (15 mL), using disposable syringes, followed by the addition of EDC (2.8 mmol, 0.53 g). The reaction was kept under room temperature and stirred for 20 min before aniline (2.6 mmol, 0.23 mL) was added. Then, the flask was sealed with a rubber septum, and a needle was applied on the septum as a vent. Upon reaction completion, monitored by thin layer chromatography or after 24 h, the solvent was removed under

reduced pressure until <5 mL of solvent was left in the reaction flask. Once concentrated, the solution was diluted in ethyl acetate (20 mL) and added with 1M HCl (20 mL). The aqueous layer was extracted again with ethyl acetate (20 mL x 2). The organic layers were combined and washed with 1M HCl (10 mL), saturated NaHCO₃ (15 mL x 2), and brine (10 mL). The organic layer was separated, dried over MgSO₄, filtered, and concentrated under reduced pressure. The crude reaction mixture was purified by flash column chromatography, employing 1:2 ethyl acetate:hexane as eluent to give **1a** as a white solid (0.23 g, yield 61%): R_f 0.58 (1:2 ethyl acetate:hexane); IR (cast film): 3298, 3057, 2984, 1660, 1622, 1595, 1529, 1440, 1334, 1246, 1187, 936, 760 cm⁻¹; ¹H NMR (500 MHz, CDCl₃) δ 7.57–7.55 (m, 3H), 7.33 (t, *J* = 7.5 Hz, 2H), 7.12 (t, *J* = 7.5 Hz, 1H), 5.79 (s, 1H), 5.45 (s, 1H), 2.06 (s, 3H); ¹³C {¹H} NMR(125 MHz, CDCl₃) δ 166.6, 141.0, 137.8, 129.0, 124.4, 120.1, 119.8, 18.8; HRMS (ESI, [M+H]⁺) calcd for C₁₀H₁₂NO 162.0913, found: *m/z* 162.0917.

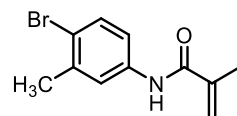
N-(4-isopropylphenyl)methacrylamide (**1b**)



1b

Synthesized according to the previous procedure, using methacrylic acid (2.0 mmol, 0.17 mL), 4-isopropylaniline (2.2 mmol, 0.47 mL), and EDC (2.4 mmol, 0.46 g) in THF (15 mL) to give **1b** (0.18 g, yield 45%): R_f 0.54 (1:2 ethyl acetate:hexane) as a brown solid; IR (cast film): 3343, 3044, 2954, 1659, 1625, 1595, 1415, 926, 829 cm⁻¹; ¹H NMR (500 MHz, CDCl₃) δ 7.47 (d, *J* = 8.5 Hz, 2H), 7.43 (br s, 1H), 7.20 (d, *J* = 8.5 Hz, 2H), 5.77 (s, 1H), 5.44 (s, 1H), 2.89 (sept, *J* = 7.0 Hz, 1H), 2.06 (s, 3H), 1.24 (d, *J* = 7.0 Hz, 6H); ¹³C {¹H} NMR (125 MHz, CDCl₃) δ 166.5, 145.2, 141.1, 135.4, 126.9, 120.1, 119.6, 33.6, 24.0, 18.8; HRMS (ESI, [M+Na]⁺) calcd for C₁₃H₁₈NNaO 226.1202, found: *m/z* 226.1204.

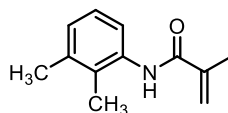
***N*-(4-bromo-3-methylphenyl)methacrylamide (1c)**



1c

Synthesized according to the previous procedure, using methacrylic acid (1.0 mmol, 82 μ L), 4-bromo-3-methylaniline (1.1 mmol, 0.20 g), and EDC (1.2 mmol, 0.22 g) in THF (15 mL) to give **1c** (0.17 g, yield 61%): R_f 0.50 (1:2 ethyl acetate:hexane) as a brown oil; IR (cast film): 3258 (sharp), 3092, 2979, 2961, 1867, 1663, 1624, 1579, 1527, 1473, 1399, 1195, 1028, 931, 801 cm^{-1} ; ^1H NMR (500 MHz, CDCl_3) δ 7.51 (d, $J = 2.5$ Hz, 1H), 7.46 (d, $J = 8.5$ Hz, 1H), 7.44 (br s, 1H), 7.25 (dd, $J = 9.0, 2.5$ Hz, 1H), 5.78 (s, 1H), 5.47 (s, 1H), 2.38 (s, 3H), 2.06 (s, 3H); ^{13}C $\{^1\text{H}\}$ NMR (125 MHz, CDCl_3) δ 166.5, 140.8, 138.7, 137.0, 132.7, 122.2, 120.1, 119.6, 119.0, 23.1, 18.8; HRMS (ESI, $[\text{M}+\text{H}]^+$) calcd for $\text{C}_{11}\text{H}_{13}\text{BrNO}$ 254.0175, found: m/z 254.0175.

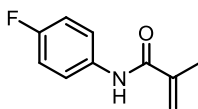
***N*-(2,3-dimethylphenyl)methacrylamide (1d)**



1d

Synthesized according to the previous procedure, using methacrylic acid (2.1 mmol, 0.18 mL), 2,3-dimethylaniline (2.3 mmol, 0.28 mL), and EDC (2.5 mmol, 0.49 g) in THF (15 mL) to give **1d** (0.16 g, yield 41%): R_f 0.49 (1:2 ethyl acetate:hexane) as pale brown solid; IR (cast film): 3257, 3020, 2951, 1660, 1622, 1519, 1454, 1385, 932, 773 cm^{-1} ; ^1H NMR (500 MHz, CDCl_3) δ 7.56 (d, $J = 8.0$ Hz, 1H), 7.36 (br s, 1H), 7.11 (dd, $J = 8.0, 7.5$ Hz, 1H), 7.02 (d, $J = 7.5$ Hz, 1H), 5.82 (s, 1H), 5.46 (s, 1H), 2.31 (s, 3H), 2.16 (s, 3H), 2.08 (s, 3H); ^{13}C $\{^1\text{H}\}$ NMR (125 MHz, CDCl_3) δ 166.7, 140.9, 137.4, 135.3, 129.0, 127.4, 126.0, 121.8, 119.8, 20.7, 18.9, 13.7; HRMS (ESI, $[\text{M}+\text{H}]^+$) calcd for $\text{C}_{12}\text{H}_{16}\text{NO}$ 190.1226, found: m/z 190.1228.

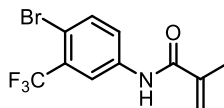
***N*-(4-fluorophenyl)methacrylamide (1e)**



1e

Synthesized according to the previous procedure, using methacrylic acid (3.5 mmol, 0.29 mL), 4-fluoroaniline (3.8 mmol, 0.43 g), and EDC (4.2 mmol, 0.80 g) in THF (20 mL) to give **1e** (0.49 g, yield 71%): R_f 0.50 (1:2 ethyl acetate:hexane) as a brown solid; IR (cast film): 3313, 3054, 2987, 2931, 1658, 1623, 1612, 1530, 1452, 1405, 1215, 1096, 931, 831 cm^{-1} ; ^1H NMR (500 MHz, CDCl_3) δ 7.54–7.47 (m, 3H), 7.07–6.98 (m, 2H), 5.78 (s, 1H), 5.46 (s, 1H), 2.06 (s, 3H); ^{13}C $\{^1\text{H}\}$ NMR (125 MHz, CDCl_3) δ 166.5, 159.5 (d, $J_{\text{C-F}} = 242.5$ Hz), 140.8, 133.8 (d, $J_{\text{C-F}} = 2.5$ Hz), 121.9 (d, $J_{\text{C-F}} = 7.5$ Hz), 120.0, 115.7 (d, $J_{\text{C-F}} = 22.5$ Hz), 18.8; HRMS (ESI, $[\text{M}+\text{Na}]^+$) calcd for $\text{C}_{10}\text{H}_{10}\text{FNNaO}$ 202.0639, found: m/z 202.0637.

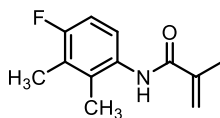
***N*-(4-bromo-3-(trifluoromethyl)phenyl)methacrylamide (1f)**



1f

Synthesized according to the previous procedure, using methacrylic acid (1.9 mmol, 0.16 mL), 4-bromo-3-trifluoromethylaniline (2.1 mmol, 0.50 g), and EDC (2.3 mmol, 0.44 g) in THF (15 mL) to give **1f** (0.25 g, yield 43%) as a colorless oil: R_f 0.49 (1:2 ethyl acetate:hexane); IR (cast film): 3311, 3117, 2985, 1668, 1629, 1526, 1479, 1412, 1322, 1166, 1141 1023 cm^{-1} ; ^1H NMR(500 MHz, CDCl_3) δ 7.87 (d, $J = 2.5$ Hz, 1H), 7.74 (br s, 1H), 7.69 (dd, $J = 8.5, 2.5$ Hz, 1H), 7.63 (d, $J = 8.5$ Hz, 1H), 5.81 (s, 1H), 5.51 (s, 1H), 2.05 (s, 3H); ^{13}C $\{^1\text{H}\}$ NMR (125 MHz, CDCl_3) δ 166.7, 140.3, 137.2, 135.5, 130.6 (q, $J_{\text{C-F}} = 31.3$ Hz), 124.1, 122.6 (q, $J_{\text{C-F}} = 272.5$ Hz), 120.8, 119.3 (q, $J_{\text{C-F}} = 6.3$ Hz), 114.1 (q, $J_{\text{C-F}} = 1.3$ Hz), 18.6; HRMS (ESI, $[\text{M}-\text{H}]^-$) calcd for $\text{C}_{11}\text{H}_8\text{BrF}_3\text{NO}$ 305.9747, found: m/z 305.9749.

***N*-(4-fluoro-2,3-dimethylphenyl)methacrylamide (1g)**

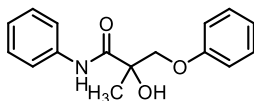


1g

Synthesized according to the previous procedure, using methacrylic acid (1.3 mmol, 0.11 mL), 2,3-dimethyl-4-fluoroaniline (1.4 mmol, 0.20 g), and EDC (1.6 mmol, 0.30 mg) in THF (15 mL) to give **1g** (0.19 g, yield 70%) as a pale yellow solid: R_f 0.49 (1:2 ethyl acetate:hexane); IR (cast film): 3289, 3045, 2930, 1657, 1621, 1533, 1482, 1426, 1241, 1043, 924, 817 cm^{-1} ; ^1H NMR (500 MHz, CDCl_3) δ 7.39 (dd, $J = 9.0, 5.5$ Hz, 1H), 7.25 (br s, 1H), 6.89 (t, $J = 9.0$ Hz, 1H), 5.83 (s, 1H), 5.47 (s, 1H), 2.21 (d, $J = 2.5$ Hz, 3H), 2.17 (s, 3H), 2.08 (s, 3H); ^{13}C $\{^1\text{H}\}$ NMR (125 MHz, CDCl_3) δ 166.9, 159.2 (d, $J_{\text{C-F}} = 241.3$ Hz), 140.7, 132.7 (d, $J_{\text{C-F}} = 5.0$ Hz), 130.9 (d, $J_{\text{C-F}} = 3.8$ Hz), 124.2 (d, $J_{\text{C-F}} = 16.3$ Hz), 123.5 (d, $J_{\text{C-F}} = 8.8$ Hz), 120.0, 112.7 (d, $J_{\text{C-F}} = 25.0$ Hz), 18.9, 14.3 (d, $J_{\text{C-F}} = 2.5$ Hz), 11.6 (d, $J_{\text{C-F}} = 5.0$ Hz); HRMS (ESI, $[\text{M}+\text{H}]^+$) calcd for $\text{C}_{12}\text{H}_{15}\text{FNO}$ 208.1132, found: m/z 208.1133.

Synthesis of aryl propionamides 2

Representative procedure: 2-Hydroxy-2-methyl-3-phenoxy-*N*-phenylpropanamide (2aa)

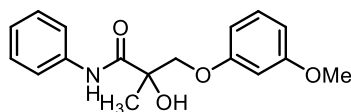


2aa

To a solution of **1a** (1.2 mmol, 0.20 g) with CH_2Cl_2 (40 mL) in a 100 mL round bottom flask was added trifluoroacetic anhydride (TFAA) (9.9 mmol, 0.76 mL), using a disposable syringe. Then, H_2O_2 (30% w/w in H_2O , 7.4 mmol, 0.58 mL) was added to the reaction mixture dropwise over 5 min, using a disposable syringe. The reaction was sealed with a rubber septum, and a needle was applied to the septum as a vent. It was stirred vigorously to ensure the proper mixture of the solution. After stirring

under room temperature for 24 h or when the reaction has gone to completion, as determined by thin layer chromatography, the reaction was poured over water and extracted with CH₂Cl₂ (20 mL x 2). The organic layers were combined and washed with H₂O (15 mL x 3), saturated NaHCO₃ (10 mL x 3), Na₂S₂O₃ (5 % w/v, 10 mL x 3), and brine (10 mL). The organic layer was separated, dried over MgSO₄, filtered, and concentrated under reduced pressure. The synthesized epoxide was used in the next reaction without further purification. To a new 50 mL round bottom flask was added phenol (1.4 mmol, 0.13 g), sodium hydride (60% dispersion in mineral oil, 1.4 mmol, 55 mg), and THF (15 mL). The reaction mixture was stirred under room temperature for 30 min before the addition of the previously synthesized epoxide. The reaction was purged with N₂, sealed with a rubber septum, and stirred under room temperature for 16 h. Upon reaction completion, the solvent was removed under reduced pressure. The residue was poured over H₂O (20 mL), and the aqueous layer was extracted with CH₂Cl₂ (20 mL x 2). The organic layers were combined and washed with H₂O (15 mL) and brine (15 mL). Then, the organic layer was separated, dried over MgSO₄, filtered, and concentrated under reduced pressure. The reaction crude was purified, using flash column chromatography, employing 1:2 ethyl acetate:hexane as eluent, to give **2aa** (72 mg, yield 21%) as a white solid: R_f 0.58 (1:2 ethyl acetate:hexane); IR (cast film): 3408, 3367, 3057, 2977, 2924, 1665, 1601, 1540, 1494, 1444, 1313, 1250, 1073, 1043, 754 cm⁻¹; ¹H NMR (400 MHz, CDCl₃) δ 8.73 (br s, 1H), 7.64–7.56 (m, 2H), 7.38–7.27 (m, 4H), 7.18–7.09 (m, 1H), 7.04–6.95 (m, 1H), 6.95–6.89 (m, 2H), 4.43 (d, *J* = 9.0 Hz, 1H), 4.01 (d, *J* = 9.0 Hz, 1H), 3.44 (s, 1H), 1.60 (s, 3H); ¹³C {¹H} NMR (125 MHz, CDCl₃) δ 171.9, 157.9, 137.4, 129.6, 129.1, 124.6, 121.8, 119.7, 114.8, 75.2, 72.5, 23.2; HRMS (ESI, [M+Na]⁺) calcd for C₁₆H₁₇NNaO₃ 294.1101, found: *m/z* 294.1099.

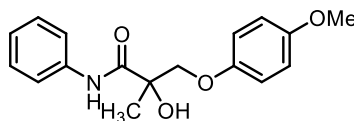
2-Hydroxy-3-(3-methoxyphenoxy)-2-methyl-*N*-phenylpropanamide (2ab)



2ab

Synthesized according to the previous procedure, using **1a** (1.3 mmol, 0.20 g), trifluoroacetic anhydride (TFAA) (9.9 mmol, 0.76 mL), H₂O₂ (30% w/w in H₂O, 7.4 mmol, 0.58 mL), and CH₂Cl₂ (40 mL), followed by the synthesized epoxide (0.62 mmol, 0.11 g), 3-methoxyphenol (0.68 mmol, 74 μL), sodium hydride 60% dispersion in mineral oil, 0.68 mmol, 27 mg), and THF (15 mL) to give **2aa** (0.15 g, yield 40%) as a white solid: *R_f* 0.37 (1:2 ethyl acetate:hexane); IR(cast film): 3371, 3062, 2935, 1688, 1600, 1533, 1493, 1444, 1314, 1289, 1202, 1153, 1051, 755 cm⁻¹; ¹H NMR (500 MHz, CDCl₃) δ 8.77 (br s, 1H), 7.60 (d, *J* = 8.0 Hz, 2H), 7.34 (t, *J* = 7.5 Hz, 2H), 7.18 (t, *J* = 8.0 Hz, 1H), 7.13 (t, *J* = 7.5 Hz, 1H), 6.58–6.47 (m, 3H), 4.40 (d, *J* = 9.0 Hz, 1H), 3.99 (d, *J* = 9.0 Hz, 1H), 3.77 (s, 3H), 3.63 (s, 1H), 1.59 (s, 3H); ¹³C {¹H} NMR(125 MHz, CDCl₃) δ 172.0, 160.9, 159.2, 137.3, 130.0, 129.0, 124.6, 119.7, 107.4, 106.9, 101.3, 75.3, 72.6, 55.3, 23.2; HRMS (ESI, [M+H]⁺) calcd for C₁₇H₂₀NO₄ 302.1387, found: *m/z* 302.1389.

2-Hydroxy-3-(4-methoxyphenoxy)-2-methyl-*N*-phenylpropanamide (**2ac**)

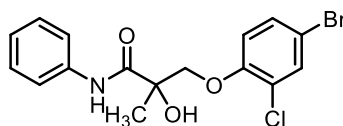


2ac

Synthesized according to the previous procedure, using **1a** (0.75 mmol, 0.12 g), trifluoroacetic anhydride (TFAA) (6.0 mmol, 0.46 mL), H₂O₂ (30% w/w in H₂O, 4.5 mmol, 0.35 mL), and CH₂Cl₂ (15 mL), followed by the synthesized epoxide (0.57 mmol, 0.10 g), 4-methoxyphenol (2.8 mmol, 0.35 g), sodium hydride (60% dispersion in mineral oil, 2.8 mmol, 0.11 g), and THF (15 mL) to give **2ac** (95 mg, yield 42%) as a pale brown solid: *R_f* 0.29 (1:2 ethyl acetate:hexane); IR (cast film): 3372, 3060, 2931, 1668, 1600, 1532, 1509, 1443, 1315, 1230, 1047, 825, 755 cm⁻¹; ¹H NMR (500 MHz, CDCl₃) δ 8.74 (br s, 1H), 7.62–7.56 (m, 2H), 7.38–7.30 (m, 2H), 7.17–7.09 (m, 1H), 6.89–6.85 (m, 2H), 6.84–6.80 (m, 2H), 4.38 (d, *J* = 9.0 Hz, 1H), 3.94 (d, *J* = 9.0 Hz, 1H), 3.76 (s, 3H), 3.52 (s, 1H), 1.57 (s, 3H); ¹³C {¹H} NMR (125 MHz, CDCl₃) δ 172.1, 154.7, 152.1, 137.4, 129.1, 124.6, 119.7,

116.0, 114.8, 75.3, 73.5, 55.8, 23.2; HRMS (ESI, $[M+Na]^+$) calcd for $C_{17}H_{19}NNaO_4$ 324.1206, found: m/z 324.1204.

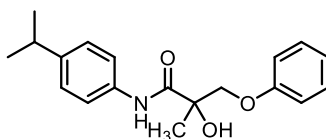
3-(4-Bromo-2-chlorophenoxy)-2-hydroxy-2-methyl-*N*-phenylpropanamide (2ad)



2ad

Synthesized according to the previous procedure, using **1a** (0.62 mmol, 0.10 g), trifluoroacetic anhydride (TFAA) (5.0 mmol, 0.38 mL), H_2O_2 (30% w/w in H_2O , 3.7 mmol, 0.29 mL), and CH_2Cl_2 (10 mL), followed by the synthesized epoxide (0.53 mmol, 93 mg), 4-methoxyphenol (1.3 mmol, 0.27 g), sodium hydride (60% dispersion in mineral oil, 1.3 mmol, 0.050 g), and THF (10 mL) to give **2ad** (89 mg, yield 38%) as a pale pink solid: R_f 0.27 (1:2 ethyl acetate:hexane); IR (cast film): 3370, 3065, 2931, 1667, 1600, 1534, 1484, 1445, 1292, 1266, 1248, 1065, 752 cm^{-1} ; 1H NMR (500 MHz, $CDCl_3$) δ 8.71 (br s, 1H), 7.58 (d, $J = 8.0$ Hz, 2H), 7.49 (d, $J = 2.5$ Hz, 1H), 7.37–7.29 (m, 3H), 7.14 (t, $J = 7.5$ Hz, 1H), 6.82 (d, $J = 9.0$ Hz, 1H), 4.38 (d, $J = 9.0$ Hz, 1H), 4.03 (d, $J = 9.0$ Hz, 1H), 3.78 (s, 1H), 1.62 (s, 3H); ^{13}C $\{^1H\}$ NMR (125 MHz, $CDCl_3$) δ 171.8, 152.7, 137.2, 132.7, 130.9, 129.1, 124.8, 124.1, 119.9, 115.5, 114.0, 74.8, 74.0, 23.3; HRMS (ESI, $[M+Na]^+$) calcd for $C_{16}H_{15}BrClNNaO_3$ 405.9816, found: m/z 405.9813.

2-Hydroxy-*N*-(4-isopropylphenyl)-2-methyl-3-phenoxypropanamide (2ba)

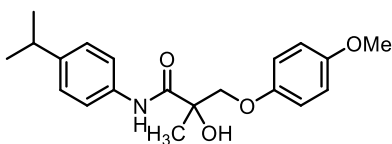


2ba

Synthesized according to the previous procedure, using **1b** (0.49 mmol, 0.10 g), trifluoroacetic anhydride (TFAA) (3.9 mmol, 0.30 mL), H_2O_2 (30% w/w in H_2O , 3.0 mmol, 0.23 mL), and CH_2Cl_2 (10 mL), followed by the synthesized epoxide (0.30 mmol, 65 mg), phenol (1.5 mmol, 0.14 g), sodium hydride (60% dispersion in

mineral oil, 1.5 mmol, 0.060 g), and THF (10 mL) to give **2ba** (0.090 g, yield 58%) as a pale yellow solid: R_f 0.36 (1:2 ethyl acetate:hexane); IR (cast film): 3325, 3045, 2953, 1658, 1602, 1547, 1498, 1245, 1177, 1051, 841, 748 cm^{-1} ; ^1H NMR (500 MHz, CDCl_3) δ 8.72 (br s, 1H), 7.52 (d, $J = 8.0$ Hz, 2H), 7.29 (app. t, $J = 8.0$ Hz, 2H), 7.20 (d, $J = 8.0$ Hz, 2H), 7.00 (app. t, $J = 7.5$ Hz, 1H), 6.93 (d, $J = 8.0$ Hz, 2H), 4.42 (d, $J = 9.0$ Hz, 1H), 4.00 (d, $J = 9.0$ Hz, 1H), 3.60 (s, 1H), 2.89 (sept, $J = 7.0$ Hz, 1H), 1.59 (s, 3H), 1.25 (d, $J = 7.0$ Hz, 6H); ^{13}C $\{^1\text{H}\}$ NMR (125 MHz, CDCl_3) δ 171.9, 158.0, 145.3, 135.1, 129.6, 126.9, 121.8, 119.8, 114.8, 75.2, 72.6, 33.7, 24.1, 23.2; HRMS (ESI, $[\text{M}+\text{Na}]^+$) calcd for $\text{C}_{19}\text{H}_{23}\text{NNaO}_3$ 336.1570, found: m/z 336.1564.

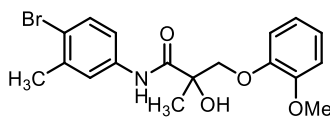
2-Hydroxy-*N*-(4-isopropylphenyl)-3-(4-methoxyphenoxy)-2-methylpropanamide (**2bb**)



2bb

Synthesized according to the previous procedure, using **1b** (0.49 mmol, 0.10 g), trifluoroacetic anhydride (TFAA) (3.9 mmol, 0.30 mL), H_2O_2 (30% w/w in H_2O , 3.0 mmol, 0.23 mL), and CH_2Cl_2 (10 mL), followed by the synthesized epoxide (0.30 mmol, 65 mg), 4-methoxyphenol (0.90 mmol, 0.11 g), sodium hydride (60% dispersion in mineral oil, 0.90 mmol, 36 mg), and THF (10 mL) to give **2bb** (74 mg, yield 44%) as a brown solid: R_f 0.33 (1:2 ethyl acetate:hexane); IR (cast film): 3377, 2960, 2933, 1666, 1593, 1528, 1509, 1461, 1231, 1051, 826 cm^{-1} ; ^1H NMR (500 MHz, CDCl_3) δ 8.69 (br s, 1H), 7.50 (d, $J = 8.5$ Hz, 2H), 7.20 (d, $J = 8.5$ Hz, 2H), 6.87–6.85 (m, 2H), 6.83–6.81 (m, 2H), 4.37 (d, $J = 9.0$ Hz, 1H), 3.93 (d, $J = 9.0$ Hz, 1H), 3.76 (s, 3H), 3.53 (s, 1H), 2.88 (sept, $J = 7.0$ Hz, 1H), 1.56 (s, 3H), 1.23 (d, $J = 7.0$ Hz, 6H); ^{13}C $\{^1\text{H}\}$ NMR (125 MHz, CDCl_3) δ 171.9, 154.6, 152.1, 145.3, 135.1, 127.0, 119.8, 116.0, 114.8, 75.2, 73.5, 55.8, 33.7, 24.1, 23.2; HRMS (ESI, $[\text{M}+\text{Na}]^+$) calcd for $\text{C}_{20}\text{H}_{25}\text{NNaO}_4$ 366.1676, found: m/z 366.1675.

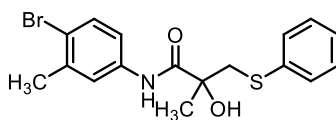
***N*-(4-Bromo-3-methylphenyl)-2-hydroxy-3-(2-methoxyphenoxy)-2-methylpropanamide (2ca)**



2ca

Synthesized according to the previous procedure, using **1c** (0.39 mmol, 0.10 g), trifluoroacetic anhydride (TFAA) (3.1 mmol, 0.24 mL), H₂O₂ (30% w/w in H₂O, 2.4 mmol, 0.18 mL), and CH₂Cl₂ (15 mL), followed by the synthesized epoxide (0.30 mmol, 0.80 g), 2-methoxyphenol (1.5 mmol, 0.18 g), sodium hydride (60% dispersion in mineral oil, 1.5 mmol, 59 mg), and THF (15 mL) to give **2ca** (51 mg, yield 33%) as a white solid: R_f 0.31 (1:2 ethyl acetate:hexane); IR (cast film): 3371, 3065, 2957, 2923, 1864, 1594, 1528, 1506, 1480, 1255, 1224, 1028, 744 cm⁻¹; ¹H NMR (500 MHz, CDCl₃) δ 8.92 (br s, 1H), 7.52 (d, *J* = 2.5 Hz, 1H), 7.46 (d, *J* = 8.5 Hz, 1H), 7.28 (dd, *J* = 8.5, 2.5 Hz, 1H), 7.05–6.96 (m, 2H), 6.95–6.88 (m, 2H), 4.46–4.43 (m, 2H), 3.92 (d, *J* = 9.0 Hz, 1H), 3.86 (s, 3H), 2.38 (s, 3H), 1.55 (s, 3H); ¹³C {¹H} NMR (125 MHz, CDCl₃) δ 172.7, 150.0, 147.6, 138.5, 136.8, 132.6, 123.4, 122.0, 121.4, 119.6, 118.9, 117.1, 112.1, 75.6, 74.6, 55.9, 23.6, 23.1; HRMS (ESI, [M+Na]⁺) calcd for C₁₈H₂₀BrNNaO₄ 416.0468, found: *m/z* 416.0462.

***N*-(4-Bromo-3-methylphenyl)-2-hydroxy-2-methyl-3-(phenylthio)propanamide (2cb)**

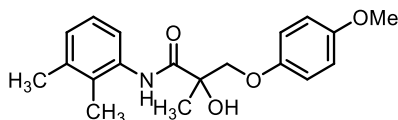


2cb

Synthesized according to the previous procedure, using **1c** (0.39 mmol, 0.10 g), trifluoroacetic anhydride (TFAA) (3.1 mmol, 0.24 mL), H₂O₂ (30% w/w in H₂O, 2.4 mmol, 0.18 mL), and CH₂Cl₂ (15 mL), followed by the synthesized epoxide (0.30 mmol, 82 mg), thiophenol (0.33 mmol, 36 mg), sodium hydride (60% dispersion in mineral oil, 0.33 mmol, 13 mg), and THF (10 mL) to give **2cb**

(66 mg, yield 45%) as a pale brown solid: R_f 0.54 (1:2 ethyl acetate:hexane); IR (cast film): 3366, 3059, 2927, 1665, 1604, 1583, 1538, 1480, 1204, 1028, 741 cm^{-1} ; ^1H NMR (400 MHz, CDCl_3) δ 8.63 (br s, 1H), 7.46–7.42 (m, 3H), 7.39 (d, $J = 2.4$ Hz, 1H), 7.29–7.18 (m, 3H), 7.16 (dd, $J = 8.4, 2.4$ Hz, 1H), 3.76 (d, $J = 14.0$ Hz, 1H), 3.49 (s, 1H), 3.23 (d, $J = 14.0$ Hz, 1H), 2.38 (s, 3H), 1.55 (s, 3H); ^{13}C $\{^1\text{H}\}$ NMR (125 MHz, CDCl_3) δ 172.2, 138.5, 136.4, 134.4, 132.5, 130.7, 129.2, 127.2, 121.9, 119.6, 118.7, 75.4, 44.9, 26.1, 23.0; HRMS (ESI, $[\text{M}+\text{Na}]^+$) calcd for $\text{C}_{17}\text{H}_{18}\text{BrNNaO}_2\text{S}$ 402.0134, found: m/z 402.0131.

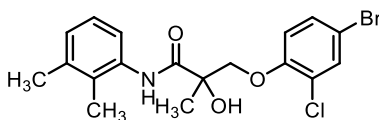
***N*-(2,3-Dimethylphenyl)-2-hydroxy-3-(4-methoxyphenoxy)-2-methylpropanamide (2da)**



2da

Synthesized according to the previous procedure using **1d** (0.48 mmol, 0.90 g), trifluoroacetic anhydride (TFAA) (3.8 mmol, 0.29 mL), H_2O_2 (30% w/w in H_2O , 2.9 mmol, 0.23 mL), and CH_2Cl_2 (10 mL), followed by the synthesized epoxide (0.32 mmol, 65 mg), 4-methoxyphenol (0.95 mmol, 0.12 g), sodium hydride (60% dispersion in mineral oil, 0.95 mmol, 38 mg), and THF (10 mL) to give **2da** (38 mg, yield 24%) as a white solid: R_f 0.33 (1:2 ethyl acetate:hexane); IR (cast film): 3377, 3067, 2932, 1667, 1587, 1508, 1462, 1231, 1048, 824, 770 cm^{-1} ; ^1H NMR (500 MHz, CDCl_3) δ 8.63 (br s, 1H), 7.64 (d, $J = 8.0$ Hz, 1H), 7.11 (dd, $J = 8.0, 7.5$ Hz, 1H), 7.01 (d, $J = 7.5$ Hz, 1H), 6.90–6.86 (m, 2H), 6.86–6.81 (m, 2H), 4.34 (d, $J = 9.0$ Hz, 1H), 3.97 (d, $J = 9.0$ Hz, 1H), 3.77 (s, 3H), 3.67 (s, 1H), 2.31 (s, 3H), 2.18 (s, 3H), 1.60 (s, 3H); ^{13}C $\{^1\text{H}\}$ NMR (125 MHz, CDCl_3) δ 172.3, 154.6, 152.1, 137.4, 135.0, 128.5, 127.25, 126.0, 121.1, 115.9, 114.8, 75.2, 73.6, 55.7, 23.4, 20.6, 13.6; HRMS (ESI, $[\text{M}+\text{Na}]^+$) calcd for $\text{C}_{19}\text{H}_{23}\text{NNaO}_4$ 352.1519, found: m/z 352.1517.

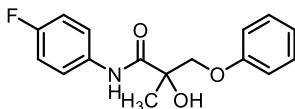
3-(4-Bromo-2-chlorophenoxy)-*N*-(2,3-dimethylphenyl)-2-hydroxy-2-methylpropanamide (2db)



2db

Synthesized according to the previous procedure, using **1d** (0.53 mmol, 0.10 g), trifluoroacetic anhydride (TFAA) (4.2 mmol, 0.32 mL), H₂O₂ (30% w/w in H₂O, 3.2 mmol, 0.25 mL), and CH₂Cl₂ (10 mL), followed by the synthesized epoxide (0.51 mmol, 65 mg), 4-bromo-2-chlorophenol (1.5 mmol, 0.32 g), sodium hydride (60% dispersion in mineral oil, 1.5 mmol, 61 mg), and THF (10 mL) to give **2db** (65 mg, yield 30%) as a white solid: R_f 0.27 (1:2 ethyl acetate:hexane); IR (cast film): 3368, 3070, 2923, 1666, 1583, 1526, 1484, 1385, 1291, 1265, 1065, 779 cm⁻¹; ¹H NMR (500 MHz, CDCl₃) δ 8.60 (br s, 1H), 7.54 (d, *J* = 8.0 Hz, 1H), 7.50 (d, *J* = 2.0 Hz, 1H), 7.33 (dd, *J* = 8.0, 2.5 Hz, 1H), 7.11 (dd, *J* = 8.0, 7.5 Hz, 1H), 7.02 (d, *J* = 7.5 Hz, 1H), 6.84 (d, *J* = 8.0 Hz, 1H), 4.43 (d, *J* = 9.0 Hz, 1H), 4.03 (d, *J* = 9.0 Hz, 1H), 3.76 (s, 1H), 2.30 (s, 3H), 2.16 (s, 3H), 1.63 (s, 3H); ¹³C {¹H} NMR (125 MHz CDCl₃) δ 172.0, 152.8, 137.5, 134.7, 132.7, 130.9, 129.2, 127.6, 125.9, 124.2, 121.5, 115.4, 113.9, 75.1, 74.1, 23.3, 20.6, 13.6; HRMS (ESI, [M+Na]⁺) calcd for C₁₈H₁₉BrClNaO₃ 434.0129, found: *m/z* 434.0124.

***N*-(4-Fluorophenyl)-2-hydroxy-2-methyl-3-phenoxypropanamide (2ea)**

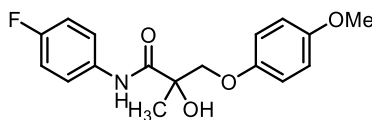


2ea

Synthesized according to the previous procedure, using **1e** (0.55 mmol, 0.10 g), trifluoroacetic anhydride (TFAA) (4.4 mmol, 0.34 mL), H₂O₂ (30% w/w in H₂O, 3.3 mmol, 0.26 mL), and CH₂Cl₂ (15 mL), followed by the synthesized epoxide (0.49 mmol, 96 mg), phenol (0.54 mmol, 51 mg), sodium hydride (60% dispersion in mineral oil, 0.54 mmol, 22 mg), and THF (10 mL) to give **2ea** (54 mg, yield 34%) as

a white solid: R_f 0.38 (1:2 ethyl acetate:hexane); IR (cast film): 3338, 3073, 2926, 1657, 1699, 1541, 1509, 1230, 1175, 1054, 839, 753 cm^{-1} ; ^1H NMR (400 MHz, CDCl_3) δ 8.72 (s, 1H), 7.58–7.53 (m, 2H), 7.32–7.27 (m, 2H), 7.06–6.98 (m, 3H), 6.95–6.91 (m, 2H), 4.43 (d, $J = 9.0$ Hz, 1H), 4.00 (d, $J = 9.0$ Hz, 1H), 3.44 (s, 1H), 1.59 (s, 3H); ^{13}C $\{^1\text{H}\}$ NMR (125 MHz, CDCl_3) δ 171.9, 159.5 (d, $J = 242.5$ Hz), 157.9, 133.4 (d, $J = 3.8$ Hz), 129.7, 121.9, 121.5 (d, $J = 7.5$ Hz), 115.7 (d, $J = 22.5$ Hz), 114.9, 75.3, 72.5, 23.2; HRMS (ESI, $[\text{M}+\text{Na}]^+$) calcd for $\text{C}_{16}\text{H}_{16}\text{FNNaO}_3$ 312.1006, found: m/z 312.1004.

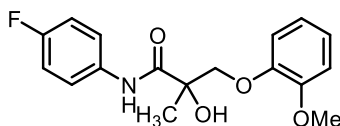
***N*-(4-Fluorophenyl)-2-hydroxy-3-(4-methoxyphenoxy)-2-methylpropanamide
(2eb)**



2eb

Synthesized according to the previous procedure, using **1e** (0.84 mmol, 0.15 g), trifluoroacetic anhydride (TFAA) (6.7 mmol, 0.51 mL), H_2O_2 (30% w/w in H_2O , 5.0 mmol, 0.39 mL), and CH_2Cl_2 (15 mL), followed by the synthesized epoxide (0.49 mmol, 95 mg), 4-methoxyphenol (0.54 mmol, 58 mg), sodium hydride (60% dispersion in mineral oil, 0.54 mmol, 22 mg), and THF (10 mL) to give **2eb** (76 mg, yield 28%) as a pale brown solid: R_f 0.33 (1:2 ethyl acetate:hexane); IR (cast film): 3372, 3051, 2933, 1667, 1610, 1534, 1509, 1457, 1231, 1181, 1048, 828 cm^{-1} ; ^1H NMR (400 MHz, CDCl_3) δ 8.74 (br s, 1H), 7.57–7.52 (m, 2H), 7.06–6.99 (m, 2H), 6.88–6.79 (m, 4H), 4.37 (d, $J = 8.8$ Hz, 1H), 3.93 (d, $J = 8.8$ Hz, 1H), 3.76 (s, 3H), 3.57 (s, 1H), 1.56 (s, 3H); ^{13}C $\{^1\text{H}\}$ NMR (125 MHz, CDCl_3) δ 172.1, 159.5 (d, $J_{\text{C-F}} = 242.5$ Hz), 154.6, 152.1, 133.4 (d, $J_{\text{C-F}} = 2.5$ Hz), 121.5 (d, $J_{\text{C-F}} = 7.5$ Hz), 116.0, 115.7 (d, $J_{\text{C-F}} = 21.3$ Hz), 114.8, 75.4, 73.5, 55.7, 23.1; HRMS (ESI, $[\text{M}+\text{Na}]^+$) calcd for $\text{C}_{17}\text{H}_{18}\text{FNNaO}_4$ 342.1112, found: m/z 342.1111.

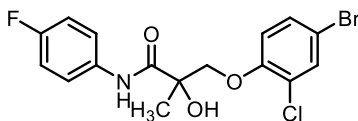
***N*-(4-Fluorophenyl)-2-hydroxy-3-(2-methoxyphenoxy)-2-methylpropanamide (2ec)**



2ec

Synthesized according to the previous procedure, using **1e** (0.84 mmol, 0.15 g), trifluoroacetic anhydride (TFAA) (6.7 mmol, 0.51 mL), H₂O₂ (30% w/w in H₂O, 5.0 mmol, 0.39 mL), and CH₂Cl₂ (15 mL), followed by the synthesized epoxide (0.49 mmol, 96 mg), 2-methoxyphenol (0.54 mmol, 58 mg), sodium hydride (60% dispersion in mineral oil, 0.54 mmol, 22 mg), and THF (10 mL) to give **2ec** (0.060 g, yield 22%) as a brown oil: R_f 0.56 (1:2 ethyl acetate:hexane); IR (cast film): 3376, 3068, 2933, 1676, 1594, 1530, 1509, 1455, 1256, 1214, 1124, 1028, 835, 746 cm⁻¹; ¹H NMR (400 MHz, CDCl₃) δ 8.98 (br s, 1H), 7.57–7.51 (m, 2H), 7.03–6.97 (m, 4H), 6.93–6.88 (m, 2H), 4.61 (s, 1H), 4.44 (d, *J* = 9.6 Hz, 1H), 3.94 (d, *J* = 9.6 Hz, 1H), 3.82 (s, 3H), 1.56 (s, 3H); ¹³C {¹H} NMR (125 MHz, CDCl₃) δ 172.6, 159.4 (d, *J*_{C-F} = 242.5 Hz), 149.9, 147.7, 133.7 (d, *J*_{C-F} = 2.5 Hz), 123.2, 121.5 (d, *J*_{C-F} = 7.5 Hz), 121.4, 116.8, 115.6 (d, *J*_{C-F} = 22.5 Hz), 112.1, 75.5, 74.6, 55.8, 23.5; HRMS (ESI, [M+Na]⁺) calcd for C₁₇H₁₈FNNaO₄ 342.1112, found: *m/z* 342.1106.

3-(4-Bromo-2-chlorophenoxy)-*N*-(4-fluorophenyl)-2-hydroxy-2-methylpropanamide (2ed)

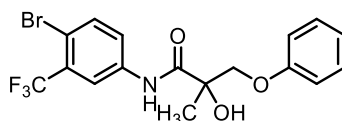


2ed

Synthesized according to the previous procedure, using **1e** (0.61 mmol, 0.12 g), trifluoroacetic anhydride (TFAA) (4.9 mmol, 0.56 mL), H₂O₂ (30% w/w in H₂O, 3.7 mmol, 0.44 mL), and CH₂Cl₂ (15 mL), followed by the synthesized epoxide (0.47 mmol, 0.10 g), 3-bromo-2-chloro-4-phenol (1.2 mmol, 0.25 g), sodium hydride

(60% dispersion in mineral oil, 1.2 mmol, 46 mg), and THF (10 mL) to give **2ed** (0.060 g, yield 25%) as a pale brown solid: R_f 0.30 (1:2 ethyl acetate:hexane); IR (cast film): 3373, 3073, 2926, 1666, 1610, 1532, 1511, 1484, 1454, 1292, 1248, 1213, 1065, 833 cm^{-1} ; ^1H NMR (500 MHz, CDCl_3) δ 8.67 (br s, 1H), 7.55–7.52 (m, 2H), 7.51 (d, $J = 2.5$ Hz, 1H), 7.34 (dd, $J = 8.5, 2.5$ Hz, 1H), 7.03 (m, 2H), 6.84 (d, $J = 9.0$ Hz, 1H), 4.39 (d, $J = 9.0$ Hz, 1H), 4.03 (d, $J = 9.0$ Hz, 1H), 3.63 (s, 1H), 1.61 (s, 3H); ^{13}C $\{^1\text{H}\}$ NMR (125 MHz, CDCl_3) δ 171.7, 159.6 (d, $J_{\text{C-F}} = 242.5$ Hz), 152.7, 133.3 (d, $J_{\text{C-F}} = 3.8$ Hz), 132.8, 131.0, 124.2, 121.7 (d, $J_{\text{C-F}} = 7.5$ Hz), 115.8 (d, $J_{\text{C-F}} = 22.5$ Hz), 115.6, 114.2, 74.8, 74.0, 23.3; HRMS (ESI, $[\text{M}+\text{Na}]^+$) calcd for $\text{C}_{16}\text{H}_{14}\text{BrClFNNaO}_3$ 423.9722, found: m/z 423.9714.

***N*-(4-Bromo-3-(trifluoromethyl)phenyl)-2-hydroxy-2-methyl-3-phenoxypropanamide (2fa)**

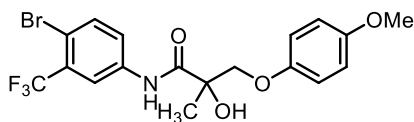


2fa

Synthesized according to the previous procedure, using **1f** (2.3 mmol, 0.70 g), trifluoroacetic anhydride (TFAA) (18 mmol, 1.4 mL), H_2O_2 (30% w/w in H_2O , 14 mmol, 1.1 mL), and CH_2Cl_2 (20 mL) to afford the corresponding epoxide (0.65 g). From there, a portion of the synthesized epoxide was taken and used in the next reaction. The epoxide (0.31 mmol, 0.10 g), phenol (0.78 mmol, 73 mg), sodium hydride (60% dispersion in mineral oil, 0.78 mmol, 31 mg), and THF (10 mL) were used to give **2fa** (0.080 g, yield 54%) as a colorless oil: R_f 0.30 (1:2 ethyl acetate:hexane); IR (cast film): 3362, 3042, 2928, 1677, 1600, 1589, 1528, 1497, 1480, 1418, 1322, 1243, 1174, 1142, 1102, 754 cm^{-1} ; ^1H NMR (500 MHz, CDCl_3) δ 8.92 (br s, 1H), 7.96 (d, $J = 2.5$ Hz, 1H), 7.70 (dd, $J = 8.5, 2.5$ Hz, 1H), 7.63 (d, $J = 8.5$ Hz, 1H), 7.32–7.26 (m, 2H), 7.00 (t, $J = 7.5$ Hz, 1H), 6.91 (d, $J = 8.0$ Hz, 2H), 4.44 (d, $J = 9.0$ Hz, 1H), 3.99 (d, $J = 9.0$ Hz, 1H), 3.55 (s, 1H), 1.58 (s, 3H); ^{13}C $\{^1\text{H}\}$ NMR (125 MHz, CDCl_3) δ 172.4, 157.8, 136.8, 135.5, 130.7 (q, $J_{\text{C-F}}$ $J = 31.3$ Hz), 129.7, 123.7, 122.6 (q, $J_{\text{C-F}} = 272.5$ Hz), 122.0, 119.0 (q, $J_{\text{C-F}} = 6.3$ Hz),

114.8, 114.2 (q, $J_{C-F} = 2.5$ Hz), 75.6, 72.4, 23.1; HRMS (ESI, $[M+Na]^+$) calcd for $C_{17}H_{15}BrF_3NNaO_3$ 440.0080, found: m/z 440.0070.

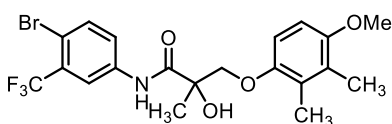
***N*-(4-Bromo-3-(trifluoromethyl)phenyl)-2-hydroxy-3-(4-methoxyphenoxy)-2-methylpropanamide (2fb)**



2fb

Synthesized according to the previous procedure, using **1f** (2.3 mmol, 0.70 g), trifluoroacetic anhydride (TFAA) (18 mmol, 1.4 mL), H_2O_2 (30% w/w in H_2O , 14 mmol, 1.1 mL), and CH_2Cl_2 (20 mL) to afford the corresponding epoxide (0.65 g). From there, a portion of the synthesized epoxide was taken and used in the next reaction. The epoxide (0.46 mmol, 0.15 g), 4-methoxyphenol (1.4 mmol, 0.17 g), sodium hydride (60% dispersion in mineral oil, 1.4 mmol, 56 mg), and THF (10 mL) was used to give **2fb** (0.18 g, yield 76%) as a brown oil: R_f 0.38 (1:2 ethyl acetate:hexane); IR (cast film): 3365, 3050, 2936, 1677, 1589, 1527, 1509, 1480, 1417, 1323, 1230, 1178, 1142, 1106, 1048, 824 cm^{-1} ; 1H NMR (500 MHz, $CDCl_3$) δ 8.93 (br s, 1H), 7.95 (d, $J = 2.5$ Hz, 1H), 7.68 (dd, $J = 9.0, 2.5$ Hz, 1H), 7.62 (d, $J = 8.5$ Hz, 1H), 6.85–6.82 (m, 2H), 6.82–6.79 (m, 2H), 4.38 (d, $J = 9.0$ Hz, 1H), 3.92 (d, $J = 9.0$ Hz, 1H), 3.75 (s, 3H), 3.63 (s, 1H), 1.55 (s, 3H); ^{13}C $\{^1H\}$ NMR (125 MHz, $CDCl_3$) δ 172.6, 154.7, 151.9, 136.8, 135.5, 130.6 (q, $J_{C-F} = 31.3$ Hz), 123.6, 122.6 (q, $J_{C-F} = 272.5$ Hz), 119.0 (q, $J_{C-F} = 6.3$ Hz), 116.0, 114.8, 114.1 (q, $J_{C-F} = 1.3$ Hz), 75.6, 73.4, 55.7, 23.0; HRMS (ESI, $[M+Na]^+$) calcd for $C_{18}H_{17}BrF_3NNaO_4$ 470.0185, found: m/z 470.0182.

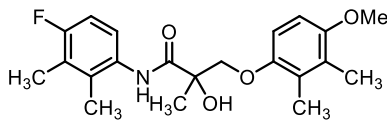
***N*-(4-Bromo-3-(trifluoromethyl)phenyl)-2-hydroxy-3-(4-methoxy-2,3-dimethylphenoxy)-2-methylpropanamide (2fc)**



2fc

Synthesized according to the previous procedure, using **1f** (2.3 mmol, 0.70 g), trifluoroacetic anhydride (TFAA) (18 mmol, 1.4 mL), H₂O₂ (30% w/w in H₂O, 14 mmol, 1.1 mL), and CH₂Cl₂ (20 mL) to afford the corresponding epoxide (0.65 g). From there, a portion of the synthesized epoxide was taken and used in the next reaction. The epoxide (0.32 mmol, 0.10 g), 2,3-dimethyl-4-methoxyphenol (0.78 mmol, 0.12 g), sodium hydride (60% dispersion in mineral oil, 0.78 mmol, 31 mg), and THF (10 mL) were used to give **2fc** (0.050 g, yield 29%) as a brown sticky oil: R_f 0.36 (1:2 ethyl acetate:hexane); IR (cast film): 3362, 2995, 2925, 1676, 1588, 1526, 1481, 1417, 1322, 1255, 1142, 1114, 1023 cm⁻¹; ¹H NMR (500 MHz, CDCl₃) δ 8.93 (br s, 1H), 7.96 (d, *J* = 2.5 Hz, 1H), 7.71 (dd, *J* = 8.5, 2.5 Hz, 1H), 7.65 (d, *J* = 8.5 Hz, 1H), 6.68 (d, *J* = 9.0 Hz, 1H), 6.63 (d, *J* = 9.0 Hz, 1H), 4.32 (d, *J* = 9.0 Hz, 1H), 3.94 (d, *J* = 9.0 Hz, 1H), 3.77 (s, 3H), 3.51 (s, 1H), 2.14 (s, 3H), 2.11 (s, 3H), 1.58 (s, 3H); ¹³C {¹H} NMR (125 MHz, CDCl₃) δ 172.7, 152.9, 149.9, 136.9, 135.5, 130.7 (q, *J*_{C-F} = 31.3 Hz), 127.0, 127.0, 123.7, 122.6 (q, *J*_{C-F} = 272.5 Hz), 119.0 (q, *J*_{C-F} = 6.3 Hz), 114.2 (q, *J*_{C-F} = 1.3 Hz), 110.5, 108.1, 75.8, 74.1, 56.0, 23.0, 12.3, 12.1; HRMS (ESI, [M+Na]⁺) calcd for C₂₀H₂₁BrF₃NNaO₄ 498.0498, found: *m/z* 498.0496.

***N*-(4-Fluoro-2,3-dimethylphenyl)-2-hydroxy-3-(4-methoxy-2,3-dimethylphenoxy)-2-methylpropanamide (2ga)**

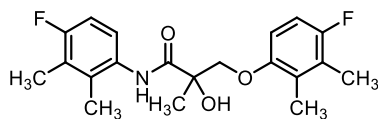


2ga

Synthesized according to the previous procedure, using **1g** (0.72 mmol, 0.15 g), trifluoroacetic anhydride (TFAA) (5.8 mmol, 0.44 mL), H₂O₂ (30% w/w in H₂O, 4.4 mmol, 0.34 mL), and CH₂Cl₂ (15 mL) to afford the corresponding epoxide (0.11 g). From there, a portion of the synthesized epoxide was taken and used in the next reaction. The epoxide (0.27 mmol, 0.060 g), 2,3-dimethyl-4-methoxyphenol (0.40 mmol, 61 mg), sodium hydride (60% dispersion in mineral oil, 0.40 mmol,

16 mg), and THF (10 mL) were used to give **2ga** (47 mg, yield 32%) as a brown sticky solid: R_f 0.26 (1:2 ethyl acetate:hexane); IR (cast film): 3369, 2995, 2932, 1664, 1590, 1521, 1484, 1254, 1212, 21140, 808, 739 cm^{-1} ; ^1H NMR (500 MHz, CDCl_3) δ 8.56 (br s, 1H), 7.45 (dd, $J = 9.0, 4.5$ Hz, 1H), 6.89 (t, $J = 9.0$ Hz, 1H), 6.70 (d, $J = 9.0$ Hz, 1H), 6.64 (d, $J = 8.5$ Hz, 1H), 4.32 (d, $J = 9.0$ Hz, 1H), 3.95 (d, $J = 9.0$ Hz, 1H), 3.78 (s, 3H), 3.60 (s, 1H), 2.20 (d, $J = 2.0$ Hz, 3H), 2.17 (s, 3H), 2.16 (s, 3H), 2.15 (s, 3H), 1.61 (s, 3H); ^{13}C $\{^1\text{H}\}$ NMR (125 MHz, CDCl_3) δ 172.7, 159.0 (d, $J_{\text{C-F}} = 240.0$ Hz), 152.8, 150.0, 132.1 (d, $J_{\text{C-F}} = 5.0$ Hz), 130.6 (d, $J_{\text{C-F}} = 3.8$ Hz), 126.9 (d, $J_{\text{C-F}} = 15.0$ Hz), 124.1 (d, $J_{\text{C-F}} = 16.3$ Hz), 122.7 (d, $J_{\text{C-F}} = 8.8$ Hz), 112.7, 112.6, 110.4, 108.0, 75.5, 74.1, 56.0, 23.3, 14.1 (d, $J_{\text{C-F}} = 3.8$ Hz), 12.3, 12.1, 11.5 (d, $J_{\text{C-F}} = 5.0$ Hz); HRMS (ESI, $[\text{M}+\text{Na}]^+$) calcd for $\text{C}_{21}\text{H}_{26}\text{FNNaO}_4$ 398.1738, found: m/z 398.1732.

3-(4-Fluoro-2,3-dimethylphenoxy)-*N*-(4-fluoro-2,3-dimethylphenyl)-2-hydroxy-2-methylpropanamide (**2gb**)



2gb

Synthesized according to the previous procedure, using **1g** (0.72 mmol, 0.15 g), trifluoroacetic anhydride (TFAA) (5.8 mmol, 0.44 mL), H_2O_2 (30% w/w in H_2O , 4.4 mmol, 0.34 mL), and CH_2Cl_2 (15 mL) to afford the corresponding epoxide (0.11 g). From there, a portion of the synthesized epoxide was taken and used in the next reaction. The epoxide (0.22 mmol, 0.050 g), 2,3-dimethyl-4-fluorophenol (0.34 mmol, 47 mg), sodium hydride (60% dispersion in mineral oil, 0.34 mmol, 14 mg), and THF (10 mL) were used to give **2gb** (45 mg, yield 39%) as a white sticky solid: R_f 0.30 (1:2 ethyl acetate:hexane); IR (cast film): 3377, 2980, 2930, 1664, 1589, 1521, 1483, 1458, 1241, 1211, 1108, 807 cm^{-1} ; ^1H NMR (500 MHz, CDCl_3) δ 8.55 (br s, 1H), 7.45 (dd, $J = 9.0, 4.5$ Hz, 1H), 6.89 (t, $J = 9.0$ Hz, 1H), 6.81 (t, $J = 9.0$ Hz, 1H), 6.67 (dd, $J = 9.0, 4.5$ Hz, 1H), 4.34 (d, $J = 9.0$ Hz, 1H), 3.96 (d, $J = 9.0$ Hz, 1H), 3.52 (s, 1H), 2.20 (d, $J = 2.5$ Hz, 3H), 2.17 (s, 6H), 2.15 (s, 3H), 1.60 (s, 3H);

^{13}C $\{^1\text{H}\}$ NMR (125 MHz, CDCl_3) δ 172.4, 159.0 (d, $J_{\text{C-F}} = 241.3$ Hz), 156.4 (d, $J_{\text{C-F}} = 235.0$ Hz), 151.8 (d, $J_{\text{C-F}} = 2.5$ Hz); 132.1 (d, $J_{\text{C-F}} = 5.0$ Hz), 130.5 (d, $J_{\text{C-F}} = 3.8$ Hz), 127.4 (d, $J_{\text{C-F}} = 3.8$ Hz), 124.8 (d, $J_{\text{C-F}} = 17.5$ Hz), 124.1 (d, $J_{\text{C-F}} = 16.3$ Hz), 122.7 (d, $J_{\text{C-F}} = 8.8$ Hz), 112.6 (d, $J_{\text{C-F}} = 23.8$ Hz), 112.1 (d, $J_{\text{C-F}} = 25.0$ Hz), 110.8 (d, $J_{\text{C-F}} = 8.8$ Hz), 75.6, 74.1, 23.2, 14.0 (d, $J_{\text{C-F}} = 2.5$ Hz), 12.2 (d, $J_{\text{C-F}} = 2.5$ Hz), 11.5 (d, $J_{\text{C-F}} = 5.0$ Hz), 11.3 (d, $J_{\text{C-F}} = 5.0$ Hz); HRMS (ESI, $[\text{M}+\text{Na}]^+$) calcd for $\text{C}_{20}\text{H}_{23}\text{F}_2\text{NNaO}_3$ 386.1538, found: m/z 386.1539.

4.5 References

- (1) Evans, R. M. The Steroid and Thyroid Hormone Receptor Superfamily. *Science* (1979) **1988**, 240 (4854), 889–895. <https://doi.org/10.1126/science.3283939>.
- (2) Tsai, M.-J.; O'Malley, B. W. Molecular Mechanisms of Action of Steroid/Thyroid Receptor Superfamily Members. *Annu. Rev. Biochem.* **1994**, 63 (1), 451–486. <https://doi.org/10.1146/annurev.bi.63.070194.002315>.
- (3) Keller, E. T.; Ershler, W. B.; Chang, C. The Androgen Receptor: A Mediator of Diverse Responses. *Front. Biosci.* **1993**, 1, 59–71.
- (4) Mooradian, A. D.; Morley, J. E.; Korenman, S. G. Biological Actions of Androgens. *Endocr. Rev.* **1987**, 8 (1), 1–28. <https://doi.org/10.1210/edrv-8-1-1>.
- (5) McLachlan, R. I.; Wreford, N. G.; O'Donnell, L.; de Kretser, D. M.; Robertson, D. M. The Endocrine Regulation of Spermatogenesis: Independent Roles for Testosterone and FSH. *J. Endocrinol.* **1996**, 148 (1), 1–9. <https://doi.org/10.1677/joe.0.1480001>.
- (6) Gao, W.; Bohl, C. E.; Dalton, J. T. Chemistry and Structural Biology of Androgen Receptor. *Chem. Rev.* **2005**, 105 (9), 3352–3370. <https://doi.org/10.1021/cr020456u>.
- (7) Baker, M. E. Albumin, Steroid Hormones and the Origin of Vertebrates. *J. Endocrinol.* **2002**, 175, 121–127.
- (8) Swerdloff, R. S.; Dudley, R. E.; Page, S. T.; Wang, C.; Salameh, W. A. Dihydrotestosterone: Biochemistry, Physiology, and Clinical Implications of Elevated Blood Levels. *Endocr. Rev.* **2017**, 38 (3), 220–254. <https://doi.org/10.1210/er.2016-1067>.
- (9) Wilson, E. M.; French, F. S. Binding Properties of Androgen Receptors. Evidence for Identical Receptors in Rat Testis, Epididymis, and Prostate. *J. Biol. Chem.* **1976**, 251 (18), 5620–5629. [https://doi.org/10.1016/S0021-9258\(17\)33103-4](https://doi.org/10.1016/S0021-9258(17)33103-4).
- (10) Thigpen, A. E.; Silver, R. I.; Guileyardo, J. M.; Casey, M. L.; McConnell, J. D.; Russell, D. W. Tissue Distribution and Ontogeny of Steroid 5 Alpha-Reductase Isozyme Expression. *J. Clin. Investig.* **1993**, 92 (2), 903–910. <https://doi.org/10.1172/JCI116665>.
- (11) Marchetti, P. M.; Barth, J. H. Clinical Biochemistry of Dihydrotestosterone. *Ann. Clin. Biochem.* **2013**, 50 (2), 95–107. <https://doi.org/10.1258/acb.2012.012159>.
- (12) Narayanan, R.; Coss, C. C.; Dalton, J. T. Development of Selective Androgen Receptor Modulators (SARMS). *Mol. Cell. Endocrinol.* **2018**, 465, 134–142. <https://doi.org/10.1016/j.mce.2017.06.013>.
- (13) Tan, M. E.; Li, J.; Xu, H. E.; Melcher, K.; Yong, E. Androgen Receptor: Structure, Role in Prostate Cancer and Drug Discovery. *Acta Pharmacol. Sin.* **2015**, 36 (1), 3–23. <https://doi.org/10.1038/aps.2014.18>.

- (14) Eder, I. E.; Culig, Z.; Putz, T.; Nessler-Menardi, C.; Bartsch, G.; Klocker, H. Molecular Biology of the Androgen Receptor: From Molecular Understanding to the Clinic. *Eur. Urol.* **2001**, *40* (3), 241–251. <https://doi.org/10.1159/000049782>.
- (15) Davey, R. A.; Grossmann, M. Androgen Receptor Structure, Function and Biology: From Bench to Bedside. *Clin. Biochem.* **2016**, *37* (1), 3–15.
- (16) Lavery, D. N.; McEwan, I. J. Structural Characterization of the Native NH₂-Terminal Transactivation Domain of the Human Androgen Receptor: A Collapsed Disordered Conformation Underlies Structural Plasticity and Protein-Induced Folding. *Biochemistry* **2008**, *47* (11), 3360–3369. <https://doi.org/10.1021/bi702221e>.
- (17) van Royen, M. E.; van Cappellen, W. A.; de Vos, C.; Houtsmuller, A. B.; Trapman, J. Stepwise Androgen Receptor Dimerization. *J. Cell Sci.* **2012**. <https://doi.org/10.1242/jcs.096792>.
- (18) Simental, J. A.; Sar, M.; Lane, M. v; French, F. S.; Wilson, E. M. Transcriptional Activation and Nuclear Targeting Signals of the Human Androgen Receptor. *J. Biol. Chem.* **1991**, *266* (1), 510–518. [https://doi.org/10.1016/S0021-9258\(18\)52466-2](https://doi.org/10.1016/S0021-9258(18)52466-2).
- (19) Alen, P.; Claessens, F.; Verhoeven, G.; Rombauts, W.; Peeters, B. The Androgen Receptor Amino-Terminal Domain Plays a Key Role in P160 Coactivator-Stimulated Gene Transcription. *Mol. Cell. Endocrinol.* **1999**, *19* (9), 6085–6097. <https://doi.org/10.1128/MCB.19.9.6085>.
- (20) Bevan, C. L.; Hoare, S.; Claessens, F.; Heery, D. M.; Parker, M. G. The AF1 and AF2 Domains of the Androgen Receptor Interact with Distinct Regions of SRC1. *Mol. Cell. Endocrinol.* **1999**, *19* (12), 8383–8392. <https://doi.org/10.1128/MCB.19.12.8383>.
- (21) Jenster, G.; Trapman, J.; Brinkmann, A. O. Nuclear Import of the Human Androgen Receptor. *Biochem. J.* **1993**, *293* (3), 761–768. <https://doi.org/10.1042/bj2930761>.
- (22) Zhou, Z. X.; Sar, M.; Simental, J. A.; Lane, M. v; Wilson, E. M. A Ligand-Dependent Bipartite Nuclear Targeting Signal in the Human Androgen Receptor. Requirement for the DNA-Binding Domain and Modulation by NH₂-Terminal and Carboxyl-Terminal Sequences. *J. Biol. Chem.* **1994**, *269* (18), 13115–13123.
- (23) Matias, P. M.; Donner, P.; Coelho, R.; Thomaz, M.; Peixoto, C.; Macedo, S.; Otto, N.; Joschko, S.; Scholz, P.; Wegg, A.; Bäsler, S.; Schäfer, M.; Egner, U.; Carrondo, M. A. Structural Evidence for Ligand Specificity in the Binding Domain of the Human Androgen Receptor. *J. Biol. Chem.* **2000**, *275* (34), 26164–26171. <https://doi.org/10.1074/jbc.M004571200>.
- (24) Eftekhazadeh, B.; Banduseela, V. C.; Chiesa, G.; Martínez-Cristóbal, P.; Rauch, J. N.; Nath, S. R.; Schwarz, D. M. C.; Shao, H.; Marin-Argany, M.; di Sanza, C.; Giorgetti, E.; Yu, Z.; Pierattelli, R.; Felli, I. C.; Brun-Heath, I.; García, J.; Nebreda, A. R.; Gestwicki, J. E.; Lieberman, A. P.; Salvatella, X. Hsp70 and Hsp40 Inhibit an Inter-Domain Interaction Necessary for Transcriptional Activity in the Androgen Receptor. *Nat. Commun.* **2019**, *10* (1), 3562. <https://doi.org/10.1038/s41467-019-11594-y>.
- (25) Schaufele, F.; Carbonell, X.; Guerbodot, M.; Borngraeber, S.; Chapman, M. S.; Ma, A. A. K.; Miner, J. N.; Diamond, M. I. The Structural Basis of Androgen Receptor Activation: Intramolecular and Intermolecular Amino–Carboxy Interactions. *Proc. Natl. Acad. Sci.* **2005**, *102* (28), 9802–9807. <https://doi.org/10.1073/pnas.0408819102>.
- (26) van Royen, M. E.; Cunha, S. M.; Brink, M. C.; Mattern, K. A.; Nigg, A. L.; Dubbink, H. J.; Verschure, P. J.; Trapman, J.; Houtsmuller, A. B. Compartmentalization of Androgen Receptor Protein–Protein Interactions in Living Cells. *J. Cell Biol.* **2007**, *177* (1), 63–72. <https://doi.org/10.1083/jcb.200609178>.
- (27) Bhasin, S.; Cunningham, G. R.; Hayes, F. J.; Matsumoto, A. M.; Snyder, P. J.; Swerdloff, R. S.; Montori, V. M. Testosterone Therapy in Men with Androgen Deficiency Syndromes: An Endocrine Society Clinical Practice Guideline. *J. Clin. Endocrinol. Metab.* **2010**, *95* (6), 2536–2559. <https://doi.org/10.1210/jc.2009-2354>.

- (28) Handelsman, D. J. Androgen Physiology, Pharmacology, Use and Misuse. In *Endotext*; 2020.
- (29) ASHP. *Testosterone*. Drugs.com. <https://www.drugs.com/monograph/testosterone.html> (accessed 2022-09-20).
- (30) Emmelot-Vonk, M. H.; Verhaar, H. J. J.; Nakhai Pour, H. R.; Aleman, A.; Lock, T. M. T. W.; Bosch, J. L. H. R.; Grobbee, D. E.; van der Schouw, Y. T. Effect of Testosterone Supplementation on Functional Mobility, Cognition, and Other Parameters in Older Men. *JAMA* **2008**, *299* (1). <https://doi.org/10.1001/jama.2007.51>.
- (31) LeBrasseur, N. K.; Lajevardi, N.; Miciek, R.; Mazer, N.; Storer, T. W.; Bhasin, S. Effects of Testosterone Therapy on Muscle Performance and Physical Function in Older Men with Mobility Limitations (The TOM Trial): Design and Methods. *Contemp. Clin. Trials* **2009**, *30* (2), 133–140. <https://doi.org/10.1016/j.cct.2008.10.005>.
- (32) Basaria, S.; Coviello, A. D.; Travison, T. G.; Storer, T. W.; Farwell, W. R.; Jette, A. M.; Eder, R.; Tennstedt, S.; Ulloor, J.; Zhang, A.; Choong, K.; Lakshman, K. M.; Mazer, N. A.; Miciek, R.; Krasnoff, J.; Elmi, A.; Knapp, P. E.; Brooks, B.; Appleman, E.; Aggarwal, S.; Bhasin, G.; Hede-Brierley, L.; Bhatia, A.; Collins, L.; LeBrasseur, N.; Fiore, L. D.; Bhasin, S. Adverse Events Associated with Testosterone Administration. *N. Engl. J. Med.* **2010**, *363* (2), 109–122. <https://doi.org/10.1056/NEJMoa1000485>.
- (33) Ponce, O. J.; Spencer-Bonilla, G.; Alvarez-Villalobos, N.; Serrano, V.; Singh-Ospina, N.; Rodriguez-Gutierrez, R.; Salcido-Montenegro, A.; Benkhadra, R.; Prokop, L. J.; Bhasin, S.; Brito, J. P. The Efficacy and Adverse Events of Testosterone Replacement Therapy in Hypogonadal Men: A Systematic Review and Meta-Analysis of Randomized, Placebo-Controlled Trials. *J. Clin. Endocrinol. Metab.* **2018**, *103* (5), 1745–1754. <https://doi.org/10.1210/jc.2018-00404>.
- (34) Grech, A.; Breck, J.; Heidelbaugh, J. Adverse Effects of Testosterone Replacement Therapy: An Update on the Evidence and Controversy. *Ther. Adv. Drug Saf.* **2014**, *5* (5), 190–200. <https://doi.org/10.1177/2042098614548680>.
- (35) Park, H.; Ahn, S.; Moon, D. Evolution of Guidelines for Testosterone Replacement Therapy. *J. Clin. Med.* **2019**, *8* (3), 410. <https://doi.org/10.3390/jcm8030410>.
- (36) Grober, E. D.; Krakowsky, Y.; Khera, M.; Holmes, D. T.; Lee, J. C.; Grantmyre, J. E.; Patel, P.; Bebb, R. A.; Fitzpatrick, R.; Campbell, J. D.; Carrier, S.; Morgentaler, A. Canadian Urological Association Clinical Practice Guideline on Testosterone Deficiency in Men: Evidence-Based Q&A. *Can. Urol. Assoc. J.* **2021**, *15* (5). <https://doi.org/10.5489/cuaj.7252>.
- (37) Negro-Vilar, A. Selective Androgen Receptor Modulators (SARMs): A Novel Approach to Androgen Therapy for the New Millennium. *J. Clin. Endocrinol. Metab.* **1999**, *84* (10), 3459–3462. <https://doi.org/10.1210/jcem.84.10.6122>.
- (38) Dalton, J. T. The Long and Winding Road for Selective Androgen Receptor Modulators. *Br. J. Clin. Pharmacol.* **2017**, *83* (10), 2131–2133. <https://doi.org/10.1111/bcp.13345>.
- (39) Narayanan, R.; Coss, C. C.; Dalton, J. T. Development of Selective Androgen Receptor Modulators (SARMs). *Mol. Cell. Endocrinol.* **2018**, *465*, 134–142. <https://doi.org/10.1016/j.mce.2017.06.013>.
- (40) Solomon, Z. J.; Mirabal, J. R.; Mazur, D. J.; Kohn, T. P.; Lipshultz, L. I.; Pastuszak, A. W. Selective Androgen Receptor Modulators: Current Knowledge and Clinical Applications. *Sex. Med. Rev.* **2019**, *7* (1), 84–94. <https://doi.org/10.1016/j.sxmr.2018.09.006>.
- (41) Fonseca, G. W. P. da; Dworatzek, E.; Ebner, N.; von Haehling, S. Selective Androgen Receptor Modulators (SARMs) as Pharmacological Treatment for Muscle Wasting in Ongoing Clinical Trials. *Expert Opin. Investig. Drugs* **2020**, *29* (8), 881–891. <https://doi.org/10.1080/13543784.2020.1777275>.

- (42) Gao, W.; Kim, J.; Dalton, J. T. Pharmacokinetics and Pharmacodynamics of Nonsteroidal Androgen Receptor Ligands. *Pharm. Res.* **2006**, *23* (8), 1641–1658. <https://doi.org/10.1007/s11095-006-9024-3>.
- (43) Narayanan, R.; Mohler, M. L.; Bohl, C. E.; Miller, D. D.; Dalton, J. T. Selective Androgen Receptor Modulators in Preclinical and Clinical Development. *Nucl. Recept. Signal.* **2008**, *6* (1), nrs.06010. <https://doi.org/10.1621/nrs.06010>.
- (44) Mohler, M. L.; Bohl, C. E.; Jones, A.; Coss, C. C.; Narayanan, R.; He, Y.; Hwang, D. J.; Dalton, J. T.; Miller, D. D. Nonsteroidal Selective Androgen Receptor Modulators (SARMs): Dissociating the Anabolic and Androgenic Activities of the Androgen Receptor for Therapeutic Benefit. *J. Med. Chem.* **2009**, *52* (12), 3597–3617. <https://doi.org/10.1021/jm900280m>.
- (45) Yin, D.; He, Y.; Perera, M. A.; Hong, S. S.; Marhefka, C.; Stourman, N.; Kirkovsky, L.; Miller, D. D.; Dalton, J. T. Key Structural Features of Nonsteroidal Ligands for Binding and Activation of the Androgen Receptor. *Mol. Pharmacol.* **2003**, *63* (1), 211–223. <https://doi.org/10.1124/mol.63.1.211>.
- (46) Gao, W.; Reiser, P. J.; Coss, C. C.; Phelps, M. A.; Kearbey, J. D.; Miller, D. D.; Dalton, J. T. Selective Androgen Receptor Modulator Treatment Improves Muscle Strength and Body Composition and Prevents Bone Loss in Orchidectomized Rats. *Endocrinology* **2005**, *146* (11), 4887–4897. <https://doi.org/10.1210/en.2005-0572>.
- (47) Srinath, R.; Dobs, A. Enobosarm (GTx-024, S-22): A Potential Treatment for Cachexia. *Future Oncol.* **2014**, *10* (2), 187–194. <https://doi.org/10.2217/fon.13.273>.
- (48) Crawford, J.; Prado, C. M. M.; Johnston, M. A.; Gralla, R. J.; Taylor, R. P.; Hancock, M. L.; Dalton, J. T. Study Design and Rationale for the Phase 3 Clinical Development Program of Enobosarm, a Selective Androgen Receptor Modulator, for the Prevention and Treatment of Muscle Wasting in Cancer Patients (POWER Trials). *Curr. Oncol. Rep.* **2016**, *18* (6), 37. <https://doi.org/10.1007/s11912-016-0522-0>.
- (49) Thigpen, A. E.; Silver, R. I.; Guileyardo, J. M.; Casey, M. L.; McConnell, J. D.; Russell, D. W. Tissue Distribution and Ontogeny of Steroid 5 Alpha-Reductase Isozyme Expression. *J. Clin. Investig.* **1993**, *92* (2), 903–910. <https://doi.org/10.1172/JCI116665>.
- (50) Gao, W.; Dalton, J. T. Ockham's Razor and Selective Androgen Receptor Modulators (SARMs): Are We Overlooking the Role of 5 α -Reductase? *Mol. Interv.* **2007**, *7* (1), 10–13. <https://doi.org/10.1124/mi.7.1.3>.
- (51) Chang, C.-Y.; McDonnell, D. P. Evaluation of Ligand-Dependent Changes in AR Structure Using Peptide Probes. *Mol. Endocrinol.* **2002**, *16* (4), 647–660. <https://doi.org/10.1210/mend.16.4.0818>.
- (52) Gao, W.; Dalton, J. T. Expanding the Therapeutic Use of Androgens via Selective Androgen Receptor Modulators (SARMs). *Drug Discov. Today* **2007**, *12* (5–6), 241–248. <https://doi.org/10.1016/j.drudis.2007.01.003>.
- (53) Thevis, M.; Geyer, H.; Kamber, M.; Schänzer, W. Detection of the Arylpropionamide-Derived Selective Androgen Receptor Modulator (SARM) S-4 (Andarine) in a Black-Market Product. *Drug Test. Anal.* **2009**, *1* (8), 387–392. <https://doi.org/10.1002/dta.91>.
- (54) Grata, E.; Perrenoud, L.; Saugy, M.; Baume, N. SARM-S4 and Metabolites Detection in Sports Drug Testing: A Case Report. *Forensic Sci. Int.* **2011**, *213* (1–3), 104–108. <https://doi.org/10.1016/j.forsciint.2011.07.014>.
- (55) Thevis, M.; Schänzer, W. Mass Spectrometry of Selective Androgen Receptor Modulators. *J. Mass Spectrom.* **2008**, *43* (7), 865–876. <https://doi.org/10.1002/jms.1438>.
- (56) Tucker, H.; Crook, J. W.; Chesterson, G. J. Nonsteroidal Antiandrogens. Synthesis and Structure-Activity Relationships of 3-Substituted Derivatives of 2-Hydroxypropionanilides. *J. Med. Chem.* **1988**, *31*, 954–959.

- (57) Jew, S.; Terashima, S.; Koga, K. Asymmetric Halolactonisation Reaction - 1. *Tetrahedron Lett.* **1979**, *35* (20), 2337–2343. [https://doi.org/10.1016/S0040-4020\(01\)93747-0](https://doi.org/10.1016/S0040-4020(01)93747-0).
- (58) Jew, S.-S.; Terashima, S.; Koga, K. Asymmetric Halolactonisation Reaction - 2. *Tetrahedron Lett.* **1979**, *35* (20), 2345–2352. [https://doi.org/10.1016/S0040-4020\(01\)93748-2](https://doi.org/10.1016/S0040-4020(01)93748-2).
- (59) Nique, F.; Hebbe, S.; Peixoto, C.; Annoot, D.; Lefrançois, J.-M.; Duval, E.; Michoux, L.; Triballeau, N.; Lemoullec, J.-M.; Mollat, P.; Thauvin, M.; Prangé, T.; Minet, D.; Clément-Lacroix, P.; Robin-Jagerschmidt, C.; Fleury, D.; Guédin, D.; Deprez, P. Discovery of Diarylhydantoin as New Selective Androgen Receptor Modulators. *J. Med. Chem.* **2012**, *55* (19), 8225–8235. <https://doi.org/10.1021/jm300249m>.
- (60) Konnert, L.; Lamaty, F.; Martinez, J.; Colacino, E. Recent Advances in the Synthesis of Hydantoin: The State of the Art of a Valuable Scaffold. *Chem. Rev.* **2017**, *117* (23), 13757–13809. <https://doi.org/10.1021/acs.chemrev.7b00067>.
- (61) Sun, C.; Robl, J. A.; Wang, T. C.; Huang, Y.; Kuhns, J. E.; Lupisella, J. A.; Beehler, B. C.; Golla, R.; Sleph, P. G.; Seethala, R.; Fura, A.; Krystek, S. R.; An, Y.; Malley, M. F.; Sack, J. S.; Salvati, M. E.; Grover, G. J.; Ostrowski, J.; Hamann, L. G. Discovery of Potent, Orally-Active, and Muscle-Selective Androgen Receptor Modulators Based on an *N*-Aryl-Hydroxybicyclohydantoin Scaffold. *J. Med. Chem.* **2006**, *49* (26), 7596–7599. <https://doi.org/10.1021/jm061101w>.
- (62) Ostrowski, J.; Kuhns, J. E.; Lupisella, J. A.; Manfredi, M. C.; Beehler, B. C.; Krystek, S. R.; Bi, Y.; Sun, C.; Seethala, R.; Golla, R.; Sleph, P. G.; Fura, A.; An, Y.; Kish, K. F.; Sack, J. S.; Mookhtiar, K. A.; Grover, G. J.; Hamann, L. G. Pharmacological and X-Ray Structural Characterization of a Novel Selective Androgen Receptor Modulator: Potent Hyperanabolic Stimulation of Skeletal Muscle with Hypostimulation of Prostate in Rats. *Endocrinology* **2007**, *148* (1), 4–12. <https://doi.org/10.1210/en.2006-0843>.
- (63) van Oeveren, A.; Pio, B. A.; Tegley, C. M.; Higuchi, R. I.; Wu, M.; Jones, T. K.; Marschke, K. B.; Negro-Vilar, A.; Zhi, L. Discovery of an Androgen Receptor Modulator Pharmacophore Based on 2-Quinolinones. *Bioorg. Med. Chem. Lett.* **2007**, *17* (6), 1523–1526. <https://doi.org/10.1016/j.bmcl.2007.01.007>.
- (64) Martinborough, E.; Shen, Y.; van Oeveren, A.; Long, Y. O.; Lau, T. L. S.; Marschke, K. B.; Chang, W. Y.; López, F. J.; Vajda, E. G.; Rix, P. J.; Viveros, O. H.; Negro-Vilar, A.; Zhi, L. Substituted 6-(1-Pyrrolidine)Quinolin-2(1*H*)-Ones as Novel Selective Androgen Receptor Modulators. *J. Med. Chem.* **2007**, *50* (21), 5049–5052. <https://doi.org/10.1021/jm070231h>.
- (65) van Oeveren, A.; Motamedi, M.; Mani, N. S.; Marschke, K. B.; López, F. J.; Schrader, W. T.; Negro-Vilar, A.; Zhi, L. Discovery of 6-*N,N*-Bis(2,2,2-Trifluoroethyl)Amino-4-Trifluoromethylquinolin-2(1*H*)-One as a Novel Selective Androgen Receptor Modulator. *J. Med. Chem.* **2006**, *49* (21), 6143–6146. <https://doi.org/10.1021/jm060792t>.
- (66) Lefebvre, O.; Marull, M.; Schlosser, M. 4-(Trifluoromethyl)Quinoline Derivatives. *Eur. J. Org. Chem.* **2003**, *2003* (11), 2115–2121. <https://doi.org/10.1002/ejoc.200200633>.
- (67) Marull, M.; Lefebvre, O.; Schlosser, M. An Improved Access to 4-Trifluoromethyl-2(1*H*)-Quinolinones: The“Watering Protocol.” *Eur. J. Org. Chem.* **2004**, *2004* (1), 54–63. <https://doi.org/10.1002/ejoc.200300531>.
- (68) Schlienger, N.; Lund, B. W.; Pawlas, J.; Badalassi, F.; Bertozzi, F.; Lewinsky, R.; Fejzic, A.; Thygesen, M. B.; Tabatabaei, A.; Bradley, S. R.; Gardell, L. R.; Piu, F.; Olsson, R. Synthesis, Structure–Activity Relationships, and Characterization of Novel Nonsteroidal and Selective Androgen Receptor Modulators. *J. Med. Chem.* **2009**, *52* (22), 7186–7191. <https://doi.org/10.1021/jm901149c>.
- (69) Barden, D.; McGregor, L. A Guide to Modern Comprehensive Two-Dimensional Gas Chromatography. *Column* **2017**, *13*, 14–20.

CHAPTER 5

General Conclusions and Future Directions

5.1 The Identification of Immunostimulator Compound A

As mentioned in Chapter 1, cancer remains an important problem and calls for a more effective, accessible, and low-cost therapy to all human beings. Tumor cells invade the immune system by immunoediting, a process that manipulates the immune response to help fight against cancer cells or facilitate tumor invasion. This process has been found to be related closely to the immune checkpoints, namely, PD-1/PD-L1 and CTLA-4, which are membrane receptors that regulate immune responses.^{1,2}

Among the common cancer therapeutics, immunotherapy has made remarkable progress over the past two decades.³ In immunotherapy, the immune system of the patients is altered, usually promoted to fight against cancerous cells. Immune checkpoint inhibitors (ICIs) have received recognition for their ability to treat various cancers in recent years. Ipilimumab and pembrolizumab are monoclonal antibody ICIs approved by the FDA. Despite their success in the clinical settings, using antibody ICIs suffers from a high occurrence of immune related adverse events (irAEs). Therefore, the development of small-molecule ICIs seeks advantages in low-cost production, improved bioavailability, and better membrane permeability.

Small molecule therapeutics have received growing interest over the years. As part of the continuing research of immunomodulators by Barakat and co-workers, they discovered **Compound A** as a potent immunostimulator.⁴ **Compound A** exhibits the ability to stimulate the production of IL-2 and the proliferation of T cells at a level that is comparable to pembrolizumab. However, during the target deconvolution of **Compound A**, they confirmed that it does not act through the PD-1/PD-L1 signalling pathway but an unknown protein target.

In this project, we aimed to reveal the identity of this unknown protein and study its mode of action. With that in mind, we applied different strategies, including streptavidin–biotin affinity purification, photoaffinity labelling, bio-orthogonal reaction, and microscopy, to modify the structure of lead **Compound A**. These

compounds later served as probe molecules towards the isolation and identification of the target protein of interest.

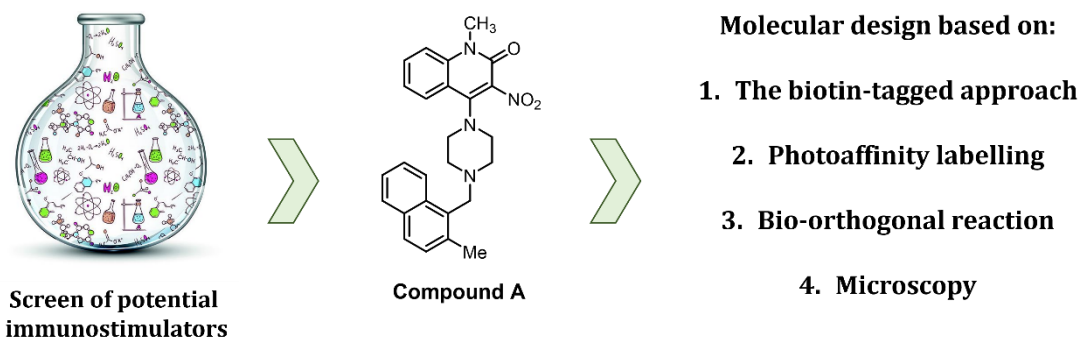


Figure 5.1. Project overview.

5.2 Synthesis of the Biotinylated Probe Molecule for Affinity Purification and the Photoaffinity Labelling Probe Molecules for a Protein Labelling Experiment

In Chapter 2, the biotin-tagged approach and the photoaffinity labelling techniques were introduced in an attempt to isolate the protein of interest.⁵ An overview is shown in Figure 5.2. In the beginning, the biotinylated probe molecule **1** was synthesized and was used towards streptavidin–biotin pull-down purification. However, due to unknown factors, the compound only exerted moderate activity to stimulate the secretion of IL-2. Therefore, we turned our focus to applying photoaffinity labelling in the project and again modified the structure of the probe molecule. Photoaffinity labelling is a technique that allows the formation of a covalent bond between the interacting protein and the ligand when in close proximity.⁶ The prerequisites of the technique are the structural modification of the molecule with a photo-crosslinker and the application of UV light.

It is important to note that the molecular probes **2** and **3**, incorporating a photo-crosslinker, were synthesized for a proof-of-concept labelling experiment. Unfortunately, the low molecular weight of the probes and the heterogeneity of the model protein, BSA, rendered the labelling experiment unsuccessful. To improve it, we decided to design two trifunctional probe molecules to overcome the problem.

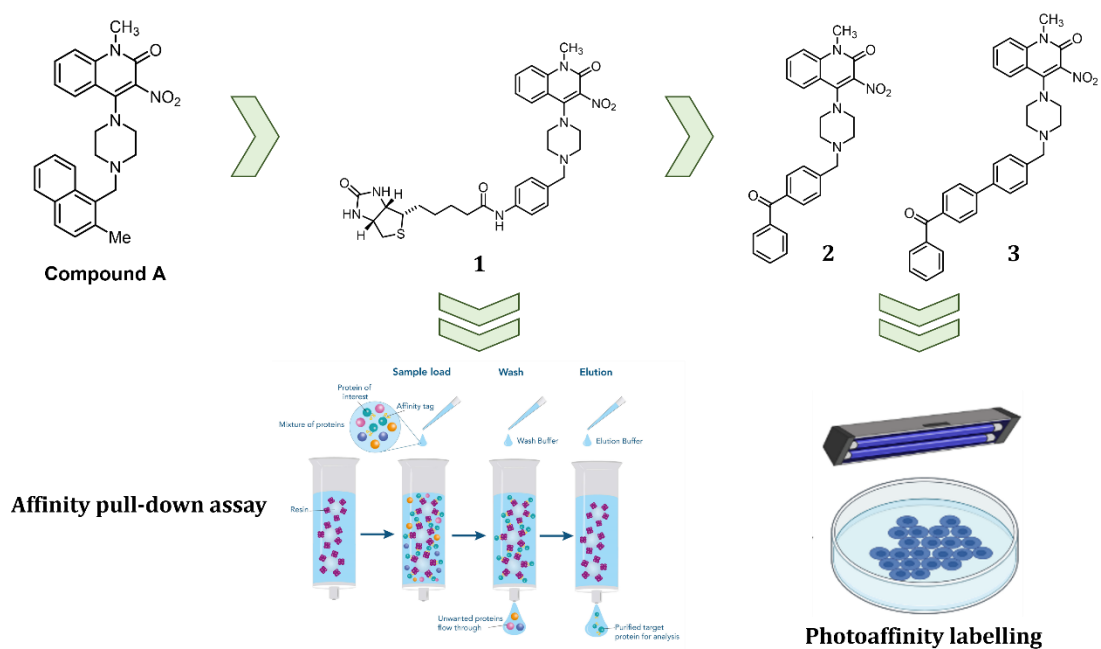


Figure 5.2. The overview of the molecular design in Chapter 2.

5.3 Synthesis of the Trifunctional Probe Molecules and the Fluorescent Probe Molecule, and Their Applications

In Chapter 3, we envisioned that furnishing the compound with a photo-crosslinker and a bio-orthogonal tag could provide a solution to the abovementioned problems. We chose benzophenone (BP) and trifluoromethyl phenyl diazirine (TPD) as the photo-crosslinker and an alkyne as the bio-orthogonal tag.^{7,8} Probes **4** and **5** were synthesized successfully and tested active towards IL-2 production. With the promising bioactivity of probe **4** and the desired photochemical property of TPD, I attempted another model labelling experiment with probe **4**. To our delight, an increase in molecular weight of the labelled BSA was observed, suggesting that probe **4** possessed the ability to modify a protein covalently.

Aside from the protein isolation, we proposed a fluorescent probe molecule to study the spatial distribution of the potential protein target.⁹ A detailed fluorescent analysis was performed to understand the correlation between fluorescent intensity and compound concentration. The fluorescent compound **6** had been used in multiple microscopy experiments, including real-time high content imaging and confocal

microscopy. Unfortunately, the results of the imaging experiments were inconclusive and lacked locational specificity, despite the good membrane permeability of probe **6**.

At the same time, the biotin-TPD probe molecule **7** was proposed to simplify the biological workflow. The biotin functionality was pre-installed to the TPD trifunctional molecule **4** so that the efficacy of the copper-catalyzed azide-alkyne cycloaddition (CuAAC) could be confirmed prior to the cell-based assay. After probe **7** was synthesized in the laboratory, it was sent to our collaborators for protein isolation and identification.

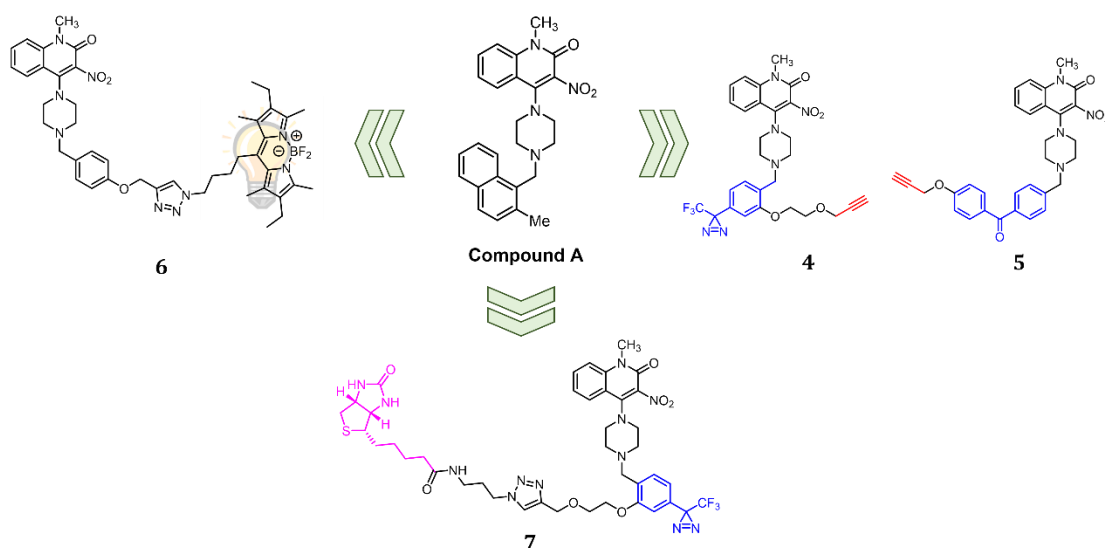


Figure 5.3. The overview of the molecular design in Chapter 3.

5.4 Development of Selective Androgen Receptor Modulators (SARMs)

In Chapter 4, a different project concerning the synthesis and characterization of aryl propionamide SARMs was described. Due to the anabolic effects of SARMs, they found useful clinical applications in treating muscle wasting disorders, however, potential abuse also has been reported.¹⁰ To the best of our knowledge, the current method of detecting SARMs relies on the comparison of the existing compounds and the clinical samples. This project was designed to provide a solution to overcome the limitation of detecting newly emerged performance-enhancing drugs (PEDs). We built a library of SARMs, containing diverse chemical structures, including aryl

propionamide, hydantoin, quinolinone, and *N*-substituted tropine/tropinone scaffolds. The compound library will be analyzed by two-dimensional gas chromatography (GC×GC) and used as a database to develop a machine-learning algorithm. The predictive model can help flag potential SARMS-based PEDs in urine or blood samples. Also, the synthesized compounds will be tested for their ability to improve muscle wasting when an appropriate collaborator is found.

5.5 Future Directions

Potential future directions regarding the immunology project will be addressed in this section, as outlined in Figure 5.4. First, the optimization of the biological workflow remains an important goal in the foreseeable future. Although the biotin functionality could be installed in the laboratory prior to the *in vitro* assay, the increase in compound size resulted in diminished bioactivity of the probe molecule, which could influence the result of the affinity pull-down assay. The biological workflow has to be optimized and the CuAAC reaction needs to be performed in the cell settings to reach a more accurate result with the least non-specific binding.

Once the result of the affinity pull-down purification is obtained and analyzed by LC-MS, validation of the result needs to be conducted. One of the feasible ways includes testing the probe molecule on a single protein after potential protein candidates are elucidated. The binding affinity (K_d) or the melting temperature (T_m) could be measured to exclude any non-specific binding proteins. Seeking out collaborators who have this expertise is required to complete the work.

The establishment of the structure-activity relationship is inevitable. If the unknown protein target and the binding pocket can be identified, structural modification of the lead **Compound A** to a more potent immunostimulator is possible. There are various possible points of modification, such as the quinolinone scaffold, the piperazine, and the naphthalene ring. This work could be aided by computational molecular modelling to analyze essential interactions between the ligand and the interacting protein to propose preferred substitutions.

In the long run, we would expect the lead compound to be tested *in vivo*, therefore, the measurement of EC_{50} and LD_{50} become vital. EC_{50} and LD_{50} are

important indexes in drug development that provide information on the potency and toxicity of the molecule. The former reflects the concentration needed to trigger a certain response, whereas the latter provides toxicity and safety assessment of a drug candidate.

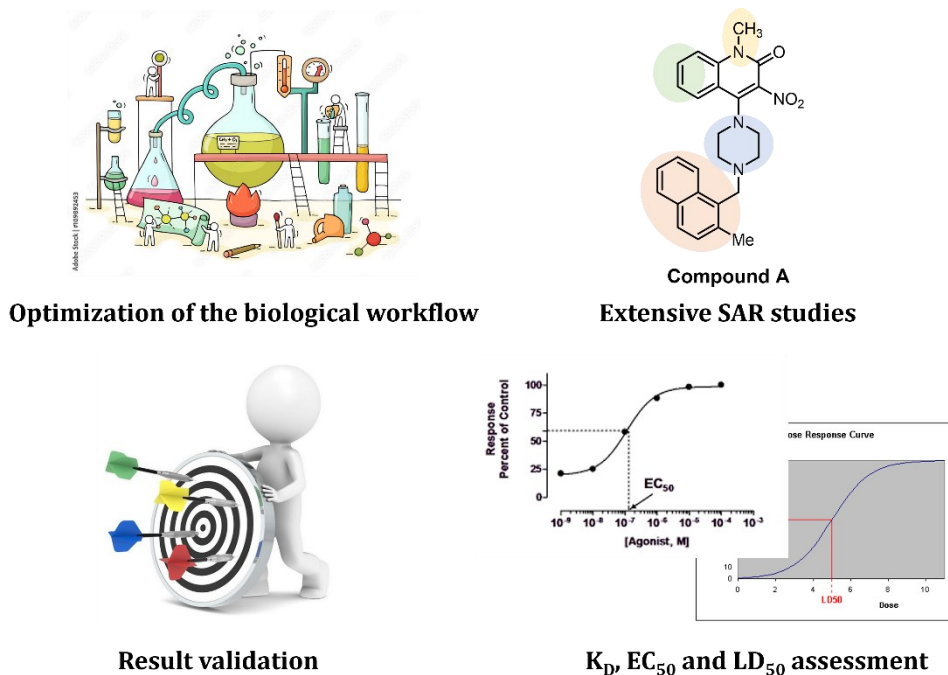


Figure 5.4. Feasible future directions of the project.

We would like to reiterate that the ongoing SARM project awaits suitable collaborations. A library of SARMS-based PEDs were synthesized originally for the development of a machine-learning system to doping detection. A wide variety of substitutions on the synthesized analogs allow the analysis by GC×GC for their fragmentation patterns, which completes the database and enables the screening of abnormal results in clinical samples. Also, the intriguing muscle-building properties of these compounds have found useful indications in diseases such as osteoporosis and cancer-related cachexia. We would like to screen these compounds in the cachexia mouse model for their ability to treat muscle wasting.

5.6 Conclusion

In this thesis, two distinct projects were introduced, both of which target clinically relevant proteins, utilizing novel small molecules. The first project concerned the

modification of a small-molecule immunostimulator with various functionalities towards protein identification. A successful target deconvolution could help reveal a clinically significant protein target and the development of drug candidates. The second project was designed to put together a library of SARMs with diverse scaffolds, which will be used to develop a machine-learning system for the detection of PEDs and tested against muscle wasting. In this chapter, a set of global conclusions and feasible future directions was addressed.

5.7 References

- (1) Egen, J. G.; Kuhns, M. S.; Allison, J. P. *CTLA-4: New Insights into Its Biological Function and Use in Tumor Immunotherapy*; 2002.
- (2) Han, Y.; Liu, D.; Li, L. *PD-1/PD-L1 Pathway: Current Researches in Cancer*; 2020; Vol. 10.
- (3) Esfahani, K.; Roudaia, L.; Buhlaiga, N.; del Rincon, S. v.; Papneja, N.; Miller, W. H. A Review of Cancer Immunotherapy: From the Past, to the Present, to the Future. *Curr. Oncol.* **2020**, *27* (S2), 87–97. <https://doi.org/10.3747/co.27.5223>.
- (4) Ganesan, A.; Ahmed, M.; Okoye, I.; Arutyunova, E.; Babu, D.; Turnbull, W. L.; Kundu, J. K.; Shields, J.; Agopsowicz, K. C.; Xu, L.; Tabana, Y.; Srivastava, N.; Zhang, G.; Moon, T. C.; Belovodskiy, A.; Hena, M.; Kandadai, A. S.; Hosseini, S. N.; Hitt, M.; Walker, J.; Smylie, M.; West, F. G.; Siraki, A. G.; Lemieux, M. J.; Elahi, S.; Nieman, J. A.; Tyrrell, D. L.; Houghton, M.; Barakat, K. Comprehensive in Vitro Characterization of PD-L1 Small Molecule Inhibitors. *Sci. Rep.* **2019**, *9* (1). <https://doi.org/10.1038/s41598-019-48826-6>.
- (5) Lee, H.; Lee, J. W. Target Identification for Biologically Active Small Molecules Using Chemical Biology Approaches. *Arch. Pharmacol. Res.* **2016**, *39* (9), 1193–1201. <https://doi.org/10.1007/s12272-016-0791-z>.
- (6) Hatanaka, Y.; Sadakane, Y. Photoaffinity Labeling in Drug Discovery and Developments: Chemical Gateway for Entering Proteomic Frontier. *Curr. Top. Med. Chem.* **2002**, *2* (3), 271–288. <https://doi.org/10.2174/1568026023394182>.
- (7) Mayer, T.; Maier, M. E. Design and Synthesis of a Tag-Free Chemical Probe for Photoaffinity Labeling. *Eur. J. Org. Chem.* **2007**, No. 28, 4711–4720. <https://doi.org/10.1002/ejoc.200700188>.
- (8) Sun, N.; Sun, Q.; Zhao, W.; Jin, L.; Hu, B.; Shen, Z.; Hu, X. Ligand-free Palladium-Catalyzed Carbonylative Suzuki Coupling of Aryl Iodides in Aqueous CH₃CN with Sub-stoichiometric Amount of Mo(CO)₆ as CO Source. *Adv. Synth. Catal.* **2019**, *361* (9), 2117–2123. <https://doi.org/10.1002/adsc.201900011>.
- (9) Bacsa, I.; Konc, C.; Orosz, A.; Kecskeméti, G.; Rigó, R.; Özvegy-Laczka, C.; Mernyák, E. Synthesis of Novel C-2- or C-15-Labeled BODIPY—Estrone Conjugates. *Molecules* **2018**, *23* (4), 821. <https://doi.org/10.3390/molecules23040821>.
- (10) Narayanan, R.; Coss, C. C.; Dalton, J. T. Development of Selective Androgen Receptor Modulators (SARMs). *Mol. Cell. Endocrinol.* **2018**, *465*, 134–142. <https://doi.org/10.1016/j.mce.2017.06.013>.

Compiled References

Chapter 1

- (1) World Health Organization: Regional Office for Europe. *World Cancer Report: Cancer Research for Cancer Development.*; IARC, 2020.
- (2) Sung, H.; Ferlay, J.; Siegel, R. L.; Laversanne, M.; Soerjomataram, I.; Jemal, A.; Bray, F. Global Cancer Statistics 2020: GLOBOCAN Estimates of Incidence and Mortality Worldwide for 36 Cancers in 185 Countries. *CA Cancer J Clin* **2021**, *71* (3), 209–249. <https://doi.org/10.3322/caac.21660>.
- (3) Schreiber, R. D.; Old, L. J.; Smyth, M. J. *Cancer Immunoediting: Integrating Immunity's Roles in Cancer Suppression and Promotion*; 2015. <http://science.sciencemag.org/>.
- (4) Dunn, G. P.; Bruce, A. T.; Ikeda, H.; Old, L. J.; Schreiber, R. D. Cancer Immunoediting: From Immuno-Surveillance to Tumor Escape. *Nat. Immunol.* **2002**, *3*, 991–998.
- (5) Janssen, L. M. E.; Ramsay, E. E.; Logsdon, C. D.; Overwijk, W. W. The Immune System in Cancer Metastasis: Friend or Foe? *J. Immunother. Cancer.* **2017**, *5* (1), 79. <https://doi.org/10.1186/s40425-017-0283-9>.
- (6) Bhatia, A.; Kumar, Y. Cellular and Molecular Mechanisms in Cancer Immune Escape: A Comprehensive Review. *Expert Review of Clinical Immunology*. January 2014, pp 41–62. <https://doi.org/10.1586/1744666X.2014.865519>.
- (7) American Cancer Society. *Cancer Treatment & Survivorship Facts & Figures 2019-2021*; 2019.
- (8) Schaeue, D.; McBride, W. H. Opportunities and Challenges of Radiotherapy for Treating Cancer. *Nat. Rev. Clin. Oncol.* **2015**, *12*, 527–540. <https://doi.org/10.1038/nrclinonc.2015.120>.
- (9) Huang, C. Y.; Ju, D. T.; Chang, C. F.; Muralidhar Reddy, P.; Velmurugan, B. K. A Review on the Effects of Current Chemotherapy Drugs and Natural Agents in Treating Non-Small Cell Lung Cancer. *Biomedicine* **2017**, *7* (4), 12–23. <https://doi.org/10.1051/bmdcn/2017070423>.
- (10) Malhotra, V.; Perry, M. C. Classical Chemotherapy: Mechanisms, Toxicities and the Therapeutic Window. *Cancer Biol. Ther.* **2003**, *2*, 1–3. <https://doi.org/10.4161/cbt.199>.
- (11) Makin, G.; Hickman, J. A. Apoptosis and Cancer Chemotherapy. *Cell Tissue Res.* **2000**, *301* (1), 143–152. <https://doi.org/10.1007/s004419900160>.
- (12) Dasari, S.; Bernard Tchounwou, P. Cisplatin in Cancer Therapy: Molecular Mechanisms of Action. *Eur. J. Pharmacol.* **2014**, *740*, 364–378. <https://doi.org/10.1016/j.ejphar.2014.07.025>.
- (13) Darwin, P.; Toor, S. M.; Sasidharan Nair, V.; Elkord, E. Immune Checkpoint Inhibitors: Recent Progress and Potential Biomarkers. *Exp. Mol. Med.* **2018**, *50* (12). <https://doi.org/10.1038/s12276-018-0191-1>.
- (14) Webster, R. M. The Immune Checkpoint Inhibitors: Where Are We Now? *Nat. Rev. Drug Discov.* **2014**, *13* (12), 883–884. <https://doi.org/10.1038/nrd4476>.
- (15) Hargadon, K. M.; Johnson, C. E.; Williams, C. J. Immune Checkpoint Blockade Therapy for Cancer: An Overview of FDA-Approved Immune Checkpoint Inhibitors. *Int. Immunopharmacol.* **2018**, *62*, 29–39. <https://doi.org/10.1016/j.intimp.2018.06.001>.

- (16) Seidel, J. A.; Otsuka, A.; Kabashima, K. Anti-PD-1 and Anti-CTLA-4 Therapies in Cancer: Mechanisms of Action, Efficacy, and Limitations. *Front. Oncol.* **2018**, *8*, 86. <https://doi.org/10.3389/fonc.2018.00086>.
- (17) Waldman, A. D.; Fritz, J. M.; Lenardo, M. J. A Guide to Cancer Immunotherapy: From T Cell Basic Science to Clinical Practice. *Nat. Rev. Immunol.* **2020**, *20* (11), 651–668. <https://doi.org/10.1038/s41577-020-0306-5>.
- (18) Savoia, P.; Astrua, C.; Fava, P. Ipilimumab (Anti-Ctla-4 Mab) in the Treatment of Metastatic Melanoma: Effectiveness and Toxicity Management. *Hum. Vaccines Immunother.* **2016**, *12* (5), 1092–1101. <https://doi.org/10.1080/21645515.2015.1129478>.
- (19) Lipson, E. J.; Drake, C. G. Ipilimumab: An Anti-CTLA-4 Antibody for Metastatic Melanoma. *Clin. Cancer. Res.* **2011**, *17* (22), 6958–6962. <https://doi.org/10.1158/1078-0432.CCR-11-1595>.
- (20) Khoja, L.; Butler, M. O.; Kang, S. P.; Ebbinghaus, S.; Joshua, A. M. Pembrolizumab. *J. Immunother. Cancer.* **2015**, *3* (1), 36. <https://doi.org/10.1186/s40425-015-0078-9>.
- (21) Hegde, P. S.; Chen, D. S. Top 10 Challenges in Cancer Immunotherapy. *Immunity* **2020**, *52* (1), 17–35. <https://doi.org/10.1016/j.immuni.2019.12.011>.
- (22) Vasan, N.; Baselga, J.; Hyman, D. M. A View on Drug Resistance in Cancer. *Nature* **2019**, *575* (7782), 299–309. <https://doi.org/10.1038/s41586-019-1730-1>.
- (23) Holohan, C.; van Schaeybroeck, S.; Longley, D. B.; Johnston, P. G. Cancer Drug Resistance: An Evolving Paradigm. *Nat. Rev. Cancer.* **2013**, *13* (10), 714–726. <https://doi.org/10.1038/nrc3599>.
- (24) Gottesman, M. M. Mechanisms of Cancer Drug Resistance. *Annu. Rev. Med* **2002**, *53*, 615–627.
- (25) Zugazagoitia, J.; Guedes, C.; Ponce, S.; Ferrer, I.; Molina-Pinelo, S.; Paz-Ares, L. Current Challenges in Cancer Treatment. *Clin. Ther.* **2016**, *38* (7), 1551–1566. <https://doi.org/10.1016/j.clinthera.2016.03.026>.
- (26) Marshall, J. S.; Warrington, R.; Watson, W.; Kim, H. L. An Introduction to Immunology and Immunopathology. *Allergy Asthma Clin. Immunol.* **2018**, *14*, 49. <https://doi.org/10.1186/s13223-018-0278-1>.
- (27) Vesely, M. D.; Kershaw, M. H.; Schreiber, R. D.; Smyth, M. J. Natural Innate and Adaptive Immunity to Cancer. *Annu. Rev. Immunol.* **2011**, *29*, 235–271. <https://doi.org/10.1146/annurev-immunol-031210-101324>.
- (28) Abbott, M.; Ustoyev, Y. Cancer and the Immune System: The History and Background of Immunotherapy. *Semin. Oncol. Nurs.* **2019**, *35* (5), 150923. <https://doi.org/10.1016/j.soncn.2019.08.002>.
- (29) Wolchok, J. D.; Saenger, Y. The Mechanism of Anti-CTLA-4 Activity and the Negative Regulation of T-Cell Activation. *Oncologist* **2008**, *13* (S4), 2–9. <https://doi.org/10.1634/theoncologist.13-s4-2>.
- (30) Meyer, M. A.; Baer, J. M.; Knolhoff, B. L.; Nywening, T. M.; Panni, R. Z.; Su, X.; Weilbaecher, K. N.; Hawkins, W. G.; Ma, C.; Fields, R. C.; Linehan, D. C.; Challen, G. A.; Faccio, R.; Aft, R. L.; Denardo, D. G. Breast and Pancreatic Cancer Interrupt IRF8-Dependent Dendritic Cell Development to Overcome Immune Surveillance. *Nat. Commun.* **2018**, *9*, 1250. <https://doi.org/10.1038/s41467-018-03600-6>.

- (31) Schaller, J.; Agudo, J. Metastatic Colonization: Escaping Immune Surveillance. *Cancers (Basel)* **2020**, *12* (11), 1–15. <https://doi.org/10.3390/cancers12113385>.
- (32) Oh, D. Y.; Fong, L. Cytotoxic CD4+ T Cells in Cancer: Expanding the Immune Effector Toolbox. *Immunity* **2021**, *54* (12), 2701–2711. <https://doi.org/10.1016/j.immuni.2021.11.015>.
- (33) Tay, R. E.; Richardson, E. K.; Toh, H. C. Revisiting the Role of CD4+ T Cells in Cancer Immunotherapy—New Insights into Old Paradigms. *Cancer Gene Ther.* **2021**, *28*, 5–17. <https://doi.org/10.1038/s41417-020-0183-x>.
- (34) Smyth, M. J.; Dunn, G. P.; Schreiber, R. D. Cancer Immunoreveillance and Immunoediting: The Roles of Immunity in Suppressing Tumor Development and Shaping Tumor Immunogenicity. *Adv. Immunol.* **2006**, *90*, 1–50. [https://doi.org/10.1016/S0065-2776\(06\)90001-7](https://doi.org/10.1016/S0065-2776(06)90001-7).
- (35) Alsaab, H. O.; Sau, S.; Alzhrani, R.; Tatiparti, K.; Bhise, K.; Kashaw, S. K.; Iyer, A. K. PD-1 and PD-L1 Checkpoint Signaling Inhibition for Cancer Immunotherapy: Mechanism, Combinations, and Clinical Outcome. *Front. Pharmacol.* **2017**, *8*, 561. <https://doi.org/10.3389/fphar.2017.00561>.
- (36) Han, Y.; Liu, D.; Li, L. PD-1/PD-L1 Pathway: Current Researches in Cancer. *Am J Cancer Res* **2020**, *10* (3), 727–742.
- (37) Pardoll, D. M. The Blockade of Immune Checkpoints in Cancer Immunotherapy. *Nat. Rev. Cancer.* **2012**, *12* (4), 252–264. <https://doi.org/10.1038/nrc3239>.
- (38) Chen, D. S.; Mellman, I. Oncology Meets Immunology: The Cancer-Immunity Cycle. *Immunity* **2013**, *39* (1), 1–10. <https://doi.org/10.1016/j.immuni.2013.07.012>.
- (39) Zou, W.; Chen, L. Inhibitory B7-Family Molecules in the Tumour Microenvironment. *Nat. Rev. Immunol.* **2008**, *8* (6), 467–477. <https://doi.org/10.1038/nri2326>.
- (40) Dong, H.; Strome, S. E.; Salomao, D. R.; Tamura, H.; Hirano, F.; Flies, D. B.; Roche, P. C.; Lu, J.; Zhu, G.; Tamada, K.; Lennon, V. A.; Cells, E.; Chen, L. Tumor-Associated B7-H1 Promotes T-Cell Apoptosis: A Potential Mechanism of Immune Evasion. *Nat. Med.* **2002**, *8* (8), 793–800. <https://doi.org/10.1038/nm730>.
- (41) Egen, J. G.; Kuhns, M. S.; Allison, J. P. CTLA-4: New Insights into Its Biological Function and Use in Tumor Immunotherapy. *Nat. Immunol.* **2002**, *3*, 611–618.
- (42) Zhang, Y.; Zhang, Z. The History and Advances in Cancer Immunotherapy: Understanding the Characteristics of Tumor-Infiltrating Immune Cells and Their Therapeutic Implications. *Cell. Mol. Immunol.* **2020**, *17* (8), 807–821. <https://doi.org/10.1038/s41423-020-0488-6>.
- (43) Dobosz, P.; Dzieciatkowski, T. The Intriguing History of Cancer Immunotherapy. *Front. Immunol.* **2019**, *10*, 2965. <https://doi.org/10.3389/fimmu.2019.02965>.
- (44) Mellman, I.; Coukos, G.; Dranoff, G. Cancer Immunotherapy Comes of Age. *Nature* **2011**, *480* (7378), 480–489. <https://doi.org/10.1038/nature10673>.
- (45) Couzin-Frankel, J. Cancer Immunotherapy. *Science*. 2013, pp 1432–1433. <https://doi.org/10.1126/science.342.6165.1432>.
- (46) Coley, M. D.; William, B. The Treatment Of Malignant Tumors By Repeated Inoculations of Erysipelas. *Am. J. Med. Sci.* **1893**, *105*, 487.

- (47) Esfahani, K.; Roudaia, L.; Buhlaiga, N.; del Rincon, S. v.; Papneja, N.; Miller, W. H. A Review of Cancer Immunotherapy: From the Past, to the Present, to the Future. *Curr. Oncol.* **2020**, *27* (S2), 87–97. <https://doi.org/10.3747/co.27.5223>.
- (48) Miller, J. F. A. P.; Mitchell, G. F.; Weiss, N. S. Cellular Basis of the Immunological Defects in Thymectomized Mice. *Nature* **1967**, *214* (5092), 992–997. <https://doi.org/10.1038/214992a0>.
- (49) Steinman, R. M.; Cohn, Z. A. Identification of a Novel Cell Type in Peripheral Lymphoid Organs of Mice. *J. Exp. Med.* **1973**, *137* (5), 1142–1162. <https://doi.org/10.1084/jem.137.5.1142>.
- (50) Kiessling, R.; Klein, E.; Pross, H.; Wigzell, H. “Natural” Killer Cells in the Mouse. II. Cytotoxic Cells with Specificity for Mouse Moloney Leukemia Cells. Characteristics of the Killer Cell. *Eur. J. Immunol.* **1975**, *5* (2), 117–121. <https://doi.org/10.1002/eji.1830050209>.
- (51) Kiessling, R.; Klein, E.; Wigzell, H. “Natural” Killer Cells in the Mouse. I. Cytotoxic Cells with Specificity for Mouse Moloney Leukemia Cells. Specificity and Distribution According to Genotype. *Eur. J. Immunol.* **1975**, *5* (2), 112–117. <https://doi.org/10.1002/eji.1830050208>.
- (52) Stutman, O. Delayed Tumour Appearance and Absence of Regression in Nude Mice Infected with Murine Sarcoma Virus. *Nature* **1975**, *253* (5487), 142–144. <https://doi.org/10.1038/253142a0>.
- (53) Stutman, O. Tumor Development after 3-Methylcholanthrene in Immunologically Deficient Athymic-Nude Mice. *Science* **1974**, *183* (4124), 534–536. <https://doi.org/10.1126/science.183.4124.534>.
- (54) van der Bruggen, P.; Traversari, C.; Chomez, P.; Lurquin, C.; de Plaen, E.; van den Eynde, B.; Knuth, A.; Boon, T. A Gene Encoding an Antigen Recognized by Cytolytic T Lymphocytes on a Human Melanoma. *Science* **1991**, *254* (5038), 1643–1647. <https://doi.org/10.1126/science.1840703>.
- (55) Rosenberg, S. A. IL-2: The First Effective Immunotherapy for Human Cancer. *J. Immunol.* **2014**, *192* (12), 5451–5458. <https://doi.org/10.4049/jimmunol.1490019>.
- (56) Ye, C.; Brand, D.; Zheng, S. G. Targeting IL-2: An Unexpected Effect in Treating Immunological Diseases. *Curr. Signal Transduct. Ther.* **2018**, *3* (1), 2. <https://doi.org/10.1038/s41392-017-0002-5>.
- (57) Jiang, T.; Zhou, C.; Ren, S. Role of IL-2 in Cancer Immunotherapy. *Oncoimmunology* **2016**, *5* (6), e1163462. <https://doi.org/10.1080/2162402X.2016.1163462>.
- (58) Brunet, J.-F.; Denizot, F.; Luciani, M.-F.; Roux-Dosseto, M.; Suzan, M.; Mattei, M.-G.; Golstein, P. A New Member of the Immunoglobulin Superfamily—CTLA-4. *Nature* **1987**, *328* (6127), 267–270. <https://doi.org/10.1038/328267a0>.
- (59) Krummel, M. F.; Allison, J. P. CD28 and CTLA-4 Have Opposing Effects on the Response of T Cells to Stimulation. *J. Exp. Med.* **1995**, *182* (2), 459–465. <https://doi.org/10.1084/jem.182.2.459>.
- (60) Leach, D. R.; Krummel, M. F.; Allison, J. P. Enhancement of Antitumor Immunity by CTLA-4 Blockade. *Science* **1996**, *271* (5256), 1734–1736. <https://doi.org/10.1126/science.271.5256.1734>.

- (61) Ishida, Y.; Agata, Y.; Shibahara, K.; Honjo, T. Induced Expression of PD-1, a Novel Member of the Immunoglobulin Gene Superfamily, upon Programmed Cell Death. *EMBO J.* **1992**, *11* (11), 3887–3895. <https://doi.org/10.1002/j.1460-2075.1992.tb05481.x>.
- (62) Nishimura, H.; Okazaki, T.; Tanaka, Y.; Nakatani, K.; Hara, M.; Matsumori, A.; Sasayama, S.; Mizoguchi, A.; Hiai, H.; Minato, N.; Honjo, T. Autoimmune Dilated Cardiomyopathy in PD-1 Receptor-Deficient Mice. *Science* **2001**, *291* (5502), 319–322. <https://doi.org/10.1126/science.291.5502.319>.
- (63) Agata, Y.; Kawasaki, A.; Nishimura, H.; Ishida, Y.; Tsubat, T.; Yagita, H.; Honjo, T. Expression of the PD-1 Antigen on the Surface of Stimulated Mouse T and B Lymphocytes. *Int. Immunopharmacol.* **1996**, *8* (5), 765–772. <https://doi.org/10.1093/intimm/8.5.765>.
- (64) Ishida, Y. PD-1: Its Discovery, Involvement in Cancer Immunotherapy, and Beyond. *Cells* **2020**, *9* (6). <https://doi.org/10.3390/cells9061376>.
- (65) Iwai, Y.; Ishida, M.; Tanaka, Y.; Okazaki, T.; Honjo, T.; Minato, N. Involvement of PD-L1 on Tumor Cells in the Escape from Host Immune System and Tumor Immunotherapy by PD-L1 Blockade. *Proc. Natl. Acad. Sci.* **2002**, *99* (19), 12293–12297. <https://doi.org/10.1073/pnas.192461099>.
- (66) Savoia, P.; Astrua, C.; Fava, P. Ipilimumab (Anti-Ctla-4 Mab) in the Treatment of Metastatic Melanoma: Effectiveness and Toxicity Management. *Hum. Vaccines Immunother.* **2016**, *12* (5), 1092–1101. <https://doi.org/10.1080/21645515.2015.1129478>.
- (67) *The Nobel Prize in Physiology or Medicine 2018*. <https://www.nobelprize.org/prizes/medicine/2018/press-release/> (accessed 2022-05-12).
- (68) Smyth, M. J.; Teng, M. W. 2018 Nobel Prize in Physiology or Medicine. *Clin Transl Immunology* **2018**, *7* (10), e1041. <https://doi.org/10.1002/cti2.1041>.
- (69) Darnell, E. P.; Mooradian, M. J.; Baruch, E. N.; Yilmaz, M.; Reynolds, K. L. Immune-Related Adverse Events (IrAEs): Diagnosis, Management, and Clinical Pearls. *Curr. Oncol. Rep.* **2020**, *22* (4), 39. <https://doi.org/10.1007/s11912-020-0897-9>.
- (70) Conroy, M.; Naidoo, J. Immune-Related Adverse Events and the Balancing Act of Immunotherapy. *Nat. Commun.* **2022**, *13* (1), 392. <https://doi.org/10.1038/s41467-022-27960-2>.
- (71) Spain, L.; Diem, S.; Larkin, J. Management of Toxicities of Immune Checkpoint Inhibitors. *Cancer Treat. Rev.* **2016**, *44*, 51–60. <https://doi.org/10.1016/j.ctrv.2016.02.001>.
- (72) Wang, D. Y.; Salem, J. E.; Cohen, J. v.; Chandra, S.; Menzer, C.; Ye, F.; Zhao, S.; Das, S.; Beckermann, K. E.; Ha, L.; Rathmell, W. K.; Ancell, K. K.; Balko, J. M.; Bowman, C.; Davis, E. J.; Chism, D. D.; Horn, L.; Long, G. v.; Carlino, M. S.; Lebrun-Vignes, B.; Eroglu, Z.; Hassel, J. C.; Menzies, A. M.; Sosman, J. A.; Sullivan, R. J.; Moslehi, J. J.; Johnson, D. B. Fatal Toxic Effects Associated With Immune Checkpoint Inhibitors: A Systematic Review and Meta-Analysis. *JAMA Oncol* **2018**, *4* (12), 1721–1728. <https://doi.org/10.1001/jamaoncol.2018.3923>.
- (73) Spain, L.; Diem, S.; Larkin, J. Management of Toxicities of Immune Checkpoint Inhibitors. *Cancer Treat. Rev.* **2016**, *44*, 51–60. <https://doi.org/10.1016/j.ctrv.2016.02.001>.
- (74) Curry, J. L.; Tetzlaff, M. T.; Nagarajan, P.; Drucker, C.; Diab, A.; Hymes, S. R.; Duvic, M.; Hwu, W.-J.; Wargo, J. A.; Torres-Cabala, C. A.; Rapini, R. P.; Prieto, V. G. Diverse Types of

Dermatologic Toxicities from Immune Checkpoint Blockade Therapy. *J. Cutan. Pathol.* **2017**, *44* (2), 158–176. <https://doi.org/10.1111/cup.12858>.

- (75) Ernstoff, M.; Puzanov, I.; Robert, C.; Diab, A.; Hersey, P. *SITC's Guide to Managing Immunotherapy Toxicity*; Demos Medical Publishing, 2019.
- (76) Brahmer, J. R.; Lacchetti, C.; Schneider, B. J.; Atkins, M. B.; Brassil, K. J.; Caterino, J. M.; Chau, I.; Ernstoff, M. S.; Gardner, J. M.; Ginex, P.; Hallmeyer, S.; Holter Chakrabarty, J.; Leigh, N. B.; Mammen, J. S.; McDermott, D. F.; Naing, A.; Nastoupil, L. J.; Phillips, T.; Porter, L. D.; Puzanov, I.; Reichner, C. A.; Santomasso, B. D.; Seigel, C.; Spira, A.; Suarez-Almazor, M. E.; Wang, Y.; Weber, J. S.; Wolchok, J. D.; Thompson, J. A. Management of Immune-Related Adverse Events in Patients Treated With Immune Checkpoint Inhibitor Therapy: American Society of Clinical Oncology Clinical Practice Guideline. *J. Clin. Oncol.* **2018**, *36* (17), 1714–1768. <https://doi.org/10.1200/JCO.2017.77.6385>.
- (77) Haanen, J. B. A. G.; Carbone, F.; Robert, C.; Kerr, K. M.; Peters, S.; Larkin, J.; Jordan, K. Management of Toxicities from Immunotherapy: ESMO Clinical Practice Guidelines for Diagnosis, Treatment and Follow-Up. *Ann. Oncol.* **2017**, *28*, iv119–iv142. <https://doi.org/10.1093/annonc/mdx225>.
- (78) Maker, A. v.; Attia, P.; Rosenberg, S. A. Analysis of the Cellular Mechanism of Antitumor Responses and Autoimmunity in Patients Treated with CTLA-4 Blockade. *J. Immunol.* **2005**, *175* (11), 7746–7754. <https://doi.org/10.4049/jimmunol.175.11.7746>.
- (79) Peggs, K. S.; Quezada, S. A.; Korman, A. J.; Allison, J. P. Principles and Use of Anti-CTLA4 Antibody in Human Cancer Immunotherapy. *Curr. Opin. Immunol.* **2006**, *18* (2), 206–213. <https://doi.org/10.1016/j.coi.2006.01.011>.
- (80) Maker, A. v.; Phan, G. Q.; Attia, P.; Yang, J. C.; Sherry, R. M.; Topalian, S. L.; Kammula, U. S.; Royal, R. E.; Haworth, L. R.; Levy, C.; Kleiner, D.; Mavroukakis, S. A.; Yellin, M.; Rosenberg, S. A. Tumor Regression and Autoimmunity in Patients Treated with Cytotoxic T Lymphocyte-Associated Antigen 4 Blockade and Interleukin 2: A Phase I/II Study. *Ann. Surg. Oncol.* **2005**, *12* (12), 1005–1016. <https://doi.org/10.1245/ASO.2005.03.536>.
- (81) Robert, C.; Thomas, L.; Bondarenko, I.; O'Day, S.; Weber, J.; Garbe, C.; Lebbe, C.; Baurain, J.-F.; Testori, A.; Grob, J.-J.; Davidson, N.; Richards, J.; Maio, M.; Hauschild, A.; Miller, W. H.; Gascon, P.; Lotem, M.; Harmankaya, K.; Ibrahim, R.; Francis, S.; Chen, T.-T.; Humphrey, R.; Hoos, A.; Wolchok, J. D. Ipilimumab plus Dacarbazine for Previously Untreated Metastatic Melanoma. *N. Engl. J. Med.* **2011**, *364* (26), 2517–2526. <https://doi.org/10.1056/NEJMoa1104621>.
- (82) Hersh, E. M.; O'Day, S. J.; Powderly, J.; Khan, K. D.; Pavlick, A. C.; Cranmer, L. D.; Samlowski, W. E.; Nichol, G. M.; Yellin, M. J.; Weber, J. S. A Phase II Multicenter Study of Ipilimumab with or without Dacarbazine in Chemotherapy-Naïve Patients with Advanced Melanoma. *Investig. New Drugs* **2011**, *29* (3), 489–498. <https://doi.org/10.1007/s10637-009-9376-8>.
- (83) Reuben, J. M.; Lee, B. N.; Shen, D. Y.; Gutierrez, C.; Hernandez, I.; Parker, C. A.; Bozon, V. A.; Gomez-Navarro, J.; Lopez-Berestein, G.; Camacho, L. H. Therapy with Human Monoclonal Anti-CTLA-4 Antibody, CP-675,206, Reduces Regulatory T Cells and IL-10 Production in Patients with Advanced Malignant Melanoma (MM). *Journal of Clinical Oncology* **2005**, *23* (16_suppl), 7505–7505. https://doi.org/10.1200/jco.2005.23.16_suppl.7505.

- (84) Yang, J. C.; Beck, K. E.; Blansfield, J. A.; Tran, K. Q.; Lowy, I.; Rosenberg, S. A. Tumor Regression in Patients with Metastatic Renal Cancer Treated with a Monoclonal Antibody to CTLA4 (MDX-010). *J. Clin. Oncol.* **2005**, *23*, 2501. https://doi.org/10.1200/jco.2005.23.16_suppl.2501.
- (85) Bertrand, A.; Kostine, M.; Barnetche, T.; Truchetet, M. E.; Schaefferbeke, T. Immune Related Adverse Events Associated with Anti-CTLA-4 Antibodies: Systematic Review and Meta-Analysis. *BMC Med.* **2015**, *13* (1), 211. <https://doi.org/10.1186/s12916-015-0455-8>.
- (86) Jiang, Y.; Chen, M.; Nie, H.; Yuan, Y. PD-1 and PD-L1 in Cancer Immunotherapy: Clinical Implications and Future Considerations. *Hum. Vaccines Immunother.* **2019**, *15* (5), 1111–1122. <https://doi.org/10.1080/21645515.2019.1571892>.
- (87) Ohaegbulam, K. C.; Assal, A.; Lazar-Molnar, E.; Yao, Y.; Zang, X. Human Cancer Immunotherapy with Antibodies to the PD-1 and PD-L1 Pathway. *Trends. Mol. Med.* **2015**, *21* (1), 24–33. <https://doi.org/10.1016/j.molmed.2014.10.009>.
- (88) World Health Organization (2021). *World Health Organization Model List of Essential Medicines: 22nd List (2021)*; 2021. <https://apps.who.int/iris/handle/10665/345533> (accessed 2022-05-17).
- (89) Hamid, O.; Robert, C.; Daud, A.; Hodi, F. S.; Hwu, W.-J.; Kefford, R.; Wolchok, J. D.; Hersey, P.; Joseph, R. W.; Weber, J. S.; Dronca, R.; Gangadhar, T. C.; Patnaik, A.; Zarour, H.; Joshua, A. M.; Gergich, K.; Elassaiss-Schaap, J.; Algazi, A.; Mateus, C.; Boasberg, P.; Tume, P. C.; Chmielowski, B.; Ebbinghaus, S. W.; Li, X. N.; Kang, S. P.; Ribas, A. Safety and Tumor Responses with Lambrolizumab (Anti-PD-1) in Melanoma. *N. Engl. J. Med.* **2013**, *369* (2), 134–144. <https://doi.org/10.1056/NEJMoa1305133>.
- (90) Robert, C.; Schachter, J.; Long, G. v.; Arance, A.; Grob, J. J.; Mortier, L.; Daud, A.; Carlino, M. S.; McNeil, C.; Lotem, M.; Larkin, J.; Lorigan, P.; Neyns, B.; Blank, C. U.; Hamid, O.; Mateus, C.; Shapira-Frommer, R.; Kosh, M.; Zhou, H.; Ibrahim, N.; Ebbinghaus, S.; Ribas, A. Pembrolizumab versus Ipilimumab in Advanced Melanoma. *N. Engl. J. Med.* **2015**, *372* (26), 2521–2532. <https://doi.org/10.1056/nejmoa1503093>.
- (91) Naidoo, J.; Page, D. B.; Li, B. T.; Connell, L. C.; Schindler, K.; Lacouture, M. E.; Postow, M. A.; Wolchok, J. D. Toxicities of the Anti-PD-1 and Anti-PD-L1 Immune Checkpoint Antibodies. *Ann. Oncol.* **2015**, *26* (12), 2375–2391. <https://doi.org/10.1093/annonc/mdv383>.
- (92) Perez, H. L.; Cardarelli, P. M.; Deshpande, S.; Gangwar, S.; Schroeder, G. M.; Vite, G. D.; Borzilleri, R. M. Antibody–Drug Conjugates: Current Status and Future Directions. *Drug Discov. Today* **2014**, *19* (7), 869–881. <https://doi.org/10.1016/j.drudis.2013.11.004>.
- (93) Guzik, K.; Tomala, M.; Muszak, D.; Konieczny, M.; Hec, A.; Błaszkiwicz, U.; Pustuła, M.; Butera, R.; Dömling, A.; Holak, T. A. Development of the Inhibitors That Target the PD-1/PD-L1 Interaction—a Brief Look at Progress on Small Molecules, Peptides and Macrocycles. *Molecules* **2019**, *24* (11). <https://doi.org/10.3390/molecules24112071>.
- (94) Lin, X.; Lu, X.; Luo, G.; Xiang, H. Progress in PD-1/PD-L1 Pathway Inhibitors: From Biomacromolecules to Small Molecules. *Eur. J. Med. Chem.* **2020**, *186*, 111876. <https://doi.org/10.1016/j.ejmech.2019.111876>.
- (95) Skalniak, L.; Zak, K. M.; Guzik, K.; Magiera, K.; Musielak, B.; Pachota, M.; Szelazek, B.; Kocik, J.; Grudnik, P.; Tomala, M.; Krzanik, S.; Pyrc, K.; Dömling, A.; Dubin, G.; Holak, T. A. Small-Molecule Inhibitors of PD-1/PD-L1 Immune Checkpoint Alleviate the PD-L1-Induced Exhaustion of T-Cells. *Oncotarget* **2017**, *8* (42), 72167–72181.

- (96) Konieczny, M.; Musielak, B.; Kocik, J.; Skalniak, L.; Sala, D.; Czub, M.; Magiera-Mularz, K.; Rodriguez, I.; Myrcha, M.; Stec, M.; Siedlar, M.; Holak, T. A.; Plewka, J. Di-Bromo-Based Small-Molecule Inhibitors of the PD-1/PD-L1 Immune Checkpoint. *J. Med. Chem.* **2020**, *63* (19), 11271–11285. <https://doi.org/10.1021/acs.jmedchem.0c01260>.
- (97) Sasikumar, P. G.; Ramachandra, M. Small-Molecule Immune Checkpoint Inhibitors Targeting PD-1/PD-L1 and Other Emerging Checkpoint Pathways. *BioDrugs* **2018**, *32* (5), 481–497. <https://doi.org/10.1007/s40259-018-0303-4>.
- (98) Li, K.; Tian, H. Development of Small-Molecule Immune Checkpoint Inhibitors of PD-1/PD-L1 as a New Therapeutic Strategy for Tumour Immunotherapy. *J. Drug Target.* **2019**, *27* (3), 244–256. <https://doi.org/10.1080/1061186X.2018.1440400>.
- (99) Wu, Q.; Jiang, L.; Li, S. cheng; He, Q. jun; Yang, B.; Cao, J. Small Molecule Inhibitors Targeting the PD-1/PD-L1 Signaling Pathway. *Acta Pharmacol. Sin.* **2021**, *42* (1), 1–9. <https://doi.org/10.1038/s41401-020-0366-x>.
- (100) Zak, K. M.; Kitel, R.; Przetocka, S.; Golik, P.; Guzik, K.; Musielak, B.; Dömling, A.; Dubin, G.; Holak, T. A. Structure of the Complex of Human Programmed Death 1, PD-1, and Its Ligand PD-L1. *Structure* **2015**, *23* (12), 2341–2348. <https://doi.org/10.1016/j.str.2015.09.010>.
- (101) Sasikumar, P. G. N.; Ramachandra, M.; Vadlamani, S. K.; Vemula, K. R.; Satyam, L. K.; Subbarao, K.; Shrimali, R. K.; Kandepu, S. Immunosuppression Modulating Compounds. WO2011161699A2, 2011.
- (102) Wang, T.; Wu, X.; Guo, C.; Zhang, K.; Xu, J.; Li, Z.; Jiang, S. Development of Inhibitors of the Programmed Cell Death-1/Programmed Cell Death-Ligand 1 Signaling Pathway. *J. Med. Chem.* **2019**, *62* (4), 1715–1730. <https://doi.org/10.1021/acs.jmedchem.8b00990>.
- (103) Miller, M. M.; Mapelli, C.; Allen, M. P.; Bowsher, M. S.; Gillis, E. P.; Langley, D. R.; Mull, E.; Poirier, M. A.; Sanghvi, N.; Sun, L. Q. Macrocyclic Inhibitors of the PD-1/PD-L1 and CD80(B7-1)/PD-L1 Protein/Protein Interactions. WO2016039749, March 17, 2016.
- (104) Miller, M. M.; Mapelli, C.; Allen, M. P.; Bowsher, M. S.; Boy, K. M.; Gillis, E. P.; Langley, D. R.; Mull, E.; Poirier, M. A.; Sanghvi, N. Macrocyclic Inhibitors of the PD-1/PD-L1 and CD80(B7-1)/PD-L1 Protein/Protein Interactions. WO2014151634, September 25, 2014.
- (105) Magiera-Mularz, K.; Skalniak, L.; Zak, K. M.; Musielak, B.; Rudzinska-Szostak, E.; Berlicki, Ł.; Kocik, J.; Grudnik, P.; Sala, D.; Zarganes-Tzitzikas, T.; Shaabani, S.; Dömling, A.; Dubin, G.; Holak, T. A. Bioactive Macrocyclic Inhibitors of the PD-1/PD-L1 Immune Checkpoint. *Angew. Chem. Int. Ed.* **2017**, *56* (44), 13732–13735. <https://doi.org/10.1002/anie.201707707>.
- (106) Sasikumar, P. G.; Sudarshan, N. S.; Adurthi, S.; Ramachandra, R. K.; Samiulla, D. S.; Lakshminarasimhan, A.; Ramanathan, A.; Chandrasekhar, T.; Dhudashiya, A. A.; Talapati, S. R.; Gowda, N.; Palakolanu, S.; Mani, J.; Srinivasrao, B.; Joseph, D.; Kumar, N.; Nair, R.; Atreya, H. S.; Gowda, N.; Ramachandra, M. PD-1 Derived CA-170 Is an Oral Immune Checkpoint Inhibitor That Exhibits Preclinical Anti-Tumor Efficacy. *Commun. Biol.* **2021**, *4* (1), 699. <https://doi.org/10.1038/s42003-021-02191-1>.
- (107) Sasikumar, P. G. N.; Ramachandra, M.; Naremaddepalli, S. S. S. Dual Inhibitors of V-Domain Ig Suppressor of T-Cell Activation (VISTA) and PD-1 Pathways for Treatment of Cancer and Infectious Diseases. WO2018073754A1, 2018.
- (108) Lee, J. J.; Powderly, J. D.; Patel, M. R.; Brody, J.; Hamilton, E. P.; Infante, J. R.; Falchook, G. S.; Wang, H.; Adams, L.; Gong, L.; Ma, A. W.; Wyant, T.; Lazorchak, A.; Agarwal, S.; Tuck, D. P.; Daud, A. Phase 1 Trial of CA-170, a Novel Oral Small Molecule Dual Inhibitor of

Immune Checkpoints PD-1 and VISTA, in Patients (Pts) with Advanced Solid Tumor or Lymphomas. *J. Clin. Oncol.* **2017**, *35*, TPS3099. https://doi.org/10.1200/JCO.2017.35.15_suppl.TPS3099.

- (109) Sasikumar, P. N. G.; Ramachandra, M.; Naremaddepalli, S. S. S. 1,3,4-Oxadiazole and 1,3,4-Thiadiazole Derivatives as Immunomodulators. WO2015033301, 2015.
- (110) Sasikumar, P. G. N.; Ramachandra, M.; Naremaddepalli, S. S. S. 1,2,4-Oxadiazole and Thiadiazole Compounds as Immunomodulators. US20180044303, 2018.
- (111) Gillman, K. W.; Goodrich, J.; Boy, K. M.; Zhang, Y.; Mapelli, C.; Poss, M. A.; Sun, L. Q.; Zhao, Q.; Mull, E.; Scola, P. M.; Langley, D. R. Macrocyclic Peptides Useful as Immunomodulators. WO2016077518A1, 2016.
- (112) Chupak, L. S.; Ding, M.; Martin, S. W.; Zheng, X.; Hewawasam, P.; Connolly, T. P.; Xu, N.; Yeung, K. S.; Zhu, J.; Langley, D. R.; Tenney, D. J.; Scola, P. M. Compounds Useful as Immunomodulators. WO2015160641A3, 2015.
- (113) Chupak, L. S.; Zheng, X. Compounds Useful as Immunomodulators. WO2015034820A1, 2015.
- (114) Zak, K. M.; Grudnik, P.; Guzik, K.; Zieba, B. J.; Musielak, B.; Dömling, A.; Dubin, G.; Holak, T. A. Structural Basis for Small Molecule Targeting of the Programmed Death Ligand 1 (PD-L1). *Oncotarget* **2016**, *7* (21), 30323–30335. <https://doi.org/10.18632/oncotarget.8730>.
- (115) Ganesan, A.; Ahmed, M.; Okoye, I.; Arutyunova, E.; Babu, D.; Turnbull, W. L.; Kundu, J. K.; Shields, J.; Agopsowicz, K. C.; Xu, L.; Tabana, Y.; Srivastava, N.; Zhang, G.; Moon, T. C.; Belovodskiy, A.; Hena, M.; Kandadai, A. S.; Hosseini, S. N.; Hitt, M.; Walker, J.; Smylie, M.; West, F. G.; Siraki, A. G.; Lemieux, M. J.; Elahi, S.; Nieman, J. A.; Tyrrell, D. L.; Houghton, M.; Barakat, K. Comprehensive in Vitro Characterization of PD-L1 Small Molecule Inhibitors. *Sci. Rep.* **2019**, *9* (1), 12392. <https://doi.org/10.1038/s41598-019-48826-6>.
- (116) McLeod, J. D.; Walker, L. S.; Patel, Y. I.; Boulougouris, G.; Sansom, D. M. Activation of Human T Cells with Superantigen (Staphylococcal Enterotoxin B) and CD28 Confers Resistance to Apoptosis via CD95. *J. Immunol.* **1998**, *160* (5), 2072–2079.
- (117) William T Lee, D. K. J. Staphylococcal Enterotoxin B (SEB) Induces Memory CD4 T Cell Anergy in Vivo and Impairs Recall Immunity to Unrelated Antigens. *J. Clin. Cell. Immunol.* **2015**, *6* (4), 1–8. <https://doi.org/10.4172/2155-9899.1000346>.
- (118) Rödström, K. E. J.; Elbing, K.; Lindkvist-Petersson, K. Structure of the Superantigen Staphylococcal Enterotoxin B in Complex with TCR and Peptide–MHC Demonstrates Absence of TCR–Peptide Contacts. *J. Immunol.* **2014**, *193* (4), 1998–2004. <https://doi.org/10.4049/jimmunol.1401268>.
- (119) Lee, H.; Lee, J. W. Target Identification for Biologically Active Small Molecules Using Chemical Biology Approaches. *Arch. Pharmacol. Res.* **2016**, *39* (9), 1193–1201. <https://doi.org/10.1007/s12272-016-0791-z>.
- (120) Beckwith, R. E. J.; Jain, R. K. Recent Advances in Small Molecule Target Identification Methods. In *Annual Reports in Medicinal Chemistry*; Academic Press Inc., 2013; Vol. 48, pp 301–315. <https://doi.org/10.1016/B978-0-12-417150-3.00019-3>.
- (121) Lee, J.; Bogyo, M. Target Deconvolution Techniques in Modern Phenotypic Profiling. *Curr. Opin. Chem. Biol.* **2013**, *17* (1), 118–126. <https://doi.org/10.1016/j.cbpa.2012.12.022>.

- (122) Kawatani, M.; Osada, H. Affinity-Based Target Identification for Bioactive Small Molecules. *Medchemcomm* **2014**, *5* (3), 277–287. <https://doi.org/10.1039/c3md00276d>.
- (123) Lomenick, B.; Olsen, R. W.; Huang, J. Identification of Direct Protein Targets of Small Molecules. *ACS Chem. Biol.* **2011**, *6* (1), 34–46. <https://doi.org/10.1021/cb100294v>.
- (124) Stockwell, B. R. Chemical Genetics: Ligand-Based Discovery of Gene Function. *Nat. Rev. Genet.* **2000**, *1* (2), 116–125. <https://doi.org/10.1038/35038557>.
- (125) Kubota, K.; Funabashi, M.; Ogura, Y. Target Deconvolution from Phenotype-Based Drug Discovery by Using Chemical Proteomics Approaches. *Biochim. Biophys. Acta - Proteins Proteom.* **2019**, *1867* (1), 22–27. <https://doi.org/10.1016/j.bbapap.2018.08.002>.
- (126) Burdine, L.; Kodadek, T. Target Identification in Chemical Genetics. *Chem. Biol.* **2004**, *11* (5), 593–597. <https://doi.org/10.1016/j.chembiol.2004.05.001>.
- (127) Hertzberg, R. P.; Pope, A. J. High-Throughput Screening: New Technology for the 21st Century. *Curr. Opin. Chem. Biol.* **2000**, *4* (4), 445–451. [https://doi.org/10.1016/S1367-5931\(00\)00110-1](https://doi.org/10.1016/S1367-5931(00)00110-1).
- (128) Bajorath, J. Integration of Virtual and High-Throughput Screening. *Nat. Rev. Drug Discov.* **2002**, *1* (11), 882–894. <https://doi.org/10.1038/nrd941>.
- (129) Mayr, L. M.; Bojanic, D. Novel Trends in High-Throughput Screening. *Curr. Opin. Pharmacol.* **2009**, *9* (5), 580–588. <https://doi.org/10.1016/j.coph.2009.08.004>.
- (130) Swinney, D. C.; Anthony, J. How Were New Medicines Discovered? *Nat. Rev. Drug Discov.* **2011**, *10* (7), 507–519. <https://doi.org/10.1038/nrd3480>.
- (131) Schenone, M.; Dančik, V.; Wagner, B. K.; Clemons, P. A. Target Identification and Mechanism of Action in Chemical Biology and Drug Discovery. *Nat. Chem. Biol.* **2013**, *9* (4), 232–240. <https://doi.org/10.1038/nchembio.1199>.
- (132) Schreiber, S. L. The Small-Molecule Approach to Biology. *C&EN*. 2003, pp 51–61.
- (133) Sato, S.; Murata, A.; Shirakawa, T.; Uesugi, M. Biochemical Target Isolation for Novices: Affinity-Based Strategies. *Chem. Biol.* **2010**, *17* (6), 616–623. <https://doi.org/10.1016/j.chembiol.2010.05.015>.
- (134) Leslie, B. J.; Hergenrother, P. J. Identification of the Cellular Targets of Bioactive Small Organic Molecules Using Affinity Reagents. *Chem. Soc. Rev.* **2008**, *37* (7), 1347. <https://doi.org/10.1039/b702942j>.
- (135) Ziegler, S.; Pries, V.; Hedberg, C.; Waldmann, H. Target Identification for Small Bioactive Molecules: Finding the Needle in the Haystack. *Angew. Chem. Int. Ed.* **2013**, *52* (10), 2744–2792. <https://doi.org/10.1002/anie.201208749>.
- (136) Lapinsky, D. J. Tandem Photoaffinity Labeling-Bioorthogonal Conjugation in Medicinal Chemistry. *Bioorg. Med. Chem.* **2012**, *20* (21), 6237–6247. <https://doi.org/10.1016/j.bmc.2012.09.010>.
- (137) Grant, E. K.; Fallon, D. J.; Hann, M. M.; Fantom, K. G. M.; Quinn, C.; Zappacosta, F.; Annan, R. S.; Chung, C. wa; Bamborough, P.; Dixon, D. P.; Stacey, P.; House, D.; Patel, V. K.; Tomkinson, N. C. O.; Bush, J. T. A Photoaffinity-Based Fragment-Screening Platform for Efficient Identification of Protein Ligands. *Angew. Chem. Int. Ed.* **2020**, *59* (47), 21096–21105. <https://doi.org/10.1002/anie.202008361>.

- (138) Geurink, P. P.; Prely, L. M.; van der Marel, G. A.; Bischoff, R.; Overkleeft, H. S. Photoaffinity Labeling in Activity-Based Protein Profiling. *Top. Curr. Chem.* **2011**, 85–113. https://doi.org/10.1007/128_2011_286.
- (139) Hein, C. D.; Liu, X.-M.; Wang, D. Click Chemistry, A Powerful Tool for Pharmaceutical Sciences. *Pharm Res* **2008**, 25 (10), 2216–2230. <https://doi.org/10.1007/s11095-008-9616-1>.
- (140) Sletten, E. M.; Bertozzi, C. R. Bioorthogonal Chemistry: Fishing for Selectivity in a Sea of Functionality. *Angewandte Chemie International Edition* **2009**, 48 (38), 6974–6998. <https://doi.org/10.1002/anie.200900942>.
- (141) Best, M. D. Click Chemistry and Bioorthogonal Reactions: Unprecedented Selectivity in the Labeling of Biological Molecules. *Biochemistry* **2009**, 48 (28), 6571–6584. <https://doi.org/10.1021/bi9007726>.
- (142) Dormán, G.; Prestwich, G. D. Using Photolabile Ligands in Drug Discovery and Development. *Trends Biotechnol.* **2000**, 18 (2), 64–77. [https://doi.org/10.1016/S0167-7799\(99\)01402-X](https://doi.org/10.1016/S0167-7799(99)01402-X).
- (143) Hatanaka, Y.; Sadakane, Y. Photoaffinity Labeling in Drug Discovery and Developments: Chemical Gateway for Entering Proteomic Frontier. *Curr. Top. Med. Chem.* **2002**, 2, 271–288.
- (144) Cisar, J. S.; Cravatt, B. F. Fully Functionalized Small-Molecule Probes for Integrated Phenotypic Screening and Target Identification. *J. Am. Chem. Soc.* **2012**, 134 (25), 10385–10388. <https://doi.org/10.1021/ja304213w>.
- (145) Kumar, N. S.; Young, R. N. Design and Synthesis of an All-in-One 3-(1,1-Difluoroprop-2-Ynyl)-3H-Diazirin-3-Yl Functional Group for Photo-Affinity Labeling. *Bioorg. Med. Chem.* **2009**, 17 (15), 5388–5395. <https://doi.org/10.1016/j.bmc.2009.06.048>.
- (146) Zempleni, J.; Wijeratne, S. S. K.; Hassan, Y. I. Biotin. *BioFactors* **2009**, 35 (1), 36–46. <https://doi.org/10.1002/biof.8>.
- (147) Weber, P. C.; Ohlendorf, D. H.; Wendoloski, J. J.; Salemme, F. R. Structural Origins of High-Affinity Biotin Binding to Streptavidin. *Science* **1989**, 243 (4887), 85–88. <https://doi.org/10.1126/science.2911722>.
- (148) Chaiet, L.; Wolf, F. J. The Properties of Streptavidin, a Biotin-Binding Protein Produced by Streptomycetes. *Arch. Biochem. Biophys.* **1964**, 106, 1–5. [https://doi.org/10.1016/0003-9861\(64\)90150-X](https://doi.org/10.1016/0003-9861(64)90150-X).
- (149) Dundas, C. M.; Demonte, D.; Park, S. Streptavidin–Biotin Technology: Improvements and Innovations in Chemical and Biological Applications. *Appl. Microbiol. Biotechnol.* **2013**, 97 (21), 9343–9353. <https://doi.org/10.1007/s00253-013-5232-z>.
- (150) Seki, M. Biological Significance and Development of Practical Synthesis of Biotin. *Med. Res. Rev.* **2006**, 26 (4), 434–482. <https://doi.org/10.1002/med.20058>.
- (151) Trippier, P. C. Synthetic Strategies for the Biotinylation of Bioactive Small Molecules. *ChemMedChem* **2013**, 8 (2), 190–203. <https://doi.org/10.1002/cmdc.201200498>.
- (152) Zhu, S.; Wurdak, H.; Wang, J.; Lyssiotis, C. A.; Peters, E. C.; Cho, C. Y.; Wu, X.; Schultz, P. G. A Small Molecule Primes Embryonic Stem Cells for Differentiation. *Cell Stem Cell* **2009**, 4 (5), 416–426. <https://doi.org/10.1016/j.stem.2009.04.001>.

- (153) Lapinsky, D. J. Tandem Photoaffinity Labeling–Bioorthogonal Conjugation in Medicinal Chemistry. *Bioorg. Med. Chem.* **2012**, *20* (21), 6237–6247. <https://doi.org/10.1016/j.bmc.2012.09.010>.
- (154) Holland, J. P.; Gut, M.; Klingler, S.; Fay, R.; Guillou, A. Photochemical Reactions in the Synthesis of Protein–Drug Conjugates. *Chemistry – A European Journal* **2020**, *26* (1), 33–48. <https://doi.org/10.1002/chem.201904059>.
- (155) Smith, E.; Collins, I. Photoaffinity Labeling in Target- and Binding-Site Identification. *Future Med Chem* **2015**, *7* (2), 159–183. <https://doi.org/10.4155/fmc.14.152>.
- (156) Sumranjit, J.; Chung, S. Recent Advances in Target Characterization and Identification by Photoaffinity Probes. *Molecules* **2013**, *18* (9), 10425–10451. <https://doi.org/10.3390/molecules180910425>.
- (157) Murale, D. P.; Hong, S. C.; Haque, M. M.; Lee, J. S. Photo-Affinity Labeling (PAL) in Chemical Proteomics: A Handy Tool to Investigate Protein-Protein Interactions (PPIs). *Proteome Sci.* **2017**, *15* (1), 14. <https://doi.org/10.1186/s12953-017-0123-3>.
- (158) Kolb, H. C.; Sharpless, K. B. The Growing Impact of Click Chemistry on Drug Discovery. *Drug Discov Today* **2003**, *8* (24), 1128–1137. [https://doi.org/10.1016/S1359-6446\(03\)02933-7](https://doi.org/10.1016/S1359-6446(03)02933-7).
- (159) Presolski, S. I.; Hong, V. P.; Finn, M. G. Copper-Catalyzed Azide–Alkyne Click Chemistry for Bioconjugation. *Curr Protoc Chem Biol* **2011**, *3* (4), 153–162. <https://doi.org/10.1002/9780470559277.ch110148>.
- (160) Sletten, E. M.; Bertozzi, C. R. Bioorthogonal Chemistry: Fishing for Selectivity in a Sea of Functionality. *Angew. Chem. Int. Ed.* **2009**, *48* (38), 6974–6998. <https://doi.org/10.1002/anie.200900942>.
- (161) Hong, V.; Presolski, S. I.; Ma, C.; Finn, M. G. Analysis and Optimization of Copper-Catalyzed Azide-Alkyne Cycloaddition for Bioconjugation. *Angewandte Chemie - International Edition* **2009**, *48* (52), 9879–9883. <https://doi.org/10.1002/anie.200905087>.
- (162) Li, S.; Wang, L.; Yu, F.; Zhu, Z.; Shobaki, D.; Chen, H.; Wang, M.; Wang, J.; Qin, G.; Erasquin, U. J.; Ren, L.; Wang, Y.; Cai, C. Copper-Catalyzed Click Reaction on/in Live Cells. *Chem Sci* **2017**, *8* (3), 2107–2114. <https://doi.org/10.1039/c6sc02297a>.
- (163) Cañeque, T.; Müller, S.; Rodriguez, R. Visualizing Biologically Active Small Molecules in Cells Using Click Chemistry. *Nat. Rev. Chem.* **2018**, *2* (9), 202–215. <https://doi.org/10.1038/s41570-018-0030-x>.
- (164) Ghosh, B.; Jones, L. H. Target Validation Using In-Cell Small Molecule Clickable Imaging Probes. *Medchemcomm* **2014**, *5* (3), 247–254. <https://doi.org/10.1039/c3md00277b>.
- (165) le Droumaguet, C.; Wang, C.; Wang, Q. Fluorogenic Click Reaction. *Chem. Soc. Rev.* **2010**, *39* (4), 1233–1239. <https://doi.org/10.1039/b901975h>.
- (166) Singh, A.; Thronton, E. R.; Westheimer, F. H. The Photolysis of Diazoacetylchymotrypsin. *J. Biol. Chem.* **1962**, *237*, 3006–3008.
- (167) Pattison, D. I.; Rahmanto, A. S.; Davies, M. J. Photo-Oxidation of Proteins. *Photochem. Photobiol. Sci.* **2012**, *11* (1), 38–53. <https://doi.org/10.1039/C1PP05164D>.

- (168) Sakurai, K.; Ozawa, S.; Yamada, R.; Yasui, T.; Mizuno, S. Comparison of the Reactivity of Carbohydrate Photoaffinity Probes with Different Photoreactive Groups. *ChemBioChem* **2014**, *15* (10), 1399–1403. <https://doi.org/10.1002/cbic.201402051>.
- (169) Fleming, S. A. Chemical Reagents in Photoaffinity Labeling. *Tetrahedron* **1995**, *51*, 12419–12520. [https://doi.org/10.1016/0040-4020\(95\)00598-3](https://doi.org/10.1016/0040-4020(95)00598-3).
- (170) Hassan, M. M.; Olaoye, O. O. Recent Advances in Chemical Biology Using Benzophenones and Diazirines as Radical Precursors. *Molecules* **2020**, *25* (10), 2285. <https://doi.org/10.3390/molecules25102285>.
- (171) Galardy, R. E.; Craig, L. C.; Printz, M. P. Benzophenone Triplet: A New Photochemical Probe of Biological Ligand-Receptor Interactions. *Nature New Biol.* **1973**, *242* (117), 127–128. <https://doi.org/10.1038/newbio242127a0>.
- (172) Dormán, G.; Nakamura, H.; Pulsipher, A.; Prestwich, G. D. The Life of Pi Star: Exploring the Exciting and Forbidden Worlds of the Benzophenone Photophore. *Chem. Rev.* **2016**, *116* (24), 15284–15398. <https://doi.org/10.1021/acs.chemrev.6b00342>.
- (173) Prestwich, G. D.; Dormán, G.; Elliott, J. T.; Marecak, D. M.; Chaudhary, A. Benzophenone Photoprobes for Phosphoinositides, Peptides and Drugs. *Photochem. Photobiol.* **1997**, *65* (2), 222–234. <https://doi.org/10.1111/j.1751-1097.1997.tb08548.x>.
- (174) Sherratt, A. R.; Nasheri, N.; McKay, C. S.; O'Hara, S.; Hunt, A.; Ning, Z.; Figeys, D.; Goto, N. K.; Pezacki, J. P. A New Chemical Probe for Phosphatidylinositol Kinase Activity. *ChemBioChem* **2014**, *15* (9), 1253–1256. <https://doi.org/10.1002/cbic.201402155>.
- (175) Hashimoto, M.; Hatanaka, Y. Recent Progress in Diazirine-Based Photoaffinity Labeling. *Eur. J. Org. Chem.* **2008**, *15*, 2513–2523. <https://doi.org/10.1002/ejoc.200701069>.
- (176) Geurink, P. P.; Prely, L. M.; van der Marel, G. A.; Bischoff, R.; Overkleeft, H. S. Photoaffinity Labeling in Activity-Based Protein Profiling. *Top. Curr. Chem.* **2011**, *324*, 85–113. https://doi.org/10.1007/128_2011_286.
- (177) Korneev, S. M. Valence Isomerization between Diazo Compounds and Diazirines. *Eur. J. Org. Chem.* **2011**, *31*, 6153–6175. <https://doi.org/10.1002/ejoc.201100224>.
- (178) Das, J. Aliphatic Diazirines as Photoaffinity Probes for Proteins: Recent Developments. *Chem. Rev.* **2011**, *111* (8), 4405–4417. <https://doi.org/10.1021/cr1002722>.
- (179) Bonneau, R.; Liu, M. T. H.; Kim, K. C.; Goodman, J. L. Rearrangement of Alkylchlorocarbenes: 1,2-H Shift in Free Carbene, Carbene–Olefin Complex, and Excited States of Carbene Precursors. *J. Am. Chem. Soc.* **1996**, *118* (16), 3829–3837. <https://doi.org/10.1021/ja952700n>.
- (180) Bayley, H.; Knowles, J. R. Photogenerated Reagents for Membrane Labeling. 2. Phenylcarbene and Adamantylidene Formed within the Lipid Bilayer. *Biochemistry* **1978**, *17* (12), 2420–2423. <https://doi.org/10.1021/bi00605a026>.
- (181) Smith, R. A. G.; Knowles, J. R. Aryldiazirines. Potential Reagents for Photolabeling of Biological Receptor Sites. *J. Am. Chem. Soc.* **1973**, *95* (15), 5072–5073. <https://doi.org/10.1021/ja00796a062>.
- (182) Smith, R. A. G.; Knowles, J. R. The Preparation and Photolysis of 3-Aryl-3H-Diazirines. *J. Chem. Soc., Perkin trans. II* **1975**, *7*, 686. <https://doi.org/10.1039/p29750000686>.

- (183) Brunner, J.; Serin, H.; Richards, F. M. 3-Trifluoromethyl-3-Phenyldiazirine. A New Carbene Generating Group for Photolabeling Reagents. *J. Biol. Chem.* **1980**, *255* (8), 3313–3318.
- (184) Djordjevic, I.; Wicaksono, G.; Solic, I.; Steele, T. W. J. Diazoalkane Decay Kinetics from UVA-Active Protein Labelling Molecules: Trifluoromethyl Phenyl Diazirines. *Results Chem.* **2020**, *2*, 100066. <https://doi.org/10.1016/j.rechem.2020.100066>.
- (185) Zhang, Y.; Burdzinski, G.; Kubicki, J.; Platz, M. S. Direct Observation of Carbene and Diazo Formation from Aryldiazirines by Ultrafast Infrared Spectroscopy. *J. Am. Chem. Soc.* **2008**, *130* (48), 16134–16135. <https://doi.org/10.1021/ja805922b>.
- (186) Hill, J. R.; Robertson, A. A. B. Fishing for Drug Targets: A Focus on Diazirine Photoaffinity Probe Synthesis. *J. Med. Chem.* **2018**, *61* (16), 6945–6963. <https://doi.org/10.1021/acs.jmedchem.7b01561>.
- (187) Mayer, T.; Maier, M. E. Design and Synthesis of a Tag-Free Chemical Probe for Photoaffinity Labeling. *Eur. J. Org. Chem.* **2007**, No. 28, 4711–4720. <https://doi.org/10.1002/ejoc.200700188>.
- (188) Wixe, T.; Almqvist, F. An Improved Synthesis of 3-[3-(Trifluoromethyl)-3H-1,2-Diazirin-3-Yl]Aniline: A Key Intermediate in the Synthesis of Photoaffinity Probes. *Tetrahedron Lett.* **2017**, *58* (34), 3350–3352. <https://doi.org/10.1016/j.tetlet.2017.07.031>.
- (189) Scinto, S. L.; Bilodeau, D. A.; Hincapie, R.; Lee, W.; Nguyen, S. S.; Xu, M.; am Ende, C. W.; Finn, M. G.; Lang, K.; Lin, Q.; Pezacki, J. P.; Prescher, J. A.; Robillard, M. S.; Fox, J. M. Bioorthogonal Chemistry. *Nat. Rev. Methods. Primers.* **2021**, *1* (1), 30. <https://doi.org/10.1038/s43586-021-00028-z>.
- (190) Bird, R. E.; Lemmel, S. A.; Yu, X.; Zhou, Q. A. Bioorthogonal Chemistry and Its Applications. *Bioconjug. Chem.* **2021**, *32* (12), 2457–2479. <https://doi.org/10.1021/acs.bioconjchem.1c00461>.
- (191) Bertozzi, C. R. A Decade of Bioorthogonal Chemistry. *Acc. Chem. Res.* **2011**, *44* (9), 651–653. <https://doi.org/10.1021/ar200193f>.
- (192) Hang, H. C.; Yu, C.; Kato, D. L.; Bertozzi, C. R. A Metabolic Labeling Approach toward Proteomic Analysis of Mucin-Type O-Linked Glycosylation. *Proc. Natl. Acad. Sci.* **2003**, *100* (25), 14846–14851. <https://doi.org/10.1073/pnas.2335201100>.
- (193) Rudolf, G. C.; Sieber, S. A. Copper-Assisted Click Reactions for Activity-Based Proteomics: Fine-Tuned Ligands and Refined Conditions Extend the Scope of Application. *ChemBioChem* **2013**, *14* (18), 2447–2455. <https://doi.org/10.1002/cbic.201300551>.
- (194) Lallana, E.; Riguera, R.; Fernandez-Megia, E. Reliable and Efficient Procedures for the Conjugation of Biomolecules through Huisgen Azide-Alkyne Cycloadditions. *Angew. Chem. Int. Ed.* **2011**, *50* (38), 8794–8804. <https://doi.org/10.1002/anie.201101019>.
- (195) Köhn, M.; Breinbauer, R. The Staudinger Ligation - A Gift to Chemical Biology. *Angew. Chem. Int. Ed.* **2004**, *43* (24), 3106–3116. <https://doi.org/10.1002/anie.200401744>.
- (196) Staudinger, von H.; Meyer, J. Über Neue Organische Phosphorverbindungen III. Phosphinmethylenderivate Und Phosphinimine. *Helv. Chim. Acta.* **1919**, *2*, 635–646.
- (197) Saxon, E.; Armstrong, J. I.; Bertozzi, C. R. A “Traceless” Staudinger Ligation for the Chemoselective Synthesis of Amide Bonds. *Org. Lett.* **2000**, *2* (14), 2141–2143. <https://doi.org/10.1021/ol006054v>.

- (198) Saxon, E.; Bertozzi, C. R. Cell Surface Engineering by a Modified Staudinger Reaction. *Science* **2000**, *287* (5460), 2007–2010. <https://doi.org/10.1126/science.287.5460.2007>.
- (199) Huisgen, R. Kinetics and Mechanism of 1,3-Dipolar Cycloadditions. *Angew. Chem. Int. Ed.* **1963**, *2* (11), 633–645. <https://doi.org/10.1002/anie.196306331>.
- (200) Rostovtsev, V. v.; Green, L. G.; Fokin, V. v.; Sharpless, K. B. A Stepwise Huisgen Cycloaddition Process: Copper(I)-Catalyzed Regioselective “Ligation” of Azides and Terminal Alkynes. *Angew. Chem. Int. Ed.* **2002**, *41* (14), 2596–2599. [https://doi.org/10.1002/1521-3773\(20020715\)41:14<2596::AID-ANIE2596>3.0.CO;2-4](https://doi.org/10.1002/1521-3773(20020715)41:14<2596::AID-ANIE2596>3.0.CO;2-4).
- (201) Tornøe, C. W.; Christensen, C.; Meldal, M. Peptidotriazoles on Solid Phase: [1,2,3]-Triazoles by Regiospecific Copper(I)-Catalyzed 1,3-Dipolar Cycloadditions of Terminal Alkynes to Azides. *J. Org. Chem.* **2002**, *67* (9), 3057–3064. <https://doi.org/10.1021/jo011148j>.
- (202) Worrell, B. T.; Malik, J. A.; Fokin, V. v. Direct Evidence of a Dinuclear Copper Intermediate in Cu(I)-Catalyzed Azide-Alkyne Cycloadditions. *Science* **2013**, *340* (6131), 457–460. <https://doi.org/10.1126/science.1229506>.
- (203) Kennedy, D. C.; McKay, C. S.; Legault, M. C. B.; Danielson, D. C.; Blake, J. A.; Pegoraro, A. F.; Stolow, A.; Mester, Z.; Pezacki, J. P. Cellular Consequences of Copper Complexes Used To Catalyze Bioorthogonal Click Reactions. *J. Am. Chem. Soc.* **2011**, *133* (44), 17993–18001. <https://doi.org/10.1021/ja2083027>.
- (204) Haldón, E.; Nicasio, M. C.; Pérez, P. J. Copper-Catalysed Azide-Alkyne Cycloadditions (CuAAC): An Update. *Org. Biomol. Chem.* **2015**, *13* (37), 9528–9550. <https://doi.org/10.1039/c5ob01457c>.
- (205) Agard, N. J.; Prescher, J. A.; Bertozzi, C. R. A Strain-Promoted [3 + 2] Azide-Alkyne Cycloaddition for Covalent Modification of Biomolecules in Living Systems. *J. Am. Chem. Soc.* **2004**, *126* (46), 15046–15047. <https://doi.org/10.1021/ja044996f>.
- (206) Wittig, G.; Krebs, A. Zur Existenz Niedergliedriger Cycloalkine, I. *Chem. Ber.* **1961**, *94* (12), 3260–3275. <https://doi.org/10.1002/cber.19610941213>.
- (207) Sletten, E. M.; Bertozzi, C. R. From Mechanism to Mouse: A Tale of Two Bioorthogonal Reactions. *Acc. Chem. Res.* **2011**, *44* (9), 666–676. <https://doi.org/10.1021/ar200148z>.

Chapter 2

- (1) Weber, P. C.; Ohlendorf, D. H.; Wendoloski, J. J.; Salemme, F. R. Structural Origins of High-Affinity Biotin Binding to Streptavidin. *Science* **1989**, *243* (4887), 85–88. <https://doi.org/10.1126/science.2911722>.
- (2) Green, N. M. Avidin. In *Advances in Protein Chemistry*; New York, 1975; pp 85–133. [https://doi.org/10.1016/S0065-3233\(08\)60411-8](https://doi.org/10.1016/S0065-3233(08)60411-8).
- (3) Bayer, E. A.; Meir, W. The Avidin-Biotin Complex in Bioanalytical Applications. *Anal. Biochem.* **1988**, *171*, 1–32.
- (4) Sano, T.; Vajda, S.; Reznik, G. O.; Smith, C. L.; Cantor, C. R. Molecular Engineering of Streptavidin. *Ann. N. Y. Acad. Sci.* **1996**, *799* (1), 383–390. <https://doi.org/10.1111/j.1749-6632.1996.tb33229.x>.

- (5) Trippier, P. C. Synthetic Strategies for the Biotinylation of Bioactive Small Molecules. *ChemMedChem* **2013**, *8* (2), 190–203. <https://doi.org/10.1002/cmdc.201200498>.
- (6) Wilchek, M.; Bayer, E. A. [13] Biotin-Containing Reagents. In *Methods in Enzymology*; 1990; Vol. 184, pp 123–138. [https://doi.org/10.1016/0076-6879\(90\)84267-K](https://doi.org/10.1016/0076-6879(90)84267-K).
- (7) Murakami, N.; Ye, Y.; Kawanishi, M.; Aoki, S.; Kudo, N.; Yoshida, M.; Nakayama, E. E.; Shioda, T.; Kobayashi, M. New Rev-Transport Inhibitor with Anti-HIV Activity from Valerianae Radix. *Bioorganic Med. Chem. Lett.* **2002**, *12* (20), 2807–2810. [https://doi.org/10.1016/S0960-894X\(02\)00624-8](https://doi.org/10.1016/S0960-894X(02)00624-8).
- (8) Shioiri, T.; Ninomiya, K.; Yamada, S. Diphenylphosphoryl Azide. New Convenient Reagent for a Modified Curtius Reaction and for Peptide Synthesis. *J. Am. Chem. Soc.* **1972**, *94* (17), 6203–6205. <https://doi.org/10.1021/ja00772a052>.
- (9) Szalecki, W. Synthesis of Norbiotinamine and Its Derivatives. *Bioconjug. Chem.* **1996**, *7* (2), 271–273. <https://doi.org/10.1021/bc950094f>.
- (10) Foulon, C. F.; Alston, K. L.; Zalutsky, M. R. Synthesis and Preliminary Biological Evaluation of (3-Iodobenzoyl)Norbiotinamide and ((5-Iodo-3-Pyridinyl)Carbonyl)Norbiotinamide: Two Radioiodinated Biotin Conjugates with Improved Stability. *Bioconjug. Chem.* **1997**, *8* (2), 179–186. <https://doi.org/10.1021/bc970006m>.
- (11) Malik, M. S.; Ahmed, S. A.; Althagafi, I. I.; Ansari, M. A.; Kamal, A. Application of Triazoles as Bioisosteres and Linkers in the Development of Microtubule Targeting Agents. *RSC Med. Chem.* **2020**, *11* (3), 327–348. <https://doi.org/10.1039/C9MD00458K>.
- (12) Surana, K.; Chaudhary, B.; Diwaker, M.; Sharma, S. Benzophenone: A Ubiquitous Scaffold in Medicinal Chemistry. *Medchemcomm* **2018**, *9* (11), 1803–1817. <https://doi.org/10.1039/C8MD00300A>.
- (13) Sartori, G.; Maggi, R. Update 1 of: Use of Solid Catalysts in Friedel–Crafts Acylation Reactions. *Chem. Rev.* **2011**, *111* (5), PR181–PR214. <https://doi.org/10.1021/cr100375z>.
- (14) Hwang, J. P.; Surya Prakash, G. K.; Olah, G. A. Trifluoromethanesulfonic Acid Catalyzed Novel Friedel–Crafts Acylation of Aromatics with Methyl Benzoate. *Tetrahedron Lett.* **2000**, *56* (37), 7199–7203. [https://doi.org/10.1016/S0040-4020\(00\)00633-5](https://doi.org/10.1016/S0040-4020(00)00633-5).
- (15) Yamazaki, Y.; Sumikura, M.; Masuda, Y.; Hayashi, Y.; Yasui, H.; Kiso, Y.; Chinen, T.; Usui, T.; Yakushiji, F.; Potts, B.; Neuteboom, S.; Palladino, M.; Lloyd, G. K.; Hayashi, Y. Synthesis and Structure–Activity Relationships of Benzophenone-Bearing Diketopiperazine-Type Anti-Microtubule Agents. *Bioorg. Med. Chem.* **2012**, *20* (14), 4279–4289. <https://doi.org/10.1016/j.bmc.2012.05.059>.
- (16) Ishiyama, T.; Kizaki, H.; Miyaura, N.; Suzuki, A. Synthesis of Unsymmetrical Biaryl Ketones via Palladium-Catalyzed Carbonylative Cross-Coupling Reaction of Arylboronic Acids with Iodoarenes. *Tetrahedron Lett.* **1993**, *34* (47), 7595–7598. [https://doi.org/10.1016/S0040-4039\(00\)60409-4](https://doi.org/10.1016/S0040-4039(00)60409-4).
- (17) Ishiyama, T.; Kizaki, H.; Hayashi, T.; Suzuki, A.; Miyaura, N. Palladium-Catalyzed Carbonylative Cross-Coupling Reaction of Arylboronic Acids with Aryl Electrophiles: Synthesis of Biaryl Ketones. *J. Org. Chem.* **1998**, *63* (14), 4726–4731. <https://doi.org/10.1021/jo980417b>.
- (18) Haddach, M.; McCarthy, J. R. A New Method for the Synthesis of Ketones: The Palladium-Catalyzed Cross-Coupling of Acid Chlorides with Arylboronic Acids. *Tetrahedron Lett.* **1999**, *40* (16), 3109–3112. [https://doi.org/10.1016/S0040-4039\(99\)00476-1](https://doi.org/10.1016/S0040-4039(99)00476-1).
- (19) Qi, X.; Jiang, L.-B.; Li, H.-P.; Wu, X.-F. A Convenient Palladium-Catalyzed Carbonylative Suzuki Coupling of Aryl Halides with Formic Acid as the Carbon Monoxide Source. *Eur. J. Chem.* **2015**, *21* (49), 17650–17656. <https://doi.org/10.1002/chem.201502943>.
- (20) Sun, N.; Sun, Q.; Zhao, W.; Jin, L.; Hu, B.; Shen, Z.; Hu, X. Ligand-free Palladium-Catalyzed Carbonylative Suzuki Coupling of Aryl Iodides in Aqueous CH₃CN with Sub-stoichiometric

- Amount of Mo(CO)₆ as CO Source. *Adv. Synth. Catal.* **2019**, *361* (9), 2117–2123. <https://doi.org/10.1002/adsc.201900011>.
- (21) Huang, Y.-C.; Majumdar, K. K.; Cheng, C.-H. Nickel-Catalyzed Coupling of Aryl Iodides with Aromatic Aldehydes: Chemoselective Synthesis of Ketones. *J. Org. Chem.* **2002**, *67* (5), 1682–1684. <https://doi.org/10.1021/jo010289i>.
- (22) Wakaki, T.; Togo, T.; Yoshidome, D.; Kuninobu, Y.; Kanai, M. Palladium-Catalyzed Synthesis of Diaryl Ketones from Aldehydes and (Hetero)Aryl Halides via C–H Bond Activation. *ACS Catal.* **2018**, *8* (4), 3123–3128. <https://doi.org/10.1021/acscatal.8b00440>.
- (23) Hill, J. R.; Robertson, A. A. B. Fishing for Drug Targets: A Focus on Diazirine Photoaffinity Probe Synthesis. *J. Med. Chem.* **2018**, *61* (16), 6945–6963. <https://doi.org/10.1021/acs.jmedchem.7b01561>.
- (24) Zeifman, Yu. v.; Abduganiev, E. G.; Rokhlin, E. M.; Knunyants, I. L. Derivatives of Hexafluoroacetone Oxime. *Russ. Chem. Bull.* **1972**, *21* (12), 2667–2671. <https://doi.org/10.1007/BF00849836>.
- (25) Brunner, J.; Serin, H.; Richards, F. M. 3-Trifluoromethyl-3-Phenyldiazirine. A New Carbene Generating Group for Photolabeling Reagents. *J. Biol. Chem.* **1980**, *255* (8), 3313–3318.
- (26) Mayer, T.; Maier, M. E. Design and Synthesis of a Tag-Free Chemical Probe for Photoaffinity Labeling. *Eur. J. Org. Chem.* **2007**, No. 28, 4711–4720. <https://doi.org/10.1002/ejoc.200700188>.
- (27) Geurink, P. P.; Klein, T.; Prèly, L.; Paal, K.; Leeuwenburgh, M. A.; van der Marel, G. A.; Kauffman, H. F.; Overkleeft, H. S.; Bischoff, R. Design of Peptide Hydroxamate-Based Photoreactive Activity-Based Probes of Zinc-Dependent Metalloproteases. *Eur. J. Org. Chem.* **2010**, *2010* (11), 2100–2112. <https://doi.org/10.1002/ejoc.200901385>.
- (28) Wixe, T.; Almqvist, F. An Improved Synthesis of 3-[3-(Trifluoromethyl)-3H-1,2-Diazirin-3-Yl]Aniline: A Key Intermediate in the Synthesis of Photoaffinity Probes. *Tetrahedron Lett.* **2017**, *58* (34), 3350–3352. <https://doi.org/10.1016/j.tetlet.2017.07.031>.
- (29) Kumar, A. B.; Manetsch, R. Ammonia-Free Synthesis of 3-Trifluoromethyl-3-Phenyldiaziridine. *Synth. Commun.* **2018**, *48* (6), 626–631. <https://doi.org/10.1080/00397911.2017.1354026>.
- (30) Ning, R. Y. Employment Ad Information. *Chem. Eng. News Archive* **1973**, *51* (51), 36–37. <https://doi.org/10.1021/cen-v051n051.p028>.
- (31) Mendiola, J.; Rincón, J. A.; Mateos, C.; Soriano, J. F.; de Frutos, Ó.; Niemeier, J. K.; Davis, E. M. Preparation, Use, and Safety of *O*-Mesitylenesulfonylhydroxylamine. *Org. Process Res. Dev.* **2009**, *13* (2), 263–267. <https://doi.org/10.1021/op800264p>.
- (32) Nakashima, H.; Hashimoto, M.; Sadakane, Y.; Tomohiro, T.; Hatanaka, Y. Simple and Versatile Method for Tagging Phenyldiazirine Photophores. *J. Am. Chem. Soc.* **2006**, *128* (47), 15092–15093. <https://doi.org/10.1021/ja066479y>.
- (33) Paget, C. J.; Davis, C. S. Synthesis and in Vitro Activity of Some Aryl Diaziridines as Potential Monoamine Oxidase Inhibitors. *J. Med. Chem.* **1964**, *7* (5), 626–628. <https://doi.org/10.1021/jm00335a012>.
- (34) Mchedlidze, M. T.; Sumbatyan, N. v.; Bondar', D. A.; Taranenko, M. v.; Korshunova, G. A. New Photoreactive Cleavable Reagents with Trifluoromethyldiazirine Group. *Russ. J. Bioorg. Chem.* **2003**, *29* (2), 177–184. <https://doi.org/10.1023/A:1023268617727>.
- (35) Hashimoto, M.; Kato, Y.; Hatanaka, Y. Selective Hydrogenation of Alkene in (3-Trifluoromethyl) Phenyldiazirine Photophor with Wilkinson's Catalyst for Photoaffinity Labeling. *Chem Pharm Bull (Tokyo)* **2007**, *55* (10), 1540–1543. <https://doi.org/10.1248/cpb.55.1540>.

- (36) Ambroise, Y.; Mioskowski, C.; Djéga-Mariadassou, G.; Rousseau, B. Consequences of Affinity in Heterogeneous Catalytic Reactions: Highly Chemoselective Hydrogenolysis of Iodoarenes. *J. Org. Chem.* **2000**, *65* (21), 7183–7186. <https://doi.org/10.1021/jo0012243>.
- (37) Rennhack, A.; Jumpertz, T.; Ness, J.; Baches, S.; Pietrzik, C. U.; Weggen, S.; Bulic, B. Synthesis of a Potent Photoreactive Acidic γ -Secretase Modulator for Target Identification in Cells. *Bioorg. Med. Chem.* **2012**, *20* (21), 6523–6532. <https://doi.org/10.1016/j.bmc.2012.08.034>.
- (38) Ganesan, A.; Ahmed, M.; Okoye, I.; Arutyunova, E.; Babu, D.; Turnbull, W. L.; Kundu, J. K.; Shields, J.; Agopsowicz, K. C.; Xu, L.; Tabana, Y.; Srivastava, N.; Zhang, G.; Moon, T. C.; Belovodskiy, A.; Hena, M.; Kandadai, A. S.; Hosseini, S. N.; Hitt, M.; Walker, J.; Smylie, M.; West, F. G.; Siraki, A. G.; Lemieux, M. J.; Elahi, S.; Nieman, J. A.; Tyrrell, D. L.; Houghton, M.; Barakat, K. Comprehensive in Vitro Characterization of PD-L1 Small Molecule Inhibitors. *Sci. Rep.* **2019**, *9* (1), 12392. <https://doi.org/10.1038/s41598-019-48826-6>.
- (39) Bachmann, M. F.; Oxenius, A. Interleukin 2: From Immunostimulation to Immunoregulation and Back Again. *EMBO Rep.* **2007**, *8* (12), 1142–1148. <https://doi.org/10.1038/sj.embor.7401099>.
- (40) Hur, W.; Sun, Z.; Jiang, T.; Mason, D. E.; Peters, E. C.; Zhang, D. D.; Luesch, H.; Schultz, P. G.; Gray, N. S. A Small-Molecule Inducer of the Antioxidant Response Element. *Chem. Biol.* **2010**, *17* (5), 537–547. <https://doi.org/10.1016/j.chembiol.2010.03.013>.
- (41) Ramurthy, S.; Lin, X.; Subramanian, S.; Rico, A. Quinazolines For PDK1 Inhibition. WO 2007/117607 A2, October 18, 2007.
- (42) McGeachin, S. G. The Structures Of Two Self-Condensation Products From *o*-Aminobenzaldehyde. *Can. J. Chem.* **1966**, *44* (19), 2323–2328. <https://doi.org/10.1139/v66-348>.
- (43) Kimura, K.; Zhuang, J.-H.; Kida, M.; Yamashita, Y.; Sakaguchi, Y. Self-Assembling Polycondensation of 4-Aminobenzaldehyde. Preparation of Star-Like Aggregates of Cone-Shaped Poly(Azomethine) Crystals. *Polym. J.* **2003**, *35* (5), 455–459. <https://doi.org/10.1295/polymj.35.455>.
- (44) Fleischer, E. B.; Klem, E. The Structure of a Self-Condensation Product Of *o*-Aminobenzaldehyde in the Presence of Nickel Ions. *Inorg. Chem.* **1965**, *4* (5), 637–642. <https://doi.org/10.1021/ic50027a008>.
- (45) Owston, P. G.; Shaw (née Gözen), L. S.; Tasker, P. A. The Self-Condensation of *o*-Aminobenzaldehyde: The Polycyclic Structure of the Picrate Salt of the Diprotonated Tetra-Anhydro Tetramer, 4b,5,15b,16-Tetrahydrodibenzo[3,4:7,8][1,5]Diazocino-[2,1-b:6,5-b]Diquinazoline-11,22-Di-lum Picrate: X-Ray Crystal Structure. *J. Chem. Soc., Chem. Commun.* **1982**, *1*, 17–19. <https://doi.org/10.1039/C39820000017>.
- (46) Jircitano, A. J.; Sommerer, S. O.; Shelley, J. J.; Westcott Jnr, B. L.; Suh, I. H. The Self-Condensation of a Derivative of *o*-Aminobenzaldehyde. Structure of the Polycyclic Bisanhydro Trimer of 2-Amino-5-Bromobenzaldehyde. *Acta Crystallogr. C Struct.* **1994**, *50* (3), 445–447. <https://doi.org/10.1107/S0108270193006894>.
- (47) Yu, S. Unpublished Results. *University of Alberta*.
- (48) Smith, E.; Collins, I. Photoaffinity Labeling in Target- and Binding-Site Identification. *Future Med Chem* **2015**, *7* (2), 159–183. <https://doi.org/10.4155/fmc.14.152>.
- (49) Rej, S.; Chatani, N. Transient Imine as a Directing Group for the Metal-Free *o*-C–H Borylation of Benzaldehydes. *J. Am. Chem. Soc.* **2021**, *143* (7), 2920–2929. <https://doi.org/10.1021/jacs.0c13013>.
- (50) Li, Z.; Li, X.; Yang, Y. Conjugated Macrocyclic Polymer Nanoparticles with Alternating Pillarenes and Porphyrins as Struts and Cyclic Nodes. *Small* **2019**, *15* (12), 1805509. <https://doi.org/10.1002/sml.201805509>.

- (51) Tang, H.; Huang, L.; Zhao, D.; Sun, C.; Song, P. Interaction Mechanism of Flavonoids on Bovine Serum Albumin: Insights from Molecular Property-Binding Affinity Relationship. *Spectrochim. Acta A Mol. Biomol. Spectrosc.* **2020**, *239*, 118519. <https://doi.org/10.1016/j.saa.2020.118519>.
- (52) Cai, S.; Duan, H.; Rong, H.; Wang, D.; Li, L.; He, W.; Li, Y. Highly Active and Selective Catalysis of Bimetallic Rh₃ Ni₁ Nanoparticles in the Hydrogenation of Nitroarenes. *ACS Catal.* **2013**, *3* (4), 608–612. <https://doi.org/10.1021/cs300689w>.

Chapter 3

- (1) Shi, H.; Zhang, C.-J.; Chen, G. Y. J.; Yao, S. Q. Cell-Based Proteome Profiling of Potential Dasatinib Targets by Use of Affinity-Based Probes. *J. Am. Chem. Soc.* **2012**, *134* (6), 3001–3014. <https://doi.org/10.1021/ja208518u>.
- (2) Stephens, D. J.; Allan, V. J. Light Microscopy Techniques for Live Cell Imaging. *Science (1979)* **2003**, *300*, 82–86. <https://doi.org/10.1126/science.1082160>.
- (3) Rao, J.; Dragulescu-Andrasi, A.; Yao, H. Fluorescence Imaging in Vivo: Recent Advances. *Curr. Opin. Biotech.* **2007**, *18* (1), 17–25. <https://doi.org/10.1016/j.copbio.2007.01.003>.
- (4) Vendrell, M.; Zhai, D.; Er, J. C.; Chang, Y.-T. Combinatorial Strategies in Fluorescent Probe Development. *Chem. Rev.* **2012**, *112* (8), 4391–4420. <https://doi.org/10.1021/cr200355j>.
- (5) Liu, H.-W.; Chen, L.; Xu, C.; Li, Z.; Zhang, H.; Zhang, X.-B.; Tan, W. Recent Progresses in Small-Molecule Enzymatic Fluorescent Probes for Cancer Imaging. *Chem. Soc. Rev.* **2018**, *47* (18), 7140–7180. <https://doi.org/10.1039/C7CS00862G>.
- (6) Lichtman, J. W.; Conchello, J.-A. Fluorescence Microscopy. *Nat. Methods.* **2005**, *2* (12), 910–919. <https://doi.org/10.1038/nmeth817>.
- (7) Kobayashi, H.; Ogawa, M.; Alford, R.; Choyke, P. L.; Urano, Y. New Strategies for Fluorescent Probe Design in Medical Diagnostic Imaging. *Chem. Rev.* **2010**, *110* (5), 2620–2640. <https://doi.org/10.1021/cr900263j>.
- (8) Terai, T.; Nagano, T. Small-Molecule Fluorophores and Fluorescent Probes for Bioimaging. *Pflügers Arch.* **2013**, *465*, 347–359. <https://doi.org/10.1007/s00424-013-1234-z>.
- (9) Lavis, L. D.; Raines, R. T. Bright Ideas for Chemical Biology. *ACS Chem Biol* **2008**, *3* (3), 142–155. <https://doi.org/10.1021/cb700248m>.
- (10) Wysocki, L. M.; Lavis, L. D. Advances in the Chemistry of Small Molecule Fluorescent Probes. *Curr. Opin. Chem. Biol.* **2011**, *15* (6), 752–759. <https://doi.org/10.1016/j.cbpa.2011.10.013>.
- (11) Sherman, W. R.; Robins, Eli. Fluorescence of Substituted 7-Hydroxycoumarins. *Anal. Chem.* **1968**, *40*, 803–805. <https://doi.org/10.1021/ac60260a045>.
- (12) Baracca, A.; Sgarbi, G.; Solaini, G.; Lenaz, G. Rhodamine 123 as a Probe of Mitochondrial Membrane Potential: Evaluation of Proton Flux through F₀ during ATP Synthesis. *Biochim. Biophys. Acta* **2003**, *1606* (1–3), 137–146. [https://doi.org/10.1016/S0005-2728\(03\)00110-5](https://doi.org/10.1016/S0005-2728(03)00110-5).
- (13) Kowada, T.; Maeda, H.; Kikuchi, K. BODIPY-Based Probes for the Fluorescence Imaging of Biomolecules in Living Cells. *Chem. Soc. Rev.* **2015**, *44* (14), 4953–4972. <https://doi.org/10.1039/C5CS00030K>.
- (14) Gupta, M.; Mula, S.; Ghanty, T. K.; Naik, D. B.; Ray, A. K.; Sharma, A.; Chattopadhyay, S. Structure and Solvent-Induced Tuning of Laser Property and Photostability of a Boradiazaindacene (BODIPY) Dye. *J. Photochem. Photobiol. A* **2017**, *349*, 162–170. <https://doi.org/10.1016/j.jphotochem.2017.09.033>.

- (15) Guseva, Galina. B.; Antina, E. v.; Berezin, M. B.; Pavelyev, R. S.; Kayumov, A. R.; Sharafutdinov, I. S.; Lisovskaya, S. A.; Lodochnikova, O. A.; Islamov, D. R.; Usachev, K. S.; Boichuk, S. v.; Nikitina, L. E. Meso-Substituted-BODIPY Based Fluorescent Biomarker: Spectral Characteristics, Photostability and Possibilities for Practical Application. *J. Photochem. Photobiol. A* **2020**, *401*, 112783. <https://doi.org/10.1016/j.jphotochem.2020.112783>.
- (16) Rybczynski, P.; Smolarkiewicz-Wyczachowski, A.; Piskorz, J.; Bocian, S.; Ziegler-Borowska, M.; Kędziera, D.; Kaczmarek-Kędziera, A. Photochemical Properties and Stability of BODIPY Dyes. *Int. J. Mol. Sci.* **2021**, *22* (13), 6735. <https://doi.org/10.3390/ijms22136735>.
- (17) Hill, J. R.; Robertson, A. A. B. Fishing for Drug Targets: A Focus on Diazirine Photoaffinity Probe Synthesis. *J. Med. Chem.* **2018**, *61* (16), 6945–6963. <https://doi.org/10.1021/acs.jmedchem.7b01561>.
- (18) Beckett, A.; Porter, G. Primary Photochemical Processes in Aromatic Molecules. Part 10.—Photochemistry of Substituted Benzophenones. *Trans. Faraday Soc.* **1963**, *59* (0), 2051–2057. <https://doi.org/10.1039/TF9635902051>.
- (19) Hassan, M. M.; Olaoye, O. O. Recent Advances in Chemical Biology Using Benzophenones and Diazirines as Radical Precursors. *Molecules*. MDPI AG May 1, 2020. <https://doi.org/10.3390/molecules25102285>.
- (20) Joshi, D. K.; Sutton, J. W.; Carver, S.; Blanchard, J. P. Experiences with Commercial Production Scale Operation of Dissolving Metal Reduction Using Lithium Metal and Liquid Ammonia. *Org. Process Res. Dev.* **2005**, *9* (6), 997–1002. <https://doi.org/10.1021/op050155x>.
- (21) Kumar, A. B.; Manetsch, R. Ammonia-Free Synthesis of 3-Trifluoromethyl-3-Phenyldiaziridine. *Synth. Commun.* **2018**, *48* (6), 626–631. <https://doi.org/10.1080/00397911.2017.1354026>.
- (22) Tamura, Y.; Minamikawa, J.; Sumoto, K.; Fujii, S.; Ikeda, M. Synthesis and Some Properties of O-Acyl- and O-Nitrophenylhydroxylamines. *J. Org. Chem.* **1973**, *38* (6), 1239–1241. <https://doi.org/10.1021/jo00946a045>.
- (23) Ning, R. Y. Employment Ad Information. *Chem. Eng. News Archive* **1973**, *51* (51), 36–37. <https://doi.org/10.1021/cen-v051n051.p028>.
- (24) Mendiola, J.; Rincón, J. A.; Mateos, C.; Soriano, J. F.; de Frutos, Ó.; Niemeier, J. K.; Davis, E. M. Preparation, Use, and Safety of O-Mesitylenesulfonylhydroxylamine. *Org. Process Res. Dev.* **2009**, *13* (2), 263–267. <https://doi.org/10.1021/op800264p>.
- (25) Mayer, T.; Maier, M. E. Design and Synthesis of a Tag-Free Chemical Probe for Photoaffinity Labeling. *Eur. J. Org. Chem.* **2007**, No. 28, 4711–4720. <https://doi.org/10.1002/ejoc.200700188>.
- (26) Haldón, E.; Nicasio, M. C.; Pérez, P. J. Copper-Catalysed Azide–Alkyne Cycloadditions (CuAAC): An Update. *Org. Biomol. Chem.* **2015**, *13* (37), 9528–9550. <https://doi.org/10.1039/C5OB01457C>.
- (27) Rostovtsev, V. v.; Green, L. G.; Fokin, V. v.; Sharpless, K. B. A Stepwise Huisgen Cycloaddition Process: Copper(I)-Catalyzed Regioselective “Ligation” of Azides and Terminal Alkynes. *Angew. Chem.* **2002**, *114*, 2708–2711. [https://doi.org/10.1002/1521-3757\(20020715\)114:14<2708::AID-ANGE2708>3.0.CO;2-0](https://doi.org/10.1002/1521-3757(20020715)114:14<2708::AID-ANGE2708>3.0.CO;2-0).
- (28) Tron, G. C.; Piralì, T.; Billington, R. A.; Canonico, P. L.; Sorba, G.; Genazzani, A. A. Click Chemistry Reactions in Medicinal Chemistry: Applications of the 1,3-Dipolar Cycloaddition between Azides and Alkynes. *Med. Res. Rev.* **2008**, *28* (2), 278–308. <https://doi.org/10.1002/med.20107>.
- (29) Wang, Q.; Chan, T. R.; Hilgraf, R.; Fokin, V. v.; Sharpless, K. B.; Finn, M. G. Bioconjugation by Copper(I)-Catalyzed Azide-Alkyne [3 + 2] Cycloaddition. *J. Am. Chem. Soc.* **2003**, *125* (11), 3192–3193. <https://doi.org/10.1021/ja021381e>.

- (30) Pujari, S. S.; Seela, F. Parallel Stranded DNA Stabilized with Internal Sugar Cross-Links: Synthesis and Click Ligation of Oligonucleotides Containing 2'-Propargylated Isoguanosine. *J. Org. Chem.* **2013**, *78* (17), 8545–8561. <https://doi.org/10.1021/jo4012706>.
- (31) Pujari, S. S.; Ingale, S. A.; Seela, F. High-Density Functionalization and Cross-Linking of DNA: “Click” and “Bis-Click” Cycloadditions Performed on Alkynylated Oligonucleotides with Fluorogenic Anthracene Azides. *Bioconjugate Chem.* **2014**, *25* (10), 1855–1870. <https://doi.org/10.1021/bc5003532>.
- (32) Staudinger, von H.; Meyer, J. Über Neue Organische Phosphorverbindungen III. Phosphinmethylderivate Und Phosphinimine. *Helv. Chim. Acta.* **1919**, *2*, 635–646.
- (33) Faucher, A.-M.; Grand-Maître, C. *Tris* (2-Carboxyethyl)Phosphine (TCEP) for the Reduction of Sulfoxides, Sulfonylchlorides, *N*-Oxides, and Azides. *Synth. Commun.* **2003**, *33* (20), 3503–3511. <https://doi.org/10.1081/SCC-120024730>.
- (34) Saneyoshi, H.; Ochikubo, T.; Mashimo, T.; Hatano, K.; Ito, Y.; Abe, H. Triphenylphosphinecarboxamide: An Effective Reagent for the Reduction of Azides and Its Application to Nucleic Acid Detection. *Org. Lett.* **2014**, *16* (1), 30–33. <https://doi.org/10.1021/ol402832w>.
- (35) Lenstra, D. C.; Wolf, J. J.; Mecinović, J. Catalytic Staudinger Reduction at Room Temperature. *J. Org. Chem.* **2019**, *84* (10), 6536–6545. <https://doi.org/10.1021/acs.joc.9b00831>.
- (36) Bednarek, C.; Wehl, I.; Jung, N.; Schepers, U.; Bräse, S. The Staudinger Ligation. *Chem. Rev.* **2020**, *120* (10), 4301–4354. <https://doi.org/10.1021/acs.chemrev.9b00665>.
- (37) Loudet, A.; Burgess, K. BODIPY Dyes and Their Derivatives: Syntheses and Spectroscopic Properties. *Chem. Rev.* **2007**, *107* (11), 4891–4932. <https://doi.org/10.1021/cr078381n>.
- (38) Ulrich, G.; Ziessel, R.; Harriman, A. The Chemistry of Fluorescent Bodipy Dyes: Versatility Unsurpassed. *Angew. Chem. Int. Ed.* **2008**, *47* (7), 1184–1201. <https://doi.org/10.1002/anie.200702070>.
- (39) Bacsa, I.; Konc, C.; Orosz, A.; Kecskeméti, G.; Rigó, R.; Özvegy-Laczka, C.; Mernyák, E. Synthesis of Novel C-2- or C-15-Labeled BODIPY—Estrone Conjugates. *Molecules* **2018**, *23* (4), 821. <https://doi.org/10.3390/molecules23040821>.
- (40) Sun, N.; Sun, Q.; Zhao, W.; Jin, L.; Hu, B.; Shen, Z.; Hu, X. Ligand-free Palladium-Catalyzed Carbonylative Suzuki Coupling of Aryl Iodides in Aqueous CH₃CN with Sub-stoichiometric Amount of Mo(CO)₆ as CO Source. *Adv. Synth. Catal.* **2019**, *361* (9), 2117–2123. <https://doi.org/10.1002/adsc.201900011>.

Chapter 4

- (1) Evans, R. M. The Steroid and Thyroid Hormone Receptor Superfamily. *Science (1979)* **1988**, *240* (4854), 889–895. <https://doi.org/10.1126/science.3283939>.
- (2) Tsai, M.-J.; O'Malley, B. W. Molecular Mechanisms of Action of Steroid/Thyroid Receptor Superfamily Members. *Annu. Rev. Biochem.* **1994**, *63* (1), 451–486. <https://doi.org/10.1146/annurev.bi.63.070194.002315>.
- (3) Keller, E. T.; Ershler, W. B.; Chang, C. The Androgen Receptor: A Mediator of Diverse Responses. *Front. Biosci.* **1993**, *1*, 59–71.
- (4) Mooradian, A. D.; Morley, J. E.; Korenman, S. G. Biological Actions of Androgens. *Endocr. Rev.* **1987**, *8* (1), 1–28. <https://doi.org/10.1210/edrv-8-1-1>.

- (5) McLachlan, R. I.; Wreford, N. G.; O'Donnell, L.; de Kretser, D. M.; Robertson, D. M. The Endocrine Regulation of Spermatogenesis: Independent Roles for Testosterone and FSH. *J. Endocrinol.* **1996**, *148* (1), 1–9. <https://doi.org/10.1677/joe.0.1480001>.
- (6) Gao, W.; Bohl, C. E.; Dalton, J. T. Chemistry and Structural Biology of Androgen Receptor. *Chem. Rev.* **2005**, *105* (9), 3352–3370. <https://doi.org/10.1021/cr020456u>.
- (7) Baker, M. E. Albumin, Steroid Hormones and the Origin of Vertebrates. *J. Endocrinol.* **2002**, *175*, 121–127.
- (8) Swerdloff, R. S.; Dudley, R. E.; Page, S. T.; Wang, C.; Salameh, W. A. Dihydrotestosterone: Biochemistry, Physiology, and Clinical Implications of Elevated Blood Levels. *Endocr. Rev.* **2017**, *38* (3), 220–254. <https://doi.org/10.1210/er.2016-1067>.
- (9) Wilson, E. M.; French, F. S. Binding Properties of Androgen Receptors. Evidence for Identical Receptors in Rat Testis, Epididymis, and Prostate. *J. Biol. Chem.* **1976**, *251* (18), 5620–5629. [https://doi.org/10.1016/S0021-9258\(17\)33103-4](https://doi.org/10.1016/S0021-9258(17)33103-4).
- (10) Thigpen, A. E.; Silver, R. I.; Guileyardo, J. M.; Casey, M. L.; McConnell, J. D.; Russell, D. W. Tissue Distribution and Ontogeny of Steroid 5 Alpha-Reductase Isozyme Expression. *J. Clin. Investig.* **1993**, *92* (2), 903–910. <https://doi.org/10.1172/JCI116665>.
- (11) Marchetti, P. M.; Barth, J. H. Clinical Biochemistry of Dihydrotestosterone. *Ann. Clin. Biochem.* **2013**, *50* (2), 95–107. <https://doi.org/10.1258/acb.2012.012159>.
- (12) Narayanan, R.; Coss, C. C.; Dalton, J. T. Development of Selective Androgen Receptor Modulators (SARMs). *Mol. Cell. Endocrinol.* **2018**, *465*, 134–142. <https://doi.org/10.1016/j.mce.2017.06.013>.
- (13) Tan, M. E.; Li, J.; Xu, H. E.; Melcher, K.; Yong, E. Androgen Receptor: Structure, Role in Prostate Cancer and Drug Discovery. *Acta Pharmacol. Sin.* **2015**, *36* (1), 3–23. <https://doi.org/10.1038/aps.2014.18>.
- (14) Eder, I. E.; Culig, Z.; Putz, T.; Nessler-Menardi, C.; Bartsch, G.; Klocker, H. Molecular Biology of the Androgen Receptor: From Molecular Understanding to the Clinic. *Eur. Urol.* **2001**, *40* (3), 241–251. <https://doi.org/10.1159/000049782>.
- (15) Davey, R. A.; Grossmann, M. Androgen Receptor Structure, Function and Biology: From Bench to Bedside. *Clin. Biochem.* **2016**, *37* (1), 3–15.
- (16) Lavery, D. N.; McEwan, I. J. Structural Characterization of the Native NH₂-Terminal Transactivation Domain of the Human Androgen Receptor: A Collapsed Disordered Conformation Underlies Structural Plasticity and Protein-Induced Folding. *Biochemistry* **2008**, *47* (11), 3360–3369. <https://doi.org/10.1021/bi702221e>.
- (17) van Royen, M. E.; van Cappellen, W. A.; de Vos, C.; Houtsmuller, A. B.; Trapman, J. Stepwise Androgen Receptor Dimerization. *J. Cell Sci.* **2012**. <https://doi.org/10.1242/jcs.096792>.
- (18) Simental, J. A.; Sar, M.; Lane, M. v; French, F. S.; Wilson, E. M. Transcriptional Activation and Nuclear Targeting Signals of the Human Androgen Receptor. *J. Biol. Chem.* **1991**, *266* (1), 510–518. [https://doi.org/10.1016/S0021-9258\(18\)52466-2](https://doi.org/10.1016/S0021-9258(18)52466-2).
- (19) Alen, P.; Claessens, F.; Verhoeven, G.; Rombauts, W.; Peeters, B. The Androgen Receptor Amino-Terminal Domain Plays a Key Role in P160 Coactivator-Stimulated Gene Transcription. *Mol. Cell. Endocrinol.* **1999**, *19* (9), 6085–6097. <https://doi.org/10.1128/MCB.19.9.6085>.
- (20) Bevan, C. L.; Hoare, S.; Claessens, F.; Heery, D. M.; Parker, M. G. The AF1 and AF2 Domains of the Androgen Receptor Interact with Distinct Regions of SRC1. *Mol. Cell. Endocrinol.* **1999**, *19* (12), 8383–8392. <https://doi.org/10.1128/MCB.19.12.8383>.
- (21) Jenster, G.; Trapman, J.; Brinkmann, A. O. Nuclear Import of the Human Androgen Receptor. *Biochem. J.* **1993**, *293* (3), 761–768. <https://doi.org/10.1042/bj2930761>.

- (22) Zhou, Z. X.; Sar, M.; Simental, J. A.; Lane, M. v; Wilson, E. M. A Ligand-Dependent Bipartite Nuclear Targeting Signal in the Human Androgen Receptor. Requirement for the DNA-Binding Domain and Modulation by NH₂-Terminal and Carboxyl-Terminal Sequences. *J. Biol. Chem.* **1994**, *269* (18), 13115–13123.
- (23) Matias, P. M.; Donner, P.; Coelho, R.; Thomaz, M.; Peixoto, C.; Macedo, S.; Otto, N.; Joschko, S.; Scholz, P.; Wegg, A.; Bäsler, S.; Schäfer, M.; Egner, U.; Carrondo, M. A. Structural Evidence for Ligand Specificity in the Binding Domain of the Human Androgen Receptor. *J. Biol. Chem.* **2000**, *275* (34), 26164–26171. <https://doi.org/10.1074/jbc.M004571200>.
- (24) Eftekharzadeh, B.; Banduseela, V. C.; Chiesa, G.; Martínez-Cristóbal, P.; Rauch, J. N.; Nath, S. R.; Schwarz, D. M. C.; Shao, H.; Marin-Argany, M.; di Sanza, C.; Giorgetti, E.; Yu, Z.; Pierattelli, R.; Felli, I. C.; Brun-Heath, I.; García, J.; Nebreda, A. R.; Gestwicki, J. E.; Lieberman, A. P.; Salvatella, X. Hsp70 and Hsp40 Inhibit an Inter-Domain Interaction Necessary for Transcriptional Activity in the Androgen Receptor. *Nat. Commun.* **2019**, *10* (1), 3562. <https://doi.org/10.1038/s41467-019-11594-y>.
- (25) Schaufele, F.; Carbonell, X.; Guerbodot, M.; Borngraeber, S.; Chapman, M. S.; Ma, A. A. K.; Miner, J. N.; Diamond, M. I. The Structural Basis of Androgen Receptor Activation: Intramolecular and Intermolecular Amino–Carboxy Interactions. *Proc. Natl. Acad. Sci.* **2005**, *102* (28), 9802–9807. <https://doi.org/10.1073/pnas.0408819102>.
- (26) van Royen, M. E.; Cunha, S. M.; Brink, M. C.; Mattern, K. A.; Nigg, A. L.; Dubbink, H. J.; Verschure, P. J.; Trapman, J.; Houtsmuller, A. B. Compartmentalization of Androgen Receptor Protein–Protein Interactions in Living Cells. *J. Cell Biol.* **2007**, *177* (1), 63–72. <https://doi.org/10.1083/jcb.200609178>.
- (27) Bhasin, S.; Cunningham, G. R.; Hayes, F. J.; Matsumoto, A. M.; Snyder, P. J.; Swerdloff, R. S.; Montori, V. M. Testosterone Therapy in Men with Androgen Deficiency Syndromes: An Endocrine Society Clinical Practice Guideline. *J. Clin. Endocrinol. Metab.* **2010**, *95* (6), 2536–2559. <https://doi.org/10.1210/jc.2009-2354>.
- (28) Handelsman, D. J. Androgen Physiology, Pharmacology, Use and Misuse. In *Endotext*; 2020.
- (29) ASHP. *Testosterone*. Drugs.com. <https://www.drugs.com/monograph/testosterone.html> (accessed 2022-09-20).
- (30) Emmelot-Vonk, M. H.; Verhaar, H. J. J.; Nakhai Pour, H. R.; Aleman, A.; Lock, T. M. T. W.; Bosch, J. L. H. R.; Grobbee, D. E.; van der Schouw, Y. T. Effect of Testosterone Supplementation on Functional Mobility, Cognition, and Other Parameters in Older Men. *JAMA* **2008**, *299* (1). <https://doi.org/10.1001/jama.2007.51>.
- (31) LeBrasseur, N. K.; Lajevardi, N.; Miciek, R.; Mazer, N.; Storer, T. W.; Bhasin, S. Effects of Testosterone Therapy on Muscle Performance and Physical Function in Older Men with Mobility Limitations (The TOM Trial): Design and Methods. *Contemp. Clin. Trials* **2009**, *30* (2), 133–140. <https://doi.org/10.1016/j.cct.2008.10.005>.
- (32) Basaria, S.; Coviello, A. D.; Travison, T. G.; Storer, T. W.; Farwell, W. R.; Jette, A. M.; Eder, R.; Tennstedt, S.; Ulloor, J.; Zhang, A.; Choong, K.; Lakshman, K. M.; Mazer, N. A.; Miciek, R.; Krasnoff, J.; Elmi, A.; Knapp, P. E.; Brooks, B.; Appleman, E.; Aggarwal, S.; Bhasin, G.; Hede-Brierley, L.; Bhatia, A.; Collins, L.; LeBrasseur, N.; Fiore, L. D.; Bhasin, S. Adverse Events Associated with Testosterone Administration. *N. Engl. J. Med.* **2010**, *363* (2), 109–122. <https://doi.org/10.1056/NEJMoa1000485>.
- (33) Ponce, O. J.; Spencer-Bonilla, G.; Alvarez-Villalobos, N.; Serrano, V.; Singh-Ospina, N.; Rodriguez-Gutierrez, R.; Salcido-Montenegro, A.; Benkhadra, R.; Prokop, L. J.; Bhasin, S.; Brito, J. P. The Efficacy and Adverse Events of Testosterone Replacement Therapy in Hypogonadal Men: A Systematic Review and Meta-Analysis of Randomized, Placebo-Controlled Trials. *J. Clin. Endocrinol. Metab.* **2018**, *103* (5), 1745–1754. <https://doi.org/10.1210/jc.2018-00404>.

- (34) Grech, A.; Breck, J.; Heidelbaugh, J. Adverse Effects of Testosterone Replacement Therapy: An Update on the Evidence and Controversy. *Ther. Adv. Drug Saf.* **2014**, *5* (5), 190–200. <https://doi.org/10.1177/2042098614548680>.
- (35) Park, H.; Ahn, S.; Moon, D. Evolution of Guidelines for Testosterone Replacement Therapy. *J. Clin. Med.* **2019**, *8* (3), 410. <https://doi.org/10.3390/jcm8030410>.
- (36) Grober, E. D.; Krakowsky, Y.; Khera, M.; Holmes, D. T.; Lee, J. C.; Grantmyre, J. E.; Patel, P.; Bebb, R. A.; Fitzpatrick, R.; Campbell, J. D.; Carrier, S.; Morgentaler, A. Canadian Urological Association Clinical Practice Guideline on Testosterone Deficiency in Men: Evidence-Based Q&A. *Can. Urol. Assoc. J.* **2021**, *15* (5). <https://doi.org/10.5489/cuaj.7252>.
- (37) Negro-Vilar, A. Selective Androgen Receptor Modulators (SARMs): A Novel Approach to Androgen Therapy for the New Millennium. *J. Clin. Endocrinol. Metab.* **1999**, *84* (10), 3459–3462. <https://doi.org/10.1210/jcem.84.10.6122>.
- (38) Dalton, J. T. The Long and Winding Road for Selective Androgen Receptor Modulators. *Br. J. Clin. Pharmacol.* **2017**, *83* (10), 2131–2133. <https://doi.org/10.1111/bcp.13345>.
- (39) Narayanan, R.; Coss, C. C.; Dalton, J. T. Development of Selective Androgen Receptor Modulators (SARMs). *Mol. Cell. Endocrinol.* **2018**, *465*, 134–142. <https://doi.org/10.1016/j.mce.2017.06.013>.
- (40) Solomon, Z. J.; Mirabal, J. R.; Mazur, D. J.; Kohn, T. P.; Lipshultz, L. I.; Pastuszak, A. W. Selective Androgen Receptor Modulators: Current Knowledge and Clinical Applications. *Sex. Med. Rev.* **2019**, *7* (1), 84–94. <https://doi.org/10.1016/j.sxmr.2018.09.006>.
- (41) Fonseca, G. W. P. da; Dworatzek, E.; Ebner, N.; von Haehling, S. Selective Androgen Receptor Modulators (SARMs) as Pharmacological Treatment for Muscle Wasting in Ongoing Clinical Trials. *Expert Opin. Investig. Drugs* **2020**, *29* (8), 881–891. <https://doi.org/10.1080/13543784.2020.1777275>.
- (42) Gao, W.; Kim, J.; Dalton, J. T. Pharmacokinetics and Pharmacodynamics of Nonsteroidal Androgen Receptor Ligands. *Pharm. Res.* **2006**, *23* (8), 1641–1658. <https://doi.org/10.1007/s11095-006-9024-3>.
- (43) Narayanan, R.; Mohler, M. L.; Bohl, C. E.; Miller, D. D.; Dalton, J. T. Selective Androgen Receptor Modulators in Preclinical and Clinical Development. *Nucl. Recept. Signal.* **2008**, *6* (1), nrs.06010. <https://doi.org/10.1621/nrs.06010>.
- (44) Mohler, M. L.; Bohl, C. E.; Jones, A.; Coss, C. C.; Narayanan, R.; He, Y.; Hwang, D. J.; Dalton, J. T.; Miller, D. D. Nonsteroidal Selective Androgen Receptor Modulators (SARMs): Dissociating the Anabolic and Androgenic Activities of the Androgen Receptor for Therapeutic Benefit. *J. Med. Chem.* **2009**, *52* (12), 3597–3617. <https://doi.org/10.1021/jm900280m>.
- (45) Yin, D.; He, Y.; Perera, M. A.; Hong, S. S.; Marhefka, C.; Stourman, N.; Kirkovsky, L.; Miller, D. D.; Dalton, J. T. Key Structural Features of Nonsteroidal Ligands for Binding and Activation of the Androgen Receptor. *Mol. Pharmacol.* **2003**, *63* (1), 211–223. <https://doi.org/10.1124/mol.63.1.211>.
- (46) Gao, W.; Reiser, P. J.; Coss, C. C.; Phelps, M. A.; Kearbey, J. D.; Miller, D. D.; Dalton, J. T. Selective Androgen Receptor Modulator Treatment Improves Muscle Strength and Body Composition and Prevents Bone Loss in Orchidectomized Rats. *Endocrinology* **2005**, *146* (11), 4887–4897. <https://doi.org/10.1210/en.2005-0572>.
- (47) Srinath, R.; Dobs, A. Enobosarm (GTx-024, S-22): A Potential Treatment for Cachexia. *Future Oncol.* **2014**, *10* (2), 187–194. <https://doi.org/10.2217/fon.13.273>.
- (48) Crawford, J.; Prado, C. M. M.; Johnston, M. A.; Gralla, R. J.; Taylor, R. P.; Hancock, M. L.; Dalton, J. T. Study Design and Rationale for the Phase 3 Clinical Development Program of Enobosarm, a Selective Androgen Receptor Modulator, for the Prevention and Treatment of

- Muscle Wasting in Cancer Patients (POWER Trials). *Curr. Oncol. Rep.* **2016**, *18* (6), 37. <https://doi.org/10.1007/s11912-016-0522-0>.
- (49) Thigpen, A. E.; Silver, R. I.; Guileyardo, J. M.; Casey, M. L.; McConnell, J. D.; Russell, D. W. Tissue Distribution and Ontogeny of Steroid 5 Alpha-Reductase Isozyme Expression. *J. Clin. Investig.* **1993**, *92* (2), 903–910. <https://doi.org/10.1172/JCI116665>.
- (50) Gao, W.; Dalton, J. T. Ockham's Razor and Selective Androgen Receptor Modulators (SARMs): Are We Overlooking the Role of 5 α -Reductase? *Mol. Interv.* **2007**, *7* (1), 10–13. <https://doi.org/10.1124/mi.7.1.3>.
- (51) Chang, C.-Y.; McDonnell, D. P. Evaluation of Ligand-Dependent Changes in AR Structure Using Peptide Probes. *Mol. Endocrinol.* **2002**, *16* (4), 647–660. <https://doi.org/10.1210/mend.16.4.0818>.
- (52) Gao, W.; Dalton, J. T. Expanding the Therapeutic Use of Androgens via Selective Androgen Receptor Modulators (SARMs). *Drug Discov. Today* **2007**, *12* (5–6), 241–248. <https://doi.org/10.1016/j.drudis.2007.01.003>.
- (53) Thevis, M.; Geyer, H.; Kamber, M.; Schänzer, W. Detection of the Arylpropionamide-Derived Selective Androgen Receptor Modulator (SARM) S-4 (Andarine) in a Black-Market Product. *Drug Test. Anal.* **2009**, *1* (8), 387–392. <https://doi.org/10.1002/dta.91>.
- (54) Grata, E.; Perrenoud, L.; Saugy, M.; Baume, N. SARM-S4 and Metabolites Detection in Sports Drug Testing: A Case Report. *Forensic Sci. Int.* **2011**, *213* (1–3), 104–108. <https://doi.org/10.1016/j.forsciint.2011.07.014>.
- (55) Thevis, M.; Schänzer, W. Mass Spectrometry of Selective Androgen Receptor Modulators. *J. Mass Spectrom.* **2008**, *43* (7), 865–876. <https://doi.org/10.1002/jms.1438>.
- (56) Tucker, H.; Crook, J. W.; Chesterson, G. J. Nonsteroidal Antiandrogens. Synthesis and Structure-Activity Relationships of 3-Substituted Derivatives of 2-Hydroxypropionanilides. *J. Med. Chem.* **1988**, *31*, 954–959.
- (57) Jew, S.; Terashima, S.; Koga, K. Asymmetric Halolactonisation Reaction - 1. *Tetrahedron Lett.* **1979**, *35* (20), 2337–2343. [https://doi.org/10.1016/S0040-4020\(01\)93747-0](https://doi.org/10.1016/S0040-4020(01)93747-0).
- (58) Jew, S.-S.; Terashima, S.; Koga, K. Asymmetric Halolactonisation Reaction - 2. *Tetrahedron Lett.* **1979**, *35* (20), 2345–2352. [https://doi.org/10.1016/S0040-4020\(01\)93748-2](https://doi.org/10.1016/S0040-4020(01)93748-2).
- (59) Nique, F.; Hebbe, S.; Peixoto, C.; Annoot, D.; Lefrançois, J.-M.; Duval, E.; Michoux, L.; Triballeau, N.; Lemoullec, J.-M.; Mollat, P.; Thauvin, M.; Prangé, T.; Minet, D.; Clément-Lacroix, P.; Robin-Jagerschmidt, C.; Fleury, D.; Guédin, D.; Deprez, P. Discovery of Diarylhydantoin as New Selective Androgen Receptor Modulators. *J. Med. Chem.* **2012**, *55* (19), 8225–8235. <https://doi.org/10.1021/jm300249m>.
- (60) Konnert, L.; Lamaty, F.; Martinez, J.; Colacino, E. Recent Advances in the Synthesis of Hydantoin: The State of the Art of a Valuable Scaffold. *Chem. Rev.* **2017**, *117* (23), 13757–13809. <https://doi.org/10.1021/acs.chemrev.7b00067>.
- (61) Sun, C.; Robl, J. A.; Wang, T. C.; Huang, Y.; Kuhns, J. E.; Lupisella, J. A.; Beehler, B. C.; Golla, R.; Sleph, P. G.; Seethala, R.; Fura, A.; Krystek, S. R.; An, Y.; Malley, M. F.; Sack, J. S.; Salvati, M. E.; Grover, G. J.; Ostrowski, J.; Hamann, L. G. Discovery of Potent, Orally-Active, and Muscle-Selective Androgen Receptor Modulators Based on an *N*-Aryl-Hydroxybicyclohydantoin Scaffold. *J. Med. Chem.* **2006**, *49* (26), 7596–7599. <https://doi.org/10.1021/jm061101w>.
- (62) Ostrowski, J.; Kuhns, J. E.; Lupisella, J. A.; Manfredi, M. C.; Beehler, B. C.; Krystek, S. R.; Bi, Y.; Sun, C.; Seethala, R.; Golla, R.; Sleph, P. G.; Fura, A.; An, Y.; Kish, K. F.; Sack, J. S.; Mookhtiar, K. A.; Grover, G. J.; Hamann, L. G. Pharmacological and X-Ray Structural Characterization of a Novel Selective Androgen Receptor Modulator: Potent Hyperanabolic Stimulation of Skeletal Muscle with Hypostimulation of Prostate in Rats. *Endocrinology* **2007**, *148* (1), 4–12. <https://doi.org/10.1210/en.2006-0843>.

- (63) van Oeveren, A.; Pio, B. A.; Tegley, C. M.; Higuchi, R. I.; Wu, M.; Jones, T. K.; Marschke, K. B.; Negro-Vilar, A.; Zhi, L. Discovery of an Androgen Receptor Modulator Pharmacophore Based on 2-Quinolinones. *Bioorg. Med. Chem. Lett.* **2007**, *17* (6), 1523–1526. <https://doi.org/10.1016/j.bmcl.2007.01.007>.
- (64) Martinborough, E.; Shen, Y.; van Oeveren, A.; Long, Y. O.; Lau, T. L. S.; Marschke, K. B.; Chang, W. Y.; López, F. J.; Vajda, E. G.; Rix, P. J.; Viveros, O. H.; Negro-Vilar, A.; Zhi, L. Substituted 6-(1-Pyrrolidine)Quinolin-2(1*H*)-Ones as Novel Selective Androgen Receptor Modulators. *J. Med. Chem.* **2007**, *50* (21), 5049–5052. <https://doi.org/10.1021/jm070231h>.
- (65) van Oeveren, A.; Motamedi, M.; Mani, N. S.; Marschke, K. B.; López, F. J.; Schrader, W. T.; Negro-Vilar, A.; Zhi, L. Discovery of 6-*N,N*-Bis(2,2,2-Trifluoroethyl)Amino-4-Trifluoromethylquinolin-2(1*H*)-One as a Novel Selective Androgen Receptor Modulator. *J. Med. Chem.* **2006**, *49* (21), 6143–6146. <https://doi.org/10.1021/jm060792t>.
- (66) Lefebvre, O.; Marull, M.; Schlosser, M. 4-(Trifluoromethyl)Quinoline Derivatives. *Eur. J. Org. Chem.* **2003**, *2003* (11), 2115–2121. <https://doi.org/10.1002/ejoc.200200633>.
- (67) Marull, M.; Lefebvre, O.; Schlosser, M. An Improved Access to 4-Trifluoromethyl-2(1*H*)-Quinolinones: The“Watering Protocol.” *Eur. J. Org. Chem.* **2004**, *2004* (1), 54–63. <https://doi.org/10.1002/ejoc.200300531>.
- (68) Schlienger, N.; Lund, B. W.; Pawlas, J.; Badalassi, F.; Bertozzi, F.; Lewinsky, R.; Fejzic, A.; Thygesen, M. B.; Tabatabaie, A.; Bradley, S. R.; Gardell, L. R.; Piu, F.; Olsson, R. Synthesis, Structure–Activity Relationships, and Characterization of Novel Nonsteroidal and Selective Androgen Receptor Modulators. *J. Med. Chem.* **2009**, *52* (22), 7186–7191. <https://doi.org/10.1021/jm901149c>.
- (69) Barden, D.; McGregor, L. A Guide to Modern Comprehensive Two-Dimensional Gas Chromatography. *Column* **2017**, *13*, 14–20.

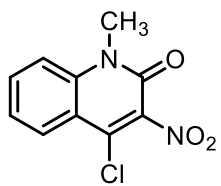
Chapter 5

- (1) Egen, J. G.; Kuhns, M. S.; Allison, J. P. *CTLA-4: New Insights into Its Biological Function and Use in Tumor Immunotherapy*; 2002.
- (2) Han, Y.; Liu, D.; Li, L. *PD-1/PD-L1 Pathway: Current Researches in Cancer*; 2020; Vol. 10.
- (3) Esfahani, K.; Roudaia, L.; Buhlaiga, N.; del Rincon, S. v.; Papneja, N.; Miller, W. H. A Review of Cancer Immunotherapy: From the Past, to the Present, to the Future. *Curr. Oncol.* **2020**, *27* (S2), 87–97. <https://doi.org/10.3747/co.27.5223>.
- (4) Ganesan, A.; Ahmed, M.; Okoye, I.; Arutyunova, E.; Babu, D.; Turnbull, W. L.; Kundu, J. K.; Shields, J.; Agopsowicz, K. C.; Xu, L.; Tabana, Y.; Srivastava, N.; Zhang, G.; Moon, T. C.; Belovodskiy, A.; Hena, M.; Kandadai, A. S.; Hosseini, S. N.; Hitt, M.; Walker, J.; Smylie, M.; West, F. G.; Siraki, A. G.; Lemieux, M. J.; Elahi, S.; Nieman, J. A.; Tyrrell, D. L.; Houghton, M.; Barakat, K. Comprehensive in Vitro Characterization of PD-L1 Small Molecule Inhibitors. *Sci. Rep.* **2019**, *9* (1). <https://doi.org/10.1038/s41598-019-48826-6>.
- (5) Lee, H.; Lee, J. W. Target Identification for Biologically Active Small Molecules Using Chemical Biology Approaches. *Arch. Pharmacol. Res.* **2016**, *39* (9), 1193–1201. <https://doi.org/10.1007/s12272-016-0791-z>.
- (6) Hatanaka, Y.; Sadakane, Y. Photoaffinity Labeling in Drug Discovery and Developments: Chemical Gateway for Entering Proteomic Frontier. *Curr. Top. Med. Chem.* **2002**, *2* (3), 271–288. <https://doi.org/10.2174/1568026023394182>.
- (7) Mayer, T.; Maier, M. E. Design and Synthesis of a Tag-Free Chemical Probe for Photoaffinity Labeling. *Eur. J. Org. Chem.* **2007**, No. 28, 4711–4720. <https://doi.org/10.1002/ejoc.200700188>.

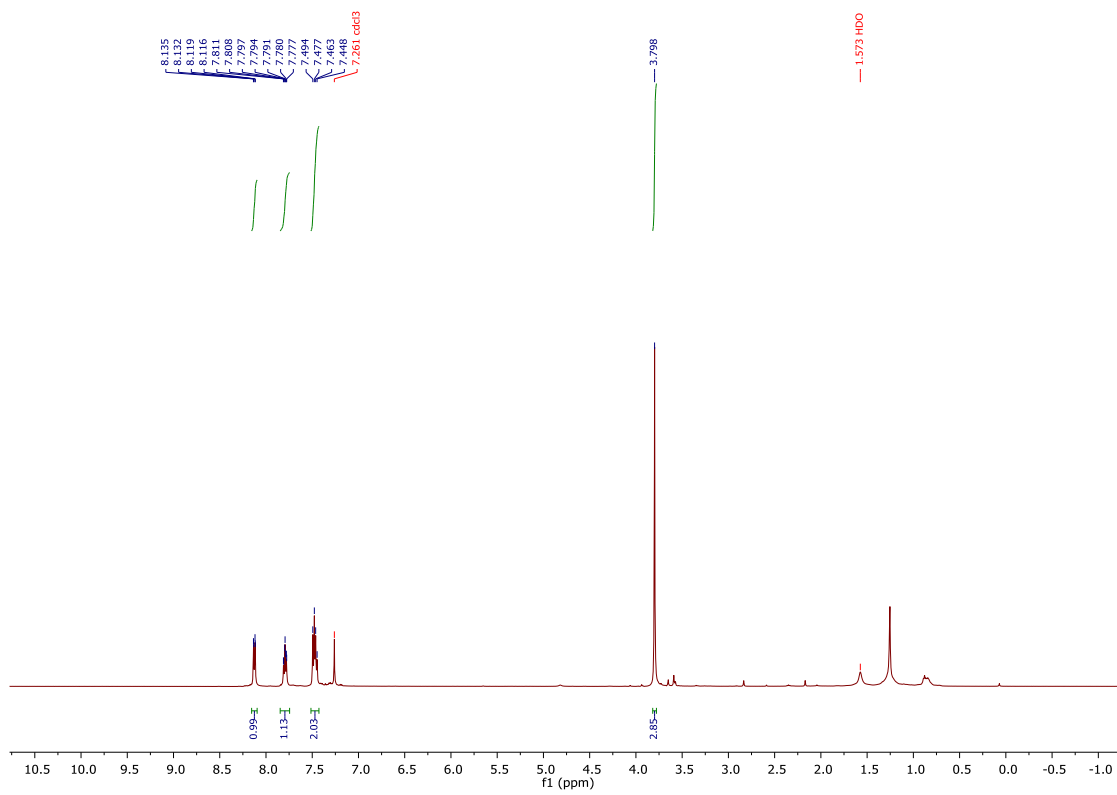
- (8) Sun, N.; Sun, Q.; Zhao, W.; Jin, L.; Hu, B.; Shen, Z.; Hu, X. Ligand-free Palladium-Catalyzed Carbonylative Suzuki Coupling of Aryl Iodides in Aqueous CH₃CN with Sub-stoichiometric Amount of Mo(CO)₆ as CO Source. *Adv. Synth. Catal.* **2019**, *361* (9), 2117–2123. <https://doi.org/10.1002/adsc.201900011>.
- (9) Bacsa, I.; Konc, C.; Orosz, A.; Kecskeméti, G.; Rigó, R.; Özvegy-Laczka, C.; Mernyák, E. Synthesis of Novel C-2- or C-15-Labeled BODIPY—Estrone Conjugates. *Molecules* **2018**, *23* (4), 821. <https://doi.org/10.3390/molecules23040821>.
- (10) Narayanan, R.; Coss, C. C.; Dalton, J. T. Development of Selective Androgen Receptor Modulators (SARMs). *Mol. Cell. Endocrinol.* **2018**, *465*, 134–142. <https://doi.org/10.1016/j.mce.2017.06.013>.

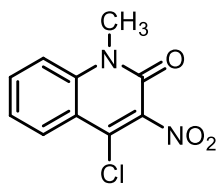
Appendix: NMR Spectra

**Appendix I:
NMR Spectra (Chapter 2)**

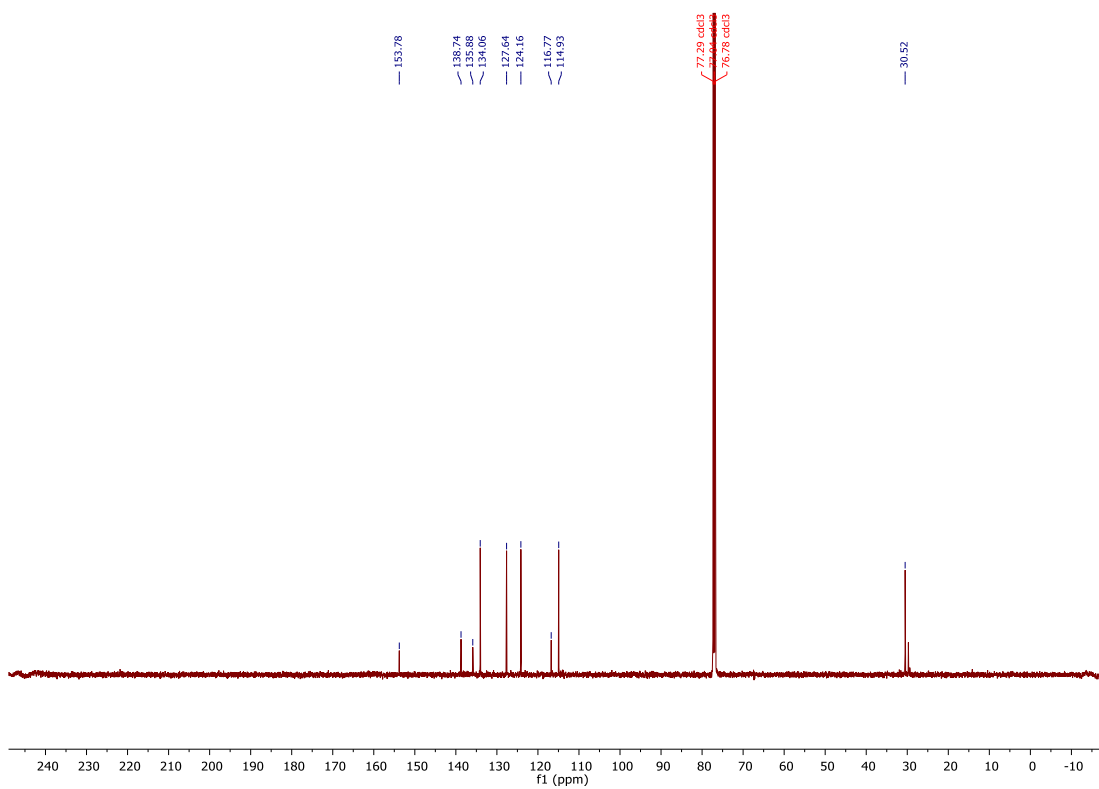


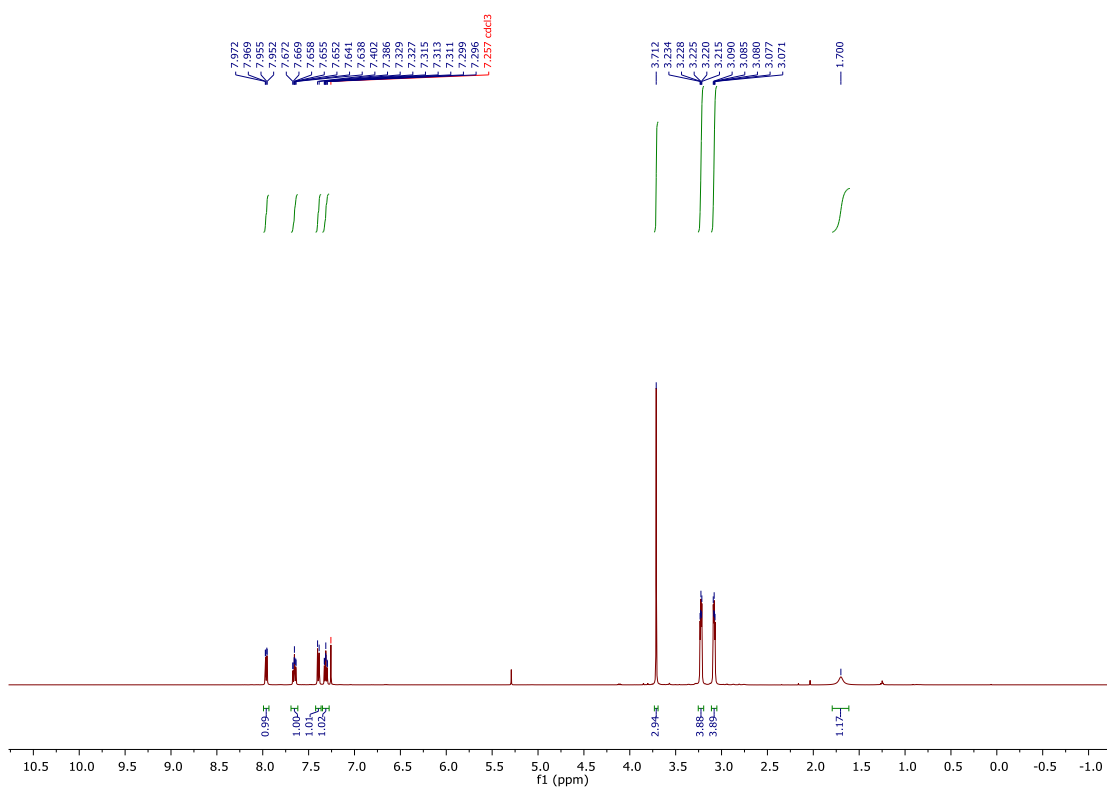
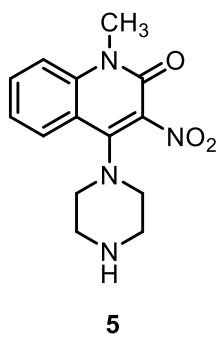
4

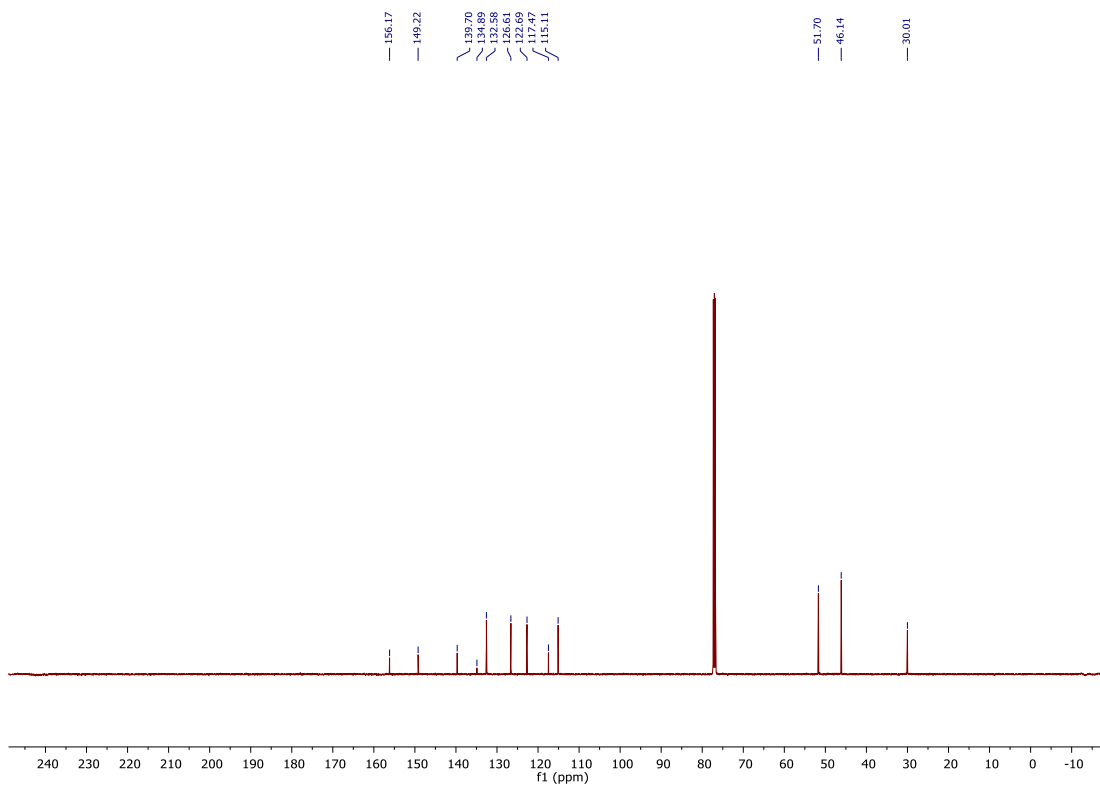
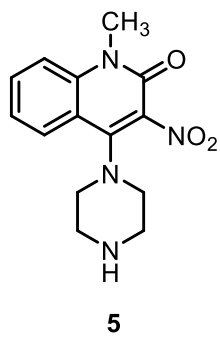


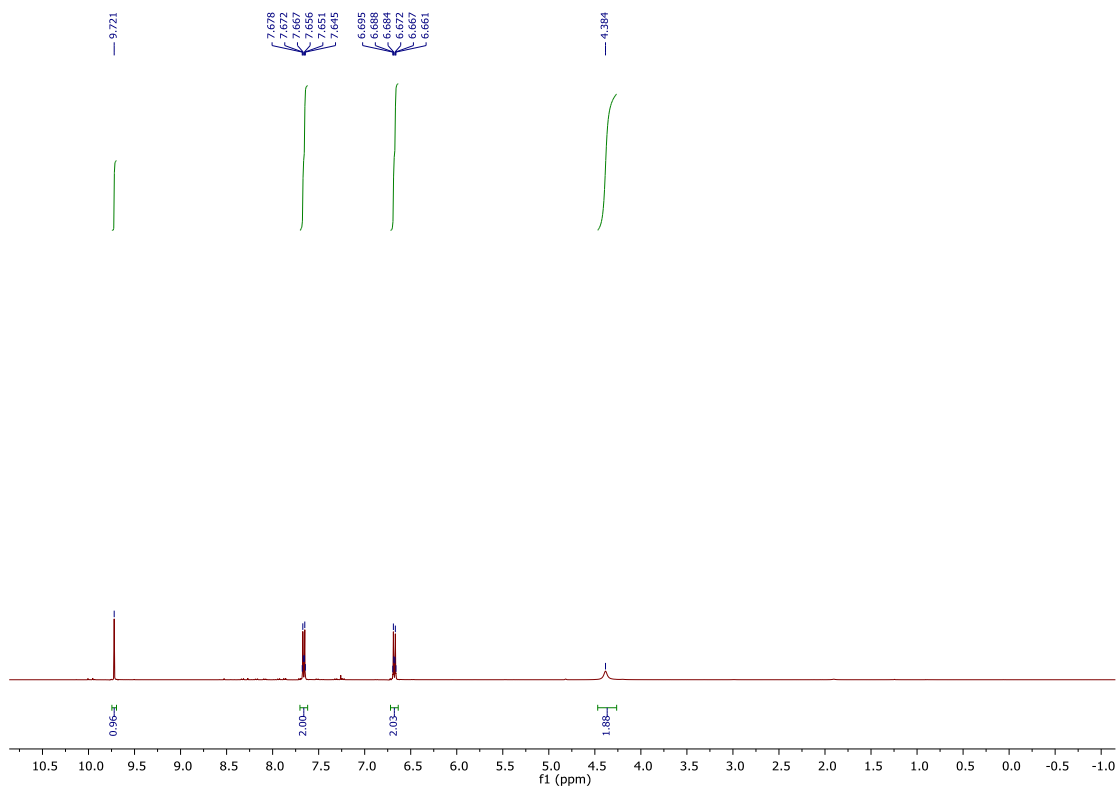
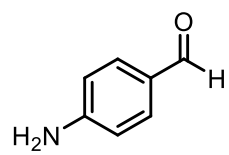


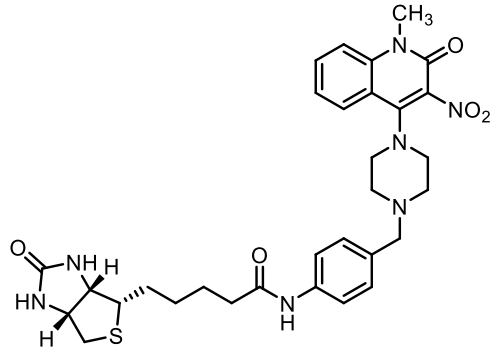
4



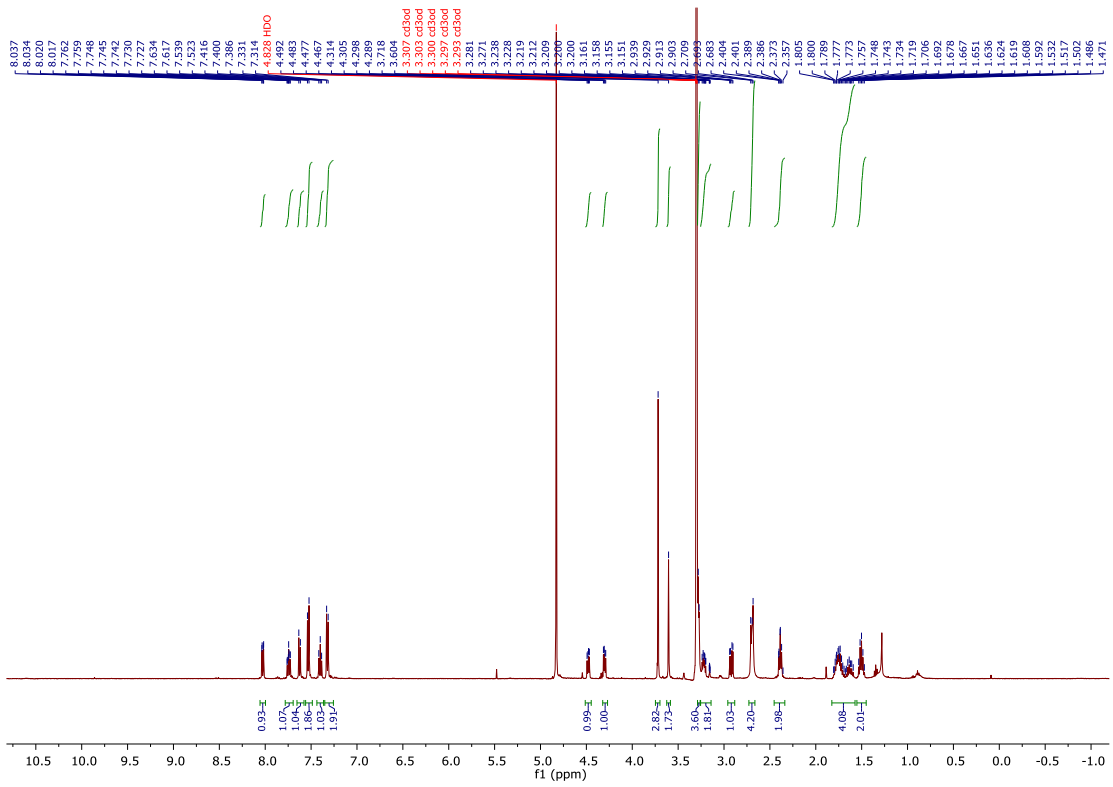


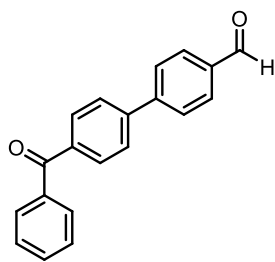




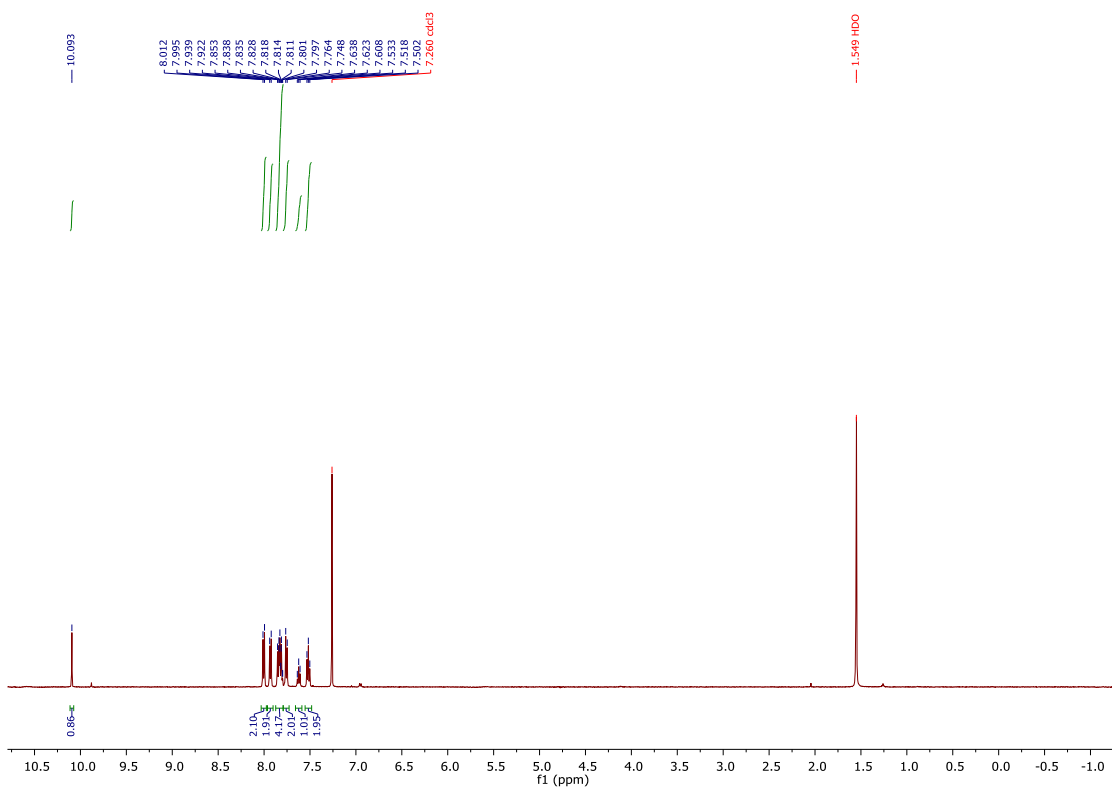


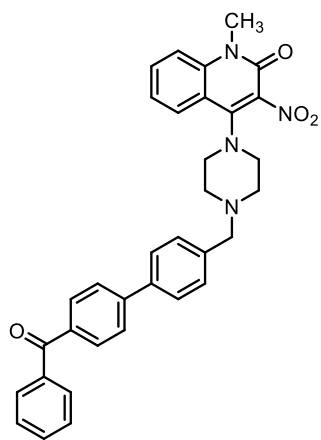
1



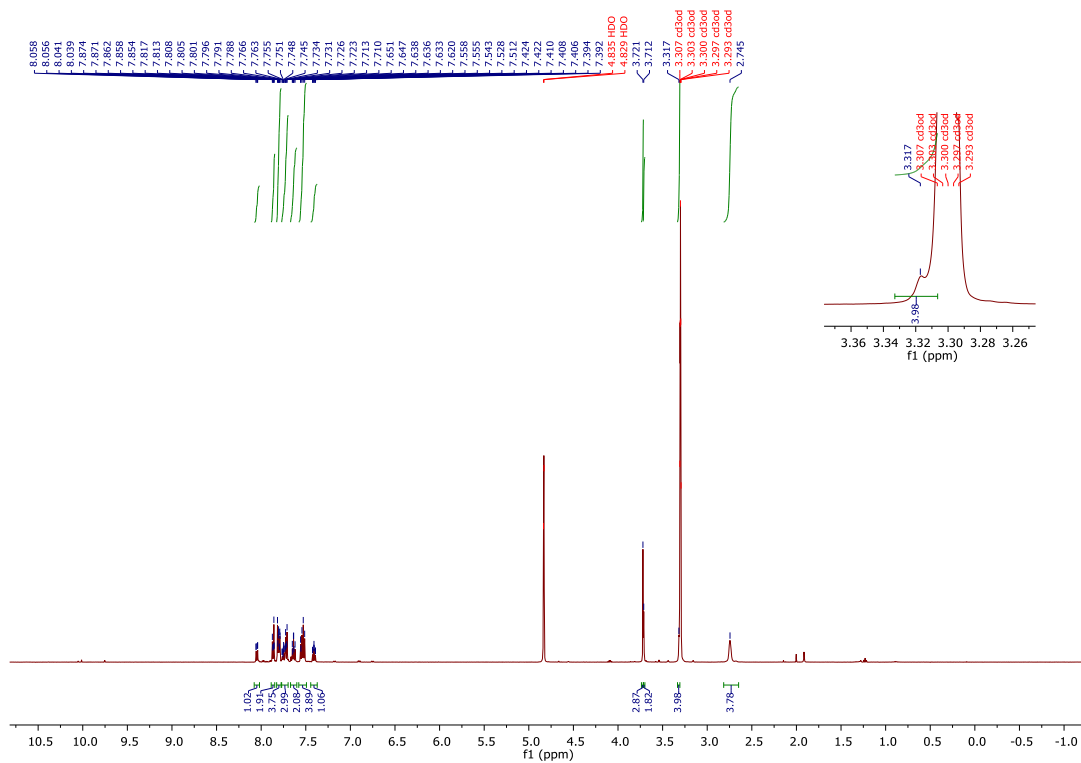


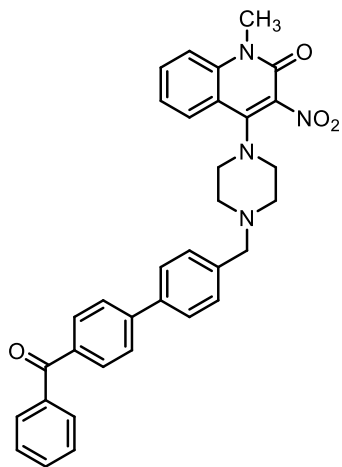
12



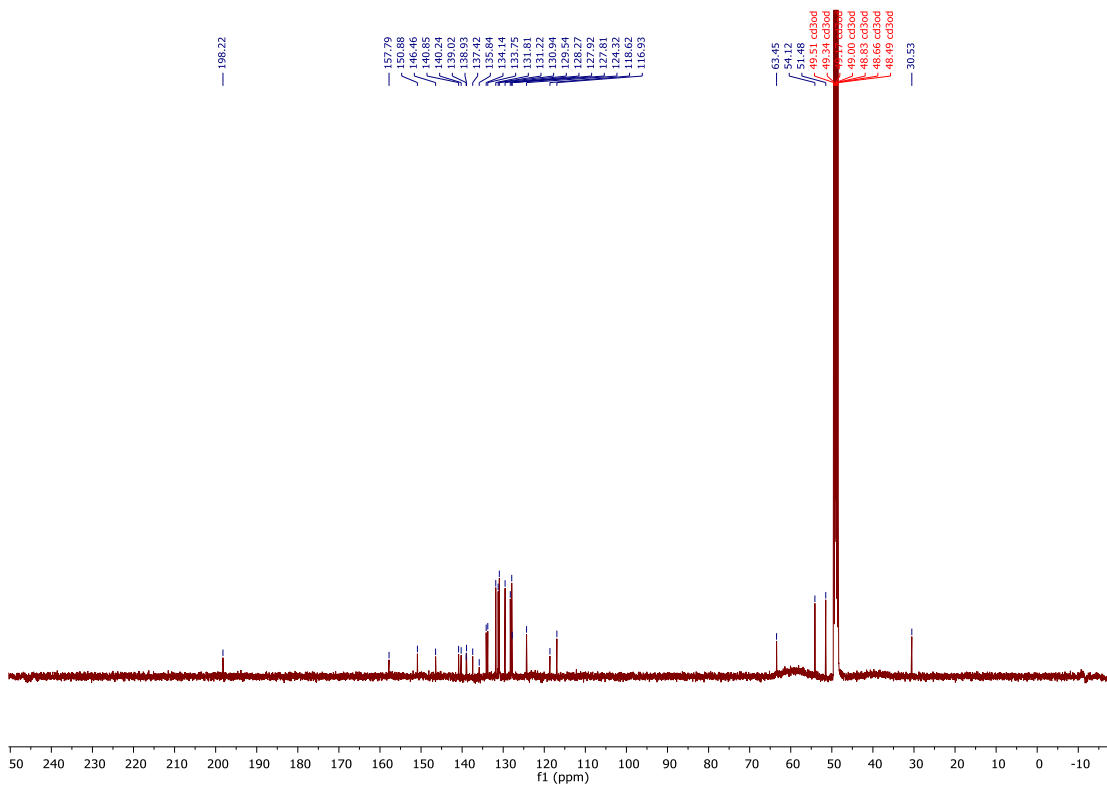


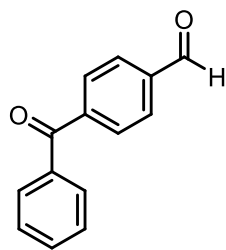
9



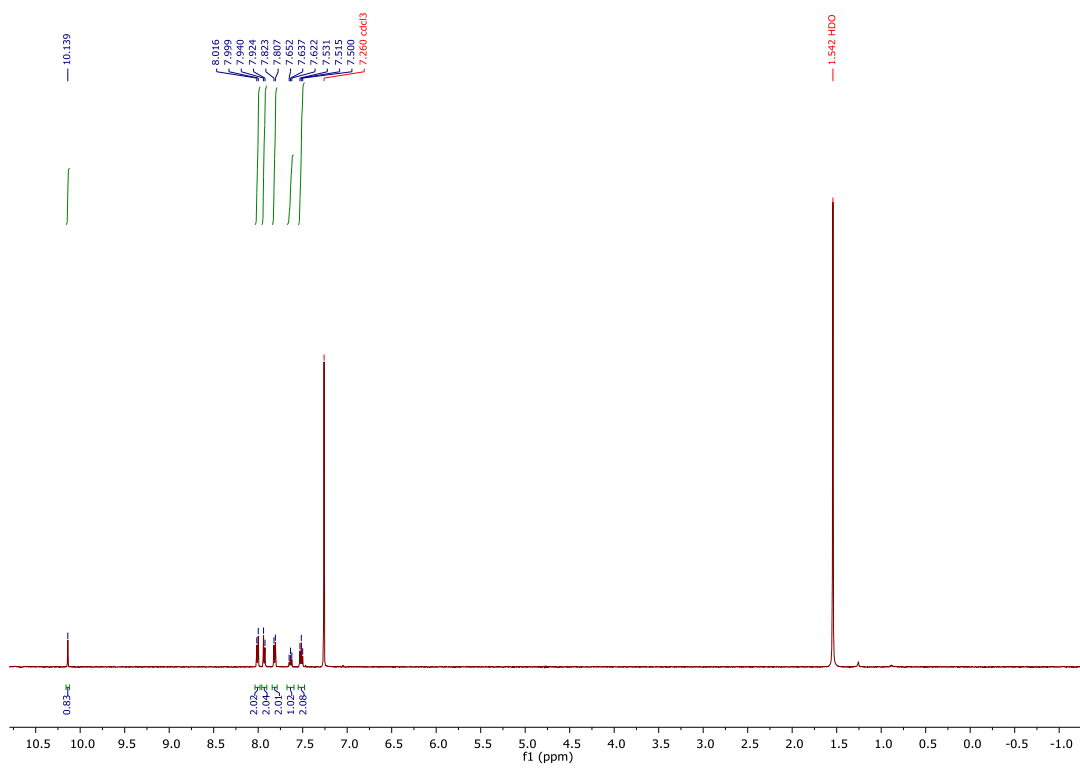


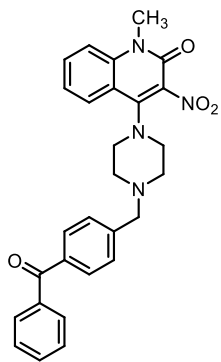
9



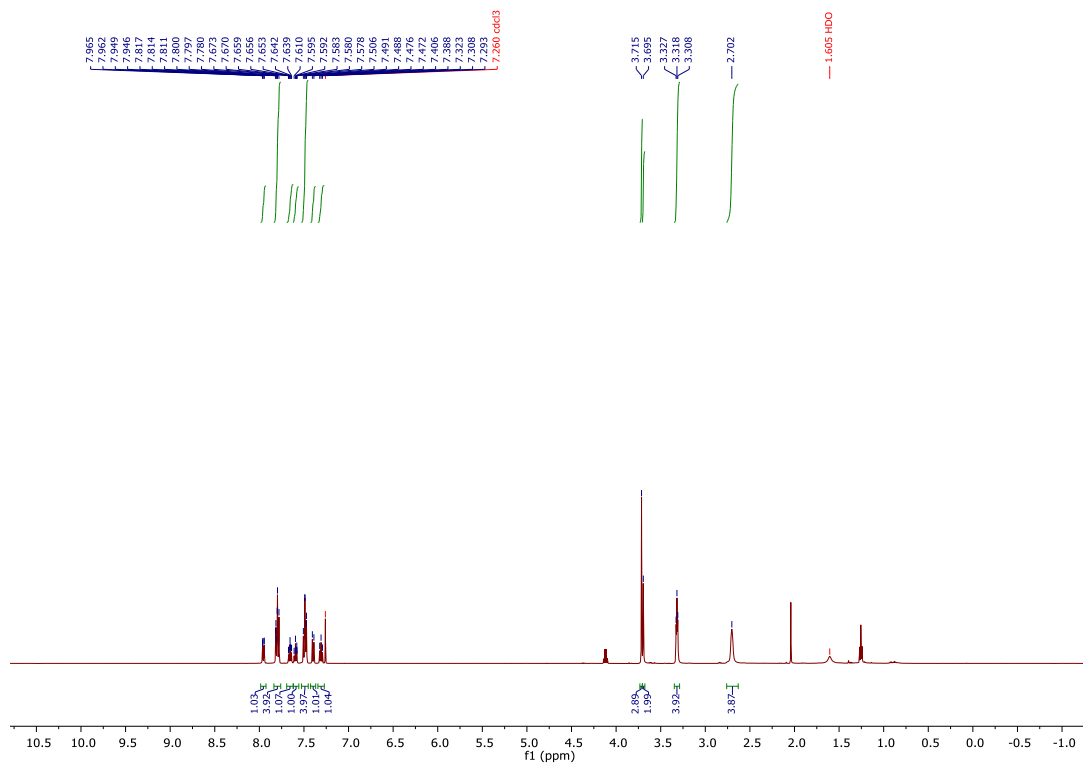


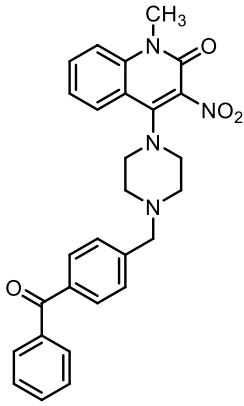
13



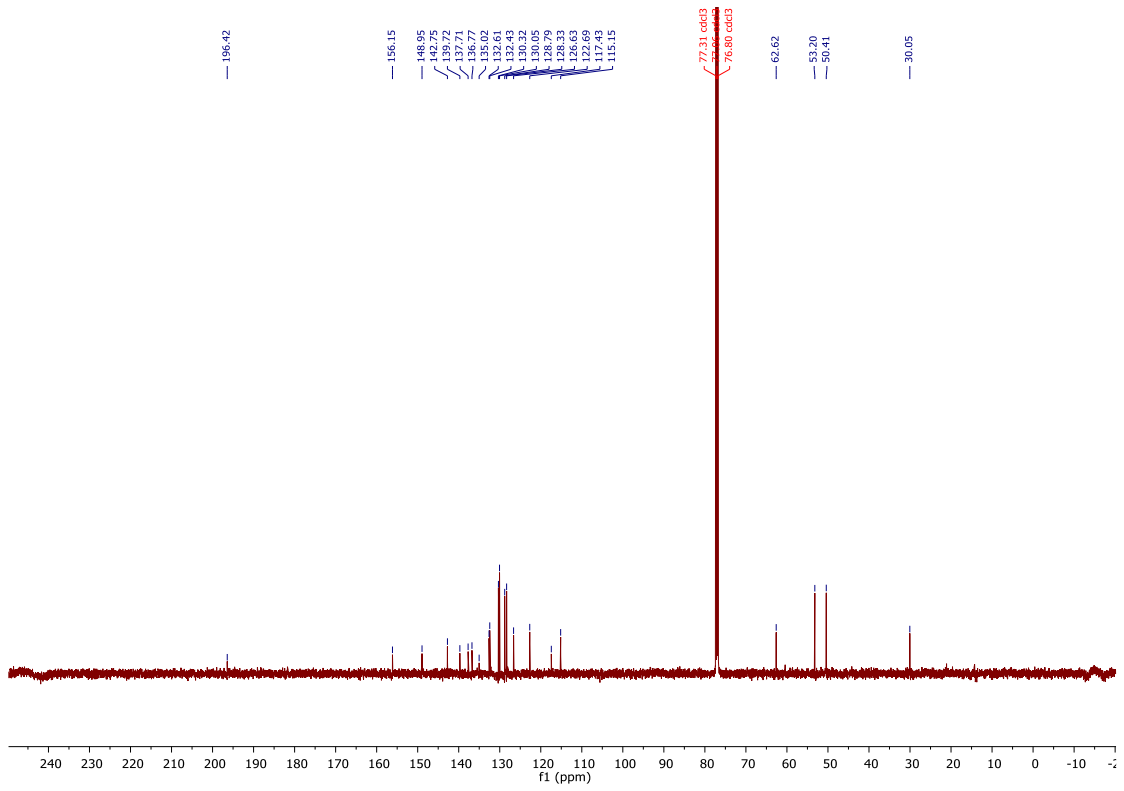


10

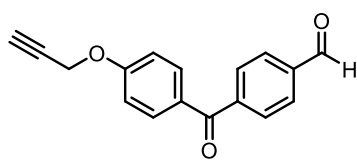




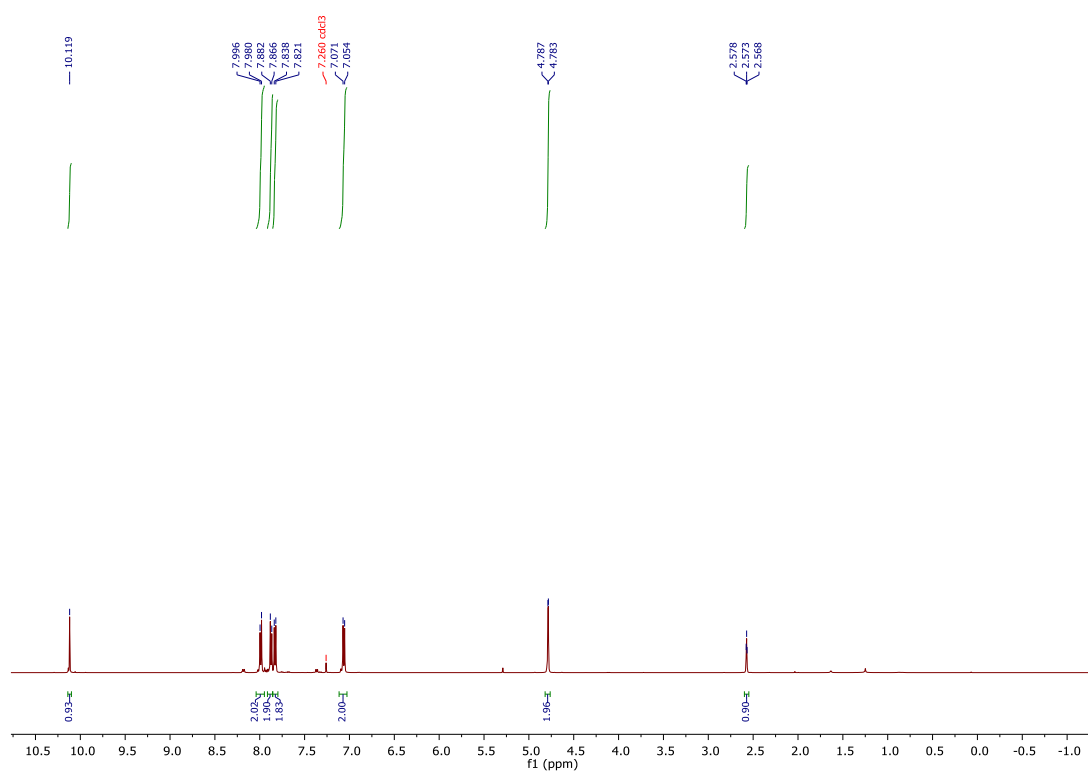
10

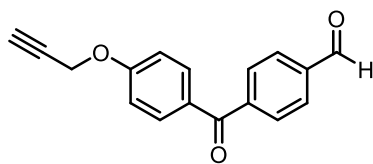


**Appendix II:
NMR Spectra (Chapter 3)**

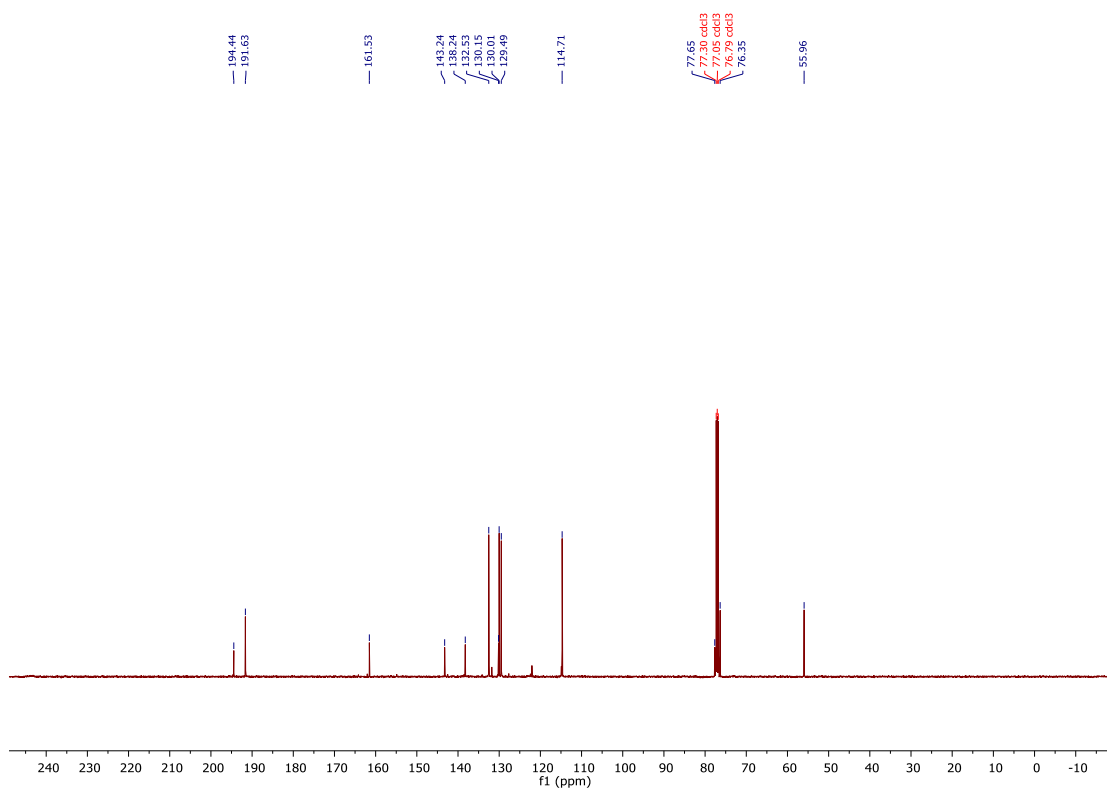


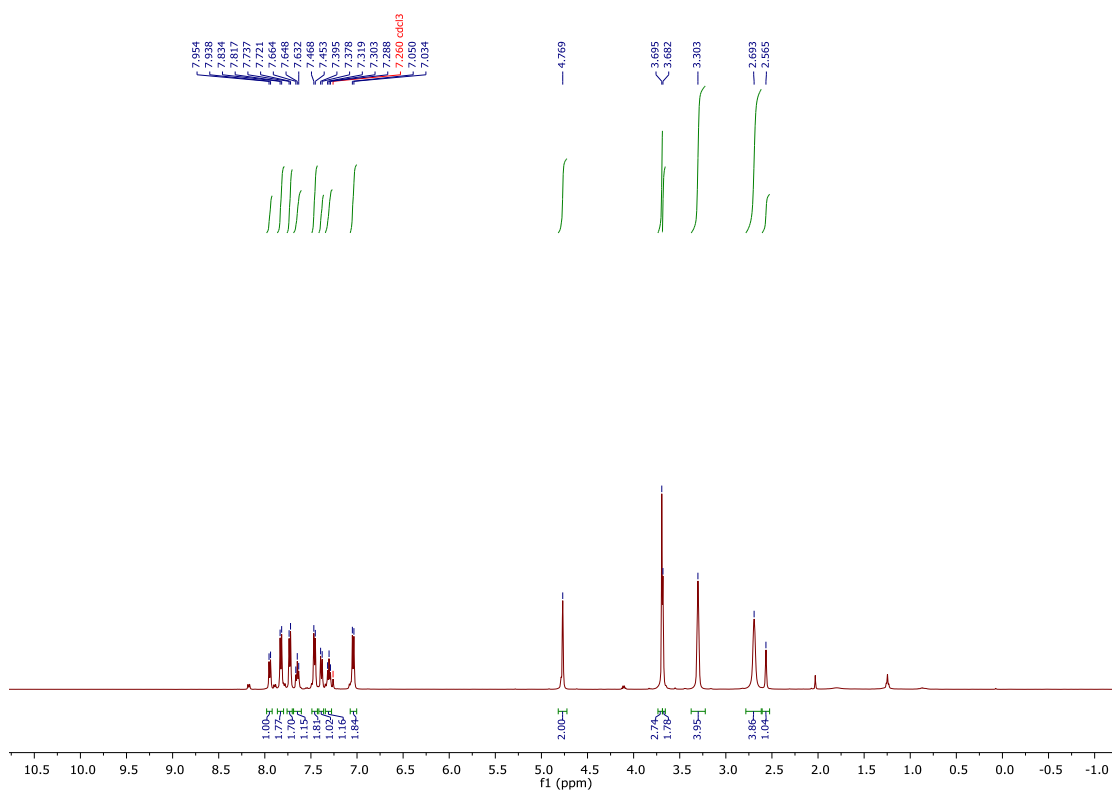
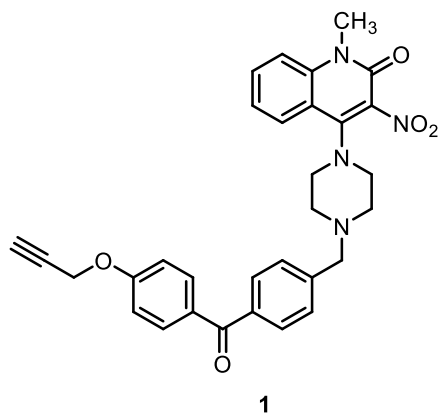
5

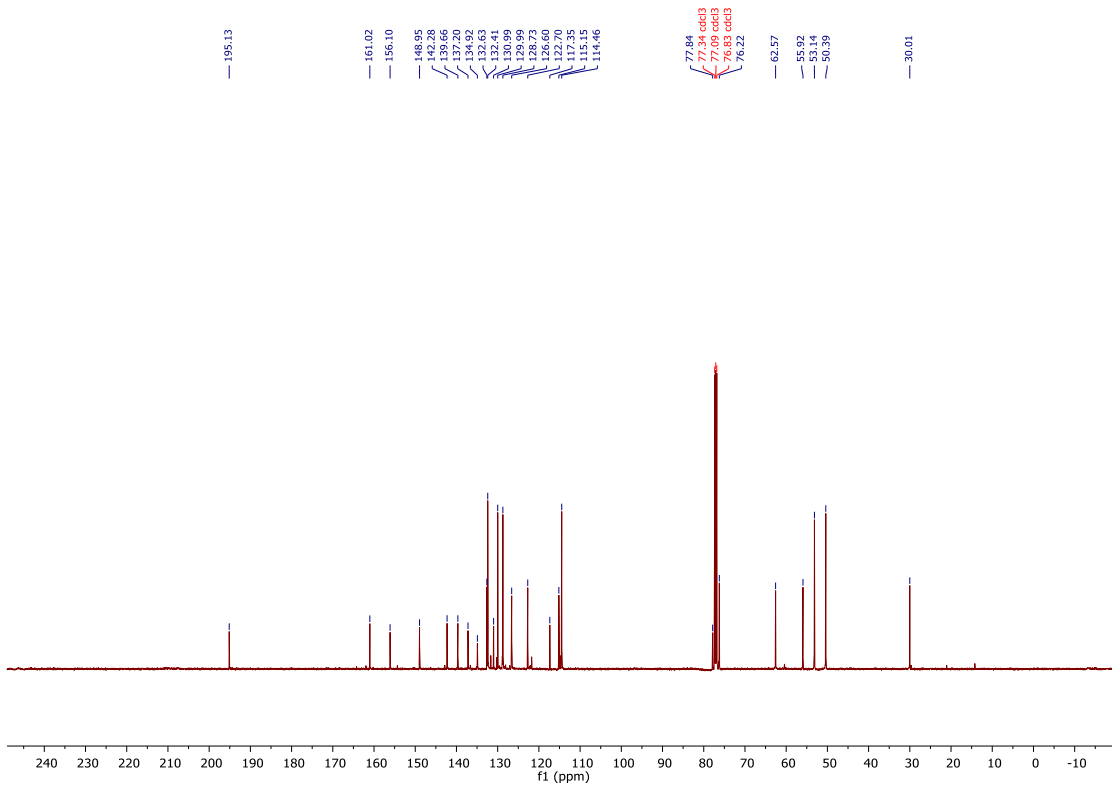
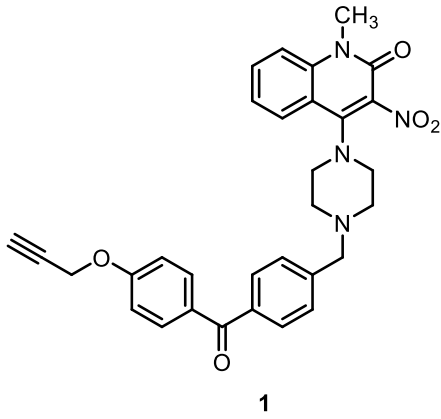


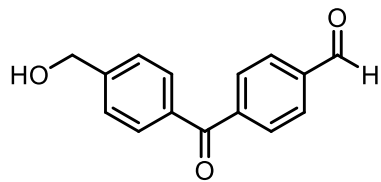


5

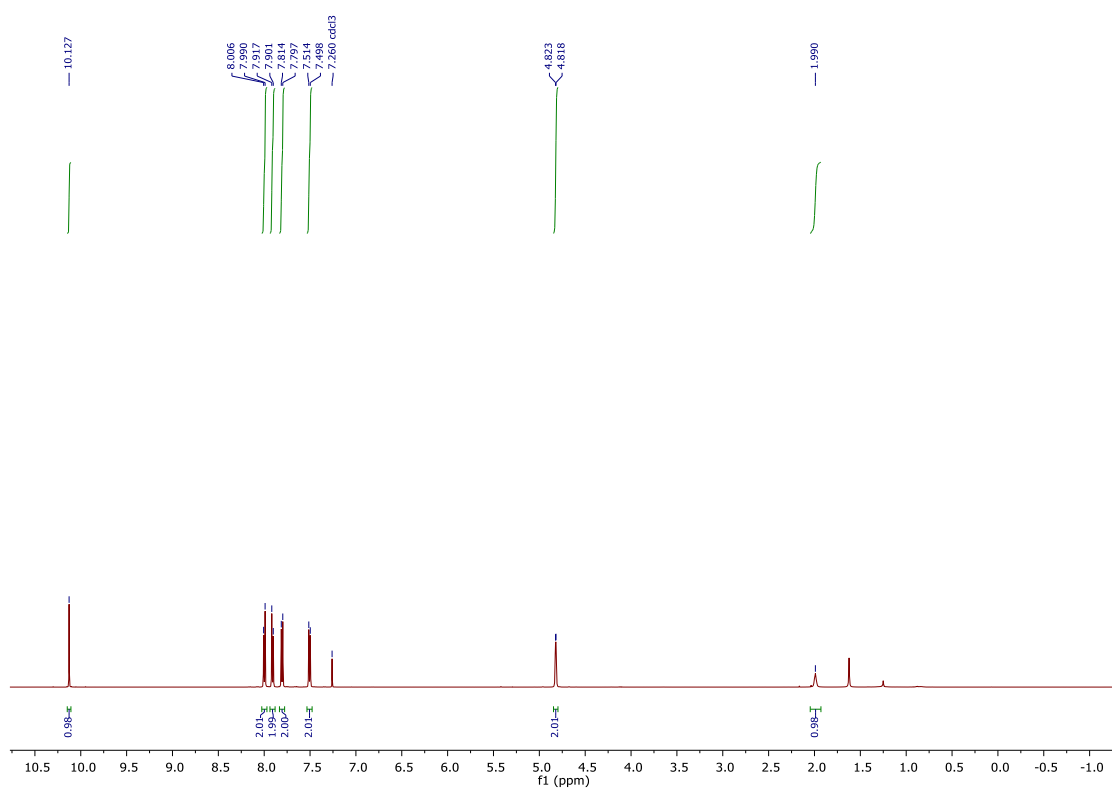


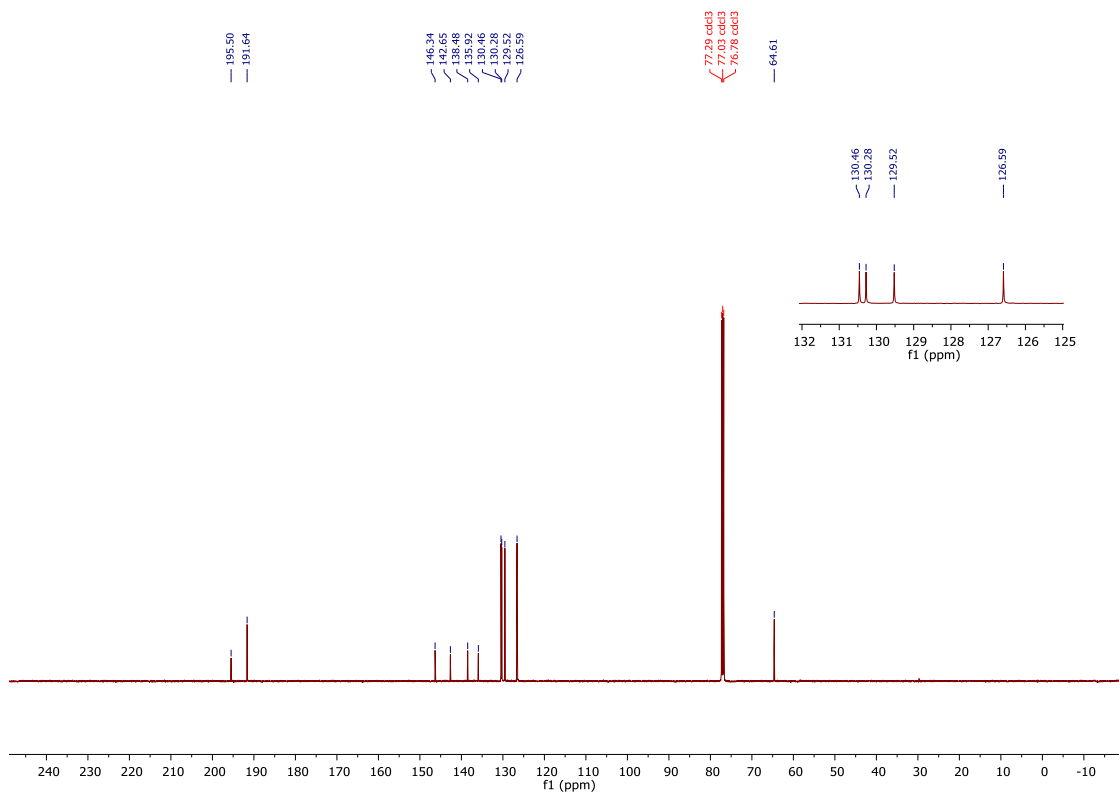
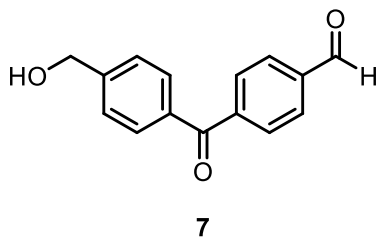


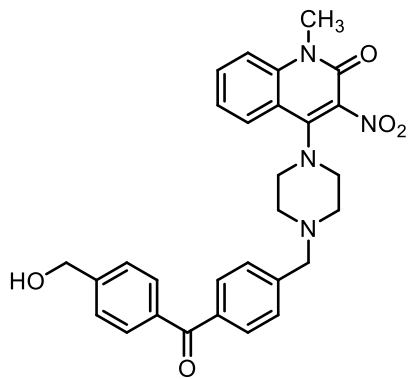




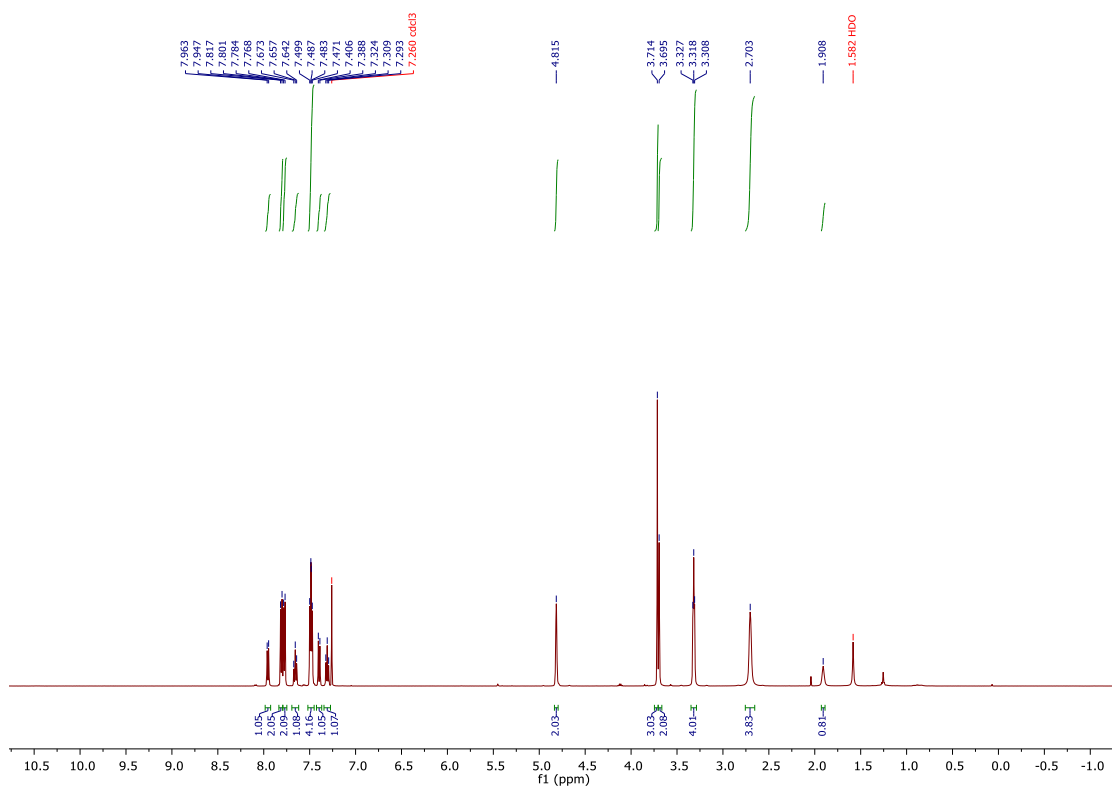
7

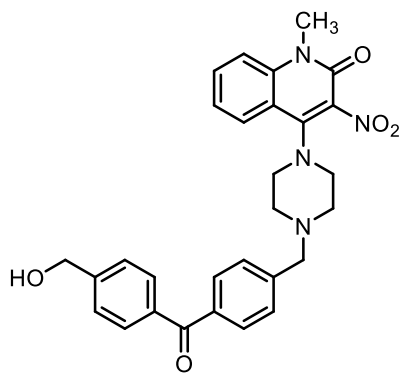




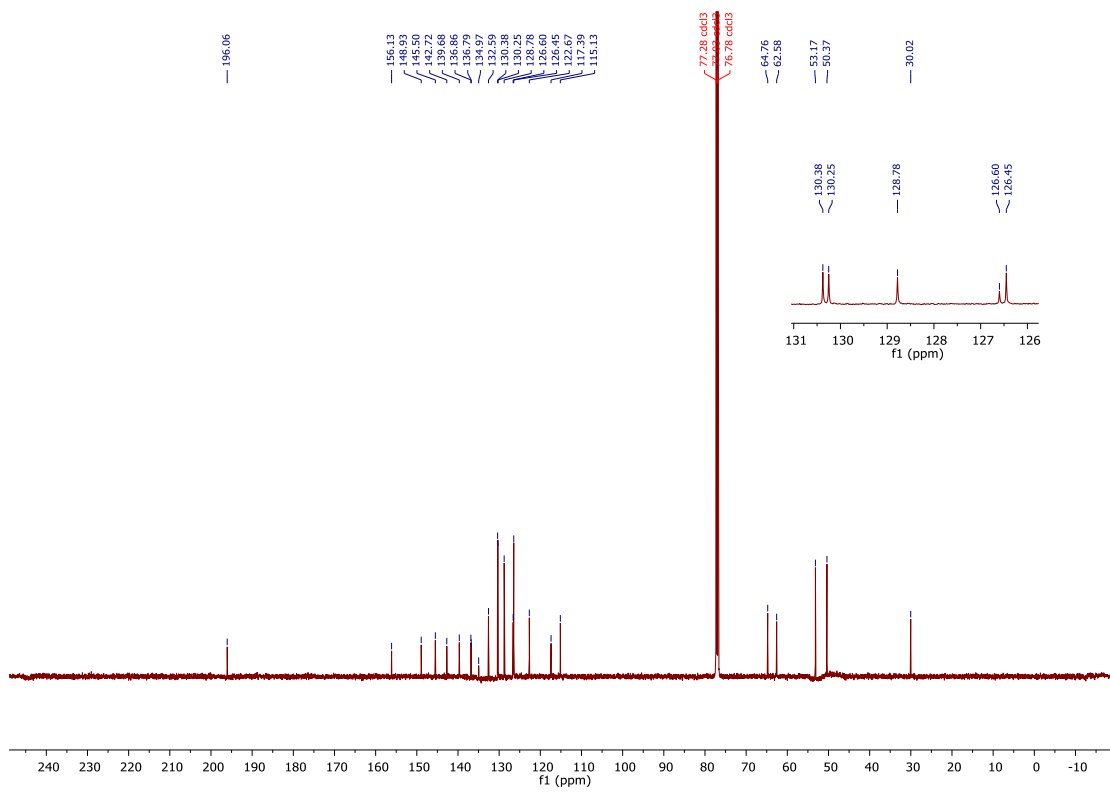


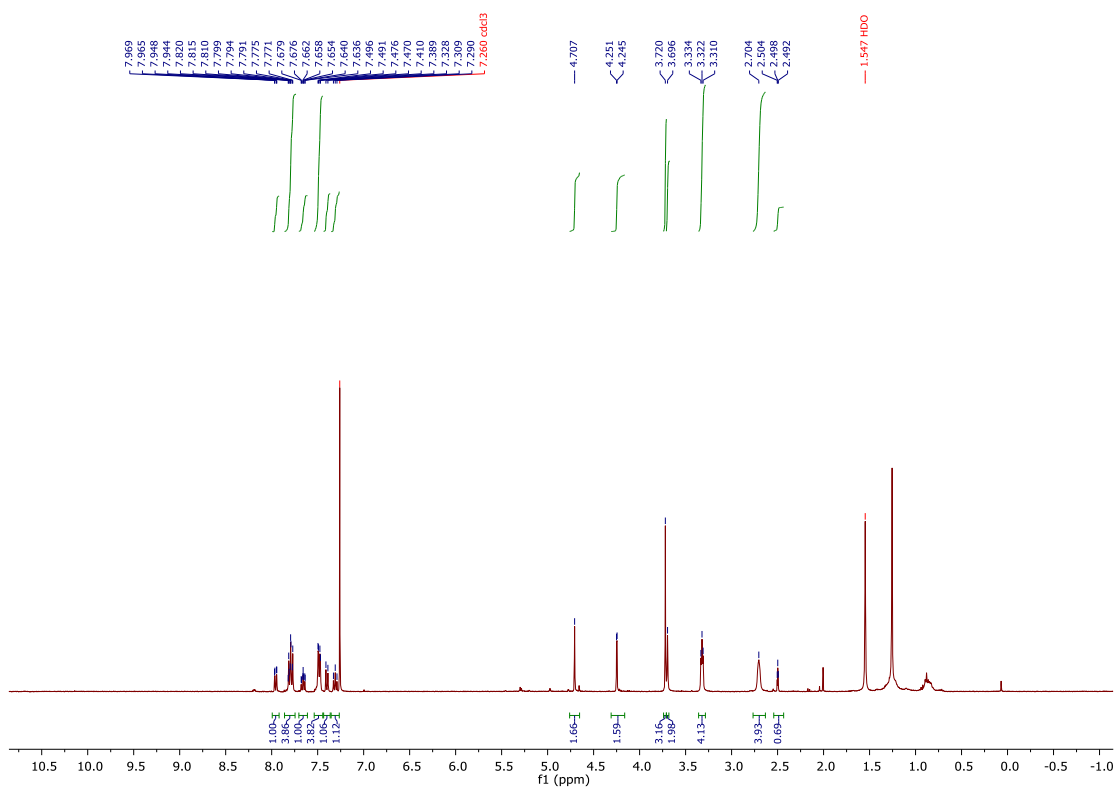
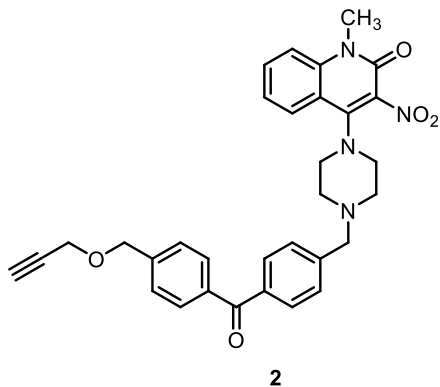
8

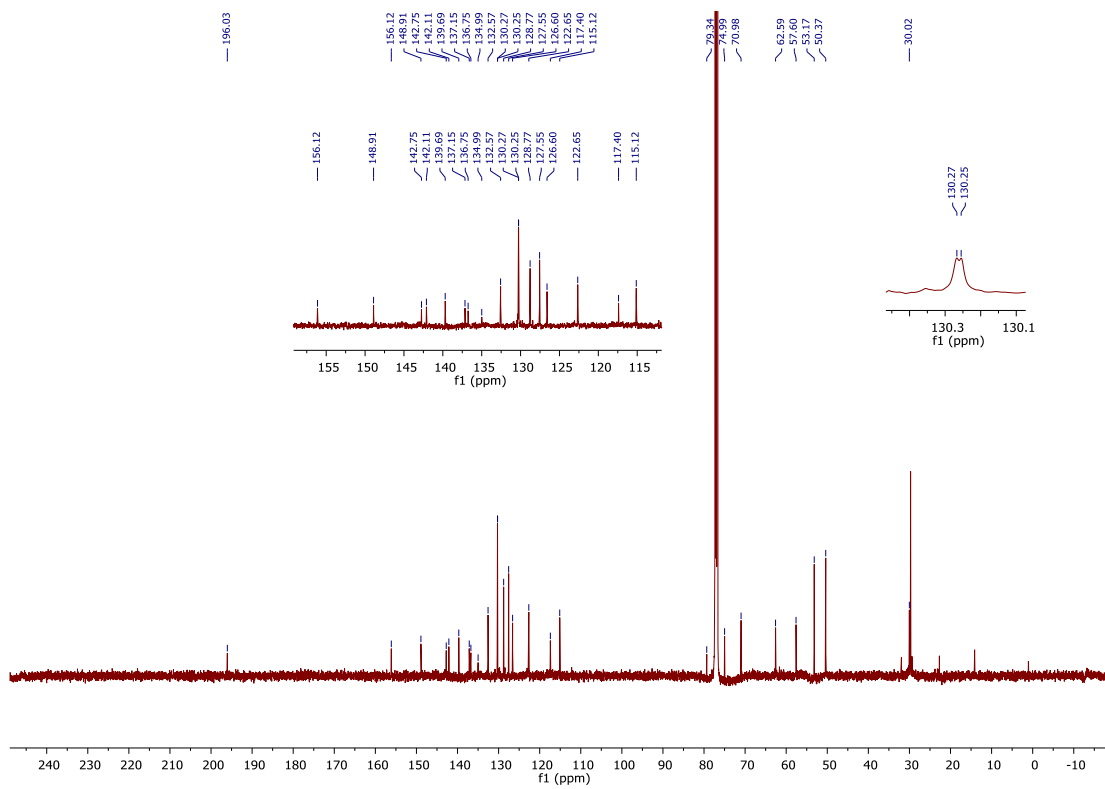
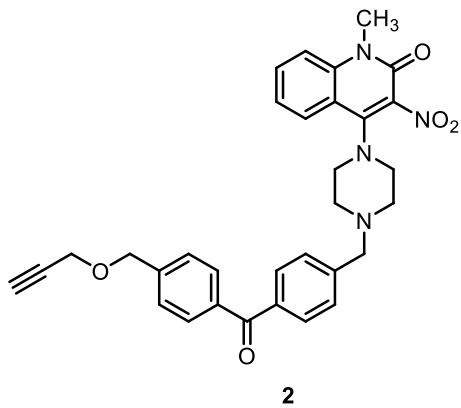


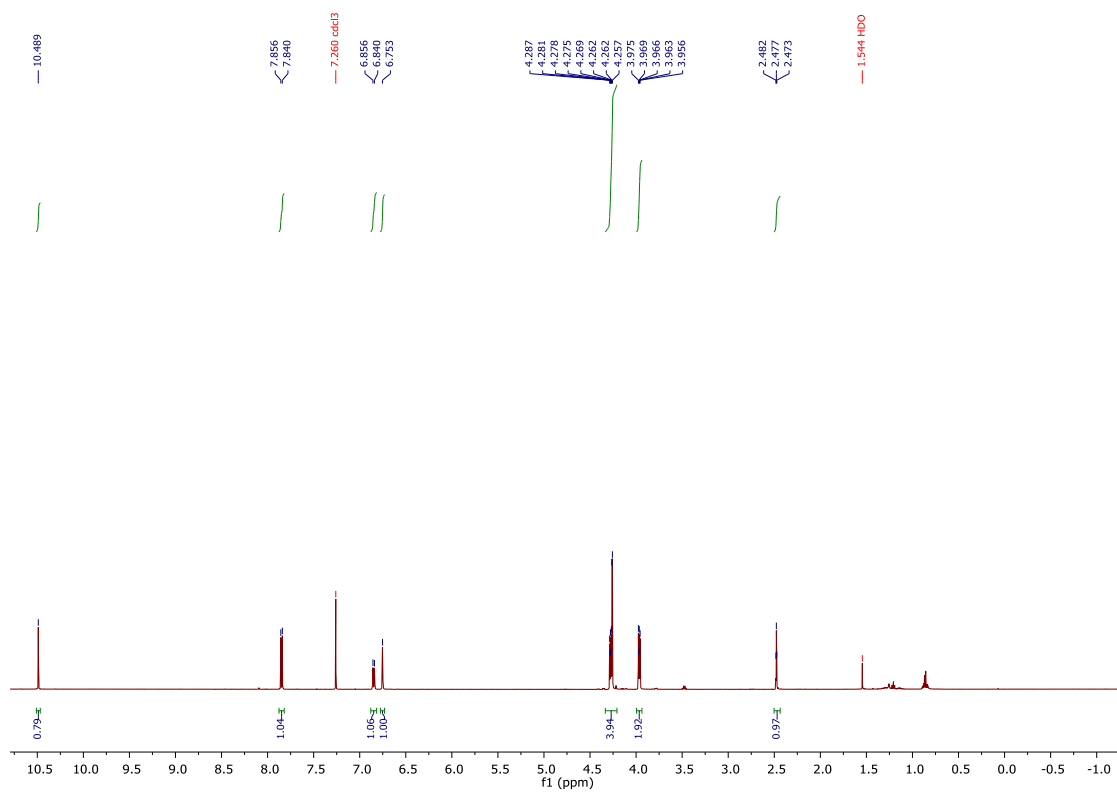
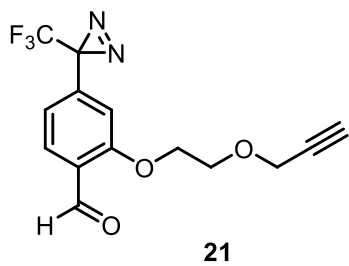


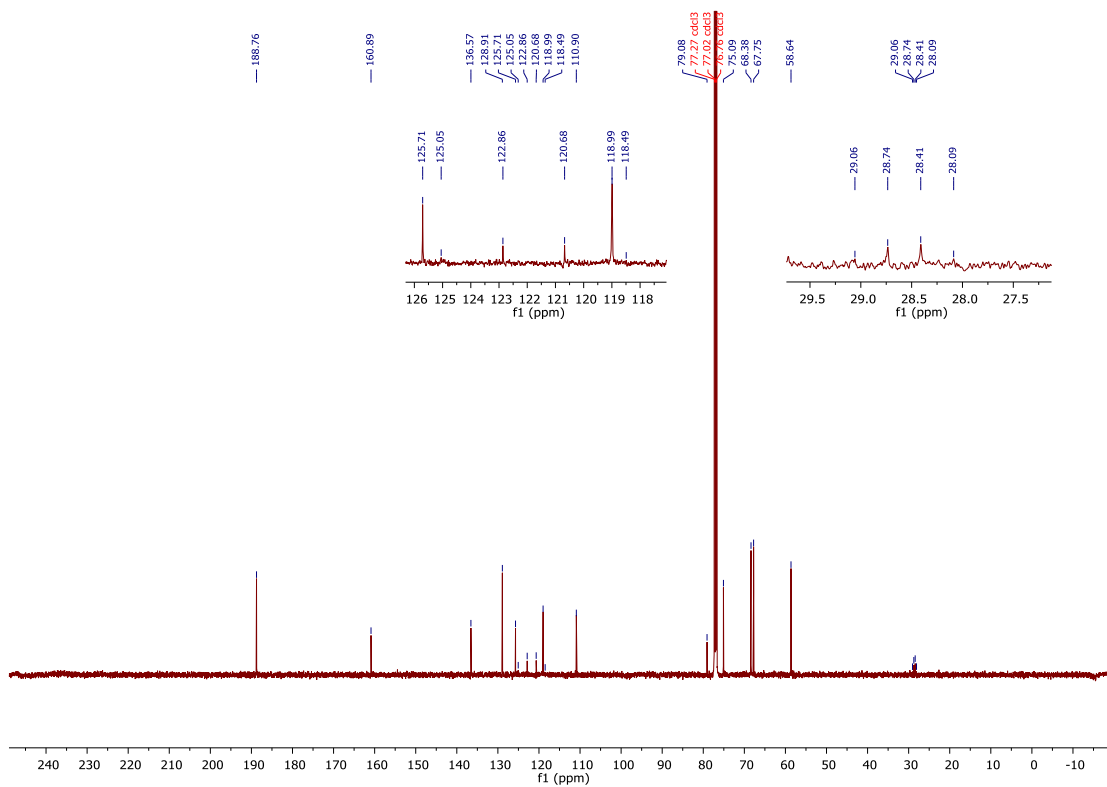
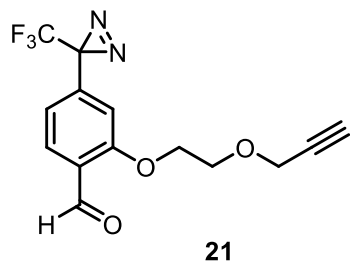
8

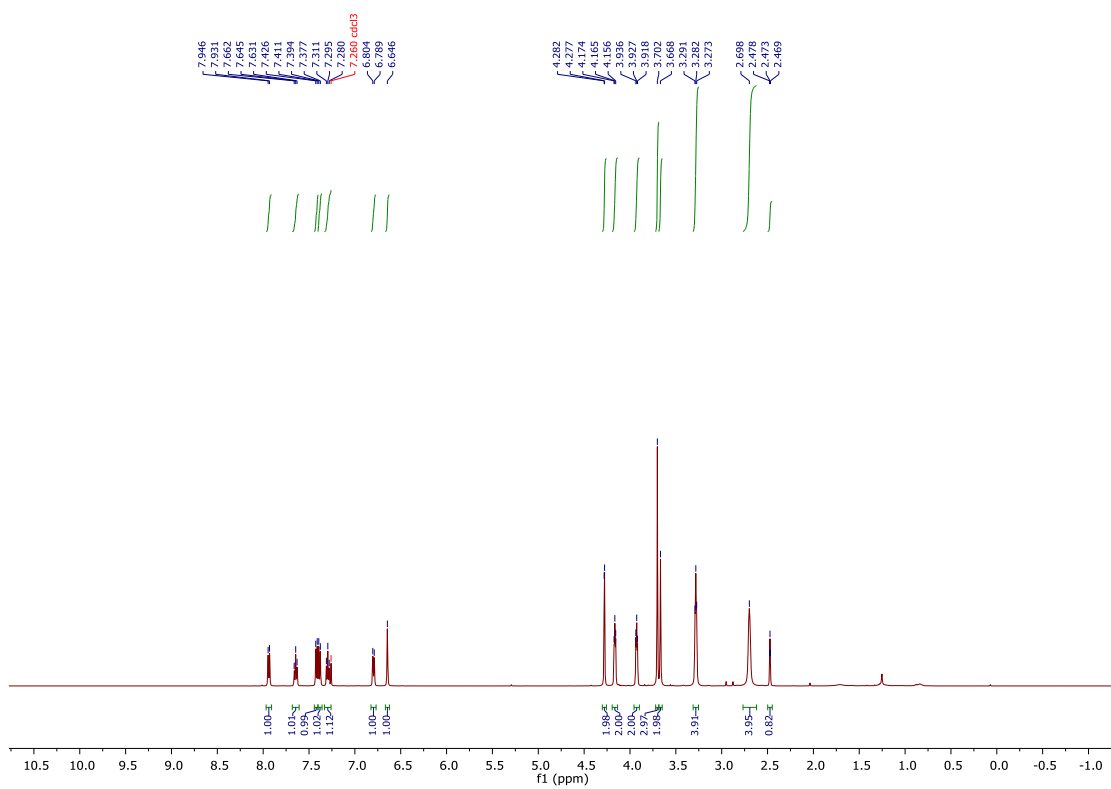
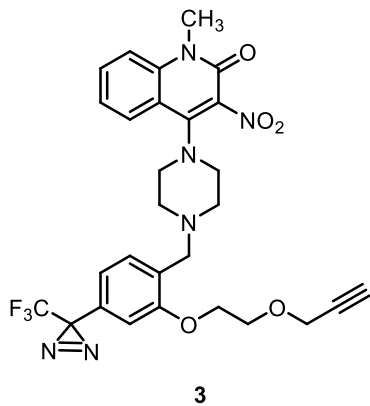


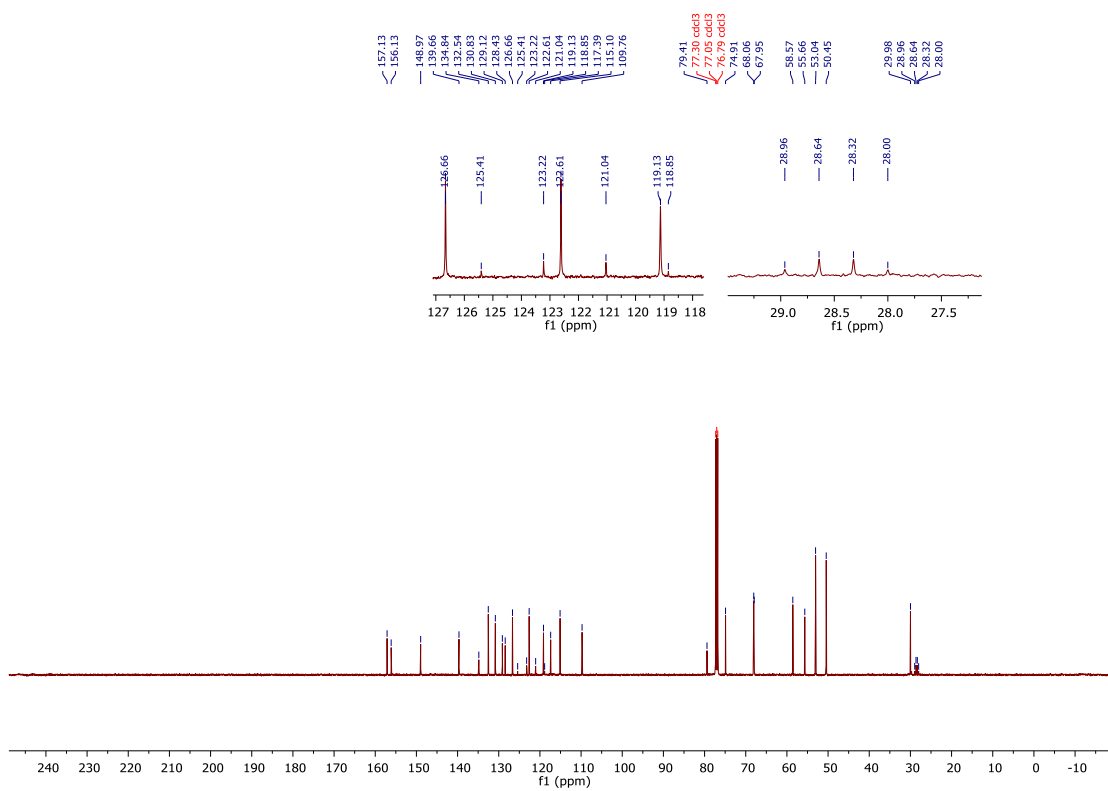
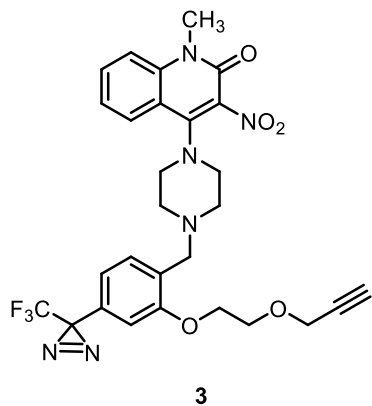


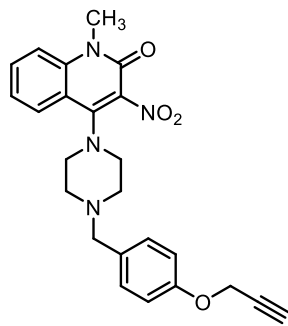




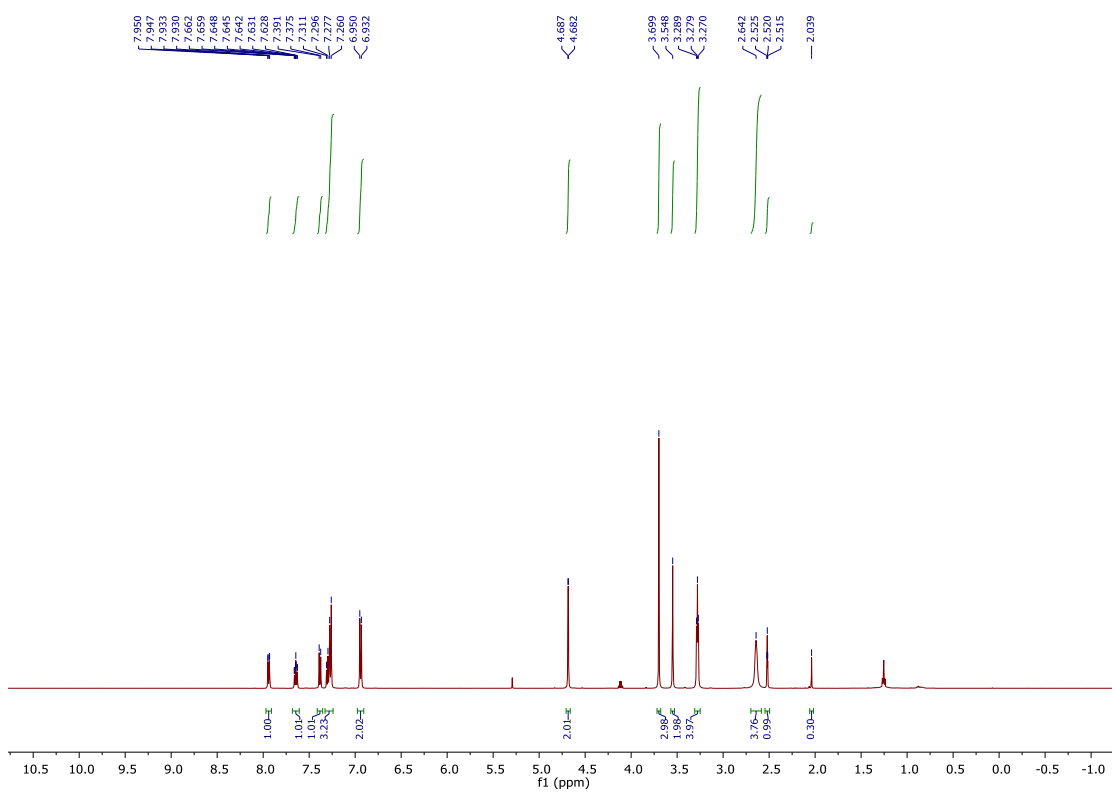


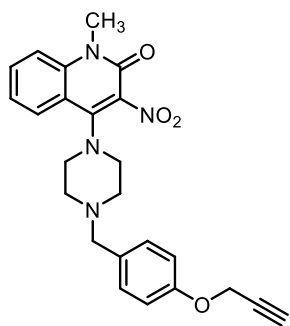




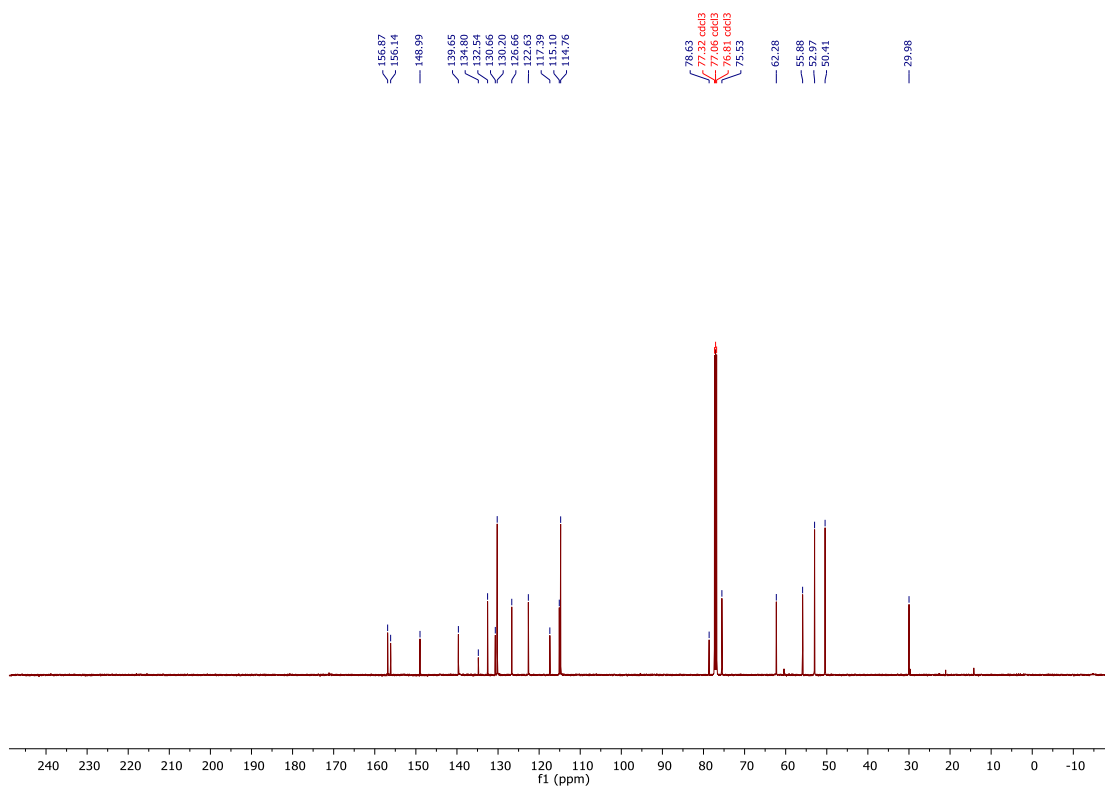


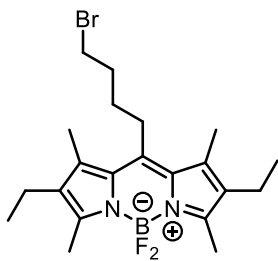
23



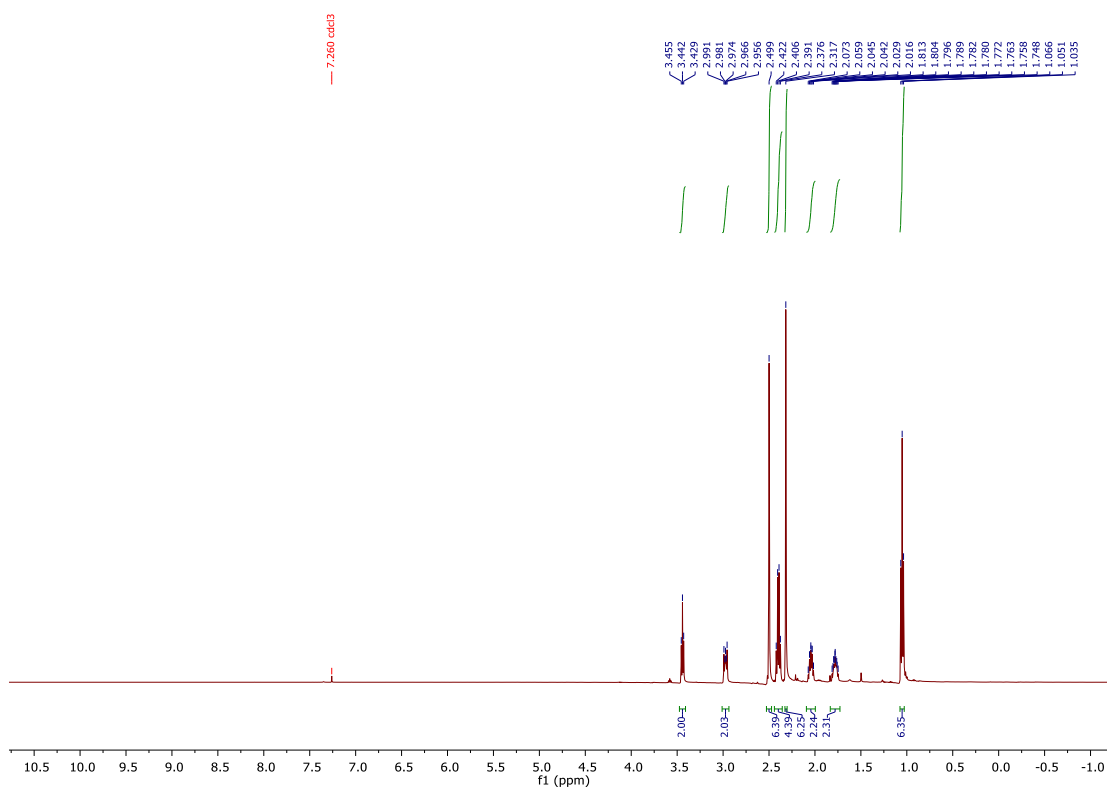


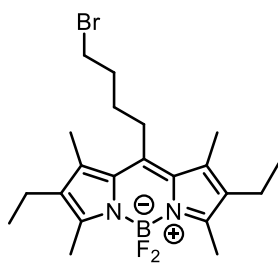
23



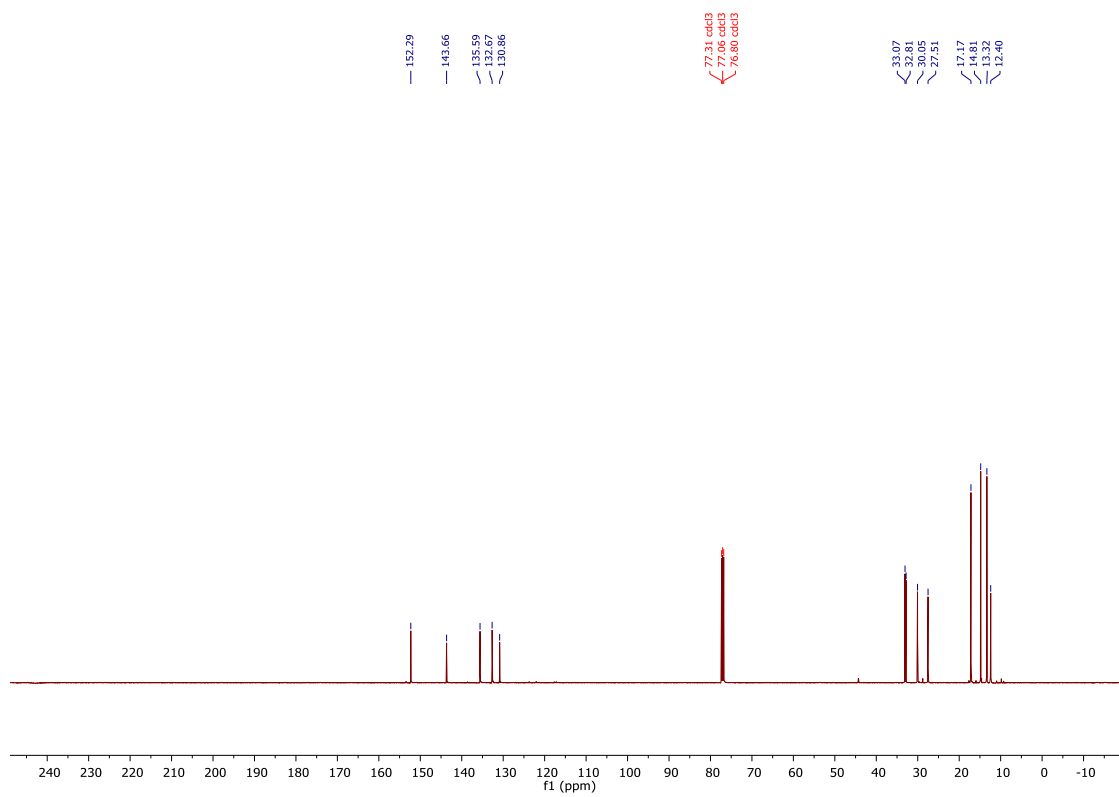


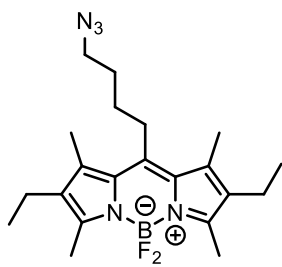
27



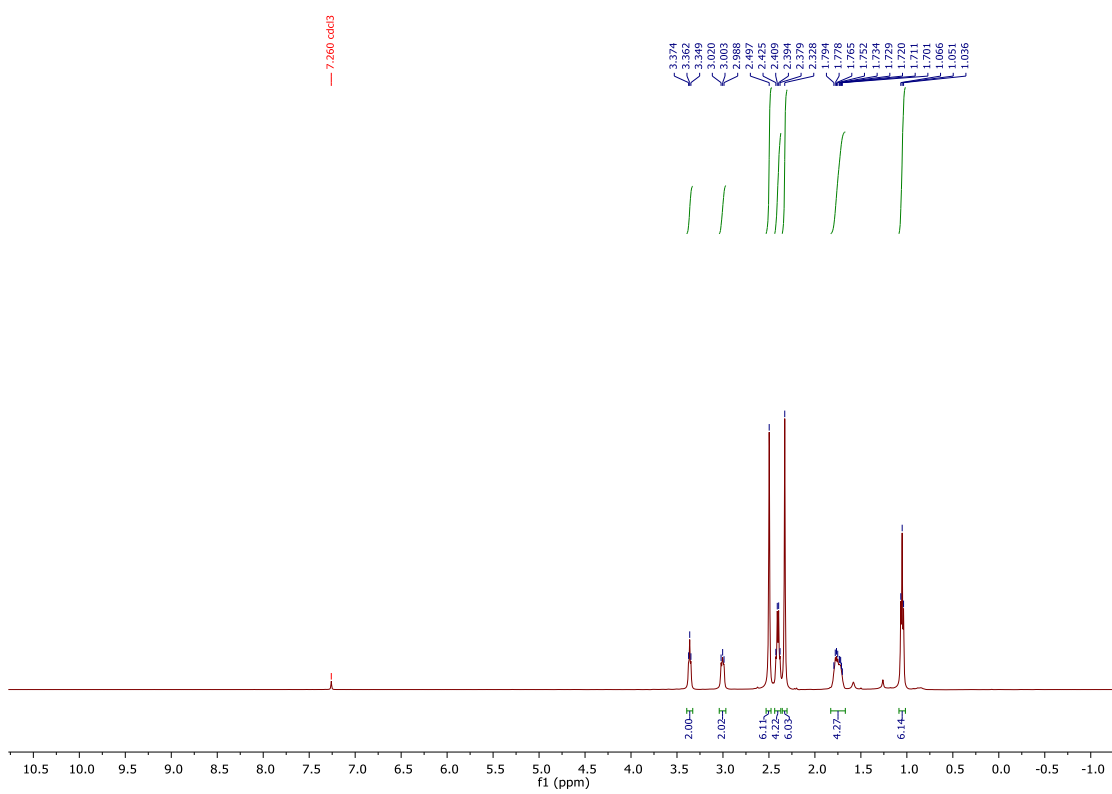


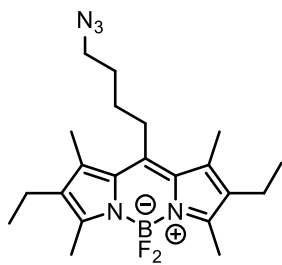
27



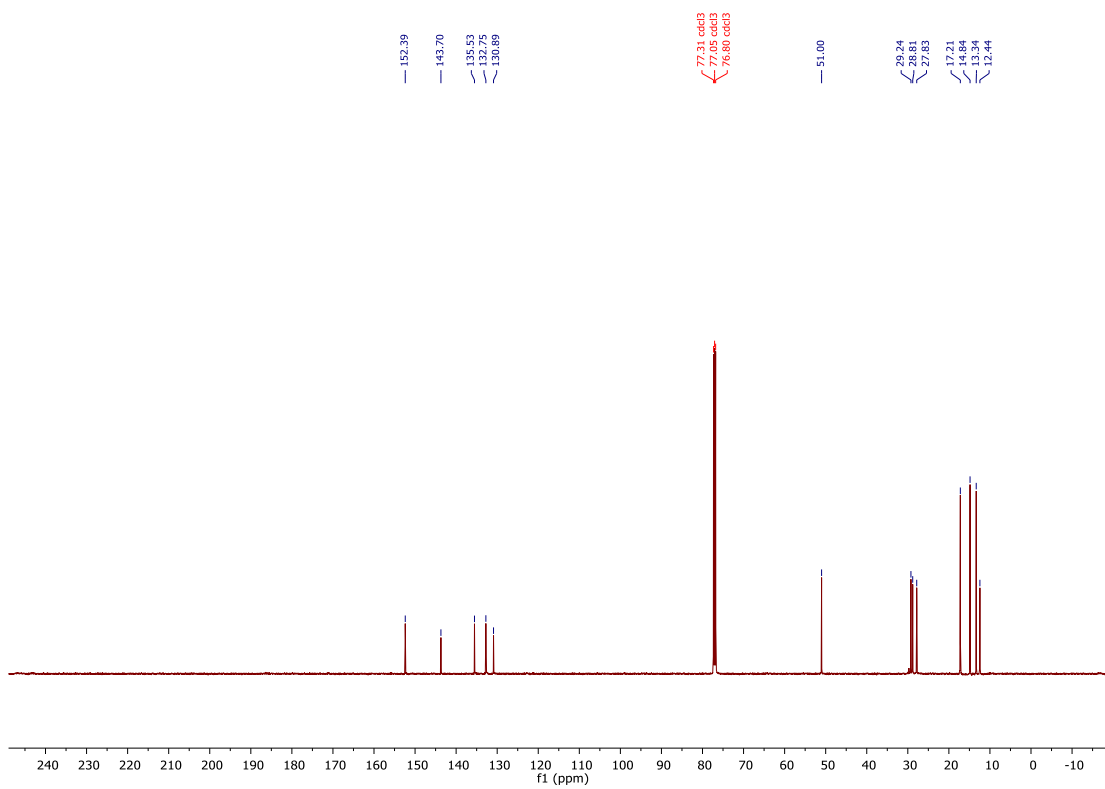


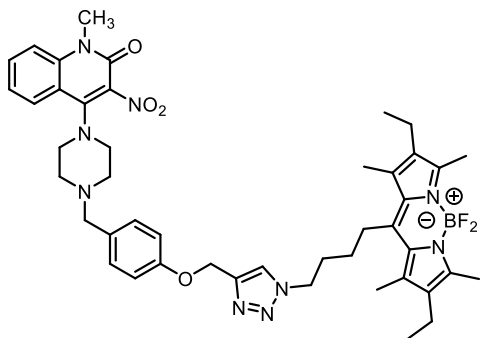
28



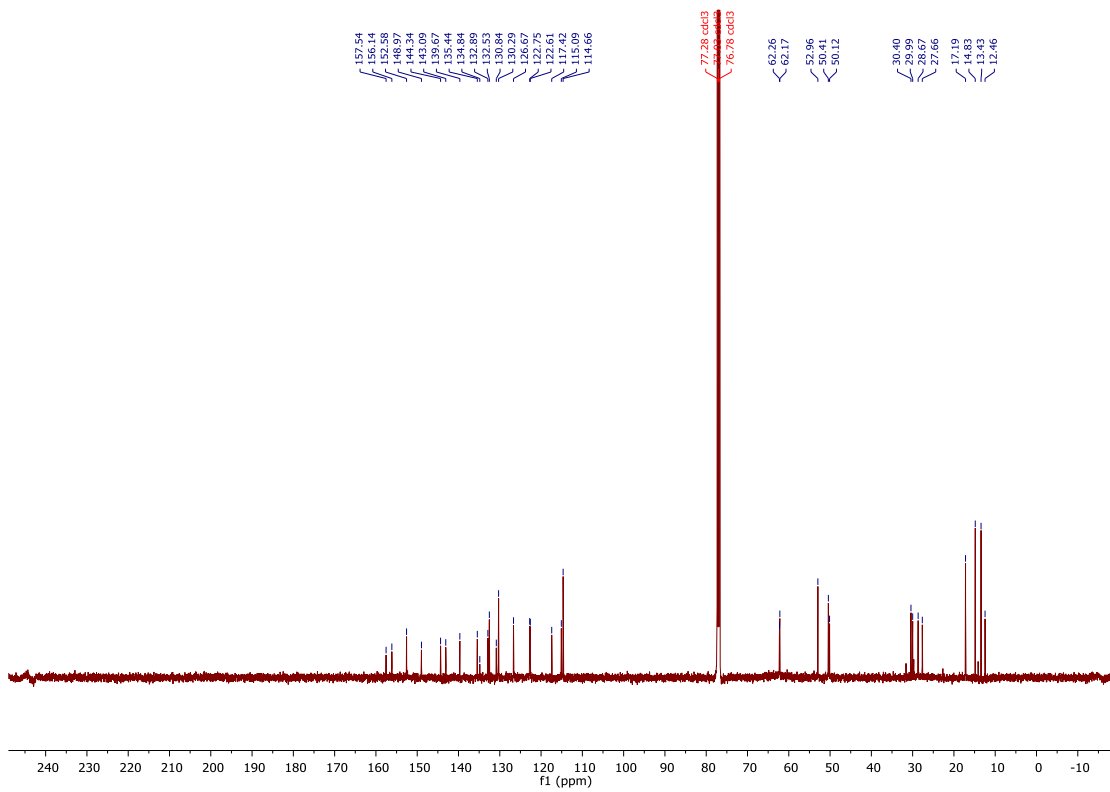


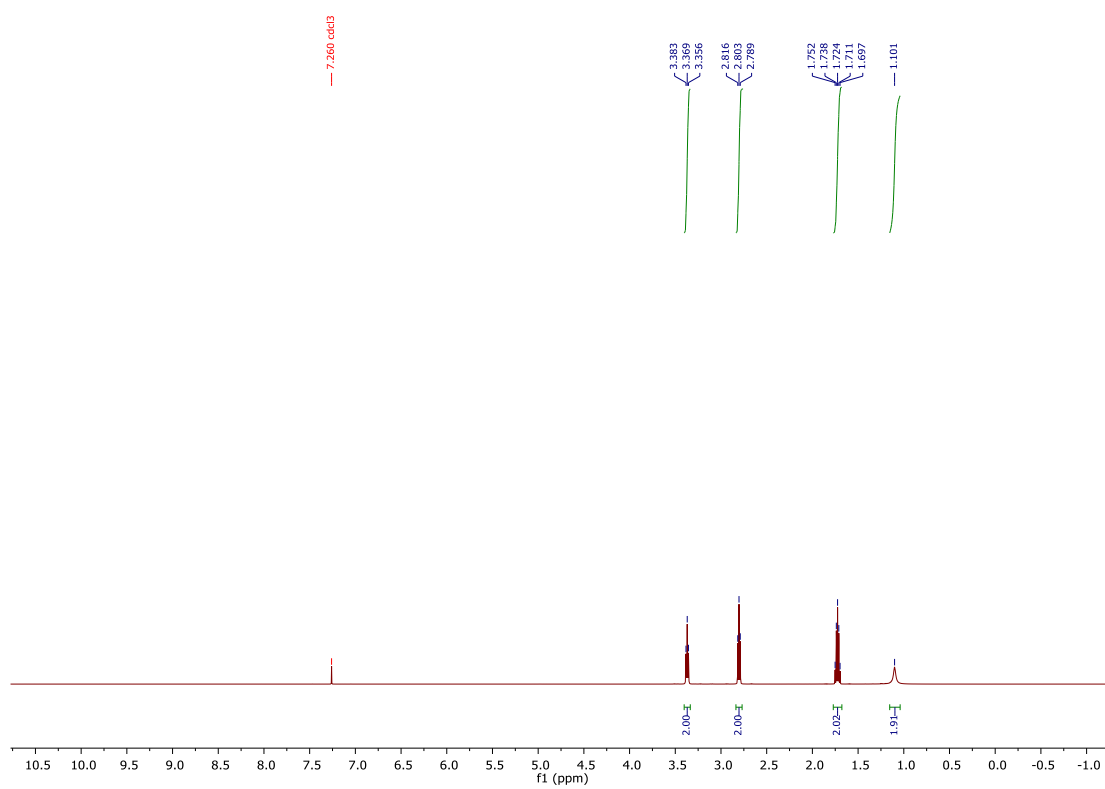
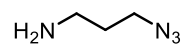
28

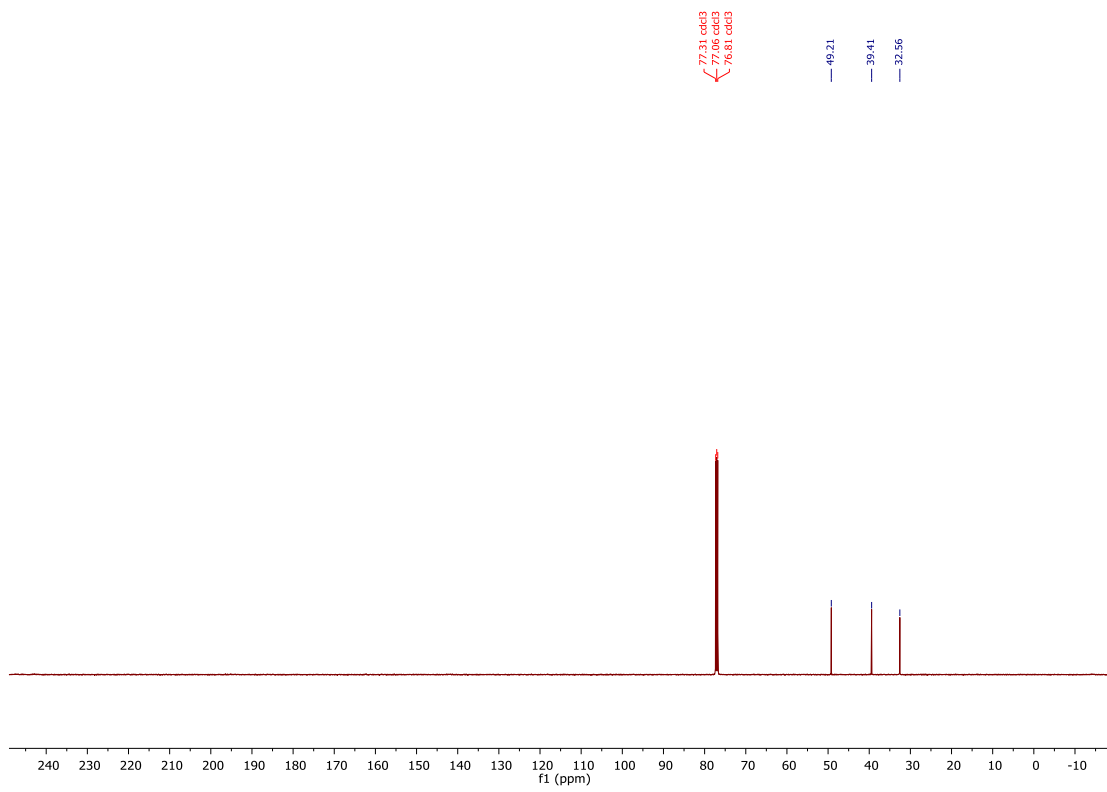
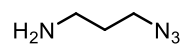


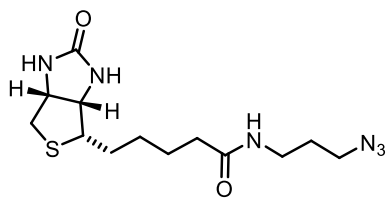


29

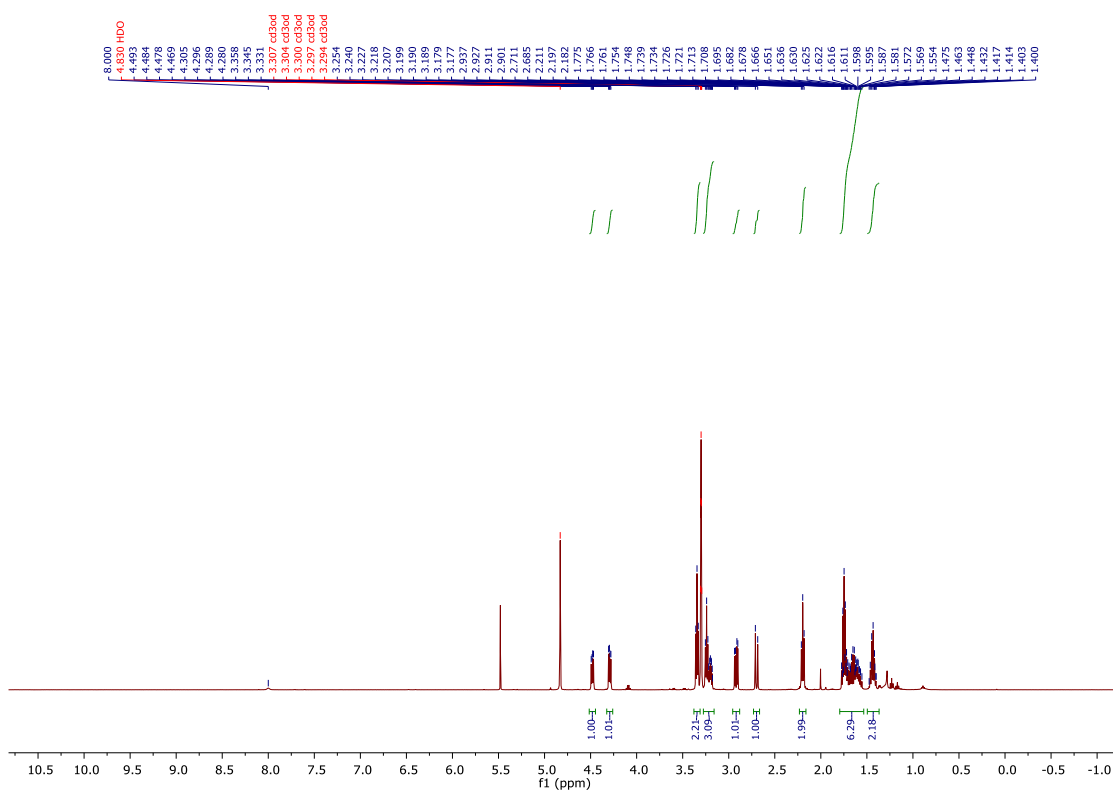


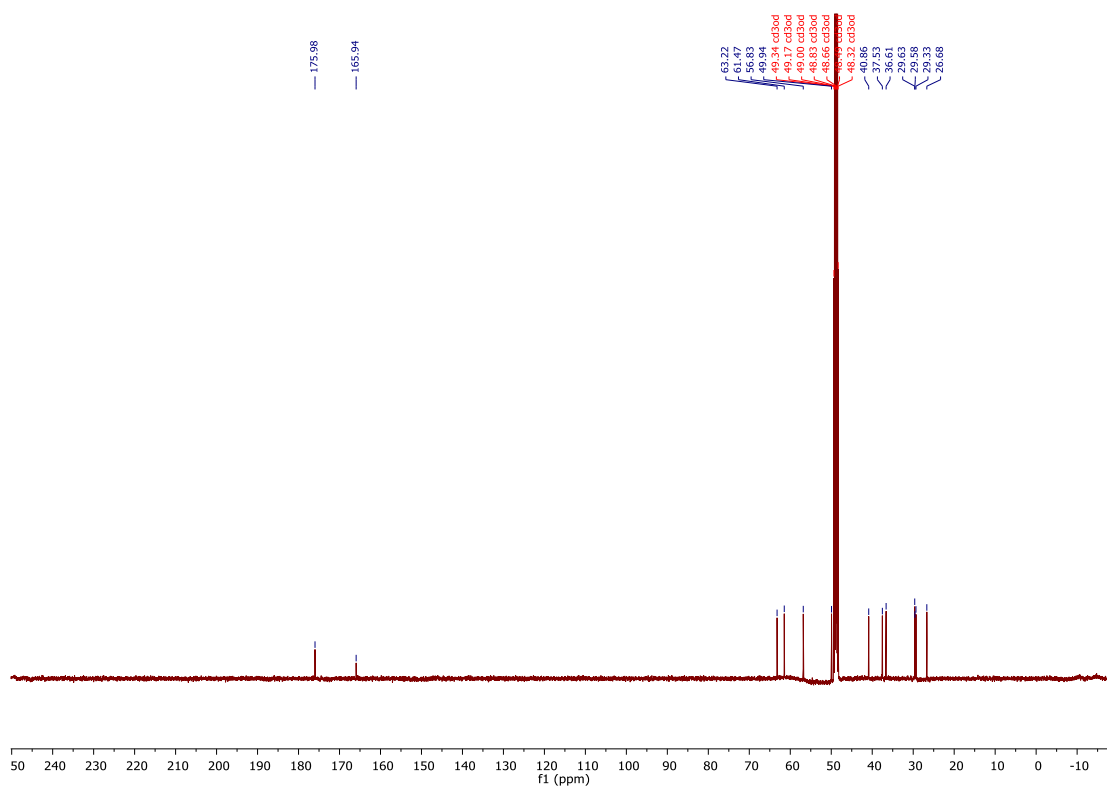
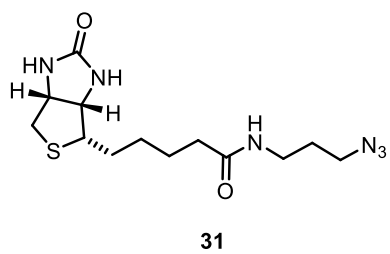


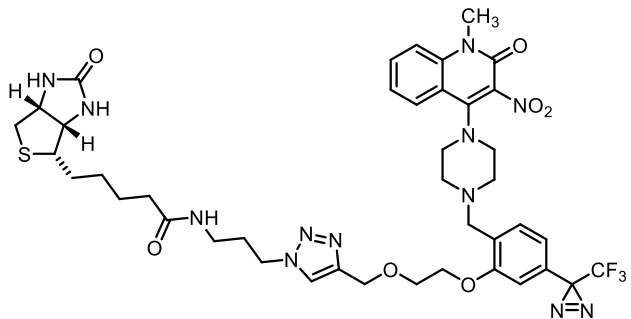




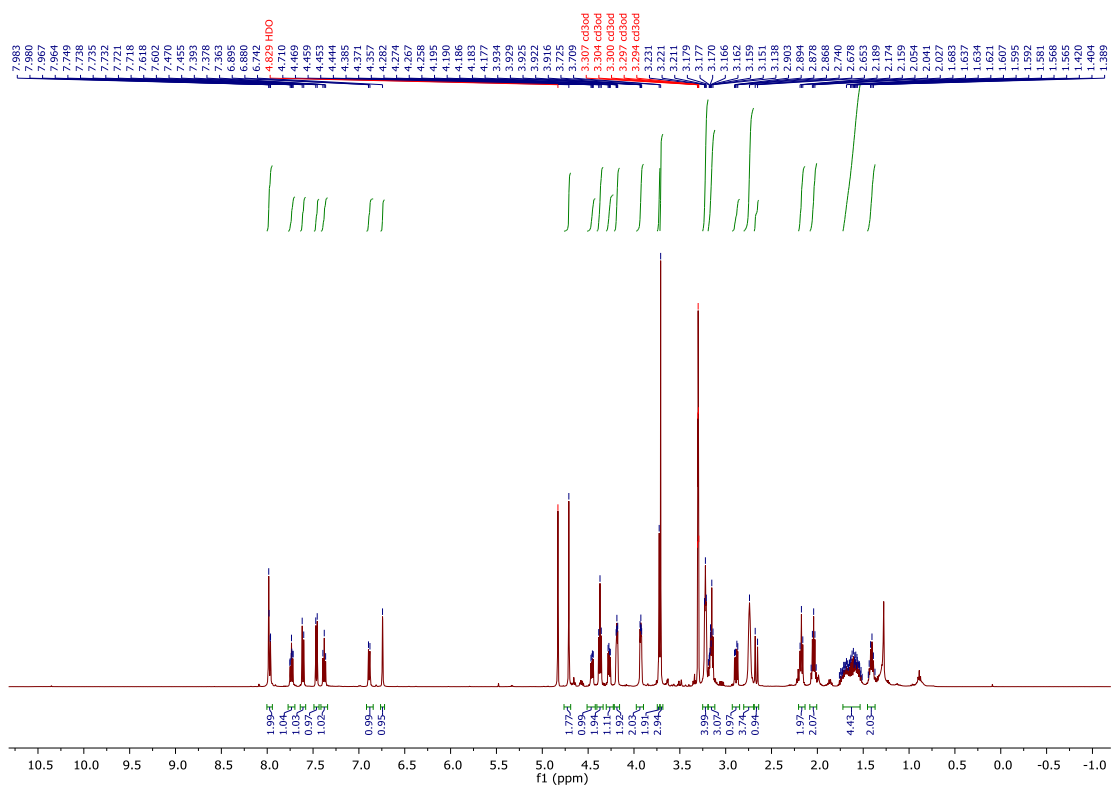
31

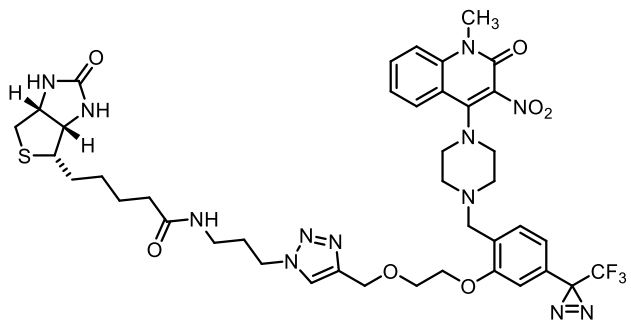




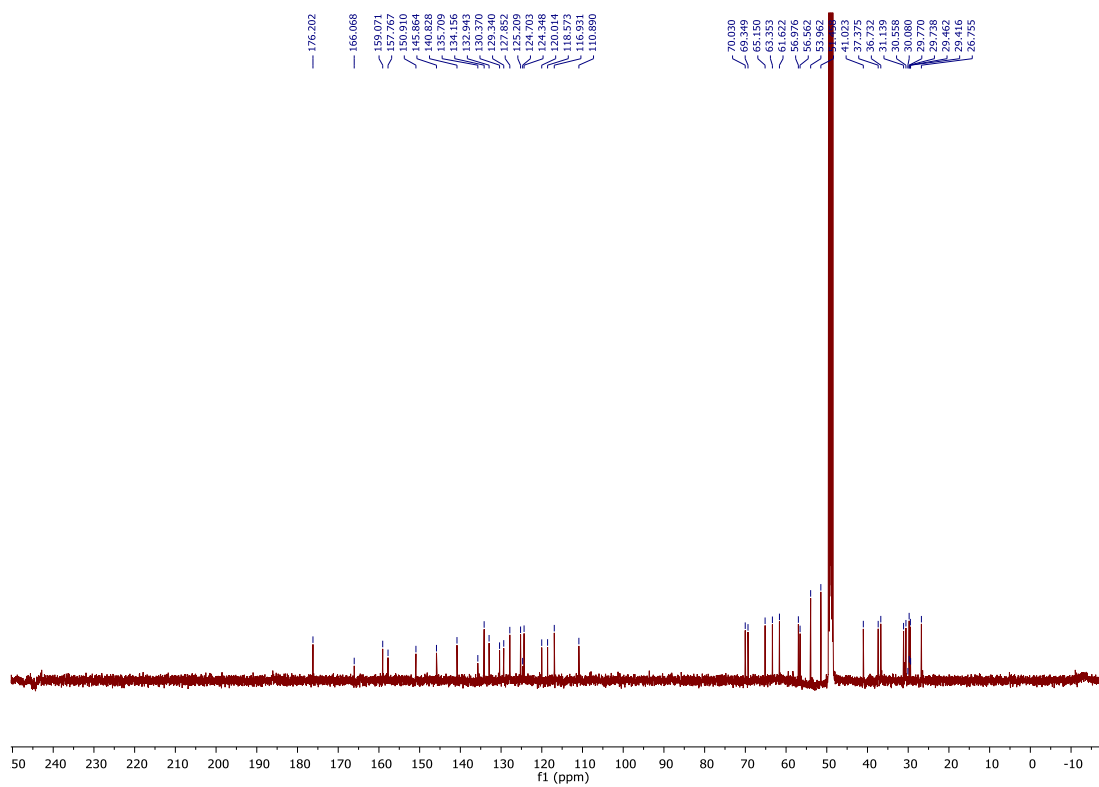


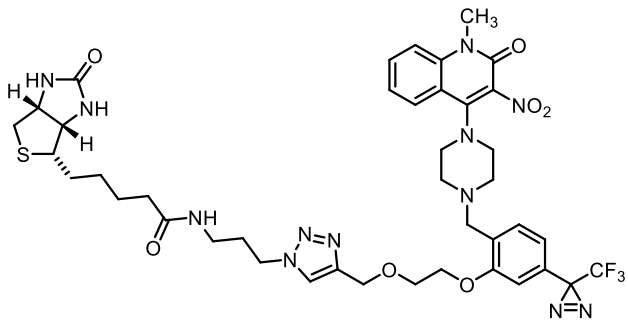
30





30

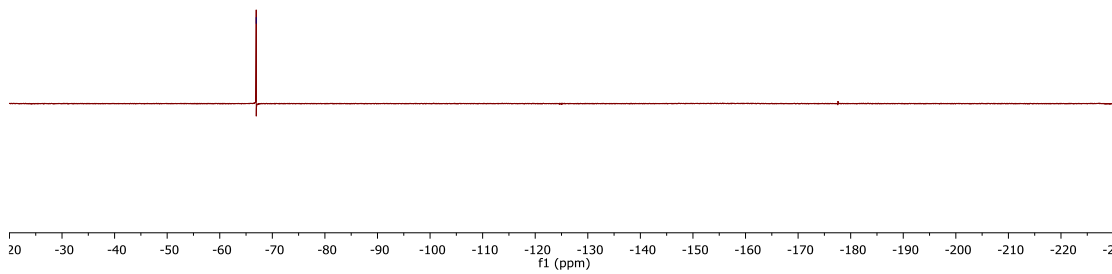


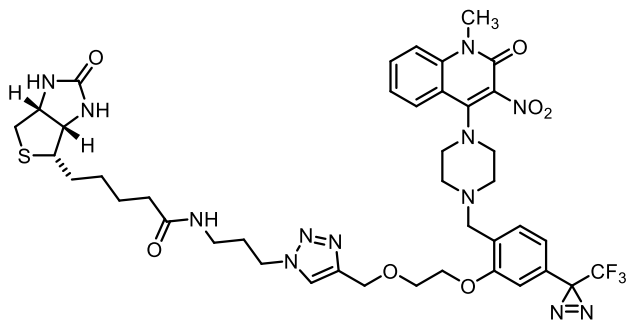


30

2022.04.26.i5_JL-B-111-F_F19_1D
JL-B-111-F
468.640 MHz F19 1D in cd3od
temp 26.9 C -> actual temp = 27.0 C, autotx probe

-66.939





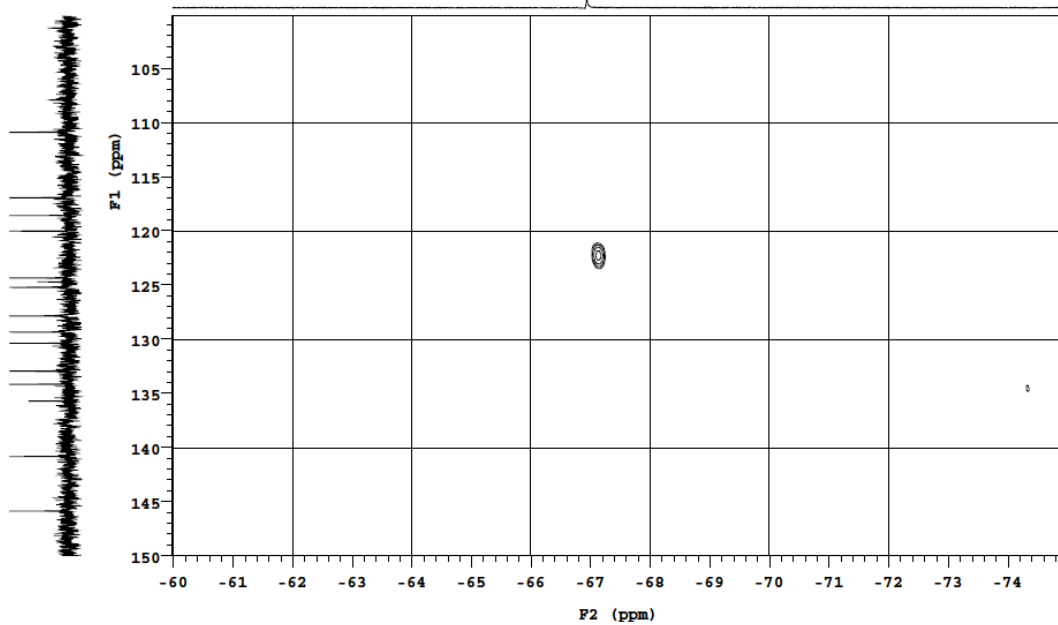
30

Department of Chemistry, University of Alberta

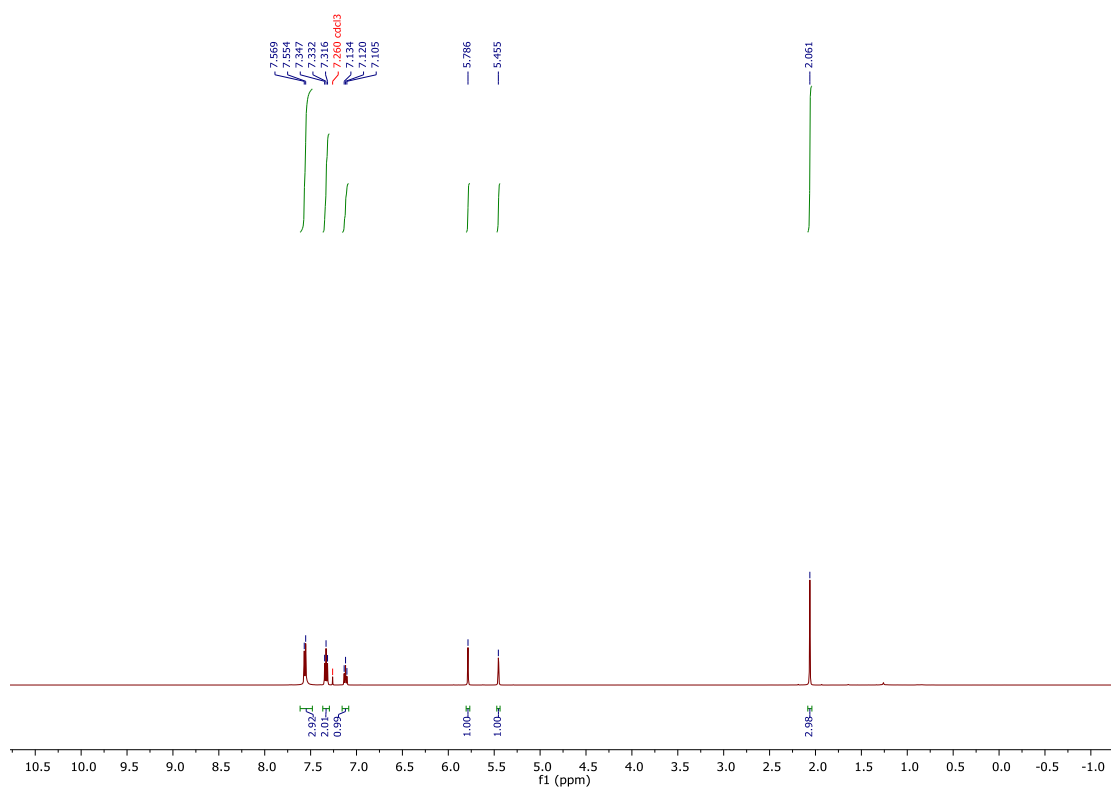
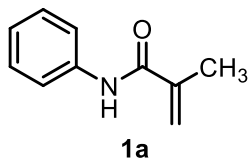
OpenVnmrj

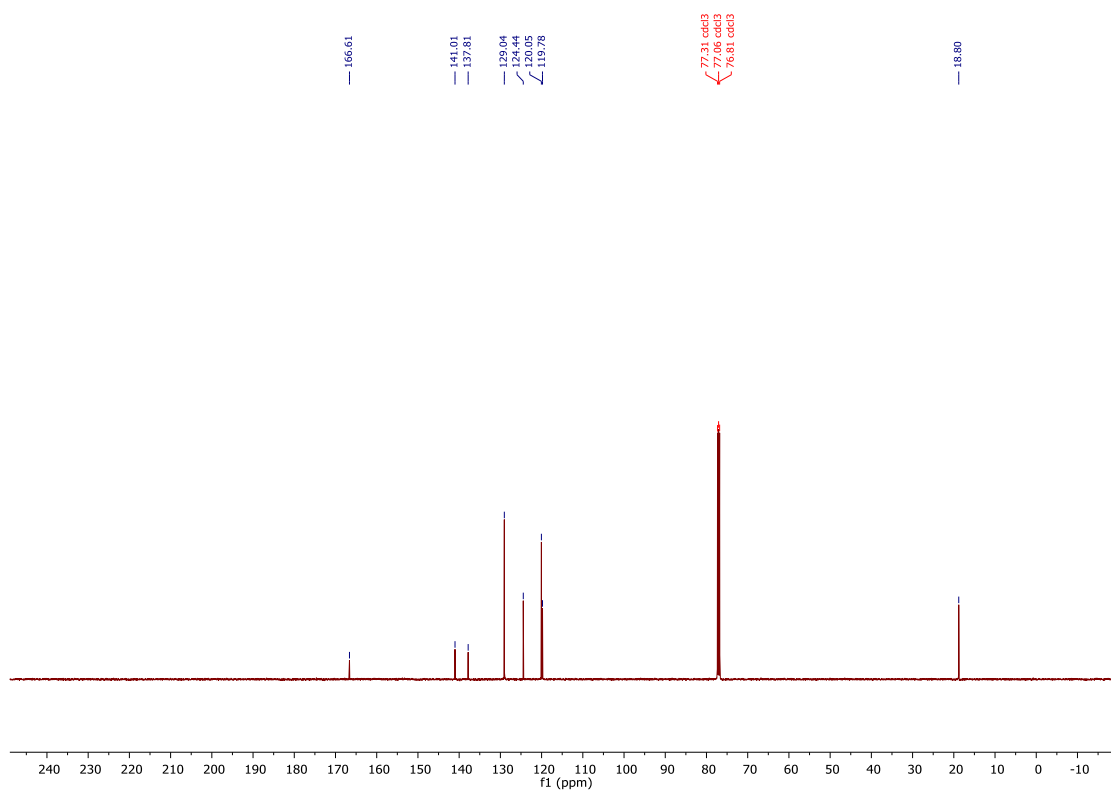
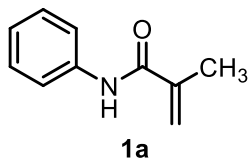
Recorded on: mr400, Apr 27 2022 Sweep Width F2[F1(Hz): 5656.11 | 5008.60] (on Time(s): 0.1 Relaxation Delay(s): 1.5
 Pulse Sequence: gq2haqc Digital Res. F2[F1(Hz/pt): 1.38 | 0.39] p64 mm F2[F1(Hz/mm): 24.10 | 30.64] of Scans/Increments 4 | 64

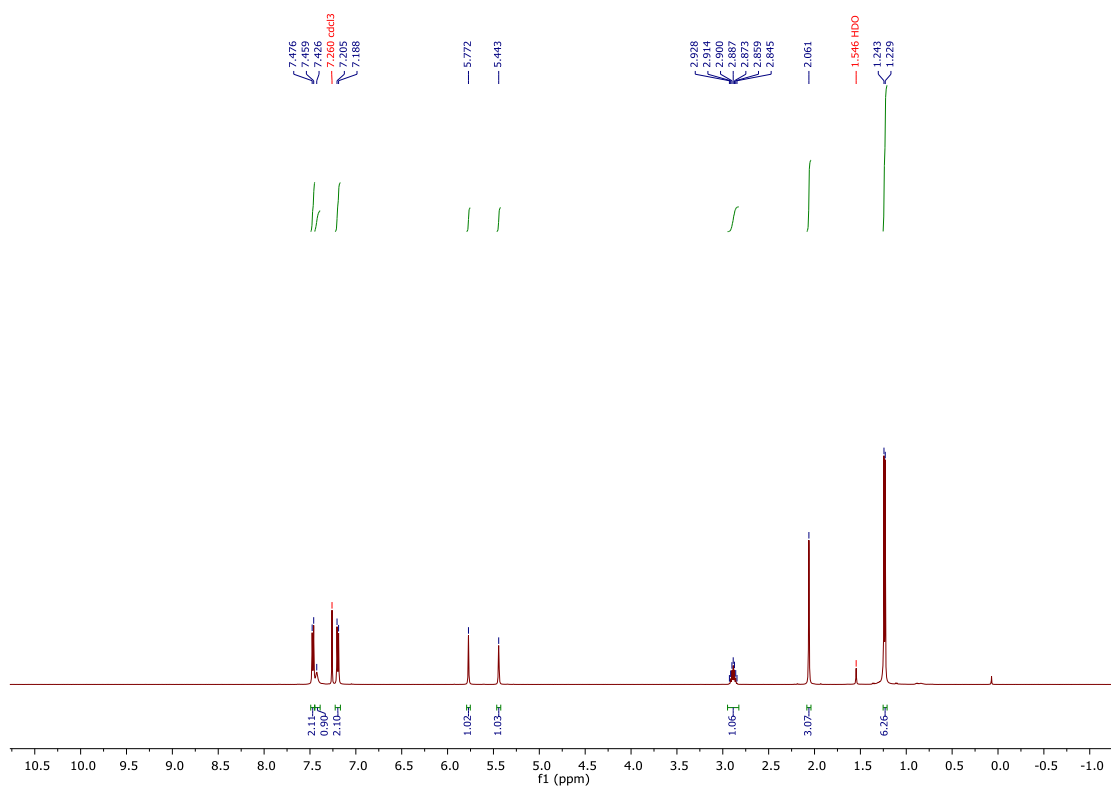
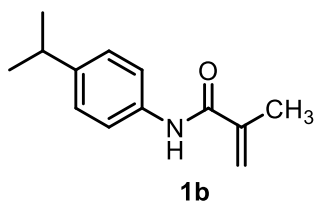
376.314 MHz F19 C13 gq2haqc in cd3od
 temp 25.9 C -> actual temp = 27.0 C, onemr probe

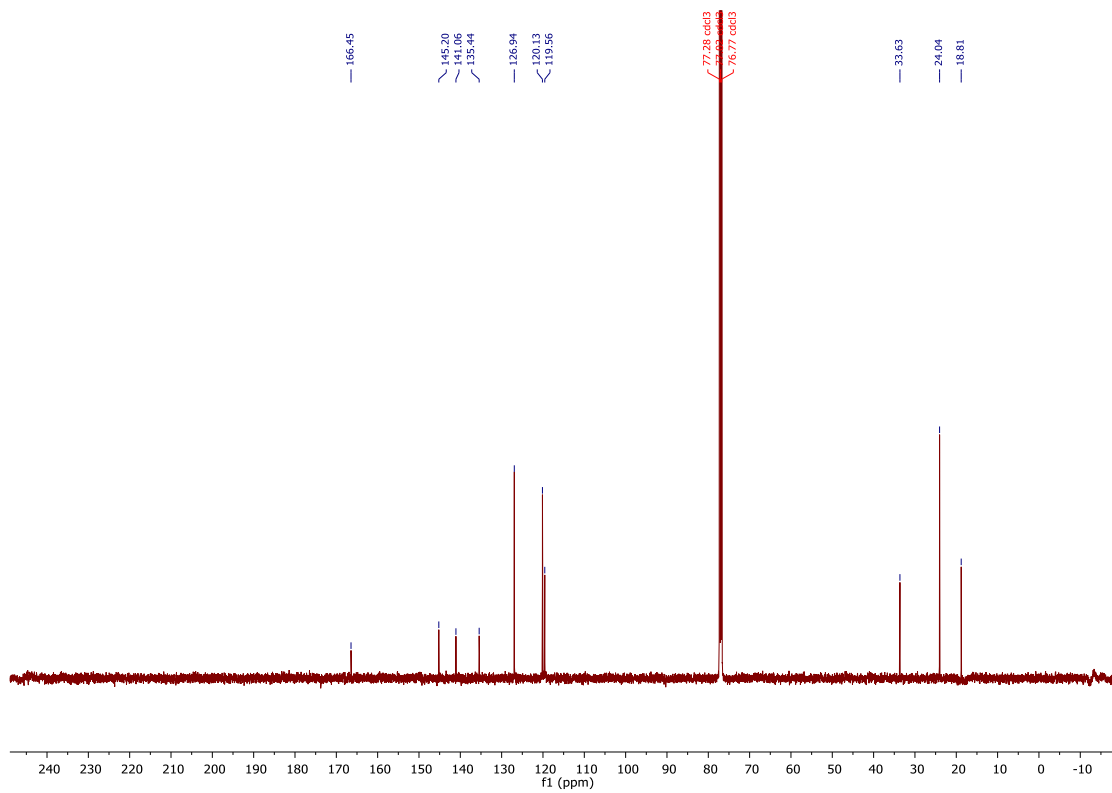
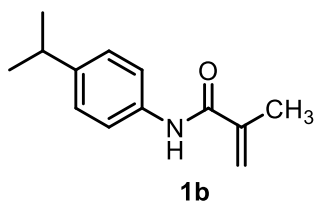


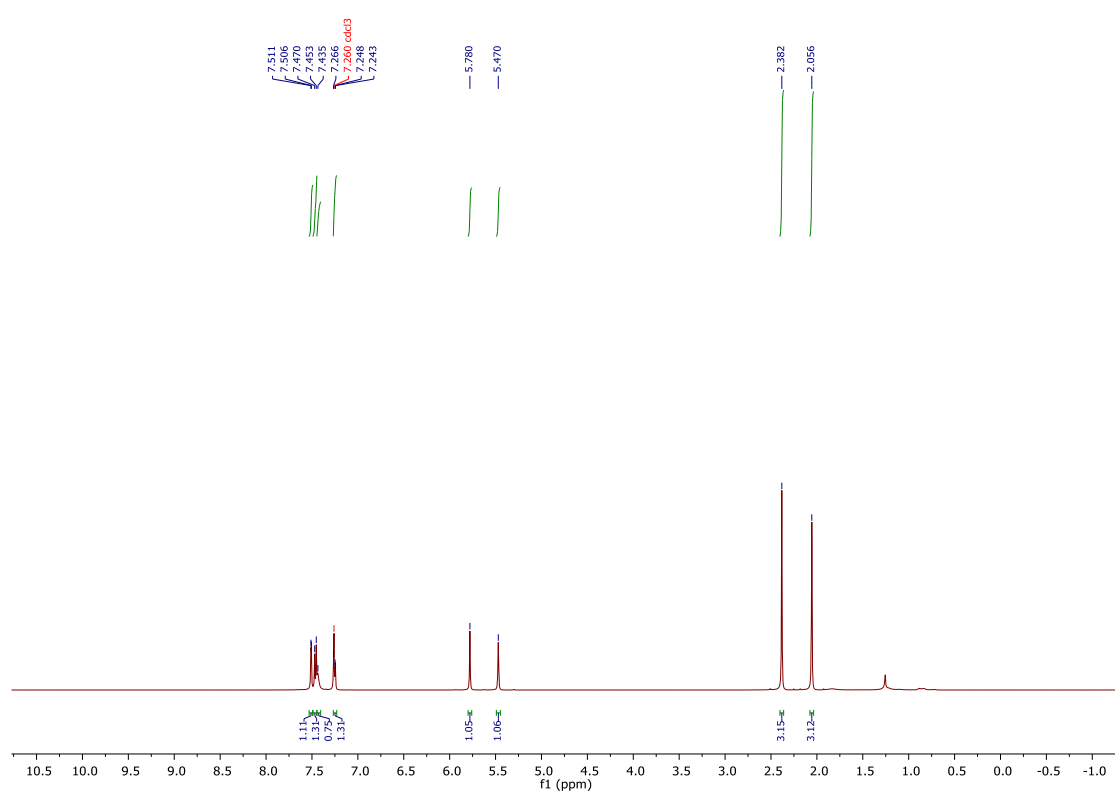
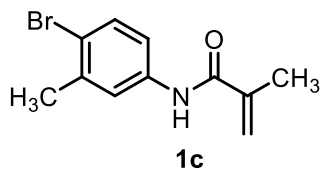
**Appendix III:
NMR Spectra (Chapter 4)**

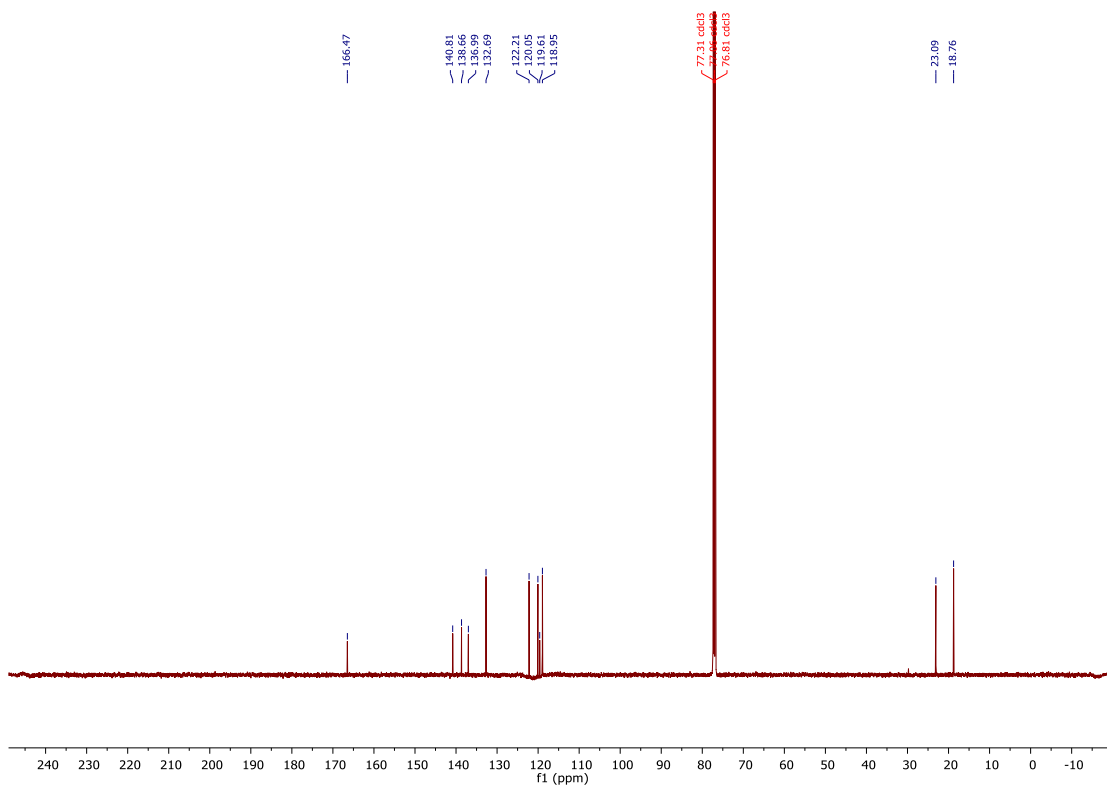
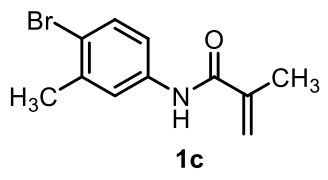


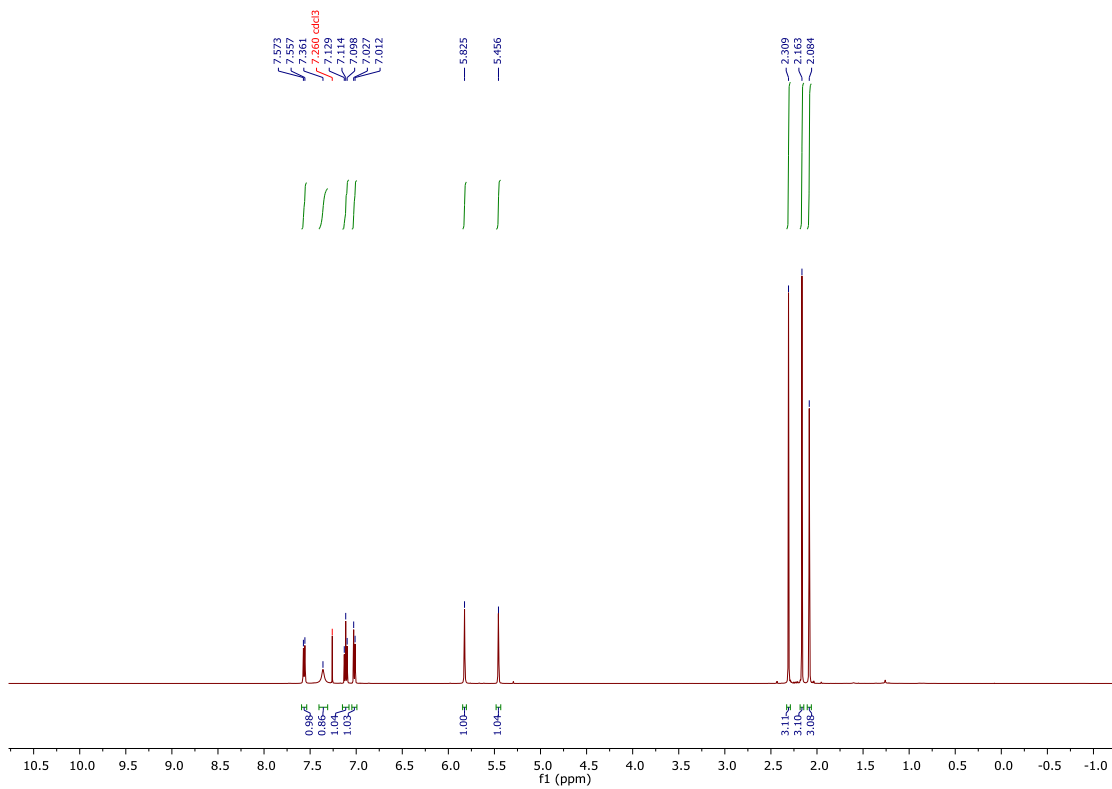
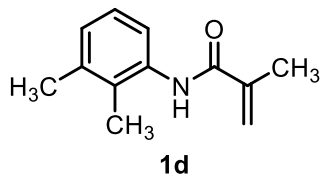


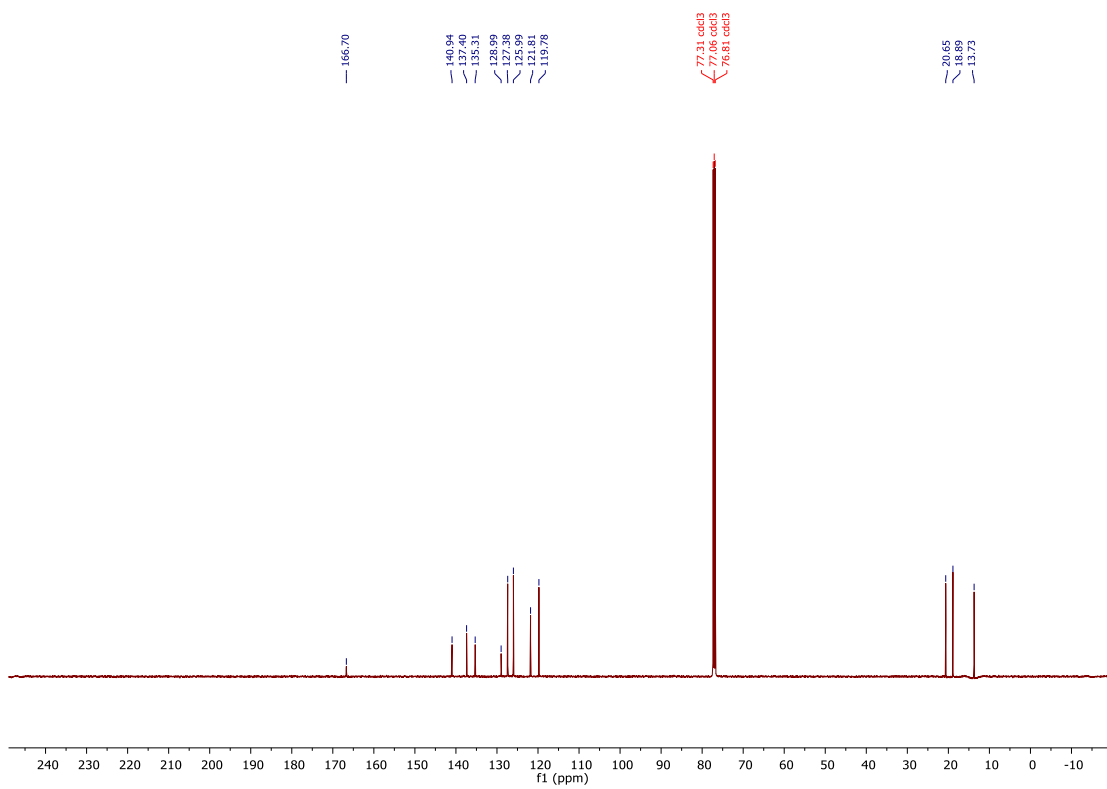
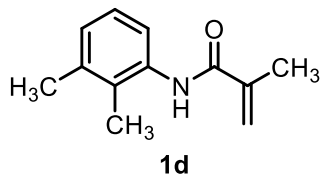


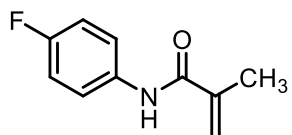




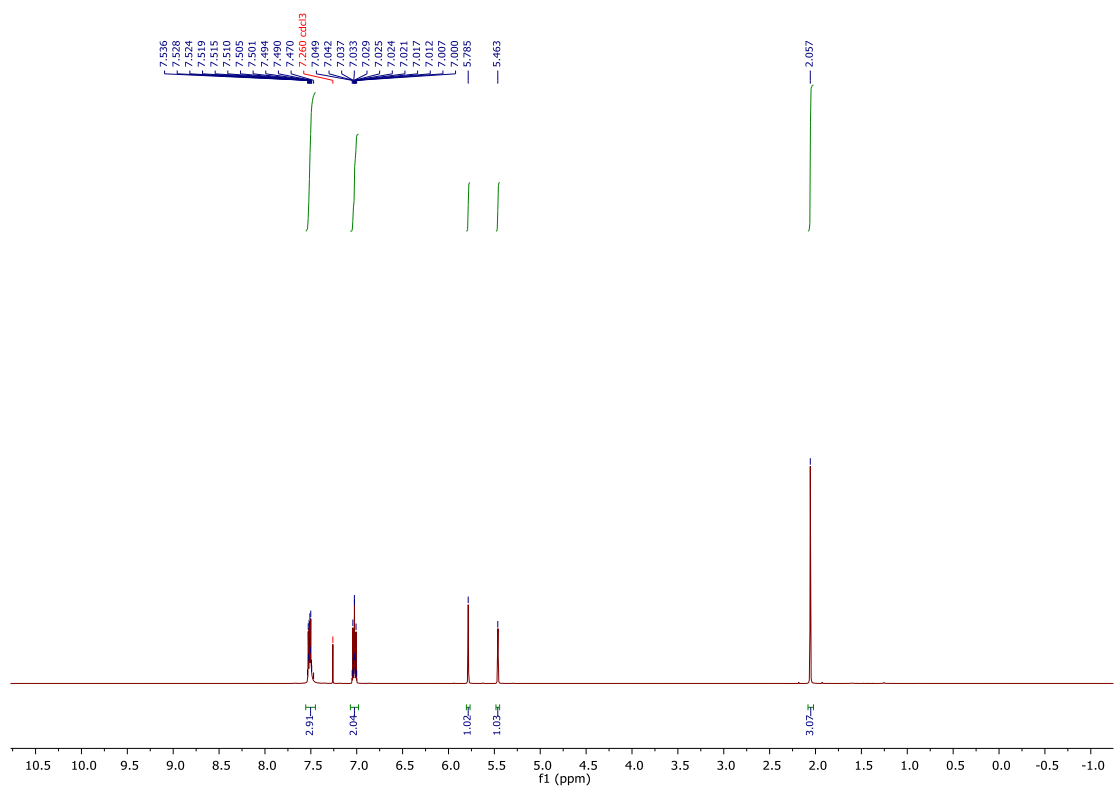


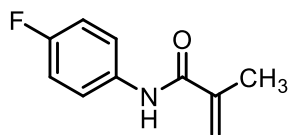






1e





1e

